**UNIVERSITÄT
DUISBURG
ESSEN**

Offen im Denken

Trefoil factor family peptide 1 (TFF1) as a biomarker, its possible receptors, signaling pathways and prospective application strategies in retinoblastoma therapy

Dissertation

zur

Erlangung des Doktorgrades

Dr. rer. nat.

der Fakultät für

Biologie

an der

Universität Duisburg-Essen

vorgelegt von

André Marcel Haase

aus Bochum

Juli 2024

Die der vorliegenden Arbeit zugrunde liegenden Experimente wurden am Institut für Anatomie II in der Abteilung für Neuroanatomie in der Universitätsmedizin Essen der Universität Duisburg-Essen durchgeführt.

    1. Gutachter: Frau Prof. Dr. Nicole Dünker
    2. Gutachter: Frau Prof. Dr. Barbara Grüner

Vorsitzender des Prüfungsausschusses: Prof. Dr. Alexander Schramm

Tag der mündlichen Prüfung: 20.11.2024

Table of Contents

List of figures

List of tables

List of abbreviations

#JM198	optimized EPI-X4 derived CXCR4 inhibitor
#JM21	optimized EPI-X4 derived CXCR4 inhibitor
AGS	adenocarcinoma cell line
AH	aqueous humor
ANP	atrial natriuretic peptide
CAM	chorioallantoic membrane
CDK	cyclin-dependent kinase
CIP	cyclin-dependent kinase inhibitor
CXCL12	C-X-C motif chemokine ligand 12
CXCR4	C-X-C motif chemokine receptor 4
ELISA	enzyme-linked immunosorbent assay
EPI-X4	endogenous peptide Inhibitor for CXCR4 receptor
GIPR	gastric inhibitory polypeptide receptor
GNP	goldnanoparticle
HA	hyaluronic acid
IAC	intraarterial chemotherapy
ICC	immunocytochemistry
IHC	immunohistochemistry
INK4	cyclin-dependent kinase inhibitor
IVC	intravitreal chemotherapy
LB	liquid biopsy
miR	microRNA
MYCN	MYCN proto-oncogene
PBT	proton beam therapy
RB	retinoblastoma

RB1	retinoblastoma gene 1
ROS	reactive oxygen species
rTFF1	recombinant TFF1
TFF1	trefoil factor family protein 1
TNM	tumor node metastasis staging system
VEGF	vascular endothelial growth factor
WB	western blot
Weri	WERI-Rb-1 retinoblastoma cell line
Y79	Y79 retinoblastoma cell line

Publications and conference contributions

Publications

<u>First authorships:</u>

Busch, M.A.*; **Haase, A.***; Alefeld, E.; Biewald, E.; Jabbarli, L.; Dünker, N. Trefoil Family Factor Peptide 1- A New Biomarker in Liquid Biopsies of Retinoblastoma under Therapy.

*shared first-authorship

Cancers 2023, 15, 4828. https://doi.org/10.3390/cancers15194828

Haase, A.*, Miroschnikov, N.*, Klein, S., Doege, A., Dünker, N., Van Meenen, D., Junker, A., Göpferich, A., Apaolaza, P.S. and Busch, M.A. (2024), New retinoblastoma (RB) drug delivery approaches: anti-tumor effect of atrial natriuretic peptide (ANP)-conjugated hyaluronic-acid-coated gold nanoparticles for intraocular treatment of chemoresistant RB.

*shared first-authorship

Mol Oncol. https://doi.org/10.1002/1878-0261.13587

Haase, A., Alefeld, E., Yalinci, F., Van Meenen, D., Dünker, N., Busch, M.A. Gastric Inhibitory Polypeptide Receptor (GIPR) Overexpression Reduces the Tumorigenic Potential of Retinoblastoma Cells.

Cancers 2024, https://doi.org/10.3390/cancers16091656

Co authorships:

Busch, M.A.; **Haase, A.**; Miroschnikov, N.; Doege, A.; Biewald, E.; Bechrakis, N.E.; Beier, M.; Kanber, D.; Lohmann, D.; Metz, K.; TFF1 in Aqueous Humor - A Potential New Biomarker for Retinoblastoma. Cancers 2022, 14, 677. https://doi.org/10.3390/cancers14030677

M. Harms, **A. Haase**, A. Rodriguez-Alfonso, J. Löffler, Y. Almeida-Hernández, Y. Ruiz-Blanco, D. Albers, A. Gilg, F. von Bank, F. Zech, M. Datta, J. Jaikishan, B. Draphoen, M. Habib, L. Ständker, S. Wiese, M. Lindén, G. Winter, V. Rasche, A. Beer, H. Jumaa, A. Abadi, F. Kirchhoff, M. Busch, N. Dünker, E. Sanchez-Garcia and J. Münch Fatty acid conjugated EPI-X4 derivatives with increased activity and in vivo stability. Under revision in Journal of Controlled Release.

Van Meenen, D.; Doege, A.; Alefeld, E.; **Haase, A**.; Beier, M.; Kiefer, T.; Biewald, E.; Metz, K.; Dräger, O.; Busch, M.A.; ADAM10 and ADAM17—Novel Players in Retinoblastoma Carcinogenesis. Int. J. Mol. Sci. 2022, 23, 12621. https://doi.org/10.3390/ijms232012621 **(not included in present work)**

Gonda S, Köhler I, **Haase A**, Czubay K, Räk A, Riedel C and Wahle P (2023) Optogenetic stimulation shapes dendritic trees of infragranular cortical pyramidal cells. Front. Cell. Neurosci. 17:1212483. doi: 10.3389/fncel.2023.1212483 **(not included in present work)**

Conference contributions

A. Haase, N. Miroschnikov, O. Dräger, E. Biewald, D. Lohmann, N. Dünker and M. Busch (2021). Establishment of primary retinoblastoma cell cultures. **Poster** presentation for "Tag der Forschung, Medical Faculty University of Duisburg Essen" in Essen.

A. Haase, N. Miroschnikov, O. Dräger, E. Biewald, D. Lohmann, N. Dünker and M. Busch (2021). Establishment of primary retinoblastoma cell cultures. **Poster**

presentation for "BIOME, graduate school of biomedical science, annual retreat" in Essen.

A. Haase, M. Busch, N. Miroschnikov, A. Doege, E. Biewald, N. Bechrakis, M. Beier, D. Kanber, D. Lohmann, K. Metz and N. Dünker (2022). TFF1 in Aqueous Humor—A Potential New Biomarker for Retinoblastoma. **Talk** for "Young Physiologists, Deutsche Physiologische Gesellschaft" in Essen.

A. Haase, M. Busch, N. Miroschnikov, A. Doege, E. Biewald, N. Bechrakis, M. Beier, D. Kanber, D. Lohmann, K. Metz and N. Dünker (2022). Trefoil factor family (TFF) peptides potential new biomarkers and pathway therapy targets in retinoblastoma therapy. **Talk** for "BIOME, graduate school of biomedical science" in Essen.

A. Haase, M. Busch and N. Dünker (2022). Role of the GIP receptor in retinoblastoma. **Poster** presentation for "Anatomische Gesellschaft" in Berlin.

A. Haase, M. Busch and N. Dünker (2022). Targeting GIPR - a new retinoblastoma treatment option? **Poster** presentation for "Gesellschaft für Biochemie und Molekularbiologie" in Bochum.

A. Haase, M. Busch and N. Dünker (2022). Gastric inhibitory polypeptide receptor (GIPR) –a novel target for retinoblastoma therapy? **Poster** presentation for "BIOME, graduate school of biomedical science, annual retreat" in Köln.

A. Haase, M. Busch and N. Dünker (2022). Gastric inhibitory polypeptide receptor (GIPR) –a novel target for retinoblastoma therapy? **Poster** presentation for "Tag der Forschung, Medical Faculty University of Duisburg Essen" in Essen.

A. Haase, E. Alefeld, F. Yalinci, D. Van Meenen M. Busch and N. Dünker (2023). The GIPR pathway - a promising target for new therapeutic approaches in retinoblastoma? **Poster** presentation for "Essen Translational Oncology Symposium" in Essen.

A. Haase, N. Miroschnikov, S. Klein, A. Doege, N. Dünker, A. Göpferich, K. Keyvani, P.S. Apaolaza, M. Busch (2023). Functionalized gold nanoparticles: A promising tool for retinoblastoma treatment. **Poster** presentation for "10th Mildred Scheel cancer conference, Deutsche Krebshilfe" in Bonn.

A. Haase, N. Miroschnikov, S. Klein, A. Doege, N. Dünker, A. Göpferich, K. Keyvani, P.S. Apaolaza, M. Busch (2023). Functionalized gold nanoparticles: A promising tool for retinoblastoma treatment. **Talk** for "BIOME, graduate school of biomedical science" in Essen.

A. Haase, M. Busch, E. Alefeld, E. Biewald, L. Jabbarli and N. Dünker (2023). New advances in retinoblastoma management: TFF1 as an aqueous humor biomarker for diagnosis and treatment monitoring. **Talk** for "BIOME, graduate school of biomedical science, annual retreat" in Essen.

A. Haase, N. Miroschnikov, S. Klein, A. Doege, N. Dünker, A. Göpferich, K. Keyvani, P.S. Apaolaza, M. Busch (2023). Efficacy of modified gold nanoparticles as a minimal invasive adjacent treatment option for chemoresistant retinoblastoma. **Poster** presentation for "Tag der Forschung, Medical Faculty University of Duisburg Essen" in Essen.

A. Haase, N. Miroschnikov, S. Klein, A. Doege, N. Dünker, A. Göpferich, K. Keyvani, P.S. Apaolaza, M. Busch (2024). Efficacy of modified gold nanoparticles as a minimal invasive adjacent treatment option for chemoresistant retinoblastoma. **Poster** presentation for "Essen Translational Oncology Symposium" in Essen.

A. Haase, E. Alefeld, F. Yalinci, D. Van Meenen M. Busch and N. Dünker (2024). GIPR overexpression reduces the tumorigenic potential of retinoblastoma cells. **Talk** for "BIOME, graduate school of biomedical science" in Essen.

Abstract

Retinoblastoma (RB) is the most common intraocular tumor in early childhood, originating from the juvenile retina and affecting approximately 7,500 patients each year. RB is most frequently caused by a biallelic loss of the tumor suppressor gene *RB1*.

The first part of this study focuses on our latest research findings in the field of liquid biopsy (LB) and describes the protein "trefoil factor family 1" (TFF1) as an LB biomarker in aqueous humor (AH) for an advanced RB subtype. TFF1 is expressed in the eye only in tumor cells of the advanced RB subtype, demonstrating the potential diagnostic and prognostic value of TFF1. In addition, we were able to demonstrate the benefit of TFF1 for therapy monitoring, as decreasing TFF1 levels after treatment with chemotherapeutic agents correlated with the onset of therapeutic success. Previous studies of our group showed that overexpression of TFF1 in RB cells leads to upregulation of the "gastric inhibitory polypeptide receptor" (GIPR).

The second part of this study, focuses on the role of GIPR in RB where our investigations showed that the expression of TFF1 and GIPR correlates in patient tumors. Further functional analysis in RB cells showed a significant decrease in cell viability, proliferation, and growth rates, with a concomitant increase in apoptosis after stable lentiviral GIPR overexpression, which was consistent with the effects after TFF1 overexpression. Further experiments in an alternative *in vivo* chicken chorioallantoic membrane (CAM) model showed that GIPR-overexpressing RB cells formed significantly smaller tumors than the control group. Furthermore, the effect of GIPR overexpression in RB cells could be reversed by the addition of a GIPR inhibitor. The addition of recombinant TFF1 showed no enhanced effect on GIPR overexpressing RB cells, suggesting that GIPR does not serve as a TFF1 receptor. Investigations into potential GIPR upstream and downstream mediators suggest the involvement of miR-542-5p and p53 in GIPR regulation and signal transduction.

The third part of this study introduces new and optimized inhibitors of the "CXC chemokine receptor type 4" (CXCR4) which were tested on RB cells and compared with previously established inhibitors. The efficiency of the inhibitors of the CXCR4 receptor was investigated in various *in vitro* studies and *in vivo* CAM assays on RB cell lines. In particular, the more stable inhibitor #JM198 was shown to have an improved

antagonistic effect compared to the CXCR4 inhibitor, resulting in a significantly improved reduction in tumor cell growth in RB cells.

The fourth part of this study discusses novel drug delivery approaches using functionalized gold nanoparticles (GNPs) which were tested for the treatment of chemoresistant RB cells. For this purpose, GNPs were functionalized with hyaluronic acid (HA) for increased uptake and with atrial natriuretic peptide (ANP), known for its inhibitory effect on neoangiogenesis, and tested in various *in vitro* and *in vivo* experiments. In addition, different application strategies were tested in an orthotopic *in vivo* RB eye model of newborn rats. Treatment of chemoresistant RB cells with ANP-HA-GNPs *in ovo* resulted in a significant reduction of tumor growth and angiogenesis compared to control groups. This effect could be verified in the rat eye model, where a non-invasive application via eye drops was also tested, which resulted in a reduction of tumor growth in the rat eye.

Overall, this study encompasses a multifaceted approach from the establishment of new biomarkers to the elucidation of molecular mechanisms and the development of targeted therapies with the aim of improving the treatment of RB, preserving patients' vision, and facilitating long-term monitoring of tumor progression.

Abstract (German)

Das Retinoblastom (RB) ist der häufigste intraokuläre Tumor im Kindesalter, der von der juvenilen Netzhaut ausgeht und jährlich etwa 7500 Patienten betrifft. Das RB entsteht fast immer durch den biallelischen Verlust des Tumorsuppressorgens *RB1*.

Der erste Teil dieser Arbeit befasst sich mit unseren neuesten Forschungsergebnissen auf dem Gebiet der "Liquid Biopsy" (LB) und beschreibt das Protein "Trefoil factor family 1" (TFF1) als LB Biomarker im Kammerwasser für einen aggressiveren RB Subtyp. TFF1 wird im Auge nur in Tumorzellen des aggressiveren RB-Subtyps exprimiert, was den potenziellen diagnostischen und prognostischen Wert von TFF1 verdeutlicht. Darüber hinaus konnten wir den Nutzen von TFF1 für die Überwachung des Therapieerfolgs aufzeigen, da sinkende TFF1-Konzentrationen nach der Behandlung mit Chemotherapeutika mit dem Therapieerfolg korrelierten. Vorangegangene Studien unserer Arbeitsgruppe haben gezeigt, dass die Überexpression von TFF1 in RB-Zellen zu einer Hochregulation des "gastric inhibitory polypeptidereceptor" (GIPR) führt.

Deshalb wurde im zweiten Teil der vorliegenden Arbeit die Rolle von GIPR im RB untersucht und gezeigt, dass die Expression von TFF1 und GIPR in Patiententumoren korreliert. Weitere funktionelle Analysen in RB-Zellen zeigten eine signifikante Reduktion der Zellviabilität, Proliferation und Teilungsrate bei gleichzeitiger Erhöhung der Apoptose nach stabiler lentiviraler GIPR-Überexpression. Diese Effekte waren denen der TFF1-Überexpression in RB-Zellen ähnlich. In weiteren Experimenten in einem alternativen *in vivo* Hühner-Chorioallantois-Membran (CAM) Modell wurde gezeigt, dass GIPR-überexprimierende RB-Zellen signifikant kleinere Tumore bildeten als die Kontrollgruppe. Darüber hinaus konnte der Effekt der GIPR-Überexpression in RB-Zellen durch Zugabe eines GIPR-Inhibitors umgekehrt werden. Die Zugabe von rekombinantem TFF1 hingegen zeigte keinen verstärkten Effekt auf GIPR-überexprimierende RB-Zellen, was darauf hindeutet, dass GIPR nicht als TFF1-Rezeptor fungiert. Die Untersuchung von potentiellen Upstream- und Downstream-Mediatoren von GIPR deutet darauf hin, dass miR-542-5p und p53 an der Regulation und der Signaltransduktion des GIPR beteiligt sind.

Im dritten Teil der vorliegenden Arbeit wurden neue und optimierte Inhibitoren des "CXC-Chemokinrezeptors Typ 4" (CXCR4) an RB-Zellen getestet und mit bereits etablierten Inhibitoren verglichen. Dabei wurde die Wirksamkeit der Inhibitoren des

CXCR4-Rezeptors in verschiedenen *in vitro* Studien und *in vivo* CAM-Assays an RB-Zelllinien untersucht. Hierbei zeigte sich, dass vor allem der stabilere Inhibitor #JM198 eine verbesserte antagonistische Wirkung auf den CXCR4-Inhibitor ausübt und dadurch das Tumorzellwachstum in RB-Zellen stärker reduziert.

Im vierten Teil der vorliegenden Arbeit wurden neue Ansätze zum Wirkstofftransport mittels funktionalisierter Goldnanopartikel (GNPs) zur Behandlung von chemoresistenten RB-Zellen getestet. Dazu wurden GNPs mit Hyaluronsäure (HA) zur besseren Aufnahme und mit atrialem natriuretischem Peptid (ANP), das für seine hemmende Wirkung auf die Neoangiogenese bekannt ist, beschichtet und in verschiedenen *in vitro-* und *in vivo-* Experimenten getestet. Außerdem wurden verschiedene Applikationsstrategien in einem zuvor neu etablierten orthotopen *in vivo* RB-Augenmodell neugeborener Ratten getestet. Die Behandlung von chemoresistenten RB-Zellen mit ANP-HA-GNPs *in ovo* führte zu einer signifikanten Reduktion des Tumorwachstums und der Angiogenese im Vergleich zu den Kontrollgruppen. Dieser Effekt konnte im Augenmodell der Ratte verifiziert werden, wobei auch eine nicht-invasive Applikationsform über Augentropfen getestet wurde, die das Tumorwachstum im Rattenauge reduzierte.

Insgesamt zeigt diese Arbeit einen vielschichtigen Ansatz von der Etablierung neuer Biomarker über die Aufklärung der molekularen Mechanismen bis hin zur Entwicklung zielgerichteter Therapien mit dem letztendlichen Ziel, die Behandlung des RB zu verbessern, das Sehvermögen der Patienten zu erhalten und die Langzeitüberwachung der Tumorprogression zu erleichtern.

Introduction

Retinoblastoma

Retinoblastoma (RB) is a rare tumor disease of the juvenile retina, with an incidence of approximately 1 case in about 15,000 - 20,000 live births worldwide (Kivelä, 2009, Dimaras *et al.*, 2012, Munier *et al.*, 2019). Although this tumor entity is not prevalent, RB is the most common intraocular tumor in early childhood (Bornfeld *et al.*, 2020, Bouchoucha *et al.*, 2023, Byroju *et al.*, 2023). Untreated retinoblastoma is lethal due to metastasis through the optic nerve to the brain or to orbital tissues (Bornfeld *et al.*, 2020).

It is currently believed that RB develops from cone photoreceptor precursor cells (Xu *et al.*, 2009, 2014, Kaewkhaw and Rojanaporn, 2020) and in over 98% of all cases is related to the biallelic loss of the *retinoblastoma gene 1* (*RB1; Cobrinik, 2024)*. About 60% of all RB cases are non-hereditary whereas the remaining 40% are hereditary (autosomal-dominant; Kleinerman et al., 2012).

In the hereditary variant, a mutation in one allele of the *RB1* gene is already present in the germline (Figure 1), followed by a second mutation of the second allele in a somatic cell. Since all somatic cells already carry one defective allele, the risk of multiple tumor locations in one eye is increased, and tumors may also develop in both eyes (bilateral). The non-hereditary variant of RB, in which both alleles of the *RB1* gene are mutated in somatic cells, usually occurs in one eye (unilateral; Knudson, 1971; Little et al., 2012).
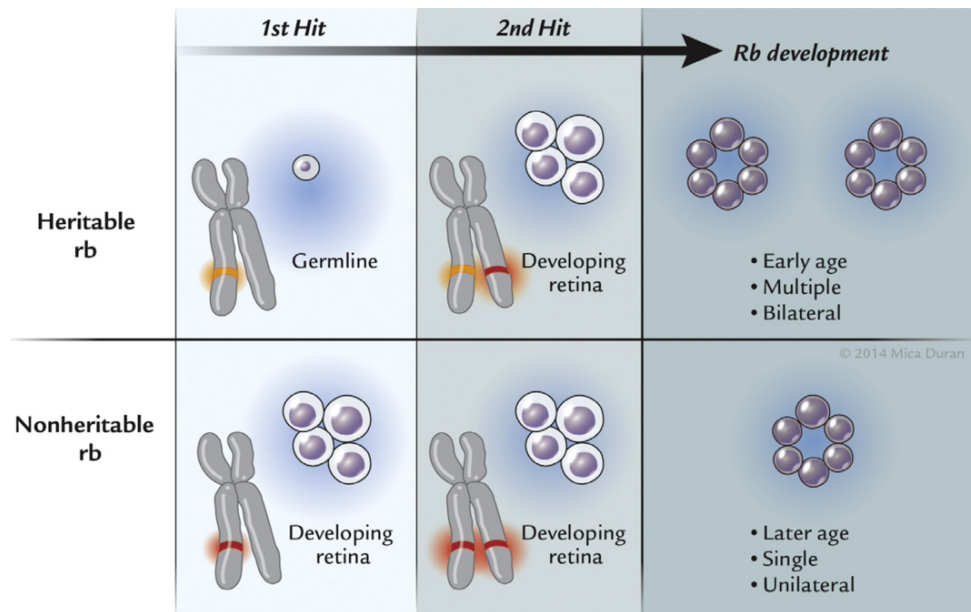
Figure 1: Inheritance of retinoblastoma. Two mutational events (two hits) in a retinal cell, most likely a developing cone photoreceptor cell, lead to damage of the *RB1* gene and finally to RB. In hereditary RB (top), an inherited germline mutation (first hit) is followed by a second mutation (second hit) in the developing retina. These tumors are usually diagnosed at an early age and form multiple tumors in both eyes. In the non-inherited variant of RB (below), two different mutation events occur in somatic cells, deactivating the *RB1* gene. These tumors are usually diagnosed later and form single, unilateral tumors. Adapted from Mendoza and Grossniklaus, 2015.

RB1 was the first described tumor suppressor gene (Knudson, 1971, Comings, 1973, Friend *et al.*, 1986), and it changed the scientific view of cancer. The *RB1* gene spans about 180,000 bases with 27 exons and is located on chromosome 13q14. Dommering and her colleagues described the distribution of *RB1* mutations in a cohort with 1173 patients and classified them as: 37% nonsense, 20% frameshift, 21% splice, 9% large insertions and deletions, 5% missense, 7% chromosomal deletions, and 1% in the promoter region (Dommering *et al.*, 2014). The *RB1* gene encodes for the RB protein, which regulates transcription of cell cycle genes by interacting with transcription factors of the E2F family; as a result, transcription of cell proliferation genes are altered (Cobrinik, 2005, Henley and Dick, 2012, Dyson, 2016). While the biallelic loss of *RB1* marks the initial stage of RB, additional mutations are needed for progression into a malignant state; otherwise it remains as non-proliferative retinoma, the precursor of RB (Gallie *et al.*, 1982, Dimaras *et al.*, 2008).

Only about 1.4% of all RB cases are not caused by the biallelic loss of the *RB1* gene, but by amplification of *MYCN* (Rushlow *et al.*, 2013, Cobrinik, 2024). Findings by

Ruschlow and colleagues suggest that RB tumors with *MYCN* amplification are derived from an earlier retinal progenitor cell rather than from a cone photoreceptor precursor cell (Rushlow *et al.*, 2013). *MYCN* amplification can also occur in addition to an *RB1* mutation, and all *MYCN*-amplified RB tumors always belong to a more aggressive subtype (Liu *et al.*, 2021, Marković *et al.*, 2023, Vempuluru *et al.*, 2024).

Using a cohort of 102 RB tumors, Liu and colleagues showed that there are two subtypes of RB, which are associated with different clinical and pathologic features (Liu *et al.*, 2021). Besides RB1 inactivation, subtype I has fewer genetic alterations and forms differentiated tumors. In contrast, almost all subtype II tumors have recurrent genetic alterations, such as *MYCN* amplifications, in addition to RB1 inactivation, and form less differentiated tumors with stemness features (see section: "Trefoil factor family peptides as biomarkers").

Diagnosis, prognosis and challenges

Retinoblastoma is diagnosed within the first five years of life in more than 90% of cases. RB is the only tumor of the central nervous system that can be seen with the naked eye. The first sign of a developing RB is a whitish reflection in the eye, often seen in photographs taken with a flash. This symptom, also known as leukocoria (Figure 2), is caused by infiltration of the tumor into the vitreous body, which causes reflection of incident light. Other common, visible symptoms include: proptosis, swelling, strabismus, and a collection of pus in the anterior chamber (hypopyon; Dimaras *et al.*, 2012). Computed tomography, magnetic resonance imaging, optical coherence tomography, fluorescence angiography and ultrasound examinations are usually used to verify the diagnosis of RB (Moulin *et al.*, 2012, Kim *et al.*, 2014, De Jong *et al.*, 2016, Gaillard *et al.*, 2018, Bornfeld *et al.*, 2020). These methods allow early diagnosis of RB with clarification of choroidal infiltration and seeding into the vitreous body (Bornfeld *et al.*, 2020). However, since diseases such as Coats' disease exhibit many, if not all, of the symptoms of RB, a definitive diagnosis is often not possible and can only be confirmed by histopathologic examination.

Major differences in mortality rates exist between various regions of the world. In Africa and Asia, the average survival rate is 30 - 60%, while in high-income countries such as Canada, the USA and countries within Europe, 95-98% of RB patients survive RB (Leal-Leal *et al.*, 2004, MacCarthy *et al.*, 2006, Kivelä, 2009, Dimaras *et al.*, 2012,

Nyamori *et al.*, 2012, Meel *et al.*, 2020). One of the reasons for the disparity in mortality rates is early diagnosis in high-income countries. Untreated RB can progress rapidly and can grow from small intraretinal tumors to extraocular tumors (Table 1) within months.

Table 1: RB tumor staging according to the TNM system. Corresponding tumors are shown in Figure 2. Adapted and modified from *Tomar et al., 2020*.

Staging Tumor	Features
T1a	Tumors < 3 mm and farther than 1.5 mm from the disc and fovea
T1b	Tumors > 3 mm or closer than 1.5 mm to the disc and fovea
T2a	Subretinal fluid > 5 mm from the base of any tumor
T2b, T3a	Tumors with vitreous seeding or subretinal seeding Phthisis or pre-phthisis bulbi
T3b	Tumor invasion of the pars plana, ciliary body, lens, zonules, iris, or anterior chamber
T4a, b, c, d	Radiologic evidence of retrobulbar optic nerve involvement or thickening of the optic nerve or involvement of the orbital tissues Extraocular tumor clinically evident with proptosis and orbital mass

While unilateral RB is diagnosed at an average age of 27 months in Canada, it is diagnosed at 36 months in Kenya (Figure 2 B; Dimaras *et al.*, 2012).
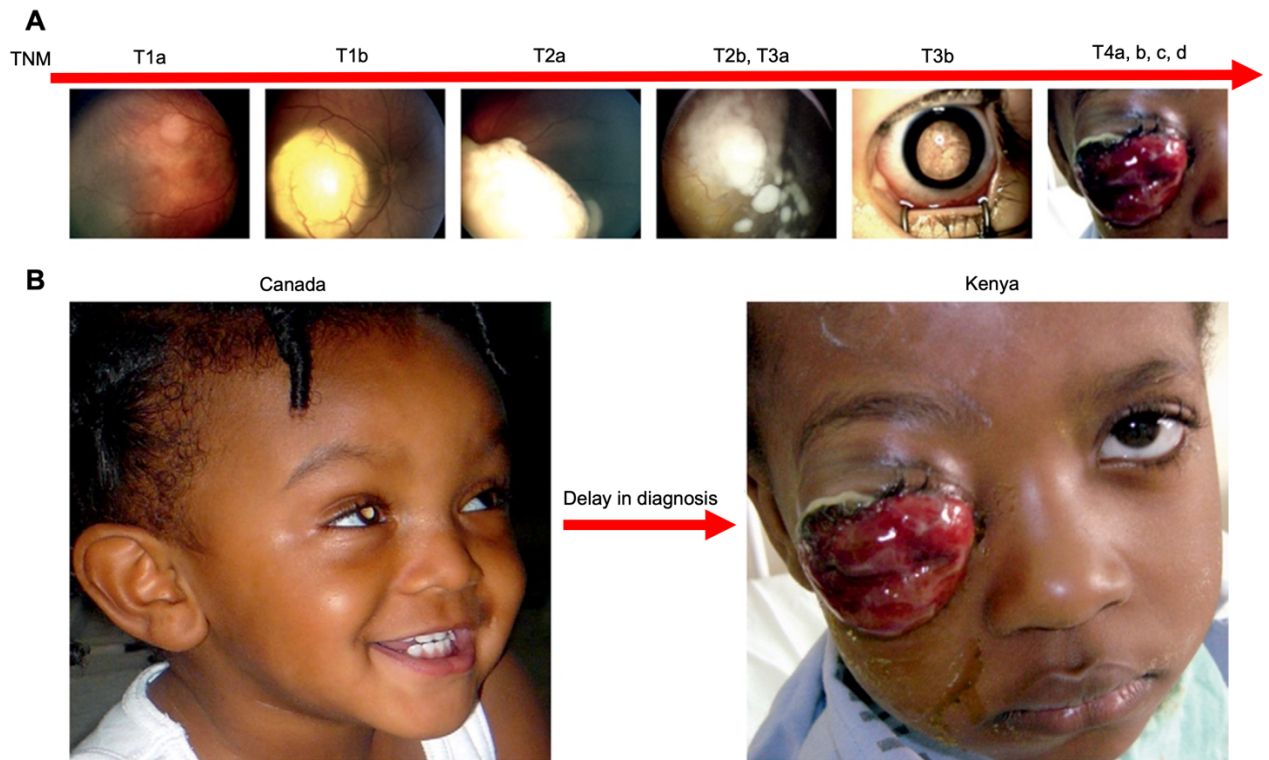
Figure 2: Progression of retinoblastoma. A) RB progresses from small intraretinal tumors (TNM T1a) to massive orbital retinoblastoma metastasizing to the brain (TNM T4a-b). **B)** The average diagnosis of unilateral RB in Canada is 9 months earlier than in Kenya. The delay in diagnosis has a negative impact on patient survival. TNM=Tumor Node Metastasis Cancer Staging. Adapted and modified from Dimaras *et al.*, 2012.

Since the *RB1* gene, a tumor suppressor that is also involved in other tumor entities, is missing in the hereditary variant of RB, the risk of developing secondary tumors such as sarcomas is significantly increased (Kleinerman *et al.*, 2005, 2012, Marees *et al.*, 2008).

Patients with bilateral RB also have a up to an 8% risk of developing pinealoblastoma (trilateral), a central nervous system malignancy originating in the pineal gland (Aerts *et al.*, 2006). The pineal gland comprises of the neuroectoderm of the posterior part of the upper part of the diencephalon and contains embryonic photoreceptor cells, therefore it can develop a tumor analogous to RB. The prognosis is significantly poorer when trilateral RB is diagnosed (Aerts *et al.*, 2006, Yamanaka *et al.*, 2019).

Current treatment strategies

A treatment strategy depends on the laterality and TNM staging (Table 1 and Figure 2). TNM staging is a classification of tumor diseases that considers the size of the primary tumor (T), potential lymph node involvement (N), and possible metastases (M). To prevent the spread of metastases, the eye may be completely removed (enucleation), which is particularly common in unilateral RB (Lu *et al.*, 2019). However, over the past 15 years there has been a shift in the direction of preserving the eye as a treatment goal (Ancona-Lezama *et al.*, 2020, Zhou *et al.*, 2022). A range of chemotherapies can be used for this purpose, which can be administered both systemically and locally. During systemic chemotherapy combinations of various cytostatic drugs such as vincristine, etoposide, and carboplatin (VEC-therapy) are administered in order to reduce tumor mass (Fabian *et al.*, 2017, Temming *et al.*, 2017, Naseripour *et al.*, 2022, Kritfuangfoo and Rojanaporn, 2024). For local chemotherapy, melphalan or topotecan is usually administered intra-arterially (intra-arterial chemotherapy, IAC) or intravitreally (intravenous chemotherapy, IVC). For IAC, a catheter is inserted via the femoral artery into the *Arteria carotis* to reach the *Arteria ophthalmica* (Suzuki and Kaneko, 2004, Castela *et al.*, 2023). In recent years, IVC has become one of the most important therapeutic options in the treatment of RB (reviewed in: Lavasidis *et al.*, 2024). It is characterized by low overall toxicity for the patient and excellent therapeutic success. The cytostatic drug is injected directly into the vitreous body of the eye. To prevent extraocular growth of the tumor, special safety precautions must be taken, such as short-term induction of bulbar hypotony by targeted paracentesis of the aqueous humor (Shields *et al.*, 2016, Francis *et al.*, 2017, Francis and Brodie *et al.*, 2017, Abramson *et al.*, 2019).

However, a problem with chemotherapy treatment is the risk of developing chemotherapy resistance. The development of resistance can hamper follow-up treatment of relapses, since resistance often occurs not only to the drug administered, but also to drugs that have a mechanism of action similar to the chemotherapeutic agent originally administered (reviewed in: Bukowski *et al.*, 2020).

Other treatment options are cryotherapy and brachytherapy, which are often used in combination with chemotherapy. Percutaneous radiotherapy was considered as a promising treatment option in the past, but long-term studies have shown that it

significantly increases the risk of secondary tumors (Kleinerman *et al.*, 2005, Temming *et al.*, 2017).

Proton beam therapy (PBT), which is more precise and less harmful to surrounding tissue than conventional radiation therapy, is also used to treat RB (reviewed in: Thomas and Timmermann, 2020; Biewald *et al.*, 2021). Long-term studies by Mouw *et al.* showed that in a cohort of 41 bilateral RB patients treated with PBT, no patient died and only one patient with hereditary RB disease developed a secondary cancer after 10 years of treatment (Mouw *et al.*, 2014).

Liquid biopsy: Aqueous humor

Liquid biopsy (LB) is a non- or minimally invasive analysis of components in various body fluids. In oncology, LB is used to analyze tumor-associated components, including extracellular vesicles, tumor-derived cell-free DNA/RNA, metabolites and secreted proteins, which provide additional information for tumor diagnosis, prognosis and therapy monitoring. The use of LB to analyze various body fluids, including blood, cerebrospinal fluid, urine, and saliva, has gained great acceptance in recent years (Russano *et al.*, 2020, Escudero *et al.*, 2021, Oshi *et al.*, 2021, Trujillo *et al.*, 2022, Kumar *et al.*, 2024).

Biomarkers are measurable parameters of biological processes that have prognostic or diagnostic value and can therefore be used as indicators of diseases. Recently, the search for biomarkers has extended to body fluids such as aqueous humor (AH; Berry *et al.*, 2020). AH is a clear, watery fluid that fills the anterior chamber of the eye, located between the cornea and the lens. Produced by the ciliary body, AH serves several important functions in maintaining ocular health. AH provides nutrients and oxygen to the avascular structures of the eye, such as the cornea and lens, while also removing metabolic waste products. Furthermore, it assists in maintaining intraocular pressure, which is vital for the shape and stability of the eyeball, thereby contributing to optimal vision (reviewed in: Goel *et al.*, 2010).

In the treatment of RB patients, AH is usually a side product of IVC to induce bulbar hypotension (see section "Current treatment strategies"). AH can be obtained easily by puncturing the anterior chamber of the eye with a fine cannula syringe (Munier *et al.*, 2012).

In addition to the easy availability of material for analysis, an advantage over tissue biopsy is that liquid biopsy can provide information about the entire tumor, and hence intratumoral heterogeneity (Venesio *et al.*, 2018, Heitzer *et al.*, 2019). In contrast, a standard tumor biopsy shows only a specific region of the tumor. These benefits may be used in the future to improve diagnosis and prognosis, and monitor responses to therapy (Escudero *et al.*, 2021, Trujillo *et al.*, 2022, Busch *et al.*, 2023, Wang *et al.*, 2023). A number of potential new biomarkers have been identified for RB in recent years (reviewed in: Ghiam *et al.*, 2019, Wu *et al.*, 2020; Galardi *et al.*, 2022).

Trefoil factor family peptides as biomarkers

Members of the trefoil factor family (TFF) possess a three-looped, trefoil-like structure containing disulfide bonds (Figure 3). TFFs are small secretory proteins particularly known for their role in the gastrointestinal tract. TFFs are expressed in various tissues of the gastrointestinal tract as well as in the uterus, salivary glands, respiratory and urinary tract. In these tissues, TFFs perform similar functions in homeostasis and mucosal repair mechanisms (Madsen *et al.*, 2007, Kjellev, 2009, Rinnert *et al.*, 2010, Braga Emidio *et al.*, 2020, Hoffmann, 2020). TFF peptides are also known to be involved in inflammatory responses (reviewed in: Hoffmann, 2021).

A

TFF1 (PDB: 1PS2)   pTFF2 (PDB: 1PCP)   TFF3 (PDB: 1E9T)

B

TFF1   EAQTET**C**T–VAPRERQN**C**GFPGVTPSQ**C**ANKG**CC**FDDTVRGVPW**C**FYPNTIDVPPEEE**C**EF[60]

TFF3   EEYVGLSANQ**C**A–VPAKDRVD**C**GYPHVTPKE**C**NNRG**CC**FDSRIPGVPW**C**FKPLQEAE**C**TF[59]

TFF2   EKPSP**C**Q**C**SRLSPHNRTN**C**GFPGITSDQ**C**FDNG**CC**FDSSVTGVPW**C**FHPL

PKQESDQ**C**V–MEVSDRRN**C**GYPGISPEE**C**ASRK**CC**FSNFIFEVPW**C**FFPKSVED**C**HY[106]
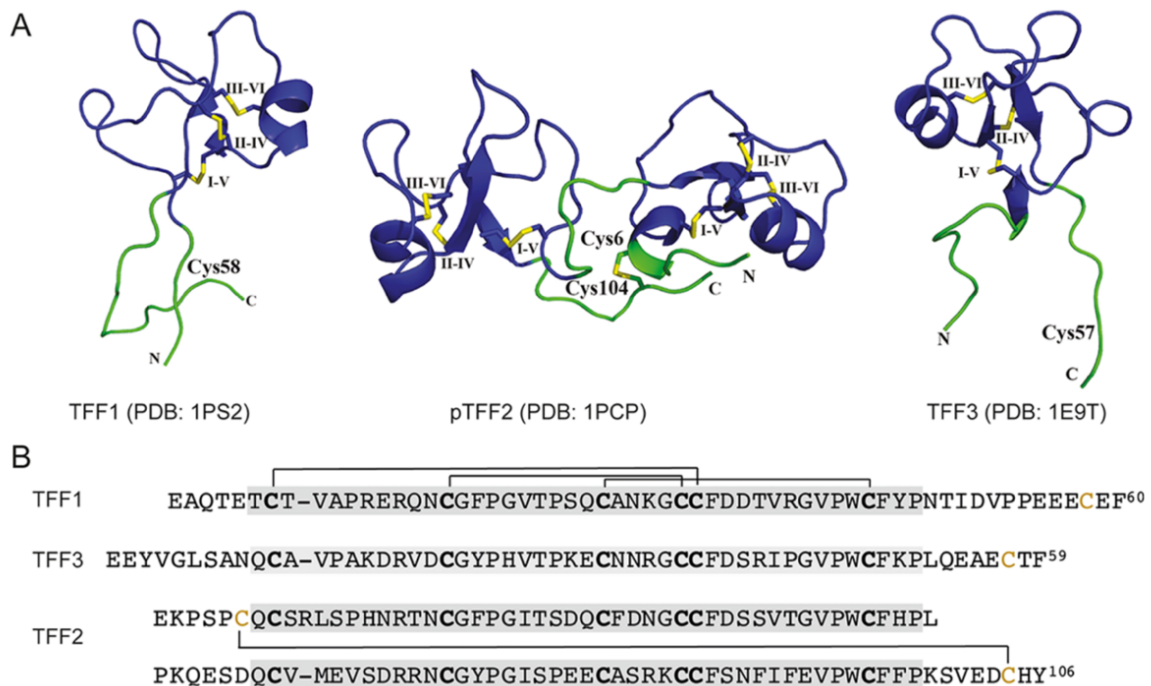
Figure 3: 3D nuclear magnetic resonance structures and amino acid sequences of the trefoil factor family peptides. A) 3D nuclear magnetic resonance structure of human TFF1, TFF3 and porcine TFF2. The TFF domains are shown in blue and the disulfide bonds in yellow. The linker region in dimeric TFF2 and the N- and C-termini are indicated in green. **B)** Amino acid sequences of human TFF1, TFF3 and porcine TFF2. Trefoil domains are highlighted in gray and disulfide bonds in orange. Adapted from Braga Emidio *et al.*, 2020.

Expression levels have also been detected in the nervous system and in various tumor entities (Probst *et al.*, 1996, Griepentrog *et al.*, 2000, Katoh, 2003, Tolušić Levak *et al.*, 2018, Hoffmann *et al.*, 2001, Hoffmann and Jagla, 2002). TFF peptides have also been described as oncogene drivers, since they can effectively stimulate cell survival (reviewed in: Perry *et al.*, 2008). While TFF1 is not expressed in healthy human retina (Weise and Dünker, 2013), our group has previously showed for the first time that RB tumors and RB cell lines express different levels of TFF1 (Weise and Dünker, 2013, Philippeit *et al.*, 2014, Busch *et al.*, 2017, Busch *et al.*, 2018). In addition, our previous findings indicated that increased TFF1 levels were associated with a later clinical stage of RB tumors (Busch *et al.*, 2018).

Liu and colleagues discovered that TFF1 allows one to immunohistochemically distinguish two subtypes of RB: subtype I has a lower risk of metastasis, slower tumor progression and is negative for TFF1. In contrast, subtype II has a high risk of metastasis, rapid tumor progression, and is predominantly positive for TFF1 (Liu *et al.*, 2021).

Studies performed as part of this PhD project showed that TFF1 levels in AH correlate with clinical and pathological features of RB. We could detect TFF1 in AH of enucleated RB eyes, and these TFF1 levels correlated with the secreted TFF1 of the corresponding cell supernatants cultured from the enucleated RB eyes (Busch *et al.*, 2022). Furthermore, we demonstrated the diagnostic and prognostic value of TFF1 as an RB biomarker by detecting TFF1 in the AH of RB patients before and during chemotherapy, and correlating TFF1 levels with treatment outcome (Busch *et al.*, 2022, 2023).

TFF1 as tumor suppressor

TFFs play a pivotal role in maintaining gastrointestinal tract integrity by orchestrating the regulation of cell apoptosis, proliferation, migration, and the process of angiogenesis (Perry *et al.*, 2008, Emidio *et al.*, 2019, Braga Emidio *et al.*, 2020, Hoffmann, 2021). TFF peptides also have diverse roles in cancer biology, since they are also described as tumor suppressors (Amiry *et al.*, 2009, Busch *et al.*, 2017). Lefebvre and colleagues showed that TFF1$^{(-/-)}$ mice develop antropyloric adenomas, about 1/3 of which progress to carcinoma (Lefebvre *et al.*, 1996). Consistent with these findings, Calnan and colleagues showed that the addition of recombinant TFF1 (rTFF1**Figure *4***) inhibited the growth of gastric adenocarcinoma cells (AGS cells; Calnan *et al.,* 1999). Bossemeyer-Pourié's results also support these findings, since the addition of rTFF1 significantly reduced the number of viable cells in different gastric carcinoma cell lines (Bossenmeyer-Pourié *et al.*, 2002). In addition, treatment with rTFF1 reduced cell proliferation, since the cell cycle was delayed by a prolongation of the G1-S cell phase. This delay is due to increased levels of INK4 and CIP, which inhibit members of the cell cycle organizing CDK family. Our group has also demonstrated that high TFF1 expression is associated with elevated CDK inhibitor levels and a downregulation of CDK6 (Weise and Dünker, 2013).

Previous studies from our group demonstrated that the addition of rTFF1 to the RB cell lines Weri and Y79 results in decreased cell viability and proliferation, but did not significantly increase apoptosis (Weise and Dünker, 2013). Lentiviral TFF1 transduction was shown to decrease the viability, proliferation, and growth of RB cells and significantly increase apoptosis. The data also strongly suggest that TFF1-induced apoptosis occurs via activation of cleaved caspase-3 and is mediated by the transcriptional activity of p53. *In vivo* assays using chicken chorioallantoic membrane (CAM) showed that overexpression of TFF1 significantly reduces tumor size (Busch *et al.*, 2017).

TFF1 and GIPR in retinoblastoma

Following TFF1 overexpression in RB cells, gene expression array analysis revealed that one of the gene expression profiles most significantly altered was that of glucose-dependent insulinotropic polypeptide receptor (GIPR; Busch *et al.*, 2017). GIPR, a 7-transmembrane (Figure 4) G-protein coupled receptor of class B, has a size of about

55 kDa and was first characterized in 1995 (Gremlich *et al.*, 1995, Volz *et al.*, 1995, Yamada *et al.*, 1995).
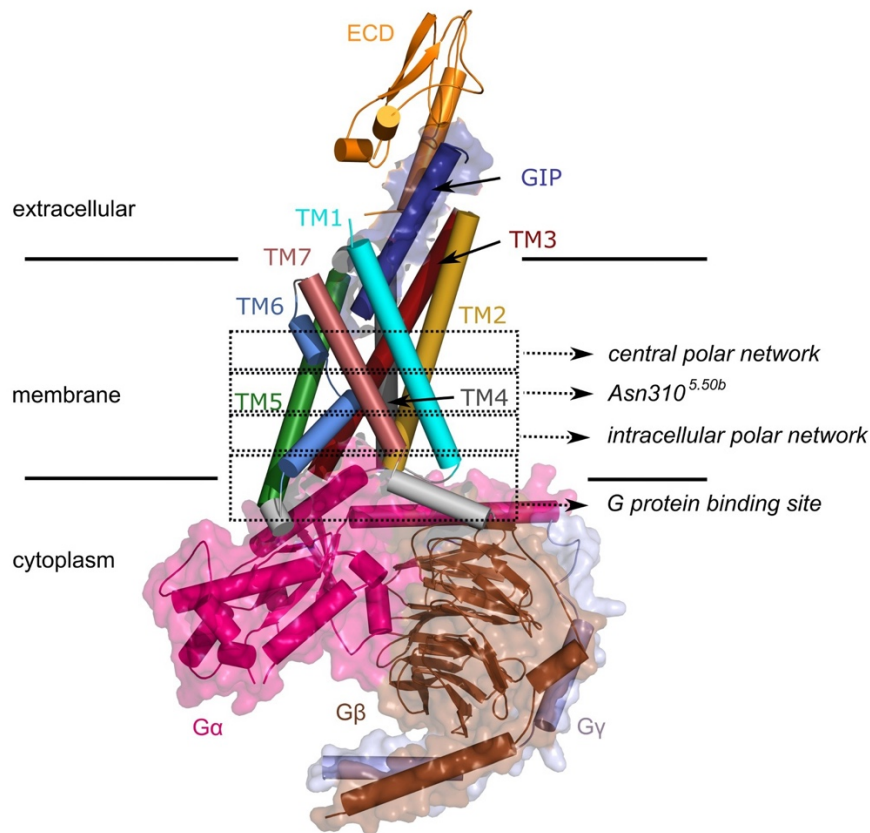

Figure 4: Structure of GIPR. Computational model of the active GIPR in a complex with GIP and Gs. Helices are shown as cylinders and loop traces have been smoothed for clarity. GIP and the G protein subunits are shown with a transparent surface. Adapted and modified from *Reubi et al., 2020*.

GIPR was initially identified as a metabolic regulator in pancreatic beta cells, where it mediates the effects of glucose-dependent insulinotropic polypeptide (GIP) on insulin release. Studies indicate that GIPR is also expressed in the nervous system and in various cancer entities (Dupre *et al.*, 1973, Usdin *et al.*, 1993, Singh *et al.*, 2010, Regazzo *et al.*, 2022, 2020). GIPR expression correlates with tumor grade in neuroendocrine tumors, making it a potential diagnostic and prognostic tool (Körner *et al.*, 2015).

Only a few receptors with low-affinity TFF binding have been described (Dubeykovskaya *et al.*, 2009; Dieckow *et al.*, 2016; see section „CXCR4 in retinoblastoma"). These receptors belongs to the same receptor family as GIPR, which suggests its potential role as a mediator in TFF signaling cascades. In addition, ligands

and receptors often have a reciprocal effect on each other's expression (Holash *et al.*, 1997, Morel *et al.*, 2000). We could show that GIPR is upregulated after overexpression of TFF1 in RB cell lines (Busch *et al.*, 2017, Haase *et al.*, 2024 A).

MicroRNAs (miRs) are small, non-coding RNA molecules that play a pivotal role in regulating gene expression. Downregulation of miR-542-5p was found in non-small-cell lung cancer tissues associated with advanced TNM stage, vascular invasion and lymphatic metastasis, with upregulation of GIPR (He *et al.*, 2017). Overall, survival analyses showed that patients with lower miR-542-5p levels had a significantly poorer prognosis (He *et al.*, 2017). MiR target scans confirm GIPR as a potential regulatory target of miR-542-5p (He *et al.*, 2017, Haase *et al.*, 2024 A). However, experimental evidence for GIPR regulation was as yet unclear.

This study focused on the role of GIPR in RB, its regulation, the link between GIPR and TFF1, potential downstream mediators and clarifying whether TFF1 is a ligand of GIPR.

CXCR4 in retinoblastoma

CXC chemokine receptor type 4 (CXCR4) is a 7-transmembrane G-protein coupled receptor expressed by a variety of cells (reviewed in: Pozzobon *et al.*, 2016). CXCR4 is one of the best studied receptors due to its pivotal role as a co-receptor for HIV entry (Feng *et al.*, 1996). Binding of the ligand CXCL12 to CXCR4 initiates a cascade of downstream signaling pathways that result in a multitude of responses (Figure 5 B), including increased intracellular calcium, gene transcription, cell migration, survival and proliferation (Ganju *et al.*, 1998). Cells that express CXCR4 have the ability to react and migrate along gradients of CXCL12, which plays an essential role in numerous physiological processes and the development of organs (Zou *et al.*, 1998, Kucia *et al.*, 2005).

Dubeykovskaya *et al.* showed that a member of the TFF family, TFF2, can bind to CXCR4 and trigger a signaling cascade (Dubeykovskaya *et al.*, 2009) making CXCR4 even more interesting for RB research. CXCR4 is upregulated in many tumor entities and is also expressed at high levels in RB cells (Wu *et al.*, 2019, Mortezaee, 2020). Moreover, there is strong evidence that the CXCR4/CXCL12 axis plays a crucial role in cancer metastasis. This is supported by studies that have identified a potential correlation between common metastatic sites (e.g. brain, lung, lymph node, liver or

bone; Figure 5 A), and high CXCL12 expression (Müller *et al.*, 2001, Yu *et al.*, 2006, Janowski, 2009, Ho *et al.*, 2012). In addition, recent studies by Yang *et al.* showed that knocking down CXCR4 reduces the metastatic potential of small cell lung cancer cells (Yang *et al.*, 2019).
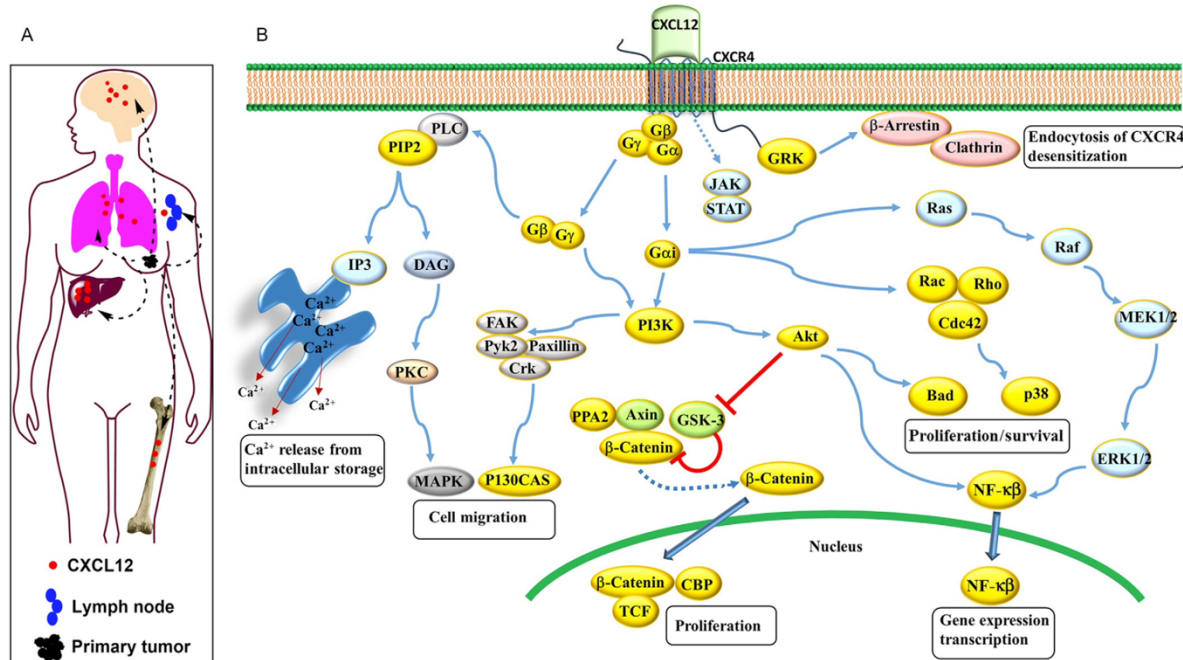

Figure 5: CXCR4/CXCL12 associated metastasis sites and signaling pathways. A) Organs that express high levels of the ligand CXCL12 are common metastasis sites for CXCR4-expressing tumors. **B)** After activation of CXCR4 various signaling pathways are initiated which trigger release of intracellular calcium, cell migration, proliferation, cell survival and expression of various genes. Adapted from Chatterjee *et al.*, 2014.

CXCR4 inhibitors are now available that have already been approved for human use. AMD3100, the first approved CXCR4 inhibitor, is successfully used to treat warts, hypogammaglobulinemia, immunodeficiency and myelokathexis (WHIM) syndrome or to release stem cells from the bone marrow (De Clercq, 2009, McDermott *et al.*, 2019). Initial tests in animal models indicate that CXCR4 inhibitors could also be potential drugs in cancer treatment, since AMD3100 induced CXCR4 inhibition leads to reduced migration and greater sensitivity to chemotherapeutic agents (Domanska *et al.*, 2012). Recent studies have shown the existence of a human endogenous CXCR4 antagonist called EPI-X4 (endogenous peptide inhibitor of CXCR4), which is derived from the proteolytic degradation of human serum albumin by pH-regulated proteases (Buske *et al.*, 2015, Zirafi *et al.*, 2015). In the present study, we investigated the effect of long-chain fatty acid-optimized variants (#JM21 and #JM198) of EPI-X4 on RB cells. These

variants exhibit significantly improved antagonistic activity and stability compared to EPI-X4 and AMD3100.

Functionalized gold nanoparticles as new treatment strategies

In recent years, gold nanoparticles (GNPs) have emerged as a promising field of cancer treatment research. GNPs can be easily adapted to the experimental setup by changing their size or shape (reviewed in: Sztandera *et al.*, 2019, Hang *et al.*, 2024). GNPs are known to have antioxidant and antiangiogenic effects in mammalian cells (BarathManiKanth *et al.*, 2010). The role of GNPs in cancer treatment are being investigated in a variety of ways, including their direct use, functionalization with other substances (DNA, drugs, etc.), and use as a radiation target for improving radio therapy (reviewed in: Bai *et al.*, 2020). Studies by Cunningham *et al.* showed that GNPs can also be used as radiosensitizers to more precisely target proton beam therapy (PBT). *In vitro* experiments showed up to 44% improved cell killing at 6 Gy after the addition of GNPs compared to the control group treated with PBT alone (Cunningham *et al.*, 2021). The nanoscale dimensions of GNPs facilitate efficient cellular uptake and penetration. Furthermore, the tunable surface chemistry of gold nanoparticles enables modification with targeted ligands, thereby increasing the specificity for cancer cells while minimizing off-target effects (Gao *et al.*, 2012, Apaolaza *et al.*, 2020).

The anatomical structure of the eye provides a robust barrier against the external environment, making noninvasive drug administration challenging. Previous studies demonstrated the potential of a nanocarrier comprising GNPs functionalized with hyaluronic acid (HA) for the treatment of ocular diseases (Apaolaza *et al.*, 2020). HA is an FDA-approved polymer that is already used as a component of numerous ocular pharmaceuticals. Ocular cells expressing CD44 receptors were shown to be capable of internalizing HA bound GNPs (Martens *et al.*, 2017, Kim *et al.*, 2018, Apaolaza *et al.*, 2020).

The atrial natriuretic peptide (ANP) is known to suppress neoangiogenesis, as evidenced by the study of Lara-Castillo *et al.*, 2009. The authors demonstrated that this process occurs via the inhibition of vascular endothelial growth factor (VEGF), which is also expressed in RB tumors and correlates with higher malignancy (Zhu *et al.*, 2019).

In the presented study, ANP-HA-functionalized GNPs were used to evaluate the effects on tumor growth in *in vivo* models. We used a newly established orthotopic rat eye animal model (Figure 6), which allows *in vivo* imaging of eye tumors. For this purpose, chemoresistant retinoblastoma cell lines were stably transduced with a luciferase vector and then injected into the eyes of newborn rats. This animal model offers the advantage of providing a developmentally suitable host environment for pediatric tumor cells that are naturally immunocompromised, thus avoiding the necessity of using immunocompromised animals (Corson *et al.*, 2014). Three distinct treatment settings were used in this experiment. First, tumor cells were directly injected together with the ANP-HA-GNPs. Subsequently, tumor growth was allowed to proceed for 14 days in the rat eye before treatment with the nanoparticles was initiated by injection or via eye drops.
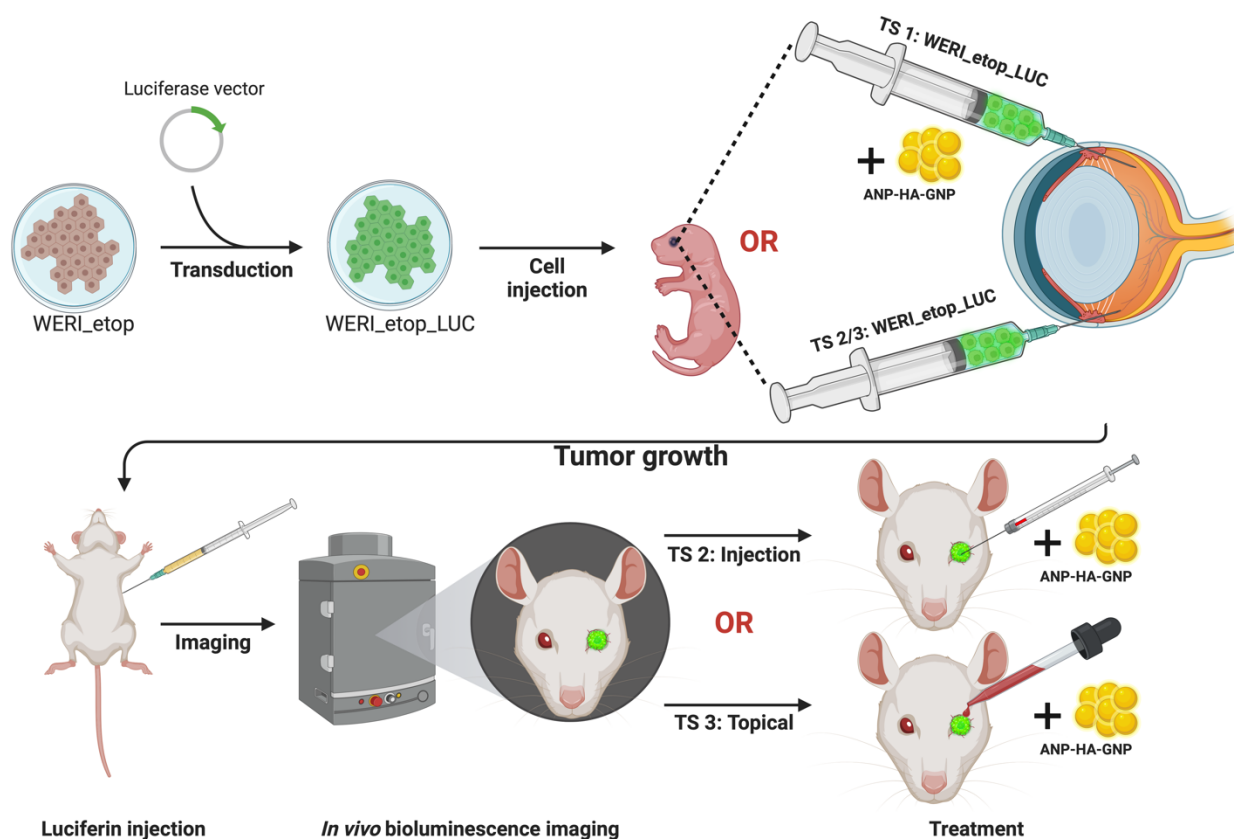

Figure 6: Scheme of the *in vivo* orthotopic rat eye model. In treatment setting 1 (TS 1), 1×10^5 etoposide-resistant and luciferase labeled Weri (WERI_etop_LUC) RB cells were injected into the right eye of P0 rat pups together with ANP-HA-GNPs (yellow). After luciferin injection, animals were imaged on defined days after injection (P3, P7, P10, P14, P21 and P28) and compared to control animals injected without ANP-HA-GNPs. In TS 2 and 3, tumors were allowed to grow 14 days prior

to treatment. Those animals with detectable RB tumor growth were treated with ANP-HA-GNPs via intravitreal injection on P14 and P21 in TS 2, or with eye drops on P14, P17, P21, and P24 in TS 3. All animals were imaged on days P10, P14, P17, P21, P24 and P28, and compared to controls injected or eye dropped with PBS under the same schedule. Created with BioRender.com

The administration of drugs via functionalized GNPs represents a potential administration alternative that enables more precise targeting of tumor cells and could thus reduce off-target effects and side effects.

Aim of the study

Although RB is a tumor with a good prognosis in high-income countries, this is not the case without early diagnosis and appropriate therapy. Therefore, further improvements are necessary in the areas of diagnosis, prognosis, and therapy monitoring. Further research is needed to improve patient safety and provide improved eye and vision-saving therapies. Moreover, advances in RB research could potentially benefit not only people diagnosed with RB, but also those diagnosed with other cancer entities.

The present work is divided into four main sections (Figure 7), to clarify various RB-related questions and issues.

The first part of the study aimed to demonstrate that TFF1 is secreted in the AH of RB patients. Since TFF1 is only expressed in an advanced subtype of RB, a simple and inexpensive ELISA analysis would provide important information about the malignancy. In addition, we aimed to clarified whether changing TFF1 levels are related to treatment success. These topics were addressed in the following two publications:

1A) TFF1 in Aqueous Humor-A Potential New Biomarker for Retinoblastoma (page 31)

1B) Trefoil Family Factor Peptide 1—A New Biomarker in Liquid Biopsies of Retinoblastoma under Therapy (page 43)

To gain a deeper understanding of TFF1 signaling we investigated the role of GIPR in RB cells, since GIPR is one of the most strongly regulated genes upon TFF1 overexpression in RB cells. To achieve this, GIPR was overexpressed in RB cell lines and various *in vitro* and *in vivo* studies were conducted. Furthermore, we wanted to clarify the role of GIPR as a potential TFF1 receptor. Additionally, we identified potential downstream targets of GIPR, examined the regulation of GIPR via

miR-542-5p, and investigated the potential link between GIPR and TFF1. These topics were addressed in the following publication:

2) Gastric Inhibitory Polypeptide Receptor (GIPR) Overexpression Reduces the Tumorigenic Potential of Retinoblastoma Cells (page 58)

In the third part of the study, we evaluated the efficacy of newly developed and optimized inhibitors of the CXCR4 receptor in various *in vitro* studies and *in ovo* CAM assays on RB cell lines. The CXCR4 inhibitors were optimized by lipidation, which enhances the antagonistic effects and appears to stabilize them. These topics were addressed in the following publication:

3) Fatty acid conjugated EPI-X4 derivatives with increased activity and *in vivo* stability (page 81)

The fourth part of this study aimed to establish a novel drug delivery approach for chemoresistant RB cells. Therefore, we investigated the effect of ANP-HA functionalized GNPs on the growth of RB tumors in various *in vivo* models.
Moreover, we used a newly established orthotopic rat eye model, which enables *in vivo* imaging of the growing tumor. Various application methods of ANP-HA-GNPs were tested, including non-invasive delivery via eye drops. These topics were addressed in the following publication:

4) New retinoblastoma (RB) drug delivery approaches: anti-tumor effect of atrial natriuretic peptide (ANP)-conjugated hyaluronic-acid-coated gold nanoparticles for intraocular treatment of chemoresistant RB (page 133)
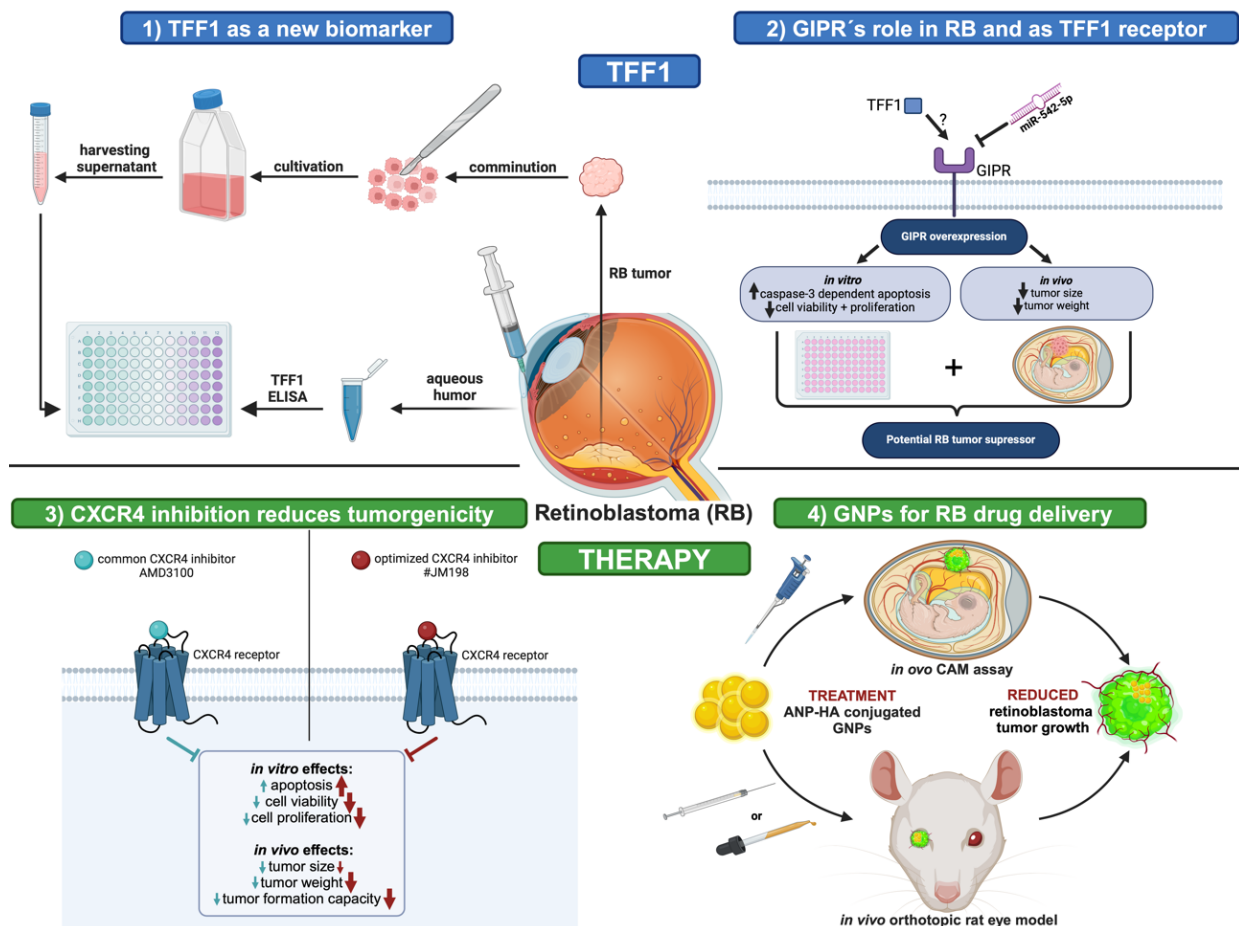
Figure 7: Graphical abstract. Top row: Trefoil factor family 1 (TFF1)-related studies (blue): **1) TFF1 as a new biomarker**. Workflow of the TFF1 ELISA analysis of aqueous humor (AH) and the supernatant of primary cell cultures. First, from right to left, AH samples were obtained from retinoblastoma (RB) patients and the corresponding primary tumors were cultured, followed by comparison of TFF1 levels detected in AH samples and primary cell culture supernatants. **2) GIPR's role in RB and as TFF1 receptor.** Since the gastric inhibitory polypeptide receptor (GIPR) is upregulated upon TFF1 overexpression in RB cells, we investigated whether TFF1 could be a potential ligand of GIPR. In addition, the role of GIPR in RB cells was investigated using various *in vitro* and *in vivo* experiments and a potential regulation of GIPR by miR-542-5p was evaluated. Bottom row: Therapy-related studies (green): **3) CXCR4 expression reduces tumorgenicity.** CXCR4 is highly expressed in RB and inhibition of this receptor might be a potential therapeutic target. Therefore, new, more effective and stable CXCR4 inhibitors (including #JM198) were tested in comparison to the current, already approved CXCR4 inhibitor AMD3100. **4) GNPs for RB drug discovery.** Gold nanoparticles (GNPs) were functionalized with hyaluronic acid (HA) for enhanced cellular uptake and the neoangiogenesis inhibitor atrial natriuretic peptide (ANP). Their effects on chemoresistant RB cells were tested in various *in vitro* and *in vivo* assays, including a novel orthotopic rat eye model, where the administration of ANP-HA-GNPs via eye drops was tested.

Publications

1A) TFF1 in Aqueous Humor - A Potential New Biomarker for Retinoblastoma

Cumulative Thesis/Extent of Contribution

Cumulative thesis of M.Sc. André Haase

Author contributions

TFF1 in Aqueous Humor—A Potential New Biomarker for Retinoblastoma

M. Busch, **A. Haase**, N. Miroschnikov, A. Doege, E. Biewald, N. Bechrakis, M. Beier, D. Kanber, D. Lohmann, K. Metz and N. Dünker

Status: published in Cancers (2022)

DOI: 10.3390/cancers14030677

Impact factor at submission: 6.6 (2021)

André Haase contributions (**co-authorship**):

- **Experimental work: 50% -** Primary cell culture, performance of/ assistance with: ELISA, WB, IHC, ICC.
- **Data analysis: 20% -** Processing, analysis, and visualization of ELISA, WB, IHC and ICC data.

_____
Signature André Haase

_____
Signature Prof. Dr. Nicole Dünker

cancers

MDPI

TFF1 in Aqueous Humor—A Potential New Biomarker for Retinoblastoma

Maike Anna Busch [1],*, André Haase [1], Natalia Miroschnikov [1], Annika Doege [1], Eva Biewald [2], Nikolaos E. Bechrakis [2], Manfred Beier [3], Deniz Kanber [4], Dietmar Lohmann [4], Klaus Metz [5] and Nicole Dünker [1]

[1] Center for Translational Neuro- and Behavioral Sciences, Institute of Anatomy II, Department of Neuroanatomy, Medical Faculty, University of Duisburg-Essen, 45147 Essen, Germany; andre.haase@uk-essen.de (A.H.); Natalia.miroschnikov@uk-essen.de (N.M.); annika.doege@uk-essen.de (A.D.); nicole.duenker@uk-essen.de (N.D.)
[2] Department of Ophthalmology, Medical Faculty, University of Duisburg-Essen, 45147 Essen, Germany; eva.biewald@uk-essen.de (E.B.); nikolaos.bechrakis@uk-essen.de (N.E.B.)
[3] Institute of Human Genetics, Medical Faculty, Heinrich-Heine University, 40225 Düsseldorf, Germany; beierm@uni-duesseldorf.de
[4] Institute of Human Genetics, Medical Faculty, University of Duisburg-Essen, 45147 Essen, Germany; deniz.kanber@uk-essen.de (D.K.); Dietmar.lohmann@uk-essen.de (D.L.)
[5] Institute of Pathology, Medical Faculty, University of Duisburg-Essen, 45147 Essen, Germany; Klaus.metz@uk-essen.de
* Correspondence: maike.busch@uk-essen.de; Tel.: +49-201-7238-4434

Simple Summary: Retinoblastoma is the most common pediatric intraocular malignancy with high cure rates in developed countries. Nevertheless, useful predictive biomarkers providing reliable evidence for therapy decisions are urgently needed to optimize therapy regimes. TFF1 is a promising candidate as it is expressed in a more advanced subtype of retinoblastoma. Additionally, TFF1 is a naturally secreted peptide. Thus, TFF1 might be detectable in the aqueous humor of RB patients' eyes, providing the opportunity to determine its expression prior to therapy without the necessity of a tumor biopsy. We therefore investigated for the first time aqueous humor samples of retinoblastoma patients in order to test for the availably and expression status of TFF1 as well as to compare it with the original tumor and established corresponding primary cell cultures.

Abstract: Retinoblastoma (RB) is the most common childhood eye cancer. The expression of trefoil factor family peptide 1 (TFF1), a small secreted peptide, has been correlated with more advanced RB stages and it might be a promising new candidate as a RB biomarker. The study presented addressed the question of if TFF1 is detectable in aqueous humor (AH) of RB patients' eyes, providing easy accessibility as a diagnostic and/or therapy accompanying predictive biomarker. The TFF1 expression status of 15 retinoblastoma AH samples was investigated by ELISA and Western blot analyses. The results were correlated with the TFF1 expression status in the tumor of origin and compared to TFF1 expression in established corresponding primary tumor cell cultures and supernatants. Nine out of fifteen AH patient samples exhibited TFF1 expression, which correlated well with TFF1 levels of the original tumor. TFF1 expression in most of the corresponding primary cell cultures reflects the levels of the original tumor, although not all TFF1-expressing tumor cells seem to secret into the AH. Together, our findings strongly suggest TFF1 as a reliable new RB biomarker.

Keywords: retinoblastoma; RB; trefoil factor family peptides; TFF1; aqueous humor; liquid biopsy; biomarker

1. Introduction

Retinoblastoma (RB) is the most common pediatric intraocular malignancy with an incidence rate of about 1 in 17,000 live births [1,2]. Although some patients develop

metastases, survival rates are over 90% in high-income countries, whereas in low-income countries, tumors remain undiagnosed and grow to an advanced, globe-threatening stage [3]. Therefore, the main therapeutic focus lies on life-saving treatment regimens including ocular tumor treatment and prevention of metastatic spread [4]. A second critical goal of RB therapy is maximization of eye and visual preservation [4]. For a long period, biopsies or the removal of eye fluid were contraindicative due to the risk of tumor dissemination [5]. However, today, paracentesis of aqueous humor (AH) is a standard procedure of the protocol for intravitreal chemotherapy injections [6] and the risk of induced extraocular spread is considered extremely low [7]. This circumstance offers the possibility for a completely new diagnostic and prognostic RB procedure using AH of patients for the evaluation of biomarkers prior to or during therapy [8]. Over the last years, different studies investigated AH in enucleated RB eyes and unraveled several markers supposed to either provide clinical values for diagnosis and clinicopathological associations or reflecting response to treatment regimens or putative therapy targets (for review see: [8]).

Our group identified trefoil factor family peptide 1 (TFF1) as a putative new RB marker correlating with higher clinical tumor-node-metastasis (TNM) stage and poorly differentiated tumor cells [9]. In addition, we could show that TFF1 functionally acts as tumor suppressor gene in RB cell lines [10] and is epigenetically regulated [11]. In a most recent study by Liu et al., the relevance of TFF1 as potential marker for RB was confirmed and connected to a subtype of RBs associated with a higher risk of metastasis [4]. TFF peptides are ectopically expressed in different human tumors (for review see: [12]) and three members—TFF1, TFF2, and TFF3—of this family of small secreted proteins have been characterized in mammals so far. TFFs possess a characteristic clover leaf-like disulfide structure, the so-called TFF domain. They are highly expressed in the gastrointestinal tract with main functions in the maintenance and protection of epithelial surfaces [13–15]. Additionally, TFFs are expressed in the central nervous system, in ocular tissues, and in the murine retina (for review see: [12,16]). Previous studies by our group revealed that TFF1 is not expressed in the healthy human retina, whereby RB cell lines and RB tumors exhibit variable levels of TFF1 [9,11,17]. Thus, TFF1 is a promising candidate as a predictive biomarker in aqueous humor of RB patients, as it is a naturally secreted peptide, which is highly expressed in RB patients harboring a higher risk of metastasis. In the study presented, we investigated TFF1 expression in AH via ELISA and Western blot and correlated the expression patterns with clinical parameters and TFF1 expression in the original tumor tissue of the enucleated patients' eyes. Additionally, we compared the TFF1 status of the corresponding RB primary cell culture cells with TFF1 levels in the tumor of origin. We showed that TFF1 is indeed detectable in the AH of patients eyes increasing its availability as a potential biomarker.

2. Materials and Methods

2.1. Human Retinoblastoma and Retina Samples

Human retinoblastoma (RB) primary tumor material, aqueous humor samples, and paraffin sections from enucleations of 15 patients, as well as post-mortem retina samples from cornea donors were used for comparative TFF1 expression studies. The Ethics Committee of the Medical Faculty of the University of Duisburg-Essen approved the use of human retina (approval # 06-30214) and retinoblastoma samples (approval # 14-5836-BO) for research conducted in the course of the study presented and written informed consent was obtained from patients' relatives or parents.

Primary tumor material and aqueous humor samples were harvested immediately after enucleation. Aqueous humor was aspirated via an anterior chamber puncture using a 30 G needle. In the next step, the actual tumor was removed from the globe via scleral fenestration. Aqueous humor samples were stored at $-80\,^\circ$C until use and the tumor tissue samples were cultured as described subsequently.

This study includes a case series of 15 untreated eyes from individual children diagnosed with intraocular retinoblastoma between 2020 and 2021. Diagnosis was confirmed

pathologically after enucleation. All RB samples were reviewed by a specialized pathologist. The data collected included patient's age at diagnosis, gender, laterality, RB1 mutation status, tumor volume, optic nerve, and choroid invasion.

2.2. Cell Lines and Primary RB Cell Culture

The human RB cell lines Rbl13 and Rbl30 were kindly provided by Dr. H. Stephan. The cell lines were cultivated as suspension cultures in Dulbecco's modified Eagle's medium (DMEM; PAN-Biotech, Aidenbach, Germany) with 15% fetal calf serum (FCS; PAN-Biotech, Aidenbach, Germany), 100 U penicillin/mL and 100 µg streptomycin/mL (Invitrogen, Darmstadt, Germany), 4 mM L-glutamine (Sigma-Aldrich, München, Germany), 50 µM ß-mercaptoethanol (Carl-Roth, Karlsruhe, Germany), and 10 µg insulin/mL (Sigma-Aldrich, München, Germany) at 37 °C, 10% CO_2, and 95% humidity as described previously (Busch et al. 2015).

The primary RB tumor material was initially cut into small pieces with a sterile scalpel and subsequently washed three times in PBS with a centrifugation step in between (800 rpm for 2 min). After the last washing step, the tumor material was cultivated under the cell culture conditions described above. Cell culture supernatants were harvested and residual cells were removed by centrifugation. Cell culture supernatants were kept at −20 °C until usage.

2.3. TFF1 ELISA Analysis

The aqueous humor samples of RB patients and the supernatant of the corresponding primary cell cultures as well as the supernatant of two RB cell lines (Rbl-13 and Rbl-30) were analyzed with a human TFF1 ELISA kit (ab213833, abcam, Cambridge, UK) following the manufacturer´s protocol. Fifty microliters sample volume was used and the concentration of the analyzed sample concentrations (pg) was calculated based on the standard curve included in the kit.

2.4. Immunocytochemistry and Immunfluorescence Stainings

For the cohort of 15 retinoblastomas included in this study, automated immunostaining for CRX and Ki-67 was performed on 5 µm paraffin-embedded samples with the OptiView DAB IHC detection kit (Santa Cruz Biotechnology, Dallas, TX, USA) or UltraView alkaline phosphatase red detection kit (Ventana Roche, Grenzach-Wyhlen, Germany). TFF1 immunostaining was performed with the Vectastin Elite ABC kit (Vector Laboratories, Burlingame, CA, USA) as previously described by our group [9]. The following antibodies were used: anti-CRX (1:50, Santa Cruz Biotechnology, Dallas, TX, USA, clone A-9), anti-Ki-67 (ready-to-use, Ventana Roche, Grenzach-Wyhlen, Germany, clone 30-9), and TFF1 (1:200, abcam, Cambridge, UK, # ab92377). Images were acquired using an Aperio ScanScope AT2 (Leica, Wetzlar, Germany) slide scanner. Two researchers, blind for additional patient information, independently assessed each stained slide by eyeballing, taking into account different staining intensities (I) defined as null (0), mild (1), moderate (2), or strong (3), and the percentage (P) of tumor cells with CRX stained nuclei and TFF1 positive cytoplasm. The quick score (QS) was then calculated as $I \times P$ (from 0 to 300). The TFF1 intensities 1 and 2 were combined and specified as "expressed", whereas intensity 0 was specified as "not expressed" and intensity 3 as "highly expressed".

For immunofluorescence staining, 1×10^5 cells were seeded on poly-D-lysine (Sigma, Hamburg, Germany) coated coverslips. Cells were fixed with 4% paraformaldehyde (PFA; Sigma-Aldrich, St. Louis, MO, USA) for 1 h at 4 °C washed three times with phosphate buffered saline (PBS; pH 7.4) and permeabilized with 100% methanol for 10 min at room temperature. Cells were washed with PBS and blocked with PBS containing 0.3% Triton™ X-100 (Sigma), 4% bovine serum albumin (BSA; Carl-Roth, Karlsruhe, Germany), and 5% normal goat serum (NGS; Dako, Glostrup, Denmark) for 1 h at room temperature. The primary antibody used (incubated overnight at 4 °C) was TFF1 1:200 (abcam, Cambridge, UK, # ab92377) diluted in PBS with 0.3% Triton™ X-100, 4% BSA, and 5% NGS. A goat anti-

rabbit antibody labeled with Alexa Flour®594 (Invitrogen, Darmstadt, Germany), diluted 1:1000 in PBS with 0.3% Triton™ X-100, 4% BSA, and 5% NGS was used to visualize the reaction. In order to stain the nuclei, cells were counter-stained with 4′,6-Diamidino-2-phenylindole (DAPI; Sigma, Hamburg, Germany). As controls, PBS was substituted for the primary antisera in order to test for non-specific labeling. Pictures were taken with a NIKON Eclipse E600 microscope equipped with a digital camera and NIKON Eclipse net software.

2.5. Western Blotting

Equal volumes of AH samples and cell culture supernatants were separated on a 12% SDS-PAGE and transferred onto nitrocellulose membranes. The primary antibodies used (incubated overnight at 4 °C) were TFF1 (1:1000 abcam, Cambridge, UK, # ab92377) and ß-actin (1:1000): #4967, Cell Signalling Technology (Cambridge, UK). The secondary antibody used was HRP-conjugated goat-anti-rabbit antibody (1:10,000); P0448; Dako (Glostrup, Denmark). Signals were developed by the WesternBright Chemiluminescence Reagent (Advansta, San Jose, CA, USA).

2.6. Statistical Analysis

Statistical analysis of tumor clinical parameters was correlated with the TFF1 expression in aqueous humor identified by ELISA analysis. Statistical analyses (Kruskal–Wallis rank sum p-values) were performed in the R statistical environment, version 3.2.0.16. Statistical analyses of the real-time PCR data were performed using GraphPad Prism 6. Results were analyzed by a Student's t-test and considered significantly different if * $p < 0.05$, ** $p < 0.01$, or *** $p < 0.001$.

3. Results

3.1. Soluble TFF1 Is Detectable in Aqueous Humor of RB Patients and Primary Cell Culture-Derived Supernatant

TFF1 is expressed in a subpopulation of RB tumors and seems to be correlated with more advanced tumor stages. Therefore, soluble TFF1 is potentially secreted from the tumor cells into the aqueous humor of RB patients. In order to investigate the accessibility of soluble TFF1 in aqueous humor, we tested AH samples of 15 RB patients by TFF1 ELISA (Figure 1a). We could show that RB tumor cells indeed secrete measurable amounts of soluble TFF1 into the aqueous humor of RB patients' eyes. We defined three TFF1 expression groups: group I) not expressed (0–30 pg/mL), group II) expressed (30–400 pg/mL), and group III) highly expressed (>400 pg/mL), based on the ELISA analysis. We identified four tumors secreting very high TFF1 concentrations (between 1000 and 4500 pg/mL; T06, T09, T14, and T18) into the AH, five tumors secreting moderate levels of TFF1 (T08, T10, T12, T13, and T17), and six tumors without TFF1 secretion into the AH (T05, T07, T11, T15, T16, and T19). Subsequently, we investigated if corresponding primary cell culture cells established from the original patient tumor samples also secrete TFF1 into the cell culture supernatant. Two RB cell lines with a known TFF1 secretion potential were used as positive controls. We could show that cultured primary RB cells from patients with TFF1 positive AH samples secrete TFF1 into the supernatant (Figure 1b), except for the cell culture of specimen T12. Two RB cell cultures (T05 and T07) do secrete TFF1 into the supernatant, whereas the corresponding AH samples were negative for TFF1. Thus, we could show that TFF1 is detectable in the AH of RB patients and that corresponding primary cell cultures mimic patients' TFF1 status, indicating their suitability as an in vitro RB model system.

In order to verify the TFF1 ELISA results, cell culture supernatants were analyzed by Western blot (Figures 2a and S1) and compared to the TFF1 levels of supernatant from the RB cell lines Rbl13 and Rbl30 serving as positive controls. TFF1 expression was detectable by Western blot in samples with TFF1 status initially defined as "highly expressed" (<400 pg/mL TFF1) in ELISA analyses (T06, T09, T14, and T18), whereas all other samples analyzed were below the detection limit of this method. Analysis of AH of

the highly TFF1 expressing sample group by Western blot confirmed the TFF1 expression pattern (Figures 2b and S2).
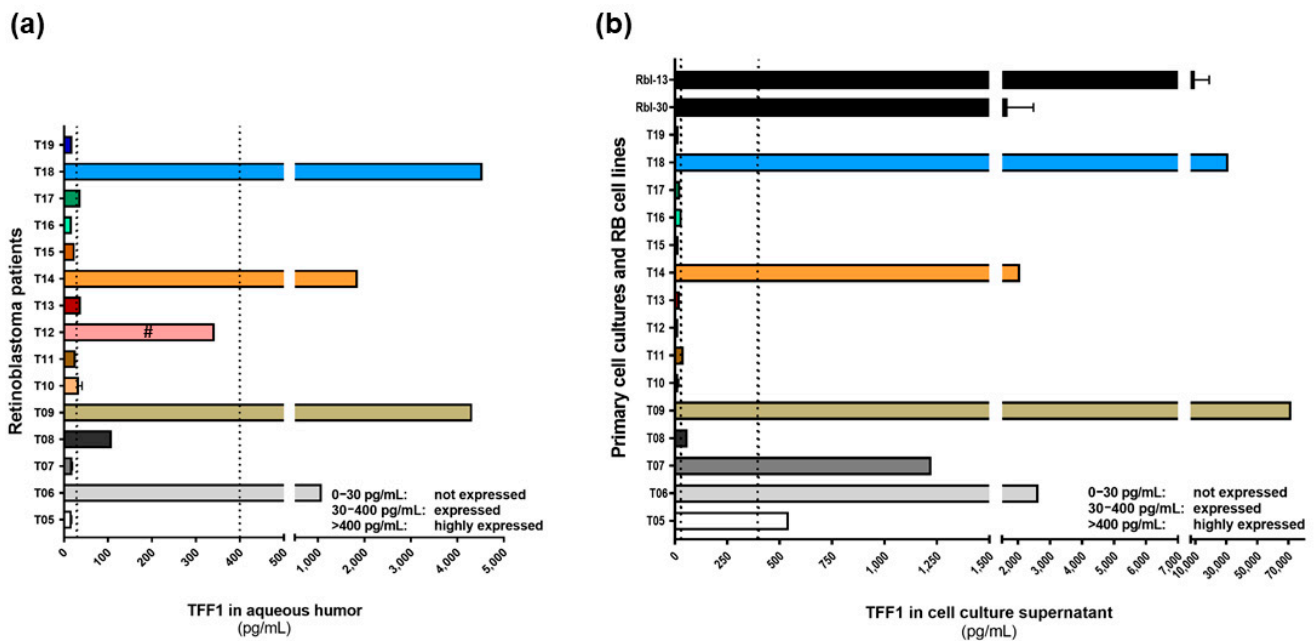

Figure 1. TFF1 expression analyses in aqueous humor samples of RB patients and corresponding primary cell culture supernatants. (**a**) TFF1 ELISA analysis of 15 aqueous humor samples of RB patients, showing four patients with highly expressed TFF1 (>400 pg/mL), five patients with expressed TFF1 (30–400 pg/mL), and six patients without TFF1 expression (0–30 pg/mL) in the aqueous humor. (**b**) The supernatants of corresponding primary cell cultures of RB patient tumors shown in (**a**) revealed six highly TFF1 expressing samples, three samples expressing TFF1, and six samples without TFF1 expression. The supernatant of two RB cell lines (Rbl-13 and Rbl-30) highly expressing and secreting TFF1 are used as internal positive controls. Vertical dotted lines indicate three TFF1 expression levels; #: sample was a vitreous body aspirate.
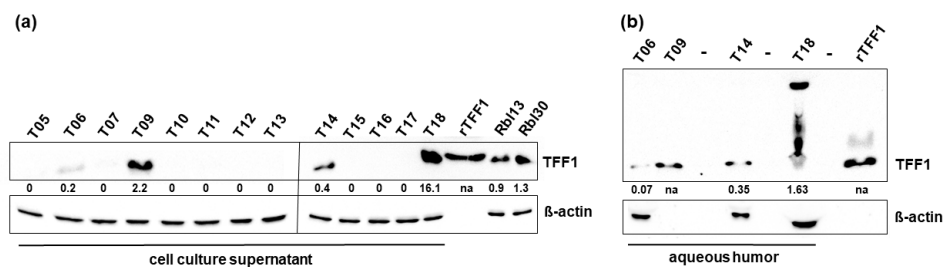

Figure 2. Western blot analysis of TFF1 expression in cell culture supernatants of primary cell cultures and aqueous humor samples of RB patients. (**a**) Western blot analysis of primary cell culture supernatants showing TFF1 expression in the highly TFF1 expressing tumors of the ELISA analysis (T06, T09, T14, and T18). Recombinant TFF1 (rTTF1) and the RB cells lines Rbl13 and Rbl30 served as positive controls. (**b**) TFF1 expression levels revealed by Western blot analysis for the four AH samples with high TFF1 expression levels in the ELISA assay. The indicated intensity ratios relative to ß-actin, used as a loading control, were calculated using MICRO MANAGER 1.4 software (University of California, San Francisco, CA, USA). -: empty lanes; na: not analyzed.

3.2. TFF1 Expression in Primary Cell Culture Cells

In order to analyze the cellular expression of TFF1 in the established primary cultures immunofluorescence staining was performed. The intracellular TFF1 expression pattern correlates well with the TFF1 secretion status described above. We found primary RB cell cultures highly expressing TFF1 (Figure 3a,b, T18) as well as cell cultures without detectable

TFF1 expression (Figure 3a,b, T19) in comparison to the RB cell line Rbl-13 used as positive control (Figure 3a,b). Real-time PCR analysis (Figure S3) revealed that in the samples analyzed, the intracellular *TFF1* mRNA expression does not correlate with the TFF1 protein concentrations measured in the AH and supernatant. Hence, *TFF1* mRNA levels are not reliable to predict expression, but TFF1 status needs to be evaluated on the protein level.
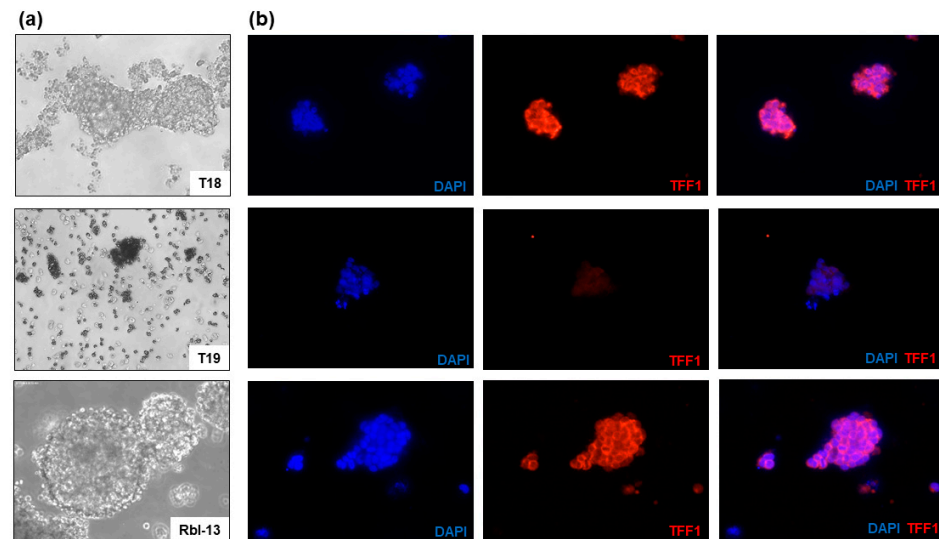

Figure 3. Immunofluorescence TFF1 staining of two primary RB cell cultures (T18 and T19) and RB cell line Rbl-13. (**a**) Morphology of the primary RB cell cultures T18 and T19 as well as RB cell line Rbl-13 revealed by phase contrast imaging (200×). (**b**) DAPI (**blue**), TFF1 (**red**), and merged DAPI/TFF1 immunofluorescence staining of the respective RB cells (200×). T18 and the positive control Rbl-13 showed a high expression of TFF1 in contrast to T19 cells without TFF1 expression.

3.3. TFF1 Expression in Primary RB Tumors

To compare the expression of TFF1 in AH and supernatant of primary cultured RB cells with its expression pattern in original tumor specimens, paraffin sections of all tumors were immunocytochemically stained for TFF1. TFF1 immunostaining revealed highly TFF1 expressing tumors, tumors with moderate TFF1 expression, and tumors without TFF1 expression (Figure 4a). The corresponding CRX staining confirmed the RB nature of the tumors and Ki67 staining the proliferation activity of the tumor cells. All RB tumor sections stained positively for Ki67 indicating that the tumor cells were still proliferative. We showed that all tumors with detectable TFF1 in the AH samples analyzed stained highly or moderately positive for TFF1 in primary tumor sections. However, not all TFF1-positive RB tumors seemed to secrete TFF1 into the AH of the patients' eye as quick score (QS) of TFF1 revealed a median QS of 60 for group III, which does not express TFF1 in AH (Figure 4b). No significant difference in TFF1 and CRX QS was detectable between the groups.

Thus, TFF1 expression in AH samples correlates to 100% with a positive TFF1 expression pattern in the primary RB tumor, however, not all TFF1 expressing tumors necessarily secrete TFF1 into the AH of the patients.

3.4. Correlation of Clinical and Pathological Characteristics of the Analyzed RB Tumors

Table 1 summarizes the clinical and pathological characteristics of the 15 RB patients analyzed. In order to correlate these parameters with TFF1 expression in AH, we divided the patients into two groups: a TFF1 expressing (60%) group and a non-expressing group (40%). No statistically significant differences between both groups in relation to sex, *RB1* germline mutations, laterality, age at diagnosis, tumor volume, optic nerve invasion, or choroid invasion could be detected (Table 1).
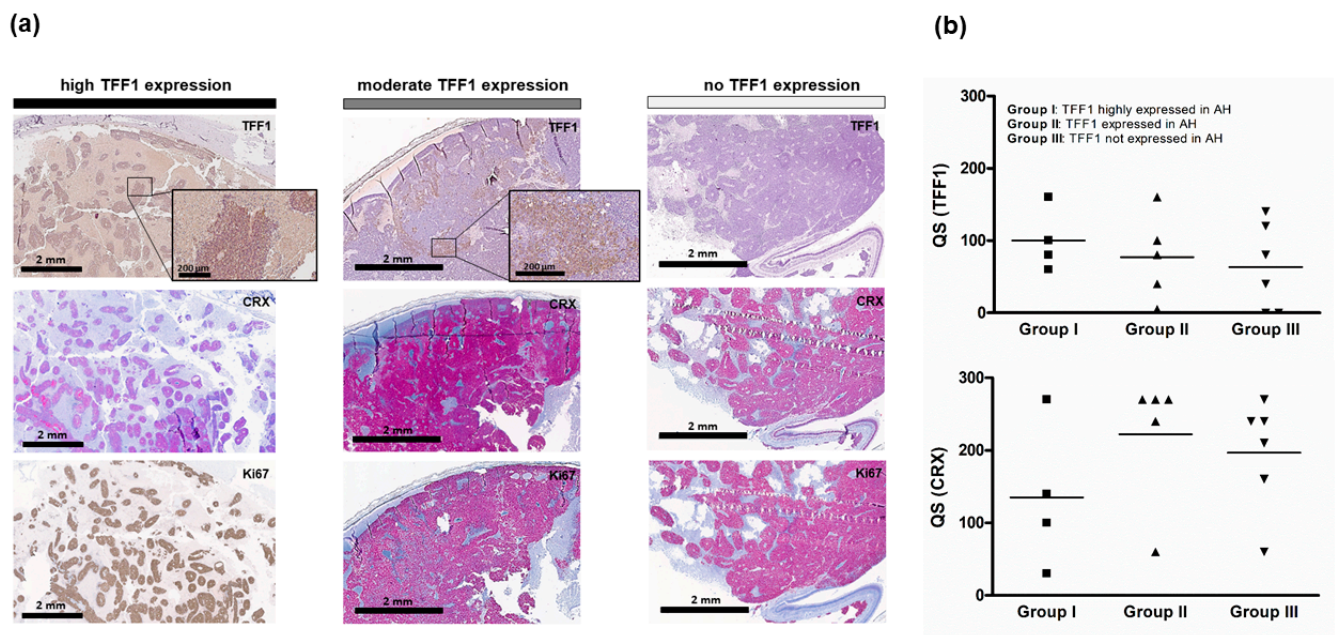
(a)

(b)

Figure 4. Histological analysis of primary RB tumors. (**a**) TFF1, CRX, and Ki67 expression levels in exemplary human RB tumor paraffin sections. Immunohistochemistry was revealed using diaminobenzidine detection (**brown signal**) or alkaline phosphatase detection (**red**) and hematoxylin counterstaining (**blue nuclei staining**). Scale bars, 2 mm and 200 μM (zoom box). (**b**) Dot plots showing the quick score (QS) for TFF1 and CRX in 15 tumors analyzed. One way ANOVA was used to assess the difference of the QS for group I (TFF1 highly expressed in AH) vs. group II (TFF1 expressed in AH) vs. group III (TFF1 not expressed in AH). No significant difference was detectable between the groups. The squares and triangles in (**b**) represent the different tumors per group.

Table 1. Clinical and pathological characteristics of RB patients stratified by TFF1 expression in aqueous humor. NA: not available, *n*: number in each group, *N*: total number. * Kruskal–Wallis rank sum *p*-value.

	TFF1 Expressed *n* (%)	TFF1 Not Expressed *n* (%)	*N*	*p*-Value *
Patients	9 (60)	6 (40)	15	
Sex				1
Female	6 (67)	4 (67)	10	
Male	3 (33)	2 (33)	5	
***RB1* germline mutations**				0.88
Yes	1 (11)	0 (0)	1	
No	5 (56)	2 (33)	7	
NA	3 (33)	4 (67)	7	
Laterality				0.79
Unilateral	7 (78)	5 (83)	12	
Bilateral	2 (22)	1 (17)	3	*
Age at diagnosis				0.47
<18 month	4 (45)	3 (50)	7	
18–36 month	3 (33)	3 (50)	6	
>36 month	2 (22)	0 (0)	2	
Tumor volume				0.26
<2 cm^3	2 (22)	1 (17)	3	
2–5 cm^3	6 (67)	2 (33)	8	
>5 cm^3	1 (11)	3 (50)	4	
Optic nerve invasion				0.89
None	1 (11)	1 (17)	2	
Pre-laminar	7 (78)	4 (67)	11	
Post-laminar	1 (11)	1 (17)	2	

Table 1. *Cont.*

	TFF1 Expressed *n* (%)	TFF1 Not Expressed *n* (%)	N	*p*-Value *
Choroid invasion				0.30
None	8 (89)	4 (67)	12	
Invasion	1 (11)	2 (33)	3	
Pre enucleation MRI				0.76
Choroid invasion	2 (22)	2 (33)	4	
Optic nerve invasion	3 (33)	3 (50)	6	

To combine and summarize all data, RB patients were categorized into three groups: group I "highly expressing TFF1", group II "expressing TFF1", and group III "without TFF1 expression" (Figure 5). In group I tumors, highly expressing TFF1 in AH (1) TFF1 could also be detected via Western Blot, (2) the original tumor stains highly positive for TFF1, and (3) primary cultured cells express and secrete TFF1. In group II tumors, TFF1 expression in the original tumor specimens correlates with the TFF1 expression in the AH. However, not all primary cell cultures secrete TFF1 into the supernatant. In group III, without detectable TFF1 in AH samples, TFF1 probably is not secreted into the AH even if the tumor bulk contained TFF1-expressing cells detectable by immunohistochemistry. TFF1 expression of group II and III is below the detection limit of Western blotting analysis. Taken together, this shows that TFF1 is indeed secreted into the AH of the patients' eyes and is readily detectable via ELISA. Even if not all TFF1 positive RB tumors secrete TFF1 into the AH, no false positive TFF1 expression was measured in AH samples.

Figure 5. TFF1 expression and clinical characteristics of retinoblastoma samples. Classification of TFF1 expression in AH, RB tumors, and primary cell culture in relation to key clinical and pathological characteristics.

4. Discussion

Aqueous humor analyses and the identification of tumor biomarkers in eyes without enucleation have the potential to renew the management of retinoblastoma. For many years, any opportunity to obtain fluid-like AH from RB eyes was contraindicated in order to prevent tumor seeding [5,18,19]. However, today, AH paracentesis is part of the protocol for intravitreal chemotherapy injections and the risk of extraocular spread is considered extremely low [7,20–24]. Aqueous fluid is routinely aspirated prior to intravitreal injection to prevent reflux from the injection site. This standardized clinical procedure offers the possibility to readily access AH in RB eyes prior and during therapy and to evaluate

biomarkers that may correlate with features of the tumor and provide diagnostic and prognostic value. Aqueous humor has been shown to give important information for intraocular diseases, including RB; however, previous studies used AH from enucleated eyes [8]. This is going to change in the near future due to the clinical applicability of AH sample aspiration and its availability for diagnosis, prognosis, and/or management of RB.

Therefore, in the study presented, we intended to investigate the potential of TFF1 as a RB biomarker and its availability in AH of RB patients' eyes. TFF1 is already described as a functional biomarker in several other tumor entities, e.g., breast cancer [25,26], esophageal squamous cell carcinoma [27], and gastric cancer [28]. In breast cancer, a correlation of high TFF1 expression in blood samples of patients with metastatic disease compared to those without metastatic disease has been demonstrated [29]. Evaluating TFF1 staining of tumor sections after enucleation, we and others already described TFF1 as a biomarker for a subset of RBs. Here, we analyzed AH, tumor of origin, and established corresponding primary cell culture cells of 15 RB patients for TFF1 expression and secretion status and compared the results with the clinical parameters. We showed that TFF1 is expressed in the AH of most patients analyzed. All patients with TFF1-positive AH also expressed TFF1 in the original tumor, whereas some RB tumors express TFF1 without secreting it into the AH. We would like to emphasize the fact that there was no false positive result within our AH analysis. It seems, however, that not all TFF1-positive RB tumors can be identified by AH sampling, probably due to a lower secreting rate of some TFF1-positive RB tumors or fewer TFF1-positive cells within the tumor bulk resulting in TFF1 concentrations in AH samples that are below the detection limit. This hypothesis is supported by the fact that those three RB tumors of group III (without measurable TFF1 in AH) that do express TFF1 protein in the original tumor also secrete TFF1 in measurable amounts into the supernatant of the corresponding primary cell cultures. Possibly, primary RB cells expressing TFF1 have a growth advantage in culture that leads to a higher concentration of TFF1 in the cell culture supernatant in comparison to the investigated AH samples of the original tumor specimens. Fortunately, the primary cultured RB tumor cells mimic the original RB tumor with regard to TFF1 expression and secretion status for most analyzed RB tumors, rendering them an excellent in vitro system for further TFF1-based RB studies.

Correlation of the clinical and pathological characteristics of the investigated RB tumors with the TFF1 expression status in the AH of the patients' eye did not allow for any stratification. The lack of correlation is most likely attributable to the comparatively small sample size, because we and others have already shown that TFF1 expression in RB tumors indeed correlates with clinical parameters [4,9]. Our group demonstrated that TFF1 correlates with a higher clinical tumor-node-metastasis (TNM) stage and poorly differentiated tumor cells [8] and a recent study showed that TFF1 is linked to RBs which are associated with a higher risk of metastasis, referred to as subtype 2 [4]. Summarizing, one can state that the identification of TFF1 in the AH of RB patients opens the field for new diagnostic approaches. Beside other AH markers already described as potentially useful for diagnosis or reflecting response to RB treatment regimens [30–33],TFF1 is a new potential valuable biomarker for subtype 2 RBs [4]. Additionally, we could show that ELISA is a reliable method for TFF1 diagnostics in AH as it is very sensitive (sensitivity < 10 pg/mL), the sample volume needed is below the volume routinely aspirated prior to chemotherapy and the assay time is short (3.5 h). Thus, we could show for the first time that TFF1 has potential as a clinically useful biomarker for future RB diagnostics.

5. Conclusions

Aqueous humor analyses and identification of tumor biomarkers have the potential to renew advanced retinoblastoma management and to assure RB diagnosis in cases of clinically uncertain differential diagnosis. TFF1, a secreted peptide, is ectopically expressed in a subset of more advanced RB tumors and its expression correlates with a higher risk for metastases. We provided evidence for TFF1 expression in the AH of RB patients, strongly suggesting TFF1 as a clinically interesting new RB biomarker.

References

1. Dimaras, H.; Kimani, K.; Dimba, E.A.O.; Gronsdahl, P.; White, A.; Chan, H.S.L.; Gallie, B.L. Retinoblastoma. *Lancet* **2012**, *379*, 1436–1446. [CrossRef]

2. Munier, F.L.; Beck-Popovic, M.; Chantada, G.L.; Cobrinik, D.; Kivelä, T.T.; Lohmann, D.; Maeder, P.; Moll, A.C.; Carcaboso, A.M.; Moulin, A.; et al. Conservative management of retinoblastoma: Challenging orthodoxy without compromising the state of metastatic grace. "Alive, with good vision and no comorbidity". *Prog. Retin. Eye Res.* **2019**, *73*, 100764. [CrossRef] [PubMed]

3. Lu, J.E.; Francis, J.H.; Dunkel, I.J.; Shields, C.L.; Yu, M.D.; Berry, J.L.; Kogachi, K.; Skalet, A.H.; Miller, A.K.; Santapuram, P.R.; et al. Metastases and death rates after primary enucleation of unilateral retinoblastoma in the USA 2007–2017. *Br. J. Ophthalmol.* **2019**, *103*, 1272–1277. [CrossRef] [PubMed]

4. Liu, J.; Ottaviani, D.; Sefta, M.; Desbrousses, C.; Chapeaublanc, E.; Aschero, R.; Sirab, N.; Lubieniecki, F.; Lamas, G.; Tonon, L.; et al. A high-risk retinoblastoma subtype with stemness features, dedifferentiated cone states and neuronal/ganglion cell gene expression. *Nat. Commun.* **2021**, *12*, 5578. [CrossRef] [PubMed]

5. Eide, N.; Walaas, L. Fine-needle aspiration biopsy and other biopsies in suspected intraocular malignant disease: A review. *Acta Ophthalmol.* **2009**, *87*, 588–601. [CrossRef] [PubMed]

6. Munier, F.L.; Soliman, S.; Moulin, A.P.; Gaillard, M.-C.; Balmer, A.; Beck-Popovic, M. Profiling safety of intravitreal injections for retinoblastoma using an anti-reflux procedure and sterilisation of the needle track. *Br. J. Ophthalmol.* **2012**, *96*, 1084–1087. [CrossRef] [PubMed]

7. Smith, S.J.; Smith, B.D. Evaluating the risk of extraocular tumour spread following intravitreal injection therapy for retinoblastoma: A systematic review. *Br. J. Ophthalmol.* **2013**, *97*, 1231–1236. [CrossRef] [PubMed]

8. Ghiam, B.K.; Xu, L.; Berry, J.L. Aqueous Humor Markers in Retinoblastoma, a Review. *Transl. Vis. Sci. Technol.* **2019**, *8*, 13. [CrossRef]

9. Busch, M.; Metz, K.; Beier, M.; Biewald, E.; Dünker, N. Trefoil Factor Family 1 Expression Correlates with Clinical Outcome in Patients With Retinoblastoma. *Retina* **2018**, *38*, 2422–2428. [CrossRef]

10. Busch, M.; Grosse-Kreul, J.; Wirtz, J.J.; Beier, M.; Stephan, H.; Royer-Pokora, B.; Metz, K.; Dunker, N. Reduction of the tumorigenic potential of human retinoblastoma cell lines by TFF1 overexpression involves p53/caspase signaling and miR-18a regulation. *Int. J. Cancer* **2017**, *141*, 549–560. [CrossRef]

11. Philippeit, C.; Busch, M.; Dünker, N. Epigenetic control of trefoil factor family (TFF) peptide expression in human retinoblastoma cell lines. *Cell. Physiol. Biochem.* **2014**, *34*, 1001–1014. [CrossRef] [PubMed]

12. Busch, M.; Dünker, N. Trefoil factor family peptides—Friends or foes? *Biomol. Concepts.* **2015**, *6*, 343–359. [CrossRef] [PubMed]

13. Hoffmann, W. Trefoil factors TFF (trefoil factor family) peptide-triggered signals promoting mucosal restitution. *Cell. Mol. Life Sci.* **2005**, *62*, 2932–2938. [CrossRef] [PubMed]

14. Hoffmann, W. Trefoil Factor Family (TFF) Peptides and Their Diverse Molecular Functions in Mucus Barrier Protection and More: Changing the Paradigm. *Int. J. Mol. Sci.* **2020**, *21*, 4535. [CrossRef] [PubMed]

15. Braga Emidio, N.; Brierley, S.M.; Schroeder, C.I.; Muttenthaler, M. Structure, Function, and Therapeutic Potential of the Trefoil Factor Family in the Gastrointestinal Tract. *ACS Pharmacol. Transl. Sci.* **2020**, *3*, 583–597. [CrossRef]

16. Schulze, U.; Hampel, U.; Sel, S.; Contreras-Ruiz, L.; Schicht, M.; Dieckow, J.; Diebold, Y.; Paulsen, F. Trefoil factor family peptide 3 (TFF3) is upregulated under experimental conditions similar to dry eye disease and supports corneal wound healing effects in vitro. *Investig. Ophthalmol. Vis. Sci.* **2014**, *55*, 3037–3042. [CrossRef]

17. Weise, A.; Dünker, N. High trefoil factor 1 (TFF1) expression in human retinoblastoma cells correlates with low growth kinetics, increased cyclin-dependent kinase (CDK) inhibitor levels and a selective down-regulation of CDK6. *Histochem. Cell Biol.* **2013**, *139*, 323–338. [CrossRef]

18. Karcioglu, Z.A. Fine needle aspiration biopsy (FNAB) for retinoblastoma. *Retina* **2002**, *22*, 707–710. [CrossRef]

19. Ali, M.J.; Honavar, S.G.; Vemuganti, G.K.; Singh, A.D. Fine needle aspiration biopsy of retinal tumors. *Monogr. Clin. Cytol.* **2012**, *21*, 72–81. [CrossRef]

20. Ghassemi, F.; Shields, C.L.; Ghadimi, H.; Khodabandeh, A.; Roohipoor, R. Combined intravitreal melphalan and topotecan for refractory or recurrent vitreous seeding from retinoblastoma. *JAMA Ophthalmol.* **2014**, *132*, 936–941. [CrossRef]

21. Lawson, B.M.; Saktanasate, J.; Say, E.A.T.; Shields, C.L. Intravitreal chemotherapy provides control for massive vitreous seeding from retinoblastoma. *J. Pediatr. Ophthalmol. Strabismus* **2014**, *51*, e92–e94. [CrossRef] [PubMed]

22. Francis, J.H.; Schaiquevich, P.; Buitrago, E.; Del Sole, M.J.; Zapata, G.; Croxatto, J.O.; Marr, B.P.; Brodie, S.E.; Berra, A.; Chantada, G.L.; et al. Local and systemic toxicity of intravitreal melphalan for vitreous seeding in retinoblastoma: A preclinical and clinical study. *Ophthalmology* **2014**, *121*, 1810–1817. [CrossRef] [PubMed]

23. Munier, F.L.; Gaillard, M.-C.; Balmer, A.; Beck-Popovic, M. Intravitreal chemotherapy for vitreous seeding in retinoblastoma: Recent advances and perspectives. *Saudi J. Ophthalmol.* **2013**, *27*, 147–150. [CrossRef] [PubMed]

24. Smith, S.J.; Smith, B.D.; Mohney, B.G. Ocular side effects following intravitreal injection therapy for retinoblastoma: A systematic review. *Br. J. Ophthalmol.* **2014**, *98*, 292–297. [CrossRef] [PubMed]

25. Yi, J.; Ren, L.; Li, D.; Wu, J.; Li, W.; Du, G.; Wang, J. Trefoil factor 1 (TFF1) is a potential prognostic biomarker with functional significance in breast cancers. *Biomed. Pharmacother.* **2020**, *124*, 109827. [CrossRef] [PubMed]

26. Schulten, H.-J.; Bangash, M.; Karim, S.; Dallol, A.; Hussein, D.; Merdad, A.; Al-Thoubaity, F.K.; Al-Maghrabi, J.; Jamal, A.; Al-Ghamdi, F.; et al. Comprehensive molecular biomarker identification in breast cancer brain metastases. *J. Transl. Med.* **2017**, *15*, 269. [CrossRef]

27. Gonzaga, I.M.; Soares Lima, S.C.; Nicolau, M.C.; Nicolau-Neto, P.; da Costa, N.M.; de Almeida Simão, T.; Hernandez-Vargas, H.; Herceg, Z.; Ribeiro Pinto, L.F. TFF1 hypermethylation and decreased expression in esophageal squamous cell carcinoma and histologically normal tumor surrounding esophageal cells. *Clin. Epigenetics* **2017**, *9*, 130. [CrossRef]

28. Shimura, T.; Dayde, D.; Wang, H.; Okuda, Y.; Iwasaki, H.; Ebi, M.; Kitagawa, M.; Yamada, T.; Yamada, T.; Hanash, S.M.; et al. Novel urinary protein biomarker panel for early diagnosis of gastric cancer. *Br. J. Cancer* **2020**, *123*, 1656–1664. [CrossRef]

29. Elnagdy, M.H.; Farouk, O.; Seleem, A.K.; Nada, H.A. TFF1 and TFF3 mRNAs Are Higher in Blood from Breast Cancer Patients with Metastatic Disease than Those without. *J. Oncol.* **2018**, *2018*, 4793498. [CrossRef]

30. Shehata, H.H.; Abou Ghalia, A.H.; Elsayed, E.K.; Ahmed Said, A.M.; Mahmoud, S.S. Clinical significance of high levels of survivin and transforming growth factor beta-1 proteins in aqueous humor and serum of retinoblastoma patients. *J. AAPOS* **2016**, *20*, 444.e1–444.e9. [CrossRef]

31. Cheng, Y.; Zheng, S.; Pan, C.-T.; Yuan, M.; Chang, L.; Yao, Y.; Zhao, M.; Liang, J. Analysis of aqueous humor concentrations of cytokines in retinoblastoma. *PLoS ONE* **2017**, *12*, e0177337. [CrossRef] [PubMed]

32. Xu, L.; Kim, M.E.; Polski, A.; Prabakar, R.K.; Shen, L.; Peng, C.-C.; Reid, M.W.; Chévez-Barrios, P.; Kim, J.W.; Shah, R.; et al. Establishing the Clinical Utility of ctDNA Analysis for Diagnosis, Prognosis, and Treatment Monitoring of Retinoblastoma: The Aqueous Humor Liquid Biopsy. *Cancers* **2021**, *13*, 1282. [CrossRef] [PubMed]

33. Berry, J.L.; Xu, L.; Polski, A.; Jubran, R.; Kuhn, P.; Kim, J.W.; Hicks, J. Aqueous Humor Is Superior to Blood as a Liquid Biopsy for Retinoblastoma. *Ophthalmology* **2020**, *127*, 552–554. [CrossRef] [PubMed]

1B) Trefoil Family Factor Peptide 1 - A New Biomarker in Liquid Biopsies of Retinoblastoma under Therapy

Cumulative Thesis/Extent of Contribution

Cumulative thesis of M.Sc. André Haase

Author contributions

Trefoil Family Factor Peptide 1 - A New Biomarker in Liquid Biopsies of Retinoblastoma under Therapy

M. Busch, **A. Haase**, E. Alefeld, E. Biewald, L. Jabbarli and N. Dünker

Status: published in Cancers (2023)

DOI: 10.3390/cancers15194828

Impact factor at submission: 5.2 (2022)

André Haase contributions (shared **first-authorship**):

- **Conception: 5% -** Study design, cohort definition, literature research.
- **Experimental work: 95% -** Organization of aqueous humor and blood samples, organization of cell culture samples, performance of/ assistance with: ELISA, IHC, ICC.
- **Data analysis: 50% -** Processing, analysis, and visualization of ELISA, IHC and ICC data.
- **Statistical analysis**: **50% -** Organization of patient data and data interpretation.
- **Writing the manuscript: 10% -** Writing of Material and Methods, figure design and legends.

_____

Signature André Haase

_____

Signature Prof. Dr. Nicole Dünker

Article

Trefoil Family Factor Peptide 1—A New Biomarker in Liquid Biopsies of Retinoblastoma under Therapy

Maike Anna Busch [1,*,†], André Haase [1,†], Emily Alefeld [1], Eva Biewald [2], Leyla Jabbarli [2] and Nicole Dünker [1]

1 Institute of Anatomy II, Department of Neuroanatomy, Medical Faculty, Center for Translational Neuro and Behavioral Sciences (C-TNBS), University of Duisburg-Essen, 45147 Essen, Germany; andre.haase@uk-essen.de (A.H.); emily.alefeld@stud.uni-due.de (E.A.); nicole.duenker@uk-essen.de (N.D.)
2 Department of Ophthalmology, Children's Hospital, University of Duisburg-Essen, 45147 Essen, Germany; eva.biewald@uk-essen.de (E.B.); leyla.jabbarli@uk-essen.de (L.J.)
* Correspondence: maike.busch@uk-essen.de; Tel.: +49-201-723-84434
† These authors contributed equally to this work.

Simple Summary: Effective management of retinoblastoma (RB), a common childhood eye cancer, requires accurate diagnosis and monitoring during therapy. In this study, the liquid biopsy marker potential of the secreted trefoil family factor peptide 1 (TFF1), described as a biomarker of a more advanced RB subtype, was explored. TFF1 expression levels were investigated in aqueous humor (AH) of RB patients after enucleation and in RB patients undergoing intravitreal chemotherapy, and compared with TFF1 expression levels in RB patients' blood serum. AH showed consistent TFF1 levels in a subgroup of RB patients, remarkably decreasing post-therapy in responsive patients. The blood serum of RB patients only displayed low-to-non-detectable and therapy-independent TFF1 levels. The study suggests TFF1 expression in AH is a reliable biomarker, aiding RB diagnosis and treatment assessment and highlights its potential for non-invasive RB therapy monitoring.

Abstract: Effective management of retinoblastoma (RB), the most prevalent childhood eye cancer, depends on reliable monitoring and diagnosis. A promising candidate in this context is the secreted trefoil family factor peptide 1 (TFF1), recently discovered as a promising new biomarker in patients with a more advanced subtype of retinoblastoma. The present study investigated TFF1 expression within aqueous humor (AH) of enucleated eyes and compared TFF1 levels in AH and corresponding blood serum samples from RB patients undergoing intravitreal chemotherapy (IVC). TFF1 was consistently detectable in AH, confirming its potential as a biomarker. Crucially, our data confirmed that TFF1-secreting cells within the tumor mass originate from RB tumor cells, not from surrounding stromal cells. IVC-therapy-responsive patients exhibited remarkably reduced TFF1 levels post-therapy. By contrast, RB patients' blood serum displayed low-to-undetectable levels of TFF1 even after sample concentration and no therapy-dependent changes were observed. Our findings suggest that compared with blood serum, AH represents the more reliable source of TFF1 if used for liquid biopsy RB marker analysis in RB patients. Thus, analysis of TFF1 in AH of RB patients potentially provides a minimally invasive tool for monitoring RB therapy efficacy, suggesting its importance for effective treatment regimens.

Keywords: retinoblastoma; TFF1; aqueous humor; liquid biopsy; therapy monitoring

1. Introduction

Retinoblastoma (RB), the most common pediatric ocular malignancy, arises from the uncontrolled proliferation of developing retinal cells [1,2]. RB is characterized by the loss or mutation of both copies of the *RB1* gene, which regulates the cell cycle and inhibits tumorigenesis [3–6]. The disease manifests predominantly in children under five years of age,

affecting both eyes in approximately 40% of all cases [5]. If left untreated, retinoblastoma can lead to severe visual impairment and, in the most unfavorable cases, metastatic spread into the central nervous system via the optic nerve [1,7,8]. Prevalent RB therapies comprise invasive procedures such as enucleation of the affected eye, leading to lifetime visual limitations, or systemic chemotherapy, bearing various risks for the young patients [9–11]. Intravitreal chemotherapy (IVC) has emerged as a highly effective therapeutic RB modality, particularly for intraocular tumors [12–18]. IVC chemotherapeutic agents are directly injected into the vitreous cavity of the affected eye, allowing for targeted treatment and reduced systemic toxicity. While IVC has shown promising results in managing RB, therapy monitoring remains crucial for the assessment of treatment efficacy and early detection of potential recurrence. A tissue biopsy is generally considered contraindicated for RB, as it is believed to promote extraocular spread [19]. Nevertheless, in some cases, tissue biopsy is relevant as it allows for a reliable confirmation of RB diagnosis and the assessment of the *RB1* mutational status for prognostic counseling [20]. Despite the use of optical coherence tomography and B-scan ultrasonography, various ocular diseases such as Coats disease, persistent fetal vasculature, retinopathy of prematurity, coloboma, and toxocariasis may be misdiagnosed as RB [19], eventually resulting in enucleation of infants for questionable diagnostic purposes [21].

Liquid biopsy offers a non-invasive alternative, helping to overcome the limitations of tumor biopsies. The term liquid biopsy (LB) refers to the detection of tumor-derived components, such as circulating tumor cells (CTCs), cell-free DNA (cfDNA), exosomes, microRNAs, and other secreted factors, in easily accessible body fluids like blood or aqueous humor (AH) [22–24]. LB allows for early detection of cancer, stratification of therapeutic intervention as well as monitoring of therapy effectiveness, and detection of metastatic relapses caused by therapy resistance [25]. Aqueous humor paracentesis is a straightforward and safe LB procedure commonly conducted under general anesthesia in conjunction with eye examinations in RB infants. AH aspiration can also be combined with intravitreal administration of chemotherapy [24]. In recent decades, the identification of specific biomarkers—also detectable in LBs—revolutionized cancer research and clinical practice [26–28]. Biomarkers are measurable indicators of biological processes or disease states and play a crucial role in early detection, diagnosis, and prognosis of various malignancies including RB [29,30]. They also provide an opportunity to develop targeted therapies and allow for real-time monitoring of cancer progression and treatment response [31,32].

Potential RB biomarkers comprise histone modification and DNA methylation markers, components of non-coding RNA regulation mechanisms, as well as proteomic and radiogenomic markers (for review see: [33]). Only a few of these potential biomarkers are, however, assessable by non-invasive procedures like LBs, e.g., in the AH and/or blood serum of RB patients. Examples are lactate dehydrogenase [34,35], survivin [36], transforming growth factor beta (TGF-β) [37], and trefoil factor family peptide 1 (TFF1). The latter has emerged as an intriguing candidate with promising implications for cancer management [1,22,38]. TFF1, a member of the trefoil factor family peptides, plays a crucial role in maintaining mucosal integrity and promoting epithelial repair in various tissues [39–42]. Previous studies by our group showed that RB cell lines and RB tumors express variable levels of TFF1 [43–45], while it is not expressed in the healthy human retina. Recent studies suggested a potential link between TFF1 and specific clinico-pathological tumor features, suggesting its diagnostic and prognostic value as an RB biomarker [1,23]. Most recently, we demonstrated that TFF1 is also detectable in the AH of RB patients [23], rendering it a highly promising candidate as an RB biomarker in LBs. As a secreted, extracellular protein, TFF1 can be detected in body fluids [23,46,47], circumventing the need for invasive procedures. Additionally, a prospective biomarker like TFF1 potentially aids with early cancer detection, monitoring treatment response, and assessing disease progression, thereby improving patient outcomes.

The objective of this study was to shed light onto the potential of TFF1 as a non-invasive diagnostic and prognostic RB marker in LBs. Monitoring TFF1 levels in RB patients' AH and blood may not only enable early cancer detection, but also serve as a valuable indicator for therapy efficacy. Changes in TFF1 expression or release during the course of RB treatment might provide insights into treatment response, and their monitoring prospectively helps identify patients that may require additional interventions. Integrating TFF1 assessment into LB protocols for RB patients could enhance therapeutic decision making and improve long-term outcomes. As such, a comprehensive understanding of TFF1 as a cancer biomarker potentially changes future RB diagnostics and personalized treatment approaches, ultimately contributing to improved clinical outcomes and quality of life for affected children.

2. Materials and Methods

2.1. Human Retinoblastoma Tumor, Aqueous Humor, and Blood Samples

Human retinoblastoma (RB) primary tumor material, aqueous humor samples from enucleations of 8 patients, as well as aqueous humor and blood serum samples from 7 RB patients under therapy and 6 healthy individuals (control group) were used for TFF1 expression studies. The Ethics Committee of the Medical Faculty of the University of Duisburg-Essen approved the use of retinoblastoma samples (approval # 14-5836-BO) for research conducted in the course of this study, and written informed consent has been obtained from patients' relatives or parents.

Primary tumor material and aqueous humor samples of eight patients were harvested immediately after enucleation (T27, T31, T32, T34, T36, T38, T40, and T41). For AH paracentesis from the anterior eye chamber, a 30 G needle was used. Subsequently, the optic bulb was fenestrated and the tumor was extracted. Aqueous humor and blood serum samples of seven patients were harvested under anesthesia prior to IVC treatment with melphalan. Subsequently, blood was centrifuged at $2500\times g$ for 15 min at 18 °C. Separated serum fraction aliquots were stored at minus 80 °C until further use. Additionally, blood was drawn from six healthy individuals as a control group. Aqueous humor was stored at minus 80 °C until use or further processing (see below), and tumor tissue samples were cultured as described below.

This study includes a case series of eight untreated eyes from individual children diagnosed with intraocular retinoblastoma (in 2022) and seven treated eyes from individual children diagnosed with intraocular retinoblastoma between 2022 and 2023. Diagnosis of the untreated eyes was confirmed by a specialized pathologist after enucleation. The data collected included patient's age at diagnosis, gender, laterality, ICRB stage (International Classification of Retinoblastoma), RB1 mutation status, tumor volume/size, optic nerve, and choroid invasion.

2.2. Primary RB Cell Culture

After the primary RB tumor material was dissected into small fragments using a sterile blade, it was washed in PBS and centrifuged three times at 800 rpm for 2 min. Afterwards, the tumor material was cultivated in supplemented Dulbecco's modified Eagle's medium (DMEM; PAN-Biotech, Aidenbach, Germany) under conditions described previously [48]. The cells separated in culture into suspension (RB tumor cells) and adherent populations (RB-derived stroma cells) and were subsequently cultured separately. Supernatants from both subcultures were harvested and residual cells were removed by centrifugation. Cell culture supernatants were kept at −20 °C until usage.

2.3. Blood Serum Concentration and TFF1 ELISA Analysis

Right before use, blood serum samples were concentrated up to 5-fold using protein concentrator column (3 kDa MWCO, Thermo Fischer Scientific, MA, USA) following the manufacturer's instructions. One hundred microliters of aqueous humor samples and concentrated blood serum from RB patients was analyzed using a human TFF1 ELISA kit

(ab213833, abcam, Cambridge, UK) according to the manufacturer's protocol. The standard curve included in the kit was used to determine the concentration of the samples analyzed. A workflow diagram is shown in Figure 1.
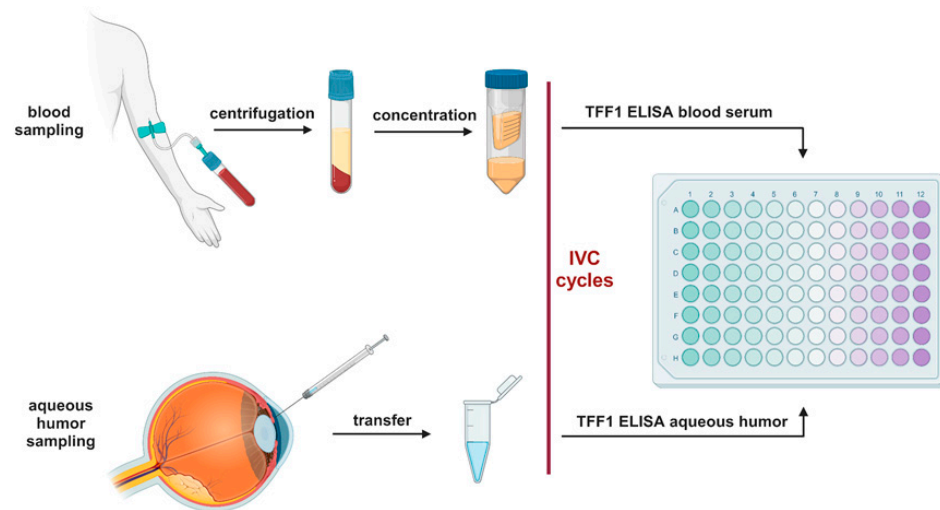

Figure 1. Workflow diagram of the TFF1 ELISA analysis. IVC: intravitreal chemotherapy. Created with BioRender.com (accessed on 13 September 2023).

2.4. Immunohistochemistry and Immunofluorescence Stainings

RB tumors were immunohistochemically stained using a specific TFF1 antibody (1:200, abcam, Cambridge, UK, # ab92377). Staining was revealed using a Vectastin Elite ABC kit (Vector Laboratories, Burlingame, CA, USA) following a protocol previously described by our group [48]. For visual documentation, an Aperio ScanScope AT2 (Leica, Wetzlar, Germany) slide scanner was used.

For immunofluorescence staining of TFF1, 1×10^5 cells were seeded on coverslips coated with poly-D-lysine (Sigma, Hamburg, Germany) and stained as previously described by our group [23]. Pictures were taken with a NIKON Eclipse E600 microscope equipped with a digital camera and NIKON Eclipse net software (version 5.20.02).

2.5. Statistical Analysis

Statistical analyses were performed using GraphPad Prism 9. Results were analyzed by a Student's t-test and considered significantly different if * $p < 0.05$, ** $p < 0.01$, *** $p < 0.001$, or **** $p < 0.0001$.

3. Results

3.1. Soluble TFF1 in Aqueous Humor of RB Patients Is Secreted by RB Tumor Cells

In a very recent study, we discovered TFF1 expression in a specific subgroup of retinoblastoma (RB) tumors with advanced stages, and found this soluble peptide to be secreted into the aqueous humor of RB patients [23]. To expand our investigation to a larger cohort of RB patients, we analyzed aqueous humor (AH) samples from eight additional RB patients after enucleation. Table 1 summarizes the clinical and pathological characteristics of the RB patients analyzed.

Using a specific, highly sensitive TFF1 ELISA (Figure 2a) allowed us to confirm that RB tumor cells secrete soluble TFF1 into the aqueous humor of RB patients' eyes.

Six out of eight tumors analyzed secreted high concentrations of TFF1 (ranging between 1000 and 4500 pg/mL; labeled as T27, T36, T31, T40, and T41) into the AH. Additionally, we found one tumor (T38) with moderate levels of TFF1 secretion. Only one (T32) out of eight tumors did not secrete any detectable TFF1 into the AH.

Table 1. Comparison of RB patients' clinical parameters and pathology reports with TFF1 levels in aqueous humor (AH). na: not available, *n*: number in each group, *N*: total number, ICRB: International Classification of Retinoblastoma.

	TFF1 Expressed *n* (%)	TFF1 Not Expressed *n* (%)	*N*
Patient's Sex	7 (87.5)	1 (12.5)	8
female	2 (28.6)	0 (0)	2
m	5 (71.4)	1 (100)	6
ICRB stage			
D	1 (14.3)	0 (0)	1
E	4 (57.1)	1 (100)	5
na	2 (28.6)	0 (0)	2
Laterality			
unilateral	7 (100)	1 (100)	8
bilateral	0 (0)	0 (0)	0
Age at diagnosis			
<18 month	0 (0)	1 (100)	1
18–36 month	6 (85.7)	0 (0)	6
>36 month	1 (14.3)	0 (0)	1
Tumor volume			
<1 cm^3	1 (14.3)	0 (0)	1
2–3 cm^3	2 (28.6)	0 (0)	2
>3 cm^3	4 (57.1)	1 (100)	5
Optic nerve invasion			
none	5 (71.4)	1 (100)	6
p-laminar	2 (28.6)	0 (0)	2
post-laminar	0 (0)	0 (0)	0
Choroid invasion			
none	7 (100)	1 (100)	8
invasion	0 (0)	0 (0)	0

In order to compare the expression pattern of TFF1 in AH with its expression in original RB tumor specimens, we performed immunohistochemical staining for TFF1 on paraffin sections of enucleated patients' eyes, barring the investigated tumors. Remarkably, all tumors displaying detectable TFF1 in the AH samples also stained positive for TFF1 in the primary tumor sections (Figure 2b).

These results further support our previous findings and indicate that detection of TFF1 in RB patients' AH represents a reliable marker for the presence of TFF1-secreting RB tumor cells. This finding holds promise for potential applications in RB patient monitoring and treatment strategies.

To investigate whether TFF1 is exclusively secreted by RB tumor cells and not by surrounding stromal tissue, we compared supernatants of a primary stromal cell culture and a primary RB tumor cell culture, both derived from enucleations of RB-tumor-bearing patient eyes. The primary stromal cells did not carry the RB1 mutation present in the primary RB tumor cells, indicating their non-tumor identity. As expected, ELISA analysis revealed no detectable TFF1 secretion in the supernatant of the stromal cell culture.

To further validate these results, we conducted immunofluorescence staining to assess the cellular expression of TFF1. The intracellular TFF1 expression pattern closely correlated with the TFF1 secretion status observed in the RB tumor cells and RB-tumor-derived stromal cells. Specifically, primary RB tumor cells exhibited high levels of TFF1 expression (Figure 3a), while the corresponding RB-derived stromal cells showed no detectable TFF1 expression (Figure 3b).
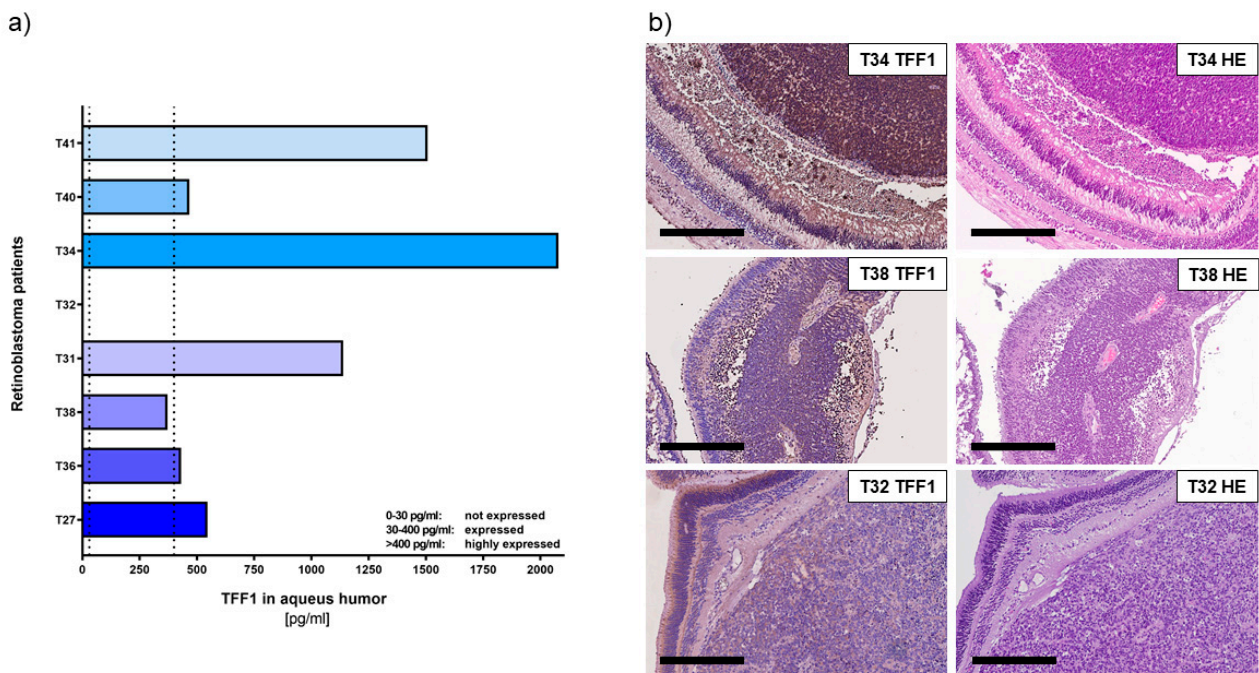
Figure 2. TFF1 expression analyses in aqueous humor samples and corresponding histological analysis of RB tumors in enucleated eyes of RB patients. (**a**) TFF1 ELISA analysis of 8 aqueous humor samples of RB patients, displaying six tumors highly expressing TFF1 (>400 pg/mL), one patient's tumor with average TFF1 expression (30–400 pg/mL), and one patient without TFF1 expression (0–30 pg/mL) in the aqueous humor. Vertical dotted lines indicate three TFF1 expression levels. (**b**) TFF1 expression in the corresponding primary tumors is shown exemplarily for T34 (high TFF1 expression in AH), T38 (moderate TFF1 expression in AH), and T32 (no TFF1 expression in AH). Immunohistochemistry was revealed using diaminobenzidine detection (brown signal) and hematoxylin counterstaining (blue nuclei staining). Scale bars: 300 μm.
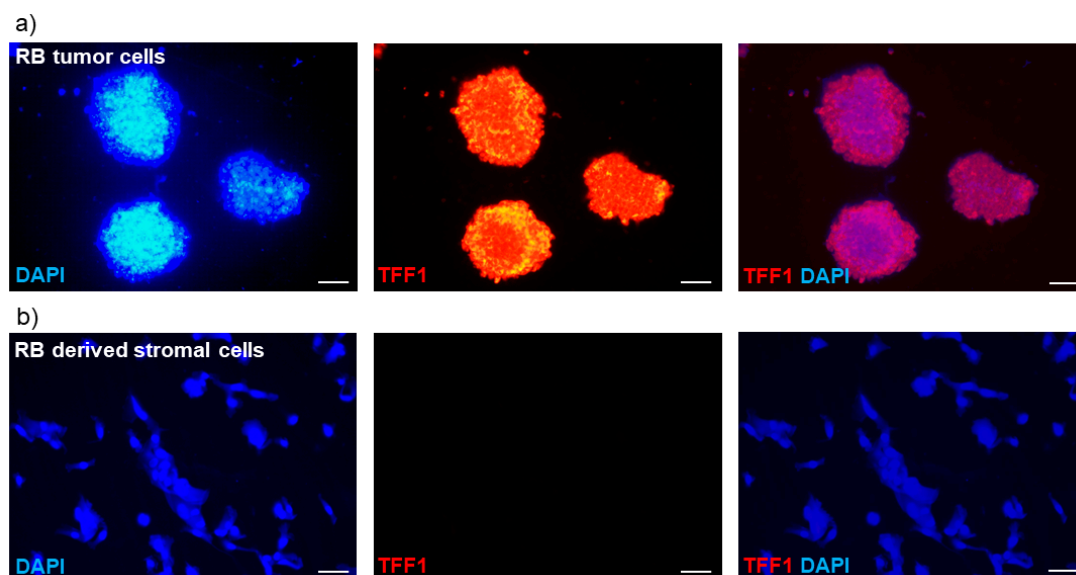
Figure 3. Immunofluorescence TFF1 staining of primary RB cell cultures. (**a**) Pictures of a primary cell culture of RB tumor cells and (**b**) corresponding RB-tumor-derived stromal cells in DAPI (blue), TFF1 (red), and merged DAPI/TFF1 immunofluorescence staining (200×). RB tumor cells showed a high expression of TFF1, in contrast to the corresponding stromal cells displaying no TFF1 expression. Scale bars: 50 μm.

In summary, our previous findings [23] were confirmed by analyzing AH samples from enucleated RB eyes via TFF1 ELISA. Additionally, we demonstrated that the cells secreting TFF1 originate from tumorigenic cells and not from the stromal compartment of the RB tumor mass. This discovery highlights TFF1 as a potential marker for minimally invasive therapy monitoring via AH aspiration.

3.2. Analysis of Soluble TFF1 Secretion in AH and Blood of RB Patients under Therapy

Monitoring and diagnosing RB is crucial in order to distinguish it from other diseases, evaluate treatment effectiveness, and identify potential recurrences. However, as RB tumor biopsies are not feasible, there is an urgent need for reliable biomarkers to determine diagnosis and treatment success in non-enucleated RB tumors.

To investigate if the expression of secreted TFF1 changes in liquid biopsies during therapy, we examined a series of AH and corresponding blood samples from seven RB patients using TFF1 ELISA. Liquid biopsies (AH and blood) were collected before the indicated intravitreal chemotherapy (IVC) treatment cycles with melphalan. We found that three out of the seven RB patients (T28, T33, and T44) expressed soluble, secreted TFF1 in their AH (Figure 4a).
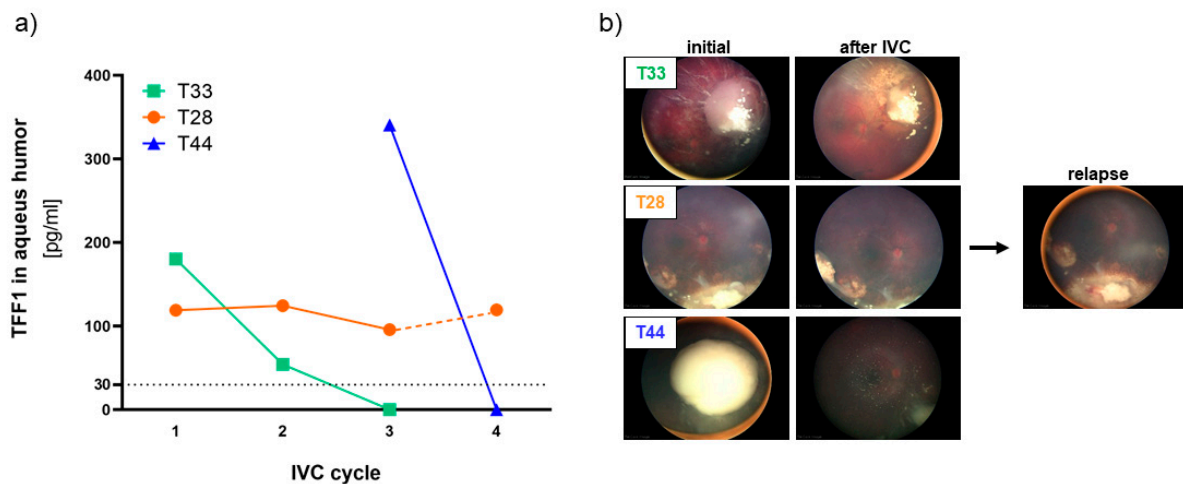
Figure 4. TFF1 expression analyses in aqueous humor samples of RB patients during therapy. (**a**) TFF1 ELISA analysis of three aqueous humor samples of RB patients taken prior to the indicated intravitreal chemotherapy (IVC) cycle with melphalan. All three patients initially expressed TFF1 (30–400 pg/mL) in the aqueous humor. Values below the vertical dotted line represent no TFF1 expression (0–30 pg/mL). (**b**) Fundoscopy pictures of the three RB patients prior (initial) and after IVC with melphalan. For patient T28, a picture of the relapse after 5 months is provided.

The first AH sample of the tumor with the highest AH TFF1 concentration (T44) observed in our study was received from the clinics after two IVC cycles with melphalan. Thus, no information about the initial TFF1 concentration in the AH prior to therapy is available. We nevertheless included this specimen in our monitoring due to a remarkable decrease in TFF1 levels under therapy, which dropped to zero after only one additional IVC cycle.

Similarly, the tumor with the second-highest AH TFF1 concentration (T33) displayed a reduction to zero after only two therapy cycles. Interestingly, the treatment outcome seems to correlate with the reduction in TFF1 expression in the AH in all RB tumors. Both tumors with TFF1 expression dropping to zero during IVC therapy responded well to treatment and showed positive outcomes as revealed by fundoscopy (Figure 4b) displaying a regression and calcification of the vitreous seeding. On the other hand, patient T28, while exhibiting a constant TFF1 expression in the AH during therapy (Figure 4a, IVC cycle 1–3), exhibited a relapse after five month (Figure 4b), while still expressing high TFF1 levels in the AH (Figure 4a, IVC cycle 4).

These findings suggest that monitoring soluble TFF1 levels in the aqueous humor of RB patients under therapy could serve as a potential biomarker to assess treatment efficacy and predict therapeutic outcomes in non-enucleated RB tumors. This could significantly improve RB therapy management and patient care.

Additionally, we examined corresponding blood serum samples from the seven RB patients who underwent therapy and compared them with three control samples from non-RB children and three healthy adolescents. Detecting TFF1 in blood serum required prior concentration of the samples (as described in the materials and methods section) and even after concentration, only fairly low TFF1 levels (~10 pg/mL) were detectable. Comparing TFF1 levels among individuals of the control groups, we found young non-RB-bearing children under the age of six to display no detectable TFF1 expression compared with the healthy adolescent group (>14 years), expressing low levels of about 10 pg/mL TFF1 (Figure 5).
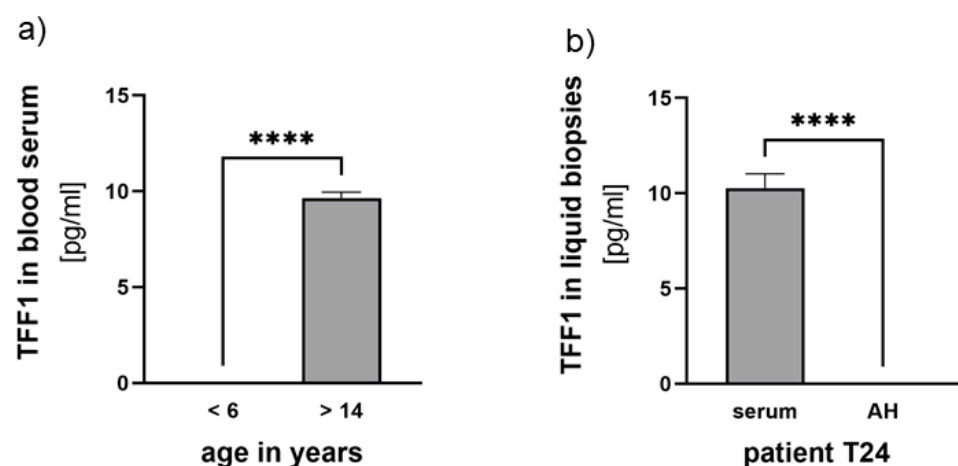
Figure 5. TFF1 expression analyses in blood serum and aqueous humor samples. (**a**) Comparison of TFF1 blood serum levels in control groups of non-RB children under the age of 6 years with healthy individuals over 14 years. (**b**) Comparison of TFF1 blood serum levels (serum) with TFF1 expression in aqueous humor (AH) of patient T24. Values are means of three samples $\pm$ SEM. **** $p < 0.0001$ statistical differences compared with the control group calculated by Student's *t*-test.

Among the seven RB serum samples investigated, we detected low concentrations of TFF1 in three samples (<12 pg/mL). However, in these patients, no TFF1 was detectable in the AH. Notably, one of the RB patients displaying detectable TFF1 expression in the blood was already 13 years old (Figure 5b), suggesting that serum expression might be related to the patient's age.

In one RB patient, TFF1 expression was neither detectable in the blood nor in the AH (T26, Table 2). Furthermore, patient T28, whose TFF1 expression in AH remained unchanged during therapy, showed no detectable TFF1 expression in their blood serum (Table 2). For patients T33 and T44, whose AH TFF1 expression dropped to zero under therapy, TFF1 expression was only randomly found in individual blood serum samples without a distinct expression pattern (Table 2).

Overall, no therapy-dependent changes in TFF1 expression were detectable in the blood serum of any of the RB patients studied (Table 2), rendering blood serum unsuitable for TFF1 biomarker analyses. These findings indicate that AH remains the most reliable source for monitoring TFF1 levels and assessing treatment responses in RB patients.

Table 2 summarizes clinical and pathological characteristics as well as TFF1 expression levels found in AH and blood serum samples of the seven RB patients analyzed during therapy.

Table 2. Clinical and pathological characteristics of RB patients under IVC therapy with melphalan stratified by TFF1 expression in liquid biopsies (aqueous humor and blood serum). Red and blue labeling indicates the respective tumor analyzed in case of bilaterality.

Case	Sex	Age at Diagnosis (Month)	Laterality	ICRB Stage	Tumor Size (mm)	Enucleation	Optic Nerve Invasion (MRI)	Choroid Invasion (MRI)	*RB1* Mutation	Sample Number	AH TFF1 (pg/mL)	Serum TFF1 (pg/mL)
T24 [#]	m	t: 23 **r: 148**	b	**ri: B** le: E	**ri: 4.5** le: >10	le: PE	no	no	yes	1 2 3	0 0 0	9.73 9.97 11.12
T25	f	18	u	D	8.7	no	no	yes	no	1 2 3 4 5 6	0 0 0 0 0 0	11.55 0 10.6 0 0 0
T26	m	14	b	D	9 (both)	**ri: no** le: SE	no	**ri: no** le: yes	yes	**1** **2** **3**	**0** **0** **0**	**0** **0** **0**
T28 [#]	f	t: 23 **r: 51** **r2: 56**	b	E	**ri: 12** le: 20	**ri: no** le: PE	**ri: no** le: yes	**ri: no** le: yes	yes	1 2 3 4	118.98 124.37 95.9 119.41	0 0 0 0
T33	m	24	u	D	n/a	no	n/a	n/a	n/a	1 2 3 4 5 6 7 8 9 10 11	180.21 54.28 0 0 0 0 0 0 0 0 0	10.65 9.23 0 0 0 9.33 0 0 9.83 10.14 0
T39	f	26	b	ri: E **le: D**	ri: 22 **le: 7**	ri: SE **le: no**	ri: yes **le: no**	ri: yes **le: no**	yes	1 2 3	0 0 0	9.93 0 9.98
T44	m	62	u	C	8	no	no	no	n/a	1 * 2	340.58 0	10.57 9.84

m: male, **f**: female, **u**: unilateral, **b**: bilateral, **ri**: right, **le**: left, **t**: primary tumor, **r**: relapse, **r2**: second relapse, **ICRB**: International Classification of Retinoblastoma, **SE**: secondary enucleation, **PE**: primary enucleation, **n/a**: not available, [#]: relapse was analyzed by TFF1 ELISA, *: specimen after two cycles of melphalan, **AH**: aqueous humor, **MRI**: magnetic resonance imaging.

4. Discussion

In contrast to other cancer entities, molecular characterization of RB tumors mainly relies on tumor samples derived from enucleations, as direct tumor biopsies bear the risk of cancer cell seeding and spread outside the eye [49–51]. The identification of tumor biomarkers in RB liquid biopsies like aqueous humor and blood serum holds the potential to improve diagnosis and therapy management of this childhood eye cancer without the need for enucleation. Aqueous humor has been suggested as a surrogate for RB tissue [26,52]. It can safely be aspirated from RB eyes and contains tumor-derived cfDNA, proteins, and metabolic targets, but also potential biomarkers like TFF1 [13,16,23,52–58]. Paracentesis of AH is minimally invasive as it is routinely aspirated from RB eyes undergoing salvage therapy with intravitreal injection of chemotherapeutics like melphalan. Nevertheless, a fine-gauge needle penetrates the cornea and thus, the procedure bears a minimal risk of complications such as bleeding, infection, cataract formation, iris trauma, and also potential spread of tumor cells [59]. Against this background, one might speculate if blood, a less invasive LB, might serve as a source for RB biomarkers like TFF1.

Our present study aimed to explore the potential of TFF1 as an RB biomarker in AH and blood serum of patients in general, and under therapy in particular. Monitoring LB biomarker levels during RB diagnosis and under therapy may ultimately enable a timely correlation between TFF1 expression levels in AH and/or blood serum and RB progression. TFF1 has previously been identified as a functional biomarker in various other

types of tumors, such as breast cancer [60,61], esophageal squamous cell carcinoma [62], and gastric cancer [63]. Notably, in breast cancer, a correlation between elevated TFF1 expression in blood samples of patients with, compared with those without, metastatic disease was observed [64]. By evaluating TFF1 staining in tumor sections post-enucleation, we and others already suggested TFF1 as a potential biomarker for a specific subset of retinoblastomas [1,38]. We previously demonstrated that TFF1 correlates with a higher clinical tumor-node-metastasis (TNM) stage and poorly differentiated tumor cells [38], later identified and specified as RB subtype 2 with a higher risk of metastasis by Liu et al. [1]. Most recently, we revealed for the first time that soluble TFF1 is secreted into the AH of RB patients [23].

Here, we analyzed AH of eight patients after enucleation as well as AH and corresponding blood serum of seven RB patients under therapy for TFF1 expression and secretion status. In addition, we investigated TFF1 expression in blood serum samples of control specimens including young children and adolescents in order to compare TFF1 levels of both groups.

The study presented verifies our previous findings [23] that TFF1 is secreted into the AH of most patients analyzed after enucleation. All patients with TFF1-positive AH also expressed TFF1 in the original tumor. Furthermore, we investigated if TFF1 is secreted exclusively by RB tumor cells or also by tumor-associated stromal cells. We therefore analyzed primary RB tumor cells and compared their endogenous TFF1 expression status and ability to secrete TFF1 into the supernatant with RB-tumor-derived stromal cells. We were able to demonstrate that only RB tumor cells and not RB-derived stromal cells express and secrete TFF1, rendering TFF1 a specific marker for RB tumor cells.

Three out of seven RB patients' tumors secreted soluble TFF1 into the AH under therapy. Two of these patients completely lost TFF1 expression in their AH during IVC therapy with melphalan, indicating a direct influence of the therapy regimen on TFF1 expression. The most obvious mechanistic explanation for this loss is death of TFF1-expressing RB tumor cells in the course of therapy. If this holds true, TFF1 expression is a direct indicator for residual-therapy-surviving and TFF1-secreting tumor cells. In line with these results, one RB tumor investigated displayed unvaried high TFF1 secretion into the AH during therapy and developed a relapse after five months, possibly indicating persisting RB tumor cells not readily visible in funduscopy and sonography. One might hypothesize that tumors with a high stromal content respond particularly well to therapy. If, however, mainly stromal, and not tumor, cells are susceptible to treatment, this distinction cannot be made by funduscopy. In this case, TFF1 would be an extraordinarily helpful marker for monitoring residual RB tumor cells. If these therapy-resistant cells still secrete TFF1, the urgent need for more frequent post-therapy screenings of the respective RB patients was indicated. However, not all RB tumors express and/or secrete TFF1 into the AH. Thus, TFF1 can probably not be considered a general minimally invasive LB-based RB biomarker, but might emerge as highly beneficial for patients with a more aggressive subtype 2 RB tumor.

Furthermore, we investigated if TFF1 can also be detected in the blood serum of RB patients and if TFF1 levels might correlate with therapy efficacy. Some RB patients' blood samples displayed detectable, yet very low, concentrations of soluble TFF1. No correlation of TFF1 levels in blood serum and corresponding AH samples was discernible and TFF1 expression likewise did not correlate with RB treatment outcome. Even in the control groups, only very low concentrations of TFF1 were detectable. Thus, AH seems to be superior to blood serum as an LB for RB, not only for detecting tumor-associated chromosomal changes in whole genome sequencing [59], but also for TFF1 monitoring. Interestingly, however, no TFF1 expression was detectable in non-RB children under the age of 6 in comparison to the older, adolescent control group (>13 years), who displayed low, but traceable levels. This may lead to the assumption that healthy young children do not secrete TFF1 into the blood.

Summarizing, one can state that the analysis of TFF1 in the AH of RB patients opens the field for additional diagnostic approaches and therapy monitoring, using TFF1 as a potential biomarker for RB tumor cells. In the future, AH paracentesis might add to the standard diagnostic RB procedure as well as to the monitoring of therapy outcomes by sonography, fundoscopy, and MRI and potentially improve early detection of residual RB tumor cells in follow-up screenings (Figure 6).
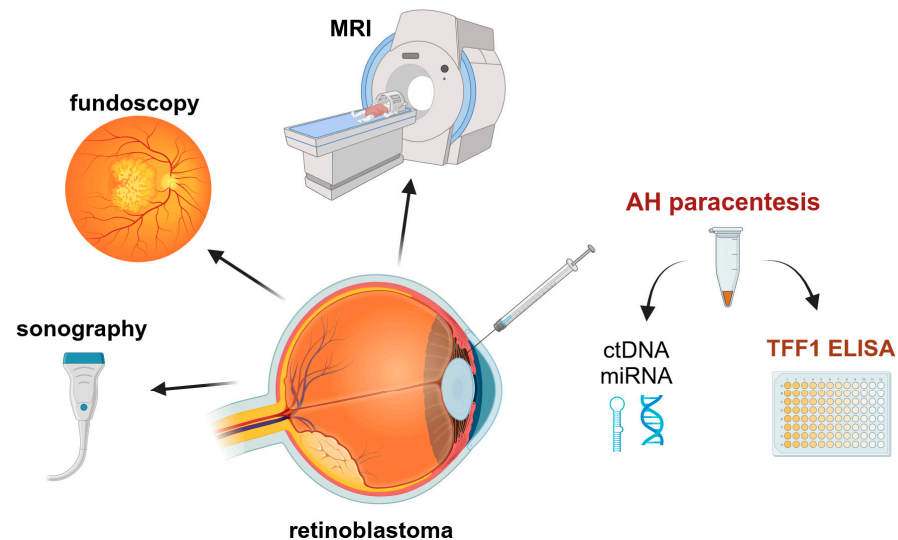

Figure 6. Potential monitoring procedures of RB patients under treatment to improve the outcome. MRI: magnetic resonance imaging; AH: aqueous humor; ctDNA: circulating tumor DNA; miRNA: micro RNA. Created with ©BioRender.com.

Nevertheless, it is necessary to further investigate TFF1 secretion into the AH during therapy in a larger cohort of RB patients to develop a save future implementation of TFF1 in clinical diagnostic and treatment regimens.

5. Conclusions

We succeeded in providing evidence for therapy-dependent changes in TFF1 expression in the AH of RB patients. Our data strongly suggest TFF1 as an LB-based RB biomarker allowing for minimally invasive, early, and unequivocal detection of RB. As TFF1 is supposed to be a marker of a subset of more advanced RB tumors with a higher risk for metastases, routinely screening for its expression might also enable a stratification of personalized intervention prior to therapy and monitoring of treatment effectiveness in the course of therapy, as well as detection of metastatic relapses caused by therapy resistance.

Author Contributions: Conceptualization, M.A.B.; methodology, A.H. and E.A.; validation, M.A.B. and A.H.; formal analysis, A.H. and E.A.; investigation, A.H. and E.A.; resources, E.B. and L.J.; data curation, A.H. and M.A.B.; writing—original draft preparation, M.A.B. and N.D.; writing—review and editing, M.A.B. and N.D.; visualization, M.A.B. and A.H.; supervision, M.A.B. and N.D.; project administration, M.A.B. and N.D. All authors have read and agreed to the published version of the manuscript.

Institutional Review Board Statement: The study was conducted in accordance with the guidelines of the Declaration of Helsinki, and approved by the Ethics Committee of the Medical Faculty of the University of Duisburg-Essen (approval # 06-30214; date of approval: 5 December 2006; approval # 14-5836-BO; date of approval: 11 March 2020).

Informed Consent Statement: Informed consent was obtained from all subjects involved in the study.

References

1. Liu, J.; Ottaviani, D.; Sefta, M.; Desbrousses, C.; Chapeaublanc, E.; Aschero, R.; Sirab, N.; Lubieniecki, F.; Lamas, G.; Tonon, L.; et al. A high-risk retinoblastoma subtype with stemness features, dedifferentiated cone states and neuronal/ganglion cell gene expression. *Nat. Commun.* **2021**, *12*, 5578. [CrossRef] [PubMed]
2. Singh, H.P.; Wang, S.; Stachelek, K.; Lee, S.; Reid, M.W.; Thornton, M.E.; Craft, C.M.; Grubbs, B.H.; Cobrinik, D. Developmental stage-specific proliferation and retinoblastoma genesis in RB-deficient human but not mouse cone precursors. *Proc. Natl. Acad. Sci. USA* **2018**, *115*, E9391–E9400. [CrossRef] [PubMed]
3. Dimaras, H.; Corson, T.W. Retinoblastoma, the visible CNS tumor: A review. *J. Neurosci. Res.* **2018**, *97*, 29–44. [CrossRef]
4. Bornfeld, N.; Lohmann, D.; Bechrakis, N.E.; Biewald, E. Retinoblastom. *Ophthalmologe* **2020**, *117*, 389–402. [CrossRef] [PubMed]
5. Roy, S.R.; Kaliki, S. Retinoblastoma: A Major Review. *Mymensingh Med. J.* **2021**, *30*, 881–895.
6. Bouchoucha, Y.; Matet, A.; Berger, A.; Carcaboso, A.M.; Gerrish, A.; Moll, A.; Jenkinson, H.; Ketteler, P.; Dorsman, J.C.; Chantada, G.; et al. Retinoblastoma: From genes to patient care. *Eur. J. Med. Genet.* **2023**, *66*, 104674. [CrossRef]
7. Chronopoulos, A.; Babst, N.; Schiemenz, C.; Schutz, J.S.; Heindl, L.M.; Ranjbar, M.; Kakkassery, V. A Narrative Review—Therapy Options and Therapy Failure in Retinoblastoma. *Neurosignals.* **2022**, *30*, 39–58. [CrossRef]
8. Shields, C.L.; Bas, Z.; Laiton, A.; Silva, A.M.V.; Sheikh, A.; Lally, S.E.; Shields, J.A. Retinoblastoma: Emerging concepts in genetics, global disease burden, chemotherapy outcomes, and psychological impact. *Eye* **2023**, *37*, 815–822. [CrossRef]
9. Kaewkhaw, R.; Rojanaporn, D. Retinoblastoma: Etiology, Modeling, and Treatment. *Cancers* **2020**, *12*, 2304. [CrossRef]
10. Munier, F.L.; Beck-Popovic, M.; Chantada, G.L.; Cobrinik, D.; Kivelä, T.T.; Lohmann, D.; Maeder, P.; Moll, A.C.; Carcaboso, A.M.; Moulin, A.; et al. Conservative management of retinoblastoma: Challenging orthodoxy without compromising the state of metastatic grace. "Alive, with good vision and no comorbidity". *Prog. Retin. Eye Res.* **2019**, *73*, 100764. [CrossRef]
11. Temming, P.; Arendt, M.; Viehmann, A.; Eisele, L.; Le Guin, C.H.D.; Schündeln, M.M.; Biewald, E.; Astrahantseff, K.; Wieland, R.; Bornfeld, N.; et al. Incidence of second cancers after radiotherapy and systemic chemotherapy in heritable retinoblastoma survivors: A report from the German reference center. *Pediatr. Blood Cancer* **2017**, *64*, 71–80. [CrossRef]
12. Campeau, E.; Ruhl, V.E.; Rodier, F.; Smith, C.L.; Rahmberg, B.L.; Fuss, J.O.; Campisi, J.; Yaswen, P.; Cooper, P.K.; Kaufman, P.D. A versatile viral system for expression and depletion of proteins in mammalian cells. *PLoS ONE* **2009**, *4*, e6529. [CrossRef] [PubMed]
13. Lawson, B.M.; Saktanasate, J.; Say, E.A.T.; Shields, C.L. Intravitreal chemotherapy provides control for massive vitreous seeding from retinoblastoma. *J. Pediatr. Ophthalmol. Strabismus* **2014**, *51*, e92–e94. [CrossRef] [PubMed]
14. Manjandavida, F.P.; Shields, C.L. The role of intravitreal chemotherapy for retinoblastoma. *Indian J. Ophthalmol.* **2015**, *63*, 141–145. [CrossRef] [PubMed]
15. Francis, J.H.; Abramson, D.H.; Ji, X.; Shields, C.L.; Teixeira, L.F.; Schefler, A.C.; Cassoux, N.; Hadjistilianou, D.; Berry, J.L.; Frenkel, S.; et al. Risk of Extraocular Extension in Eyes With Retinoblastoma Receiving Intravitreous Chemotherapy. *JAMA Ophthalmol.* **2017**, *135*, 1426–1429. [CrossRef]
16. Munier, F.L.; Gaillard, M.-C.; Balmer, A.; Beck-Popovic, M. Intravitreal chemotherapy for vitreous seeding in retinoblastoma: Recent advances and perspectives. *Saudi J. Ophthalmol.* **2013**, *27*, 147–150. [CrossRef]
17. Shields, C.L.; Douglass, A.M.; Beggache, M.; Say, E.A.T.; Shields, J.A. Intravitreous Chemotherapy for Active Vitreous Seeding from Retinoblastoma: Outcomes after 192 Consecutive Injections. The 2015 Howard Naquin Lecture. *Retina* **2016**, *36*, 1184–1190. [CrossRef]
18. Shields, C.L.; Lally, S.E.; Leahey, A.M.; Jabbour, P.M.; Caywood, E.H.; Schwendeman, R.; Shields, J.A. Targeted retinoblastoma management: When to use intravenous, intra-arterial, periocular, and intravitreal chemotherapy. *Curr. Opin. Ophthalmol.* **2014**, *25*, 374–385. [CrossRef]
19. AlAli, A.; Kletke, S.; Gallie, B.; Lam, W.-C. Retinoblastoma for Pediatric Ophthalmologists. *Asia Pac. J. Ophthalmol.* **2018**, *7*, 160–168. [CrossRef]
20. Soliman, S.E.; Racher, H.; Zhang, C.; MacDonald, H.; Gallie, B.L. Genetics and Molecular Diagnostics in Retinoblastoma—An Update. *Asia Pac. J. Ophthalmol.* **2017**, *6*, 197–207. [CrossRef]
21. Soliman, S.E.; Wan, M.J.; Heon, E.; Hazrati, L.-N.; Gallie, B. Retinoblastoma versus advanced Coats' disease: Is enucleation the answer? *Ophthalmic Genet.* **2017**, *38*, 291–293. [CrossRef] [PubMed]
22. Ghiam, B.K.; Xu, L.; Berry, J.L. Aqueous Humor Markers in Retinoblastoma, a Review. *Transl. Vis. Sci. Technol.* **2019**, *8*, 13. [CrossRef] [PubMed]
23. Busch, M.A.; Haase, A.; Miroschnikov, N.; Doege, A.; Biewald, E.; Bechrakis, N.E.; Beier, M.; Kanber, D.; Lohmann, D.; Metz, K.; et al. TFF1 in Aqueous Humor—A Potential New Biomarker for Retinoblastoma. *Cancers* **2022**, *14*, 677. [CrossRef] [PubMed]
24. Martel, A.; Baillif, S.; Nahon-Esteve, S.; Gastaud, L.; Bertolotto, C.; Roméo, B.; Mograbi, B.; Lassalle, S.; Hofman, P. Liquid Biopsy for Solid Ophthalmic Malignancies: An Updated Review and Perspectives. *Cancers* **2020**, *12*, 3284. [CrossRef]

25. Fernández-Lázaro, D.; Hernández, J.L.G.; García, A.C.; Del Castillo, A.C.; Hueso, M.V.; Cruz-Hernández, J.J. Clinical Perspective and Translational Oncology of Liquid Biopsy. *Diagnostics* **2020**, *10*, 443. [CrossRef]

26. Berry, J.L.; Xu, L.; Murphree, A.L.; Krishnan, S.; Stachelek, K.; Zolfaghari, E.; McGovern, K.; Lee, T.C.; Carlsson, A.; Kuhn, P.; et al. Potential of Aqueous Humor as a Surrogate Tumor Biopsy for Retinoblastoma. *JAMA Ophthalmol.* **2017**, *135*, 1221–1230. [CrossRef]

27. Im, D.H.; Pike, S.; Reid, M.W.; Peng, C.-C.; Sirivolu, S.; Grossniklaus, H.E.; Hubbard, G.B.; Skalet, A.H.; Bellsmith, K.N.; Shields, C.L.; et al. A Multicenter Analysis of Nucleic Acid Quantification Using Aqueous Humor Liquid Biopsy in Retinoblastoma: Implications for Clinical Testing. *Ophthalmol. Sci.* **2023**, *3*, 100289. [CrossRef]

28. Ghose, N.; Kaliki, S. Liquid biopsy in Retinoblastoma: A review. *Semin. Ophthalmol.* **2022**, *37*, 813–819. [CrossRef]

29. Zhang, Z.; Wu, H.; Chong, W.; Shang, L.; Jing, C.; Li, L. Liquid biopsy in gastric cancer: Predictive and prognostic biomarkers. *Cell Death Dis.* **2022**, *13*, 903. [CrossRef]

30. Hou, Y.; Peng, Y.; Li, Z. Update on prognostic and predictive biomarkers of breast cancer. *Semin. Diagn. Pathol.* **2022**, *39*, 322–332. [CrossRef]

31. Freitas, A.J.A.D.; Causin, R.L.; Varuzza, M.B.; Calfa, S.; Hidalgo Filho, C.M.T.; Komoto, T.T.; Souza, C.D.P.; Marques, M.M.C. Liquid Biopsy as a Tool for the Diagnosis, Treatment, and Monitoring of Breast Cancer. *Int. J. Mol. Sci.* **2022**, *23*, 9952. [CrossRef] [PubMed]

32. Galardi, A.; Stathopoulos, C.; Colletti, M.; Lavarello, C.; Russo, I.; Cozza, R.; Romanzo, A.; Carcaboso, A.M.; Locatelli, F.; Petretto, A.; et al. Proteomics of Aqueous Humor as a Source of Disease Biomarkers in Retinoblastoma. *Int. J. Mol. Sci.* **2022**, *23*, 13458. [CrossRef] [PubMed]

33. Sun, J.; Xi, H.-Y.; Shao, Q.; Liu, Q.-H. Biomarkers in retinoblastoma. *Int. J. Ophthalmol.* **2020**, *13*, 325–341. [CrossRef]

34. Abramson, D.H.; Piro, P.A.; Ellsworth, R.M.; Kitchin, F.D.; McDonald, M. Lactate dehydrogenase levels and isozyme patterns. Measurements in the aqueous humor and serum of retinoblastoma patients. *Arch. Ophthalmol.* **1979**, *97*, 870–871. [CrossRef] [PubMed]

35. Piro, P.A., Jr.; Abramson, D.H.; Ellsworth, R.M.; Kitchin, D. Aqueous humor lactate dehydrogenase in retinoblastoma patients. Clinicopathologic correlations. *Arch. Ophthalmol.* **1978**, *96*, 1823–1825. [CrossRef] [PubMed]

36. Jiang, L.-B.; Liu, X.-Q.; Li, B.; He, X.-J.; Jin, Y.-L.; Li, L.-Q.; Gao, F.; Wang, N.-L. Heat shock proteins and survivin: Relationship and effects on proliferation index of retinoblastoma cells. *Histol. Histopathol.* **2008**, *23*, 827–831. [CrossRef] [PubMed]

37. Shehata, H.H.; Abou Ghalia, A.H.; Elsayed, E.K.; Ahmed Said, A.M.; Mahmoud, S.S. Clinical significance of high levels of survivin and transforming growth factor beta-1 proteins in aqueous humor and serum of retinoblastoma patients. *J. AAPOS* **2016**, *20*, 444.e1–444.e9. [CrossRef] [PubMed]

38. Busch, M.; Metz, K.; Beier, M.; Biewald, E.; Dünker, N. Trefoil factor family 1 expression correlates with clinical outcome in patients with retinoblastoma. *Retina* **2017**, *38*, 2422–2428. [CrossRef]

39. Hoffmann, W. Trefoil factors TFF (trefoil factor family) peptide-triggered signals promoting mucosal restitution. *Cell. Mol. Life Sci.* **2005**, *62*, 2932–2938. [CrossRef]

40. Hoffmann, W. Trefoil Factor Family (TFF) Peptides and Their Diverse Molecular Functions in Mucus Barrier Protection and More: Changing the Paradigm. *Int. J. Mol. Sci.* **2020**, *21*, 4535. [CrossRef]

41. Braga Emidio, N.; Brierley, S.M.; Schroeder, C.I.; Muttenthaler, M. Structure, Function, and Therapeutic Potential of the Trefoil Factor Family in the Gastrointestinal Tract. *ACS Pharmacol. Transl. Sci.* **2020**, *3*, 583–597. [CrossRef] [PubMed]

42. Heuer, J.; Heuer, F.; Stürmer, R.; Harder, S.; Schlüter, H.; Braga Emidio, N.; Muttenthaler, M.; Jechorek, D.; Meyer, F.; Hoffmann, W. The Tumor Suppressor TFF1 Occurs in Different Forms and Interacts with Multiple Partners in the Human Gastric Mucus Barrier: Indications for Diverse Protective Functions. *Int. J. Mol. Sci.* **2020**, *21*, 2508. [CrossRef] [PubMed]

43. Weise, A.; Dünker, N. High trefoil factor 1 (TFF1) expression in human retinoblastoma cells correlates with low growth kinetics, increased cyclin-dependent kinase (CDK) inhibitor levels and a selective down-regulation of CDK6. *Histochem. Cell Biol.* **2013**, *139*, 323–338. [CrossRef] [PubMed]

44. Philippeit, C.; Busch, M.; Dünker, N. Epigenetic control of trefoil factor family (TFF) peptide expression in human retinoblastoma cell lines. *Cell. Physiol. Biochem.* **2014**, *34*, 1001–1014. [CrossRef]

45. Busch, M.; Grosse-Kreul, J.; Wirtz, J.J.; Beier, M.; Stephan, H.; Royer-Pokora, B.; Metz, K.; Dunker, N. Reduction of the tumorigenic potential of human retinoblastoma cell lines by TFF1 overexpression involves p53/caspase signaling and miR-18a regulation. *Int. J. Cancer* **2017**, *141*, 549–560. [CrossRef]

46. Katsha, A.; Soutto, M.; Sehdev, V.; Peng, D.; Washington, M.K.; Piazuelo, M.B.; Tantawy, M.N.; Manning, H.C.; Lu, P.; Shyr, Y.; et al. Aurora kinase A promotes inflammation and tumorigenesis in mice and human gastric neoplasia. *Gastroenterology* **2013**, *145*, 1312–1322.e8. [CrossRef] [PubMed]

47. Soutto, M.; Chen, Z.; Saleh, M.A.; Katsha, A.; Zhu, S.; Zaika, A.; Belkhiri, A.; El-Rifai, W. TFF1 activates p53 through down-regulation of miR-504 in gastric cancer. *Oncotarget* **2014**, *5*, 5663–5673. [CrossRef]

48. Busch, M.; Philippeit, C.; Weise, A.; Dünker, N. Re-characterization of established human retinoblastoma cell lines. *Histochem. Cell Biol.* **2015**, *143*, 325–338. [CrossRef]

49. Eide, N.; Walaas, L. Fine-needle aspiration biopsy and other biopsies in suspected intraocular malignant disease: A review. *Acta Ophthalmol.* **2009**, *87*, 588–601. [CrossRef]

50. Karcioglu, Z.A. Fine needle aspiration biopsy (FNAB) for retinoblastoma. *Retina* **2002**, *22*, 707–710. [CrossRef]

51. Ali, M.J.; Honavar, S.G.; Vemuganti, G.K.; Singh, A.D. Fine needle aspiration biopsy of retinal tumors. *Monogr. Clin. Cytol.* **2012**, *21*, 72–81. [CrossRef] [PubMed]
52. Raval, V.; Racher, H.; Wrenn, J.; Singh, A.D. Aqueous humor as a surrogate biomarker for retinoblastoma tumor tissue. *J. AAPOS* **2022**, *26*, 137.e1–137.e5. [CrossRef] [PubMed]
53. Smith, S.J.; Smith, B.D. Evaluating the risk of extraocular tumour spread following intravitreal injection therapy for retinoblastoma: A systematic review. *Br. J. Ophthalmol.* **2013**, *97*, 1231–1236. [CrossRef] [PubMed]
54. Ghassemi, F.; Shields, C.L.; Ghadimi, H.; Khodabandeh, A.; Roohipoor, R. Combined intravitreal melphalan and topotecan for refractory or recurrent vitreous seeding from retinoblastoma. *JAMA Ophthalmol.* **2014**, *132*, 936–941. [CrossRef] [PubMed]
55. Francis, J.H.; Schaiquevich, P.; Buitrago, E.; Del Sole, M.J.; Zapata, G.; Croxatto, J.O.; Marr, B.P.; Brodie, S.E.; Berra, A.; Chantada, G.L.; et al. Local and systemic toxicity of intravitreal melphalan for vitreous seeding in retinoblastoma: A preclinical and clinical study. *Ophthalmology* **2014**, *121*, 1810–1817. [CrossRef] [PubMed]
56. Smith, S.J.; Smith, B.D.; Mohney, B.G. Ocular side effects following intravitreal injection therapy for retinoblastoma: A systematic review. *Br. J. Ophthalmol.* **2014**, *98*, 292–297. [CrossRef] [PubMed]
57. Uner, O.E.; Ulrich, B.C.; Hubbard, G.B. Potential of Aqueous Humor as a Surrogate Tumor Biopsy for Retinoblastoma. *JAMA Ophthalmol.* **2018**, *136*, 597–598. [CrossRef]
58. Liu, W.; Luo, Y.; Dai, J.; Yang, L.; Huang, L.; Wang, R.; Chen, W.; Huang, Y.; Sun, S.; Cao, J.; et al. Monitoring Retinoblastoma by Machine Learning of Aqueous Humor Metabolic Fingerprinting. *Small Methods* **2022**, *6*, e2101220. [CrossRef]
59. Berry, J.L.; Xu, L.; Polski, A.; Jubran, R.; Kuhn, P.; Kim, J.W.; Hicks, J. Aqueous Humor Is Superior to Blood as a Liquid Biopsy for Retinoblastoma. *Ophthalmology* **2020**, *127*, 552–554. [CrossRef]
60. Yi, J.; Ren, L.; Li, D.; Wu, J.; Li, W.; Du, G.; Wang, J. Trefoil factor 1 (TFF1) is a potential prognostic biomarker with functional significance in breast cancers. *Biomed. Pharmacother.* **2020**, *124*, 109827. [CrossRef]
61. Schulten, H.-J.; Bangash, M.; Karim, S.; Dallol, A.; Hussein, D.; Merdad, A.; Al-Thoubaity, F.K.; Al-Maghrabi, J.; Jamal, A.; Al-Ghamdi, F.; et al. Comprehensive molecular biomarker identification in breast cancer brain metastases. *J. Transl. Med.* **2017**, *15*, 269. [CrossRef] [PubMed]
62. Gonzaga, I.M.; Soares Lima, S.C.; Nicolau, M.C.; Nicolau-Neto, P.; da Costa, N.M.; de Almeida Simão, T.; Hernandez-Vargas, H.; Herceg, Z.; Ribeiro Pinto, L.F. TFF1 hypermethylation and decreased expression in esophageal squamous cell carcinoma and histologically normal tumor surrounding esophageal cells. *Clin. Epigenet.* **2017**, *9*, 130. [CrossRef] [PubMed]
63. Shimura, T.; Dayde, D.; Wang, H.; Okuda, Y.; Iwasaki, H.; Ebi, M.; Kitagawa, M.; Yamada, T.; Yamada, T.; Hanash, S.M.; et al. Novel urinary protein biomarker panel for early diagnosis of gastric cancer. *Br. J. Cancer* **2020**, *123*, 1656–1664. [CrossRef]
64. Elnagdy, M.H.; Farouk, O.; Seleem, A.K.; Nada, H.A. TFF1 and TFF3 mRNAs Are Higher in Blood from Breast Cancer Patients with Metastatic Disease than Those without. *J. Oncol.* **2018**, *2018*, 4793498. [CrossRef] [PubMed]

2) Gastric Inhibitory Polypeptide Receptor (GIPR) Overexpression Reduces the Tumorigenic Potential of Retinoblastoma Cells

Cumulative Thesis/Extent of Contribution

Cumulative thesis of M.Sc. André Haase

Author contributions

Gastric Inhibitory Polypeptide Receptor (GIPR) Overexpression Reduces the Tumorigenic Potential of Retinoblastoma Cells

A. Haase, E. Alefeld, F. Yalinci, D. Van Meenen, M. Busch and N. Dünker

Status: published in Cancers (2024)

DOI: https://doi.org/10.3390/cancers16091656

Impact factor at submission: 5.2 (2022)

André Haase contributions (**first-authorship**):

- **Conception: 15% -** Study design, literature research.
- **Experimental work: 95% -** Planning the analysis workflow, primer design, cloning of expression vectors, production of lentivirus, conduction of transfection, transduction, RNA-isolation, Real-Time PCR, luciferase binding studies, WB, cell viability assays, cell proliferation assay, GIPR inhibitor studies, CAM assays, downstream target analysis.
- **Data analysis: 100% -** Data evaluation, processing, formal analysis, and visualization of entire data.
- **Statistical analysis**: **100% -** Data interpretation, integration, organization/correlation of patient data and performance of various statistical tests.
- **Writing the manuscript: 50% -** Writing of Material and Methods, Results, figure design and legends.
- **Revising the manuscript**: **10% -** Revising Abstract, Introduction, Results, Discussion, Material and Methods, Conclusions, Figures and supplementary materials.

_____

Signature André Haase

_____

Signature Prof. Dr. Nicole Dünker

cancers

MDPI

Article

Gastric Inhibitory Polypeptide Receptor (GIPR) Overexpression Reduces the Tumorigenic Potential of Retinoblastoma Cells

André Haase [ID], Emily Alefeld [ID], Fatma Yalinci, Dario Van Meenen, Maike Anna Busch *,† [ID] and Nicole Dünker †[ID]

Center for Translational Neuro- and Behavioral Sciences, Institute of Anatomy II, Department of Neuroanatomy, Medical Faculty, University of Duisburg-Essen, 45147 Essen, Germany; andre.haase@uk-essen.de (A.H.); emily.alefeld@stud.uni-due.de (E.A.); fatma.yalinci@stud.uni-due.de (F.Y.); dariovanmeenen@uk-essen.de (D.V.M.); nicole.duenker@uk-essen.de (N.D.)
* Correspondence: maike.busch@uk-essen.de
† These authors share senior authorship.

Simple Summary: Retinoblastoma (RB) is a malignant childhood eye cancer. In search for new or adjuvant treatment options, the gastric inhibitory polypeptide receptor (GIPR), upregulated upon the overexpression of trefoil factor family peptide 1 (TFF1), a diagnostic and prognostic biomarker for advanced RBs, came into our focus of interest. The overexpression of GIPR, found to be co-expressed with TFF1 in RB tumors, significantly reduced RB cell viability and growth and increased apoptosis levels. Moreover, GIPR-overexpressing RB cells developed significantly smaller tumors in vivo, indicating a tumor suppressor role of GIPR in RB. Although our data revealed that GIPR is not a direct TFF1 receptor, TFF1 and GIPR seem to be involved in the same signaling cascades. GIPR expression in RB cells seems to be regulated by miR-542-5p, and p53 is involved in GIPR downstream signaling, together providing potential targets for novel retinoblastoma treatment approaches.

Abstract: Retinoblastoma (RB) is the most common malignant intraocular tumor in early childhood. Gene expression profiling revealed that the gastric inhibitory polypeptide receptor (GIPR) is up-regulated following trefoil factor family peptide 1 (TFF1) overexpression in RB cells. In the study presented, we found this G protein-coupled transmembrane receptor to be co-expressed with TFF1, a new diagnostic and prognostic RB biomarker for advanced subtype 2 RBs. Functional analyses in two RB cell lines revealed a significant reduction in cell viability and growth and a concomitant increase in apoptosis following stable, lentiviral GIPR overexpression, matching the effects seen after TFF1 overexpression. In chicken chorioallantoic membrane (CAM) assays, GIPR-overexpressing RB cells developed significantly smaller CAM tumors. The effect of GIPR overexpression in RB cells was reversed by the GIPR inhibitor MK0893. The administration of recombinant TFF1 did not augment GIPR overexpression effects, suggesting that GIPR does not serve as a TFF1 receptor. Investigations of potential GIPR up- and downstream mediators suggest the involvement of miR-542-5p and p53 in GIPR signaling. Our results indicate a tumor suppressor role of GIPR in RB, suggesting its pathway as a new potential target for future retinoblastoma therapy.

1. Introduction

Affecting approximately 1 in every 18,000 live births worldwide, retinoblastoma (RB) is a rare tumor, yet it is the most common intraocular pediatric malignancy found in children under five years of age [1–3]. In bilateral RBs, which make up approx. 40% of all cases, the tumor effects both eyes [4]. The *RB1* gene regulates the cell cycle and inhibits tumorigenesis, and RB develops after a loss or mutation of both gene copies [1,2,4–6]. If diagnosed early, RB is curable, but, if left untreated, it leads to severe visual impairment

and can even become life-threatening due to metastatic spread [1,7–11]. Enucleation, the complete removal of the affected eye, is avoided whenever salvage is possible, e.g., via intraarterial chemotherapy (IAC) or intravitreal chemotherapy (IVC). IVC focusses on precise drug delivery to the hotspot of tumor seeding, the vitreous body, reducing the toxicity of systemic chemotherapy [1,11–15]. However, current therapies are associated with a considerable, sometimes even complete loss of vision and a significantly increased risk for secondary tumors [16] as well as the development of chemotherapy resistance [17]. Therefore, current therapeutic and diagnostic procedures need to be improved, and new or complementary treatment methods are required.

In humans, the trefoil factor family (TFF) comprises three peptides—TFF1, TFF2, and TFF3—all possessing a characteristic clover leaf-like disulfide structure, the so-called TFF domain (for review see [18–20]). TFF peptides have been shown to be aberrantly expressed in a wide range of human cancer entities, including retinoblastoma (for review see [21]). Our group demonstrated that TFF1 acts as a tumor suppressor in the progression of retinoblastoma by reducing RB cell viability, growth, and proliferation and increasing apoptosis in vitro as well as inhibiting tumor growth in vivo [22]. Moreover, we previously discovered that TFF1 levels correlate with a higher clinical RB tumor-node-metastasis (TNM) stage [23], and, recently, TFF1 was described as a biomarker in retinoblastoma patients with a more advanced subtype and poor prognosis [7,24]. Most recently, we demonstrated a promising role of TFF1 as a prognostic and diagnostic marker available in the aqueous humor of RB liquid biopsies in general and under therapy in particular [25,26]. After *TFF1* overexpression in RB cells, we identified several differentially expressed genes and pathways involved in cancer progression by a gene expression array analysis [22]. One of the genes with the highest fold change in its expression levels after TFF1 over-expression was the glucose-dependent insulinotropic polypeptide or gastric inhibitory polypeptide receptor (GIPR). The human *GIPR* gene encoding for a G protein-coupled class B transmembrane protein was first cloned and molecularly characterized in 1995 [27–29]. G protein-coupled receptors (GPCRs) have been described as low-affinity receptors for TFF2 and TFF3 [30,31] and might be potential mediators in TFF signaling. GIPR mediates the metabolic function of the glucose-dependent insulinotropic or gastric inhibitory polypeptide (GIP), namely, glucose-dependent stimulation of insulin release from the beta cells of the pancreas ([32]; for review see [33,34]). GIPR is, however, not only expressed in the beta cells of the pancreas, throughout the gastrointestinal tract, and in adipose tissues but also in certain regions of the rat and human brain [35–38]. In the nervous system, GIP effects on neurogenesis and neuronal survival have been reported (for overview see [37]. Recently, alterations in GIPR expression have been reported in neuroendocrine tumors [39], neuroendocrine neoplasms [40], and medullary thyroid cancer [41], suggesting a clinically significant diagnostic and prognostic potential (for review see [33,34]).

As various studies reported that signaling along the GIP/GIPR axis exerts pro-proliferative and anti-apoptotic effects [42–47], in the study presented, we investigated if the effects seen after TFF1 overexpression relating to RB cell viability, cell growth, proliferation, apoptosis, and tumorigenicity are potentially mediated via the GIPR signaling axis and if GIPR might even be a TFF1 receptor yet to be found. For this purpose, we overexpressed GIPR in the RB cell lines WERI-Rb1 and Y79 and examined the effects on RB cell behavior in vitro as well as in vivo, in ovo chorioallantoic membrane (CAM) assays. Furthermore, we investigated the expression of GIPR in primary RB tumor cells in correlation with TFF1 expression and examined up- and downstream signaling components of GIPR via luciferase binding studies and a proteome profiler oncology array.

2. Materials and Methods

2.1. Human Retina and Retinoblastoma Samples

In this study, we used postmortem healthy human retinal tissue and samples of retinoblastoma patients. This research was conducted following the principles outlined in the Declaration of Helsinki. Approval for the use of human retinal tissue (approval

no. 06-30214) and RB samples (approval no. 14-5836-BO) was granted by the Ethics Committee of the Medical Faculty at the University Hospital Essen, University of Duisburg-Essen. Informed consent was obtained from all the subjects involved in this study.

2.2. Human Cell Lines and Culture

The RB cell lines WERI-Rb1 (Weri [48] and Y79 [49], initially acquired from the Leibniz Institute DSMZ (German Collection of Microorganisms and Cell Cultures), were generously supplied by Dr. H. Stephan. The RB cell lines were cultivated as suspension cultures as described previously [50]. Human embryonic kidney (HEK293T) cells were cultivated as an adherent cell culture in DMEM medium (PAN-Biotech, Aidenbach, Germany), supplemented with 10% FBS (PAN-Biotech, Aidenbach, Germany), 4 mM L-glutamine (Gibco, Karlsruhe, Germany), 100 U penicillin/mL, and 100 µg streptomycin/mL (Gibco, Karlsruhe, Germany). The cells were maintained at 37 °C, 5% CO_2, and 95% humidity.

2.3. Expression Vectors

For the construction of the GIPR overexpression vector (GIPR_plenti), the human GIPR cDNA sequence was excised from the human hGip-R pcDNA3 plasmid (cat. #14942; Addgene, Watertown, MA, USA, [28]) using the NotI fast digest restriction enzyme (Thermo Scientific, Oberhausen, Germany). Subsequently, it was ligated to the NotI-digested pENTR4 vector (cat. #17424; Addgene, Watertown, MA, USA, [51]). Afterwards, the GIPR sequence was inserted into the plenti CMV Puro Dest vector (cat. #17452; Addgene, Watertown, MA, USA [51]) using the Gateway LR Clonase II Enzyme Mix (Invitrogen, Darmstadt, Germany), following the manufacturer's protocol. In all GIPR overexpression experiments, an empty plenti vector (empty_plenti) served as the control vector.

MicroRNA-542-5p sequences were extracted from genomic HEK293T DNA via PCR using specific primers (forward: 5′-GAATTCATTTGGGATCGGTCAAGGATG-3′; and reverse: 5′-GGATCCTTTGCTTAGGGCCCACTTTC-3′) containing EcoRI or BamHI restriction sites (underlined). After EcoRI/BamHI digestion (Thermo Scientific, Oberhausen, Germany), the miR-542-5p PCR product was integrated into the pSG5 vector (cat. #216201; Stratagene, La Jolla, CA, USA) to generate a pSG5-miR-542-5p vector. The empty pSG5 vector (pSG5) served as a control vector.

For the miR-542-5p binding studies, the wildtype miR-542-5p binding site (GIPR-BS) within the 3′-UTR of the GIPR sequence was amplified by PCR from the GIPR_plenti plasmid DNA using specific primers (forward: 5′-ACTAGTCCACACACGCTATGGAATG-3′; and reverse: 5′-GAGCTCGGGCCTTTGCCTATGCTATC-3′), containing SpeI or SacI restriction sites (underlined). Subsequently, the PCR fragments were inserted into a pCR®4-TOPO vector with the TOPO™TA Cloning™ Kit (Thermo Scientific; Oberhausen, Germany), following the manufacturer's protocol. To create a mutant binding site (GIPR-MUT), primers (forward: 5′-CACTTAAGCCAGTCGACAAAGAGGTGAAAG-3′; and reverse: 5′-CTTTCACCTCTTTGTCGACTGGCTTAAGTG-3′) containing a SalI restriction site (underlined) instead of the miR-542-5p binding site were used in combination with the wildtype primers mentioned above. Following SpeI/SacI digestion (Thermo Scientific; Oberhausen, Germany), the wildtype and mutant miR-542-5p binding site PCR products were ligated into the pmiR-TK-RNL vector [52] to generate pmiR-GIPR-BS and pmir-GIPR-MUT vectors. The empty pmiR-TK-RNL vector (pmiR) served as a control vector. Validation of all the constructed vectors was performed via Sanger sequencing (Microsynth, Balgach, Switzerland).

2.4. Luciferase Binding Studies

The interaction between miR-542-5p and the potential binding site in the 3′-UTR of the *GIPR* gene was investigated using a Dual-Luciferase® Reporter Assay System (Promega, Mannheim, Germany). HEK293T cells were transiently co-transfected with either the miR-542-5p expression vector (pSG5-miR-542-5p) or an empty control vector (pSG5), in combination with the empty pmiR-TK-RNL vector (pmiR), a vector containing the miR-542-5p binding site (pmiR-GIPR-BS), or a vector containing the mutant binding

site (pmiR-GIPR-MUT). After incubation for 48 h, the cells were lysed in $1\times$ passive lysis buffer (Promega), and luciferase activity was quantified via a dual-luciferase reporter assay (cat. #E1910, Promega, Walldorf, Germany) and visualized using a GloMax 20/20 luminometer (Promega, Walldorf, Germany) following the manufacturer's instructions. In the assay performed, binding to the potential binding site decreased luciferase activity. The relative luciferase activity was calculated as the ratio of firefly luciferase to renilla luciferase activity. All the analyses were conducted in triplicates.

2.5. Transient GIPR and miR-542-5p Overexpression

For transient GIPR and miR-542-5p overexpression, 5×10^5 Weri or Y79 cells were seeded into six-well plates with 2 mL DMEM (PAN-Biotech, Aidenbach, Germany) supplemented with 15% FBS (PAN-Biotech, Aidenbach, Germany) and 4 mM L-glutamine (Gibco, Karlsruhe, Germany). Plasmid DNA (4 µg) of GIPR_plenti, empty_plenti, pSG5-miR-542-5p, or empty pSG5 vectors was combined with transfection reagent (FuGENE® HD; Promega, Walldorf, Germany) at a ratio of 1:5 following our previously established protocol [22].

2.6. Lentivirus Production and Transduction

For lentivirus production, 6×10^6 HEK293T cells were co-transfected with 6 µg of each of the following plasmid DNAs: packaging vectors pczVSV-G [53], pCD NL-BH [54], and GIPR_plenti or empty_plenti, the latter serving as a negative control. Transfections were performed in the presence of 45 µg polyethyleneimine (PEI, Sigma-Aldrich, St. Louis, MI, USA) in DMEM medium. After 24 h, the medium was changed to Iscove's Modified Dulbecco's medium (IMDM, Pan-Biotech, Aidenbach, Germany) supplemented with 10% FBS and 1% penicillin/streptomycin. Seventy-two hours after transfection, viral supernatants were harvested, filtered (0.45 µm sterile filter), and stored at $-80\,^\circ$C until use.

For lentiviral transduction, 0.5×10^6/mL RB cells were seeded in cell culture flasks (Greiner, Kremsmünster, Austria) in DMEM cell culture medium supplemented with 15% FBS, 4 mM L-glutamine, 100 U penicillin/mL, and 100 µg streptomycin/mL. After 24 h, the medium was replaced by GIPR (GIPR_plenti) or a negative control (empty_plenti) viral supernatant. Transduction was performed in the presence of 50 µg/mL polybrene (H9268, Sigma-Aldrich, München, Germany). After 24 h, double the volume of the DMEM medium was added to the virus supernatant. Forty-eight hours later, the medium was exchanged completely with the DMEM medium.

Virus production and transduction with TFF1 lentiviral supernatant was performed as described previously [22].

2.7. RNA Extraction and Quantitative Real-Time PCR

RNA was isolated using a NucleoSpin® RNA II Kit (Macherey & Nagel, Düren, Germany), and microRNA was isolated using a miRNeasy Kit (Qiagen, Hilden, Germany), both following the manufacturers' protocols.

Complementary DNA (cDNA) was synthesized using a QuantiTect Reverse Transcription Kit (Qiagen) following the manufacturer's protocol. For quantitative Real-Time (RT) PCR analysis of *GIPR*, a SYBR™ Green PCR assay (Applied Biosystems, Dreieich, Germany) was used with specific primers (forward: 5'-GGACTATGCTGCACCCAATG-3'; and reverse: 5'-CAAAGTCCCCATTGGCCATC-3'). Human *GAPDH* (forward: 5'-ACCCACTCCTCCACCTTTGA-3'; and reverse: 5'-CTGTTGCTGTAGCCAAATTCGT-3') served as an endogenous control. RT-PCRs were performed in triplicates using 20 µL of SYBR™ Green PCR Master Mix (Applied Biosystems, Dreieich, Germany). A thermal cycling (Mastercycler X50s, Eppendorf, Hamburg, Germany) program comprised the initial denaturation step at 95 °C for 15 min, followed by 40 cycles of denaturation at 94 °C for 15 s, annealing at 55 °C for 30 s, and extension at 70 °C for 34 s.

The primers in Table 1 were used to analyze the expression levels of potential downstream targets of GIPR (see Supplementary Figure S1).

Table 1. Real-Time PCR primers for GIPR downstream signaling analyses.

Primer	5′-3′ Sequence
ENO2 FW	CTACCACCGTCTGAGTCTGC
ENO2 RV	CCTTCAGGACACCTTTGCCT
ERBB2 FW	GTTCCCGGATTTTTGTGGGC
ERBB2 RV	GTGGTACTTCAATTGCGACTCA
p27 FW	CTGCAACCGACGATTCTTCT
p27 RV	GCATTTGGGGAACCGTCTGA
p53 FW	TGTGACTTGCACGTACTCCC
p53 RV	ACCATCGCTATCTGAGCAGC
Survivin FW	TGAGAACGAGCCAGACTTGG
Survivin RV	TGGTTTCCTTTGCATGGGGT
FGFb FW	CCGTTACCTGGCTATGAAGG
FGFb RV	AAAGAAACACTCATCCGTAACACA

TaqMan Gene Expression Real-Time PCR analysis was performed according to the manufacturer's protocol using the TaqMan Universal PCR Master Mix (Applied Biosystems, Dreieich, Germany). Reactions were performed in duplicate with a total volume of 20 µL and the following cycling program: 2 min at 50 °C, 10 min at 95 °C, followed by 40 cycles of 15 s at 95 °C, and 60 s at 60 °C. The following TaqMan Real-Time PCR assays (Applied Biosystems, Dreieich, Germany) were used: 18S (Hs99999901_s1), GIPR (Hs00609210_m1), and TFF1 (Hs00907239 m1).

MiRNA expression analyses were conducted using a miScript PCR Starter Kit (cat. #2181193; Qiagen, Hilden, Germany) following the manufacturer's instructions. For miRNA quantification, miScript HiSpec buffer (Qiagen, Hilden, Germany) was used with specific primers for miR-542-5p (5′-TCGGGGATCATCATGTCACGAGA-3′) and 5.8S RNA (5′-CTACGCCTGTCTGAGCGTCGCTT-3′) as an internal control. The reactions were conducted in duplicates with the following subsequent thermal cycling program: 95 °C for 15 min, 94 °C for 15 s, 55 °C for 30 s, and 70 °C for 34 s, with a total of 40 cycles.

2.8. Western Blot Analyses

For the Western blot analyses, 10×10^6 cells were washed with phosphate-buffered saline (PBS) and subsequently lysed in RIPA buffer supplemented according to a previously described protocol [50]. Protein extraction was achieved by ultrasonic cell lysis at 4 °C, and, afterwards, the lysates were centrifuged at $10,000 \times g$ at 4 °C for 30 min. The protein concentration was determined using a bicinchoninic acid assay (BCA; Thermo Scientific, Oberhausen, Germany) following the manufacturer's instructions. Equal amounts of protein extracts were separated on a 10% SDS/PAGE gel and transferred onto nitrocellulose membranes. The membranes were blocked in 5% milk powder (Roth, Karlsruhe, Germany) and incubated overnight at 4 °C with primary antibodies against GIPR (1:2000; cat. #ab136266, Abcam, Cambridge, UK), TFF1 (1:1000; cat. #ab92377, abcam, Cambridge, UK), or β-actin (1:1000; cat. #4967; Cell Signaling Technology, Danvers, MA, USA). The blots were either cut or stripped by incubation in 0.2 N NaOH (Roth, Karlsruhe, Germany) for 15 min at RT, followed by re-blocking and incubation in an antibody solution. Horseradish peroxidase (HRP)-conjugated secondary antibodies (goat anti-rabbit; P0448, Agilent, Santa Clara, CA, USA) were applied at a dilution of 1:10,000 at room temperature for 1 h. The HRP signal was visualized with a Western Bright Chemiluminescence Reagent (Advansta, San Jose, CA, USA) and detected with a Celvin S reader (Biostep, Burkhardtsdorf, Germany).

2.9. Cell Viability Assays

For the determination of cell viability, a total of 4×10^4 cells were seeded in 100 µL of DMEM medium into a 96-well plate in quintuplicates. Following 48 h incubation, 10 µL of a water-soluble tetrazolium (WST-1) solution (Sigma-Aldrich, St. Louis, MI, USA) was added to each well, and the cells were incubated at 37 °C for 2 h. The formazan product produced

by viable cells was quantified using a microplate reader (Agilent BioTek, Santa Clara, CA, USA) at an absorbance of 450 nm.

2.10. Growth Kinetics

Growth kinetics analyses were performed using 24-well plates. A total of 3×10^5 cells were seeded in triplicates, with each well containing 500 μL of DMEM medium (see above). The quantity of viable cells was determined by manual counts of trypan blue-stained cells at defined intervals (0, 24, 48, 72, 96, and 168 h).

2.11. BrdU and Caspase-3 Assays

Cell proliferation was examined by the addition of 5 μM of BrdU (5-Bromo-2'-deoxyuridine; Sigma-Aldrich, Steinheim, Germany) to the cells. Thereafter, the cells were seeded on Poly-D-Lysin (Sigma, St. Louis, MI, USA)-coated coverslips. After 4 h at 37° and 10% CO_2, the cells were fixed in 4% paraformaldehyde (PFA). Subsequently, the cells were permeabilized with 0.1% triton X-100 (Sigma, St. Louis, MI, USA) in PBS for 30 min. To prevent unspecific binding, the cells were blocked in PBS containing 5% BSA (bovine serum albumin; Sigma, St. Louis, MI, USA) and 5% NGS (normal goat serum; Dako, Santa Clara, CA, USA). Next, the cells were incubated overnight at 4 °C with a rat anti-BrdU primary antibody (1:1000; cat. #ab6326; Abcam, Cambridge, UK). The next day the cells were washed (3×5 min with PBS) and incubated with an Alexa Fluor 594-labeled goat anti-rat secondary antibody (1:1000 in PBS; cat. #A-1007, Molecular Probes, Eugene, OR, USA). The number of proliferating cells was determined by manual counting.

Caspase-3-dependent apoptosis was investigated by seeding cells on coverslips and fixing them 2 h later with 4% PFA. The cells were treated with a blocking solution (5% BSA, 5% NGS, and 0.1% triton in PBS) for 1 h at room temperature, followed by incubation with a cleaved, active caspase-3 antibody (1:400; cat. #9664, Cell Signaling Technology, Danvers, MA, USA), overnight at 4 °C. The next day, the cells were washed with PBS three times (5 min each) and incubated with an Alexa Fluor 594-labeled goat anti-rabbit secondary antibody (1:1000 in PBS; cat. #A-11012, Molecular Probes, Eugene, OR, USA). The number of caspase-3-dependent apoptotic cells was determined by manual counting.

2.12. GIPR Inhibitor Studies

For the GIPR inhibitor studies, 4×10^4 cells transduced with GIPR or control lentiviral supernatant were seeded in 100 μL of DMEM medium in a 96-well plate (Greiner, Kremsmünster, Austria). The cells were treated with the GIPR inhibitor MK0893 (MedChemExpress, Monmouth Junction, NJ, USA) diluted in DMSO (Sigma-Aldrich, Steinheim, Germany) at a final concentration of 5 nM or a DMSO (Sigma-Aldrich, Steinheim, Germany) control. Two hours later, recombinant TFF1 (rTFF1; Preprotech, Cranbury, NJ, USA) reconstituted in water was added at a final concentration of 5 μM. The controls were treated with water.

2.13. In Ovo Chorioallantoic Membrane (CAM) Assays

In order to quantify changes in tumor formation capacity, tumor size, and weight of GIPR-overexpressing RB cells, 1×10^6 cells transduced with GIPR or control virus particles were grafted onto the chorioallantoic membrane (CAM) of fertilized chicken eggs (see Figure 1) as described previously [50] based on the protocol of Zijlstra and Palmer [55,56]. Twenty-five fertilized eggs were grafted in at least three independent experiments. On chick embryonic developmental day (EDD) 17, seven days after grafting of the RB cells at EDD10, the tumors were excised, measured, and photographed as described previously [22,57,58].
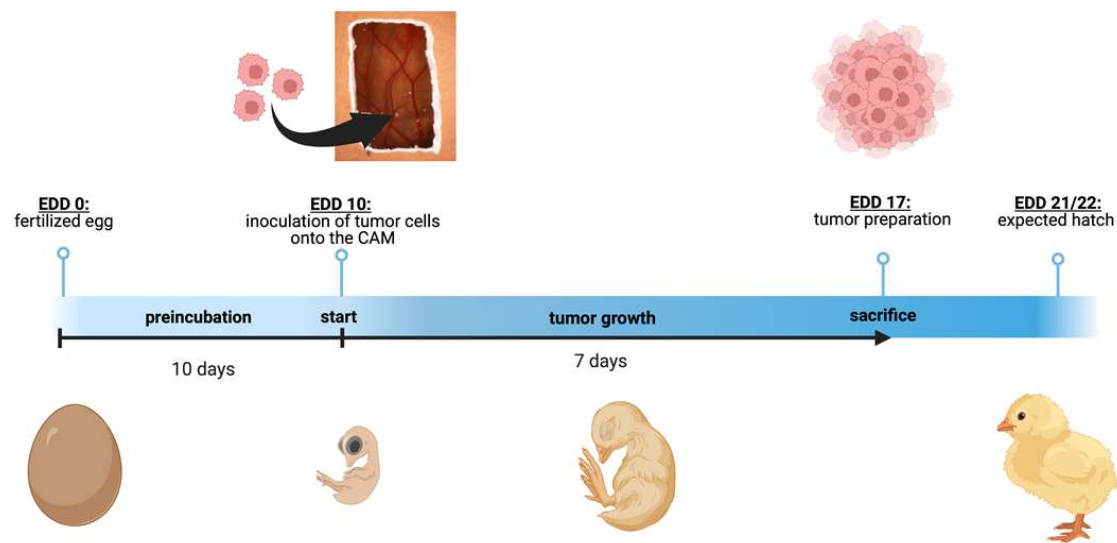
Figure 1. Schematic depiction of the chorioallantoic membrane (CAM) assay. Timeline of the in ovo chorioallantoic membrane (CAM) tumor cell graft model. Fertilized chicken eggs were incubated for 10 days. On embryonic development day (EDD) 10, the eggs were opened, and tumor cells were inoculated onto the CAM. On EDD 17, four days before hatching, the tumors were harvested and analyzed. The figure was created with BioRender© at https://www.biorender.com (accessed on 31 October 2023).

2.14. Cancer-Related Protein Expression Profiling

The expression levels of 84 human cancer-related proteins were evaluated in Weri cells transduced with either GIPR or control lentiviral supernatant using the Proteome Profiler Human XL Oncology Array (R&D Systems, Minneapolis, MN, USA). The expression levels were determined in duplicate, using 200 μg of protein following the manufacturer's protocol.

2.15. Statistical Analysis

The statistics were calculated using GraphPad Prism 9. The data presented represent the means ± standard error of the mean (SEM) from at least three experiments. The data were analyzed by Student's t-test, and statistical significance was assigned for *p*-values less than 0.05 (*), 0.01 (**), 0.001 (***), or 0.0001 (****).

Statistical analyses of growth curves were performed using a web interface (http://bioinf. wehi.edu.au/software/compareCurves/, accessed on 4 December 2023). This interface allows one to compare growth curves from the statmod statistical modeling package, which is available through the "R Project for Statistical Computing" (http://www.r-project.org, accessed on 4 December 2023).

For biological pathway and gene ontology (GO) term analyses on the target genes, we used a Kyoto encyclopedia of genes and genomes (KEGG) pathway enrichment analysis, using the database for annotation, visualization, and integration discovery (DAVID) software [59]. The analysis, based on hypergeometric distribution, utilized a significance threshold of $p < 0.05$ for the selection of GO terms and pathways.

3. Results

3.1. GIPR and TFF1 Are Co-Expressed in Retinoblastoma Tumors

Previous investigations by our group revealed that the G protein-coupled receptor (GPCR) GIPR is one of the genes with the highest fold change in expression after TFF1 overexpression in RB cells. First, we verified GIPR upregulation upon successful lentiviral TFF1 overexpression (Figure 2a,c) in the RB cell lines Weri and Y79 in terms of the RNA level by Real-Time PCR (Figure 2b). In terms of the protein level, GIPR expression was, however, only significantly upregulated in Weri RB cells, as revealed by a Western blot

analysis (Figure 2c). The uncropped blots and molecular weight markers are shown in Supplementary Figure S2.
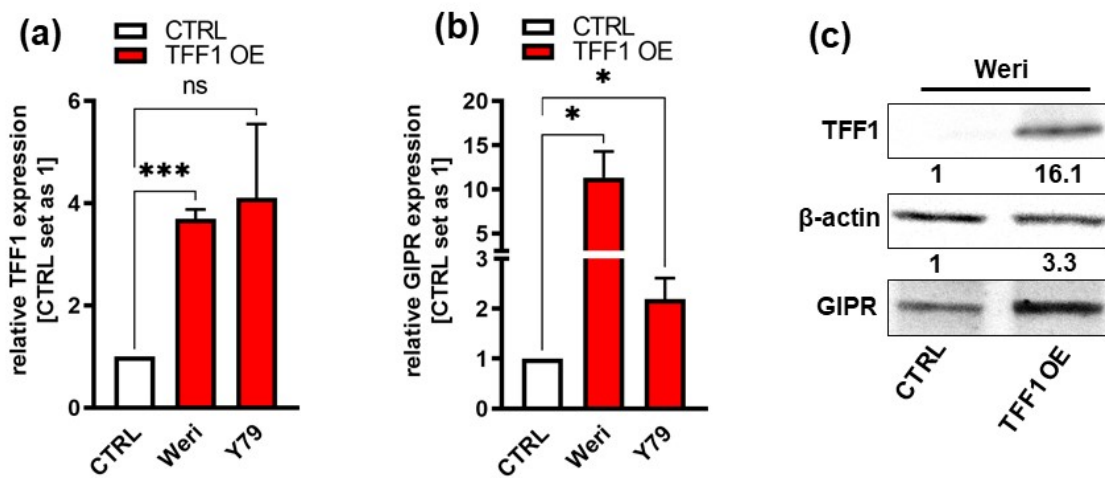

Figure 2. Verification of GIPR upregulation after lentiviral TFF1 overexpression in two retinoblastoma cell lines. (**a**) Verification of TFF1 overexpression in Weri and Y79 RB cells via Real-Time PCR. (**b**) After lentiviral TFF1 overexpression in two RB cell lines, GIPR is significantly upregulated at the mRNA level, as revealed by Real-Time PCR. (**c**) In TFF1-overexpressing Weri RB cells, GIPR is likewise upregulated at the protein level, as revealed by a Western blot analysis. CTRL = cells transduced with control vector; TFF1 OE = TFF1 overexpression. Values represent the means ± SEM; significances are calculated by an unpaired Student's *t*-test. ns: not significant; * $p < 0.05$; and *** $p < 0.001$.

Next, we investigated GIPR's expression levels in retinoblastoma primary tumor tissue and correlated them with TFF1 expression. Real-Time PCR analyses revealed that cultured primary RB patient-derived tumor cells, which do not express TFF1 (TFF1-negative; TFF1) displayed similar GIPR levels to healthy human retina (hRet; Figure 3a). TFF1-expressing (TFF1-positive; TFF1+) RB tumor cells, by contrast, showed significantly increased GIPR expression compared to TFF1-RB tumor cells and compared to hRet (Figure 3a). Formalin-fixed paraffin-embedded TFF1-RB patient tumors displayed higher, yet not significantly increased, GIPR levels compared to hRet, whereas TFF1+ tumors showed significantly increased GIPR expression compared to hRet and TFF1-RB tumors (Figure 3b). Exemplary immunohistochemical stains of RB patient tumor sections revealed that TFF1+ tumors are also positive for GIPR, whereas TFF1-tumors also stain negatively for GIPR (Figure 3c). The co-expression of GIPR and TFF1 in RB patient tumors, which did express TFF1, allowed potential TFF1 signaling via the GIPR receptor.
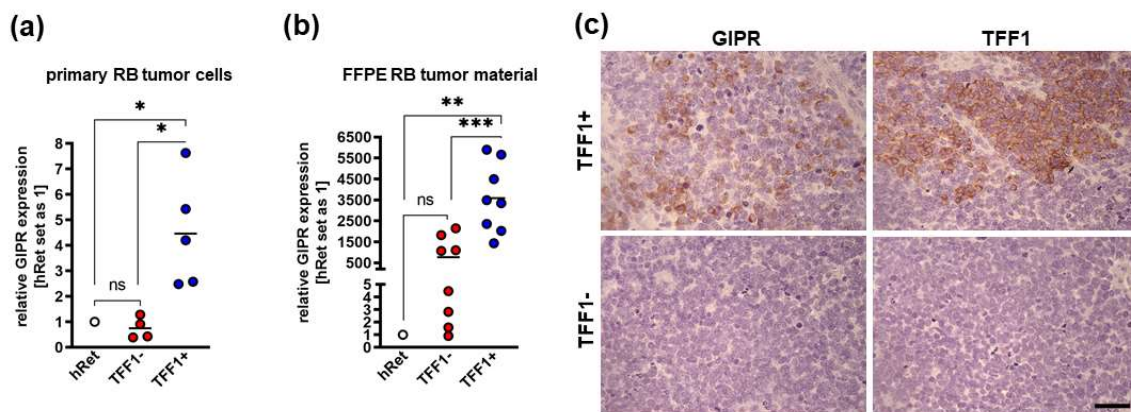
Figure 3. GIPR expression in TFF1-negative and TFF1-positive primary RB patient tumors. (**a**) Cultured TFF1-negative (TFF1-) patient-derived retinoblastoma (RB) tumor cells display similar GIPR

mRNA levels to healthy human retina (hRet) as revealed by Real-Time PCR. By contrast, TFF1-positive (TFF1+) RB tumor cells show significantly increased GIPR expression. GIPR expression in TFF1+ primary RB tumor cells is significantly increased compared to TFF1- tumor cells. (**b**) Real-Time PCR analyses with RNA extracted from formalin-fixed paraffin-embedded (FFPE) RB patient tumors revealed that TFF1-RB tumors show higher, yet not significantly increased, GIPR mRNA levels compared to hRet, whereas TFF1+ tumors display significantly increased GIPR expression compared to hRet and TFF1-RB tumors. (**c**) Exemplary immunohistochemical stains against GIPR and TFF1 (brown) in TFF1+ and TFF1- in hematoxylin counterstained (blue) paraffin sections of RB patient tumors. Scale bar: 50 μm; applies to all pictures in C. Values represent the means $\pm$ SEM; significances are calculated by an unpaired Student's *t*-test. ns = $p > 0.05$; * $p < 0.05$; ** $p < 0.01$; and *** $p < 0.001$.

3.2. GIPR Overexpression Results in Decreased Cell Viability, Cell Growth, and Proliferation as Well as Increased Apoptosis in RB Cell Lines In Vitro

In order to investigate if the decrease in RB cell viability, cell growth, proliferation, and tumorigenicity and the increase in apoptosis seen after TFF1 overexpression might be mediated via the GIPR signaling axis, we transduced GIPR in the RB cell lines Weri and Y79, generating stably GIPR-overexpressing cells. Successful GIPR overexpression was verified by Real-Time PCR (Figure 4a), Western blot analysis (Figure 4b), and immunofluorescence staining (Figure 4c). The uncropped blots and molecular weight markers are shown in Supplementary Figure S3.
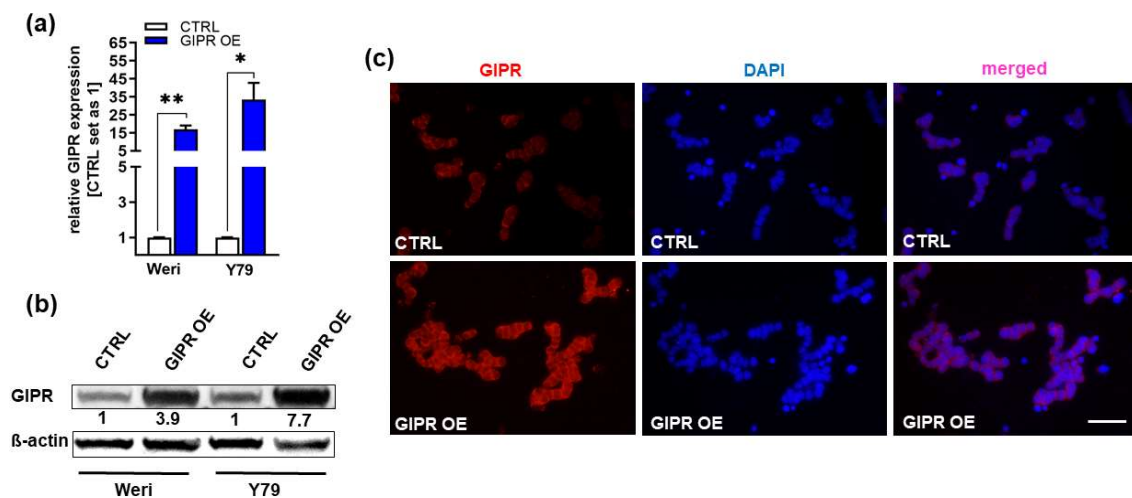
Figure 4. Verification of GIPR overexpression in retinoblastoma cell lines. (**a**) Verification of GIPR overexpression (OE) in the retinoblastoma (RB) cell lines Weri and Y79 on mRNA level via Real-Time PCR. (**b**) Verification of GIPR overexpression at the protein level via Western blot analysis in the RB cell lines Weri and Y79. (**c**) Immunofluorescent stains against GIPR (red fluorescence) with DAPI (blue) counterstaining after GIPR overexpression in Weri RB cells. Scale bar: 50 μm (applies to all pictures in (**c**). CTRL = cells transduced with control vector; GIPR OE = GIPR overexpression. Values represent the means $\pm$ SEM; significances are calculated by an unpaired Student's *t*-test. * $p < 0.05$; ** $p < 0.01$.

Cell viability was significantly decreased after GIPR overexpression in both of the RB cell lines investigated as revealed by WST-1 viability assays (Figure 5a). Accordingly, our growth curve analyses showed significantly diminished growth rates of Weri and Y79 GIPR-overexpressing cells compared to the control cells (Figure 5b,c) and the proliferation levels of both cell lines were also decreased, as revealed by the BrdU cell counts (Figure 5d,e). Additionally, a significant increase in caspase-3-dependent apoptosis was seen upon GIPR overexpression in both cell lines, as revealed by the quantification of immunofluorescent staining against cleaved caspase-3 (Figure 5f). In summary, the impact

of GIPR overexpression mirrors the effects previously seen upon TFF1 overexpression, indicating potential TFF1 signaling via the GIPR axis.
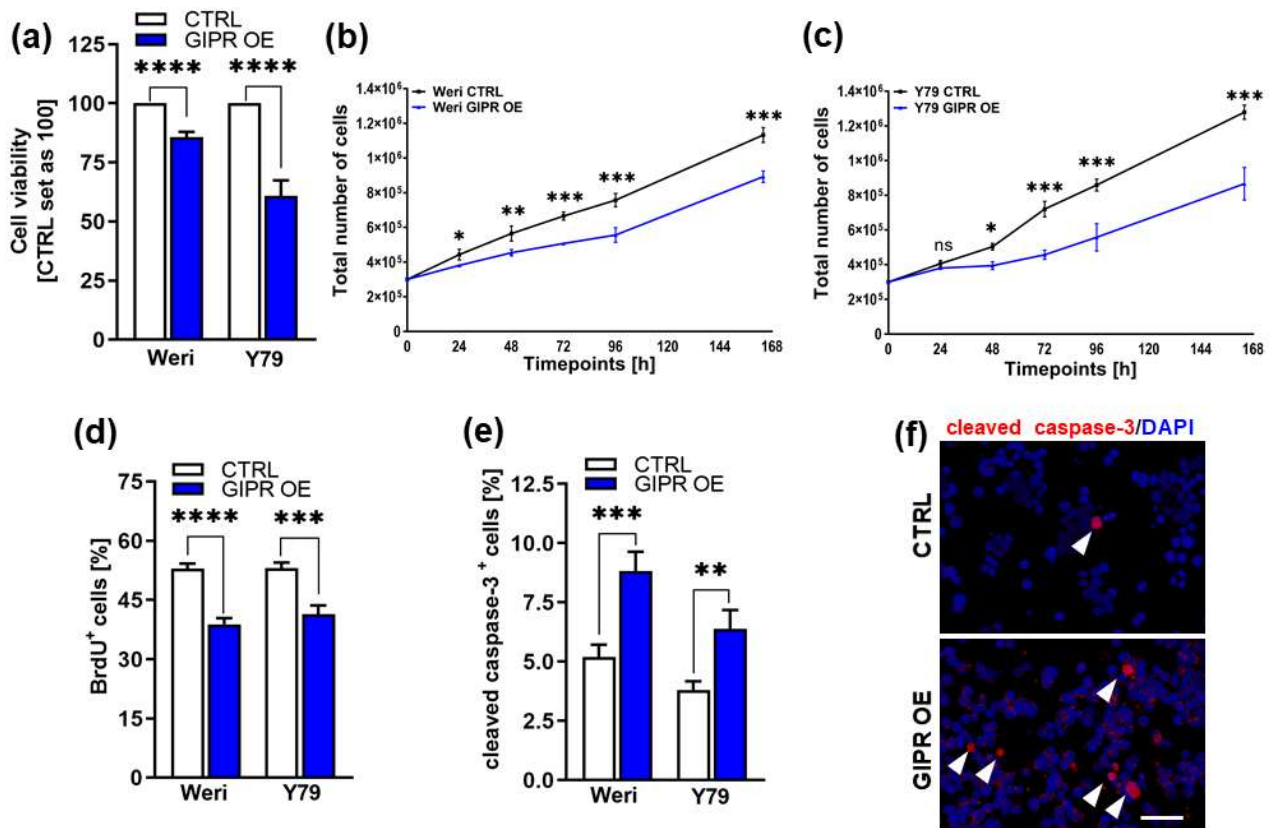

Figure 5. In vitro effects of GIPR overexpression in retinoblastoma cell lines. (**a**) Cell viability was significantly decreased following GIPR overexpression (GIPR OE; blue bars) in the retinoblastoma (RB) cell lines Weri and Y79, as revealed by WST-1 assays. (**b**,**c**) Growth kinetics of Weri (**b**) and Y79 (**c**) RB cells were significantly decreased after GIPR overexpression. (**d**) Proliferation of Weri and Y79 cells was significantly decreased after GIPR overexpression, as revealed by the quantification of BrdU stains. (**e**) The significant increase in apoptosis after GIPR overexpression in Weri and Y79 cells was caspase-3-dependent, as revealed by the quantification of immunocytochemical stains against cleaved caspase-3. (**f**) Immunocytochemical stains against cleaved caspase-3 in Weri control cells (CTRL) and GIPR-overexpressing (GIPR OE) Weri cells. Arrowheads indicate cleaved caspase-3-positive (cleaved caspase-3$^+$) cells. Scale bar 50 μm. CTRL = cells transduced with control vector. Values represent the means ± SEM; significances were calculated by an unpaired Student's *t*-test. ns = $p > 0.05$; * $p < 0.05$; ** $p < 0.01$; *** $p < 0.001$; and **** $p < 0.0001$.

3.3. GIPR-Overexpressing RB Cells Form Significantly Smaller Tumors In Vivo

Next, we used the chicken chorioallantoic membrane (CAM) assay to examine the impact of GIPR overexpression on RB cell tumor growth and formation capacity in an in vivo model (for the schematic depiction, see Figure 1). Stably GIPR-overexpressing Weri and Y79 cells were inoculated into the CAM of 10-day-old chicken embryos. The quantification of CAM tumor weight and size revealed that both GIPR-overexpressing RB cell lines investigated formed significantly lighter and smaller tumors in ovo than the control cells (Figure 6a,b,d). Compared to the controls, the tumor formation capacity was not significantly changed in the GIPR-overexpressing Weri and Y79 cells (Figure 6c).
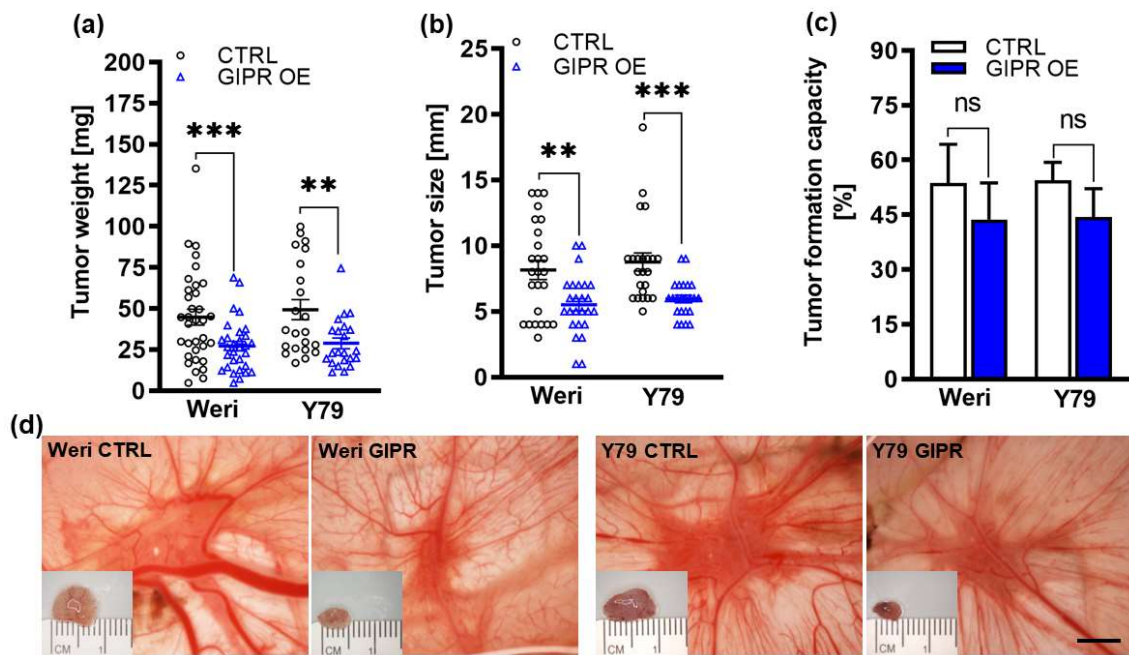
Figure 6. In vivo effects of GIPR overexpression in in ovo CAM assays. (**a–c**) Quantification of weight, size, and formation capacity of CAM tumors developing from GIPR-overexpressing (GIPR OE) Weri and Y79 RB cells inoculated in the CAM. (**d**) Representative pictures of RB CAM tumors in situ and excised tumors on a ruler (insets). GIPR-overexpressing RB cells form significantly smaller tumors in the in ovo CAM assay. Scale bar in (**d**): 5 mm; applies to all pictures. CTRL = cells transduced with control vector. Values represent the means ± SEM; significances are calculated by an unpaired Student's *t*-test. ns = $p > 0.05$; ** $p < 0.01$; and *** $p < 0.001$.

3.4. Impact of the Administration of a GIPR Inhibitor and/or Recombinant TFF1 on Cell Viability, Proliferation, and Cell Death of GIPR-Overexpressing RB Cell Lines

Next, we set out to address the question of whether the effects seen after GIPR overexpression are specific and if GIPR might be a receptor for TFF1. For this purpose, we blocked GIPR signaling after its overexpression in two RB cell lines with a specific inhibitor (MK0893) and treated the cells with recombinant TFF1 (rTFF1) alone or in combination with MK0893 and analyzed effects on cell viability, proliferation, and apoptosis.

The significant reduction in cell viability and proliferation as well as the induction of apoptosis seen after GIPR overexpression in the retinoblastoma cell lines Weri and Y79 were significantly reversed upon the administration of MK0893 (Figure 7a–f), indicating that the effects seen after GIPR overexpression on RB cells were specific. The treatment of GIPR-overexpressing RB cells with rTFF1 did not change the cell viability, proliferation, or apoptosis levels compared to those of untreated GIPR-overexpressing cells (Figure 7a–f). Thus, no additive or synergistic effect due to the binding of TFF1 to the upregulated GIPR receptor levels in GIPR-overexpressing cells could be observed. By contrast, the combined treatment with the GIPR inhibitor and rTFF1 resulted in a significant decrease in cell viability and proliferation compared to the administration of the GIPR inhibitor alone (Figure 7a–e), indicating that the effects on cell viability and proliferation induced by TFF1 were independent of GIPR. However, an induction of apoptosis upon treatment with rTFF1 in comparison to an induction of apoptosis by MK0893 alone could not been detected (Figure 7c,e). Although our data revealed that GIPR is not a direct TFF1 receptor, the fact that GIPR is upregulated after TFF1 overexpression and that the same effects are induced upon GIPR and TFF1 overexpression indicate that TFF1 and GIPR are involved in the same signaling cascades.
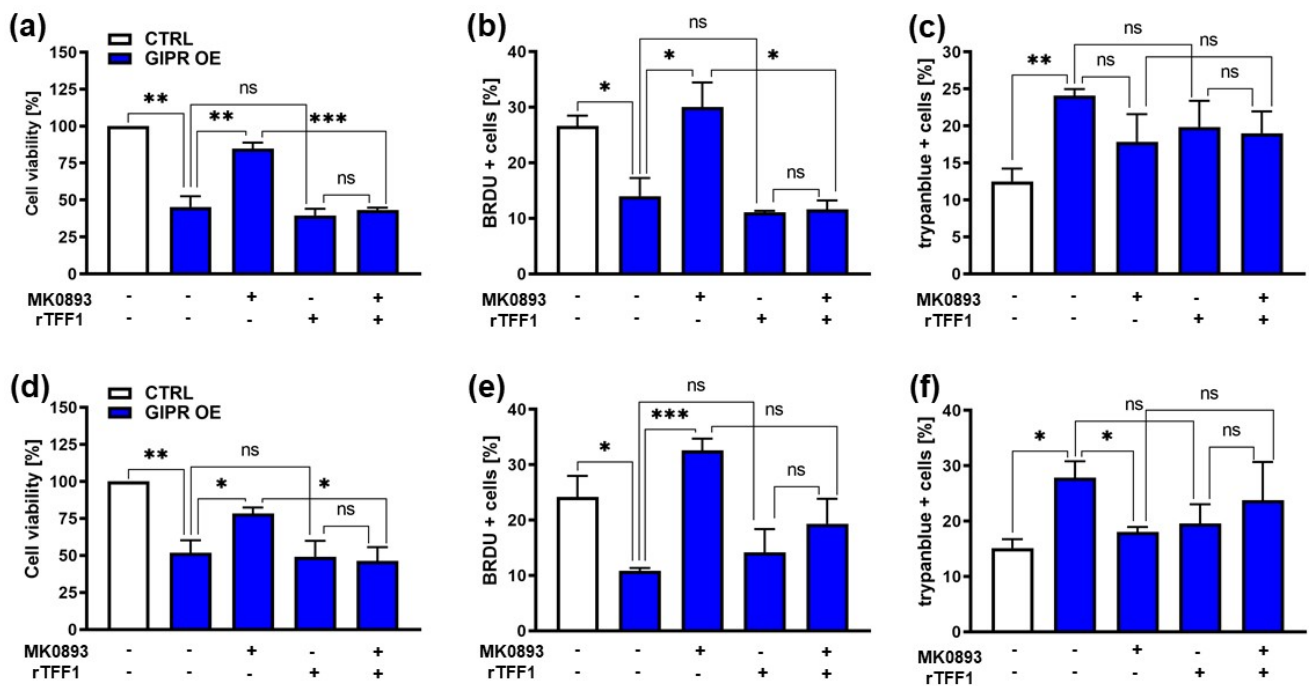
Figure 7. Effects of administration of a GIPR inhibitor and recombinant TFF1 on GIPR-overexpressing RB cells. (**a**,**d**) Cell viability was significantly decreased following GIPR overexpression (GIPR OE; blue bars) in the retinoblastoma (RB) cell lines Weri (**a**) and Y79 (**d**), as revealed by WST-1 assays after 24 h. After the administration of the GIPR inhibitor MK0893, the effect was reversed. The addition (+) of recombinant TFF1 (rTFF1) or a combination of MK0893 and rTFF1 did not lead to changes in cell viability compared to untreated GIPR-overexpressing cells (−). (**b**,**e**) Cell proliferation in Weri (**b**) as well as in Y79 (**c**) cells was decreased after GIPR overexpression, as revealed by the quantification of BrdU stains. Following the administration of MK0893, the effect was reversed, and the proliferation levels exceeded those of the control cells, transduced with a control vector (CTRL). The addition of rTFF1 did not lead to changes in proliferation compared to the untreated GIPR-overexpressing cells. (**c**,**f**) Changes in the cell death levels after GIPR overexpression were revealed by the counting of trypan blue-positive cells. GIPR overexpression resulted in an increased apoptosis level of Weri (**c**) and Y79 (**f**) cells. Following the administration of MK0893, the cell death levels dropped significantly in Y79 (**f**) but not in the Weri cell line. The addition of rTFF1 did not lead to significant changes compared to the cell death levels of the untreated controls. The legends in a and d also apply to all the other graphs. Values represent the means ± SEM; significances are calculated by an unpaired Student's *t*-test. ns = $p > 0.05$; * $p < 0.05$; ** $p < 0.01$; and *** $p < 0.001$.

3.5. GIPR Expression in Retinoblastoma Cells and Its Regulation by miR-542-5p

As GIPR has previously been described as a potential target gene of miR-542-5p [60], we analyzed the expression of this miR and GIPR in Weri and Y79 RB cells in comparison to healthy human retina. Compared to healthy human retina, GIPR expression was significantly increased in both of the RB cell lines investigated (Figure 8a), whereas the miR-542-5p expression levels were significantly decreased (Figure 8b). The opposing expression of miR-542-5p and GIPR suggests that the GIPR levels in RB cells might be regulated by mir-542-5p. This hypothesis was supported by the observation that GIPR expression significantly decreased (Figure 8d) upon transient mir-542-5p overexpression (Figure 8c) in Weri and Y79 cells. In order to analyze if TFF1 is also involved in the miR-542-5p GIPR signaling axis, we additionally investigated the expression of TFF1 after miR-542-5p overexpression as well as the miR-542-5p expression levels after TFF1 overexpression. Our data, however, did not reveal a regulatory mechanism between miR-542-5p and TTF1 (Supplementary Figure S4).
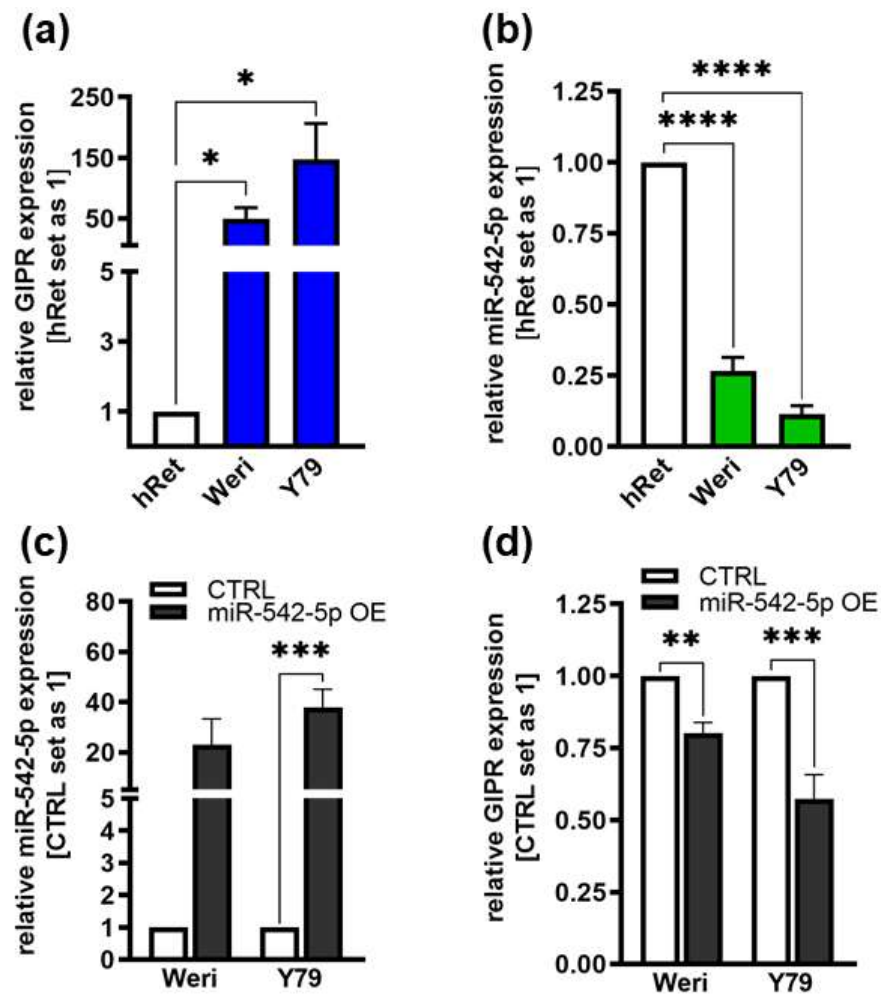
Figure 8. Endogenous GIPR and miR-542-5p expression levels in RB cell lines and expression after miR-542-5p overexpression. (**a**,**b**) Compared to healthy human retina (hRet), the RB cell lines Weri and Y79 displayed increased GIPR ((**a**); blue bars) and decreased miR-542-5p ((**b**); green bars) mRNA expression levels, as revealed by Real-Time PCR. (**c**,**d**) After successful miR-542-5p overexpression (grey bars; (**c**)), verified by Real-Time PCR, the RB cell lines displayed significantly decreased GIPR mRNA expression levels (**d**). CTRL = cells transduced with control vector. miR-542-5p OE = miR-542-5p overexpression. Values represent the means $\pm$ SEM; non-significant *p*-values are not shown. * $p < 0.05$; ** $p < 0.01$; *** $p < 0.001$; and **** $p < 0.0001$.

Target scans predicted a potential binding site for miR-542-5p within the 3′-UTR region of the *GIPR* gene (Figure 9a). Luciferase activity assays were performed to assess the binding of miR-542-5p to the GIPR 3′-UTR region. Our binding study revealed that miR-542-5p binds to the wildtype binding site of GIPR in the 3′-UTR detected by significantly reduced luciferase activity (Figure 9b). As a control for the binding specificity, we mutated the GIPR binding site (Figure 9a) and measured the binding of miR-542-5p. In this setting, luciferase activity remained unchanged compared to the binding of the empty vector control (Figure 9b), indicating that miR-542-5p has the capability to specifically bind to and regulate GIPR expression in RB cell lines.
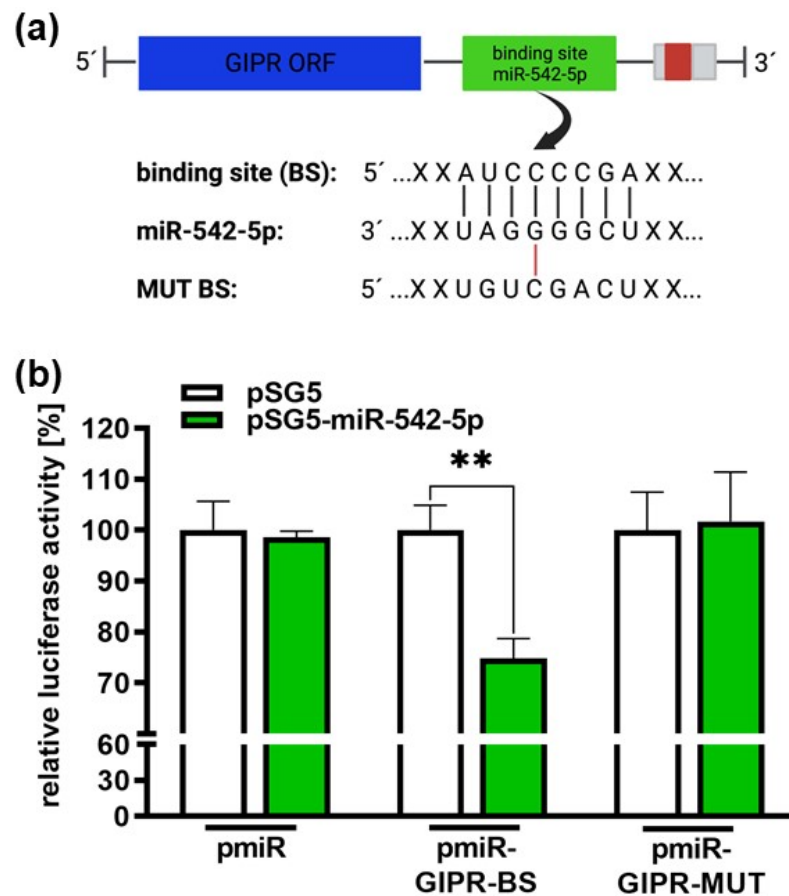
Figure 9. Binding studies of miR-542-5p to the 3′-UTR region of GIPR. (**a**) Depiction of potential binding sites of miR-542-5p at the 3′-UTR region of the GIPR gene. The GIPR 3′-UTR region contains a potential binding site for miR-542-5p adjacent to the open reading frame (GIPR ORF). MiR-542-5p can bind to the potential binding site (BS), whereas it cannot bind to the mutant binding site (MUT BS). (**b**) For the luciferase binding studies, HEK293T cells were co-transfected with a miR-542-5p expression vector (pSG5-miR542-5p) in addition to either a wildtype (pmiR-GIPR-BS) or mutant (pmiR-GIPR-MUT) vector containing the binding sequence of the GIPR 3′-UTR. Empty vectors (pSG5 and pmiR) served as the controls. After 48 h, decreased luciferase activity indicated the binding of miR-542-5p to the 3′-UTR of the GIPR gene (pmiR-GIPR-BS). No binding was observed for the mutant GIPR binding site (pmiR-GIPR-MUT). The values are the means of at least three independent experiments ± SEM; significances are calculated by an unpaired Student's *t*-test. Non-significant *p*-value calculations are not shown. ** $p < 0.01$. The figure was created with BioRender© at https://www.biorender.com (accessed on 31 October 2023).

3.6. GIPR Downstream Signaling Targets

To gain a deeper insight into GIPR downstream signaling in RB cells, cancer-associated proteins were analyzed in a human oncology array. Following GIPR overexpression 9 out of 84 proteins were differentially regulated in Weri RB cells: BCL_{XL}, enolase 2, ErbB2, FGFb, p27/Kip1, p53, and survivin were upregulated, whereas MMP3 was downregulated compared to the controls (Figure 10). The whole human oncology arrays are shown in Supplementary Figure S5.
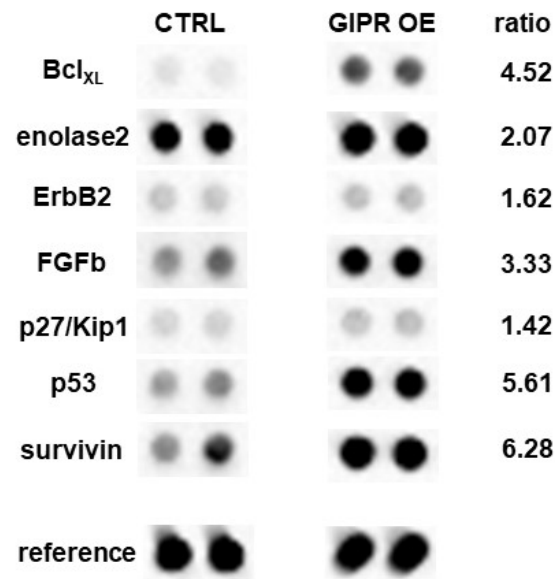
Figure 10. Expression of tumor-related proteins after GIPR overexpression in Weri cells as revealed by a human oncology array. Duplicate spots of differentially expressed proteins are shown. Grey-scale intensities were recorded and the ratios for the control cells vs. the GIPR-overexpressing cells were calculated. CTRL = cells transduced with control vector; GIPR OE = GIPR-overexpressing cells.

Differential expression of these proteins was confirmed at mRNA level via Real-Time PCR (Supplementary Figure S1). In Y79 cells, no significant regulation of the before-mentioned proteins was seen at the protein level. At the mRNA level, by contrast, all the proteins upregulated in the Weri cells were likewise upregulated; however, the levels did not reach significance (Supplementary Figure S1).

DAVID analyses of all the proteins differentially expressed in the Weri cells revealed 10 significantly enriched GO terms (Table S1) and 18 KEGG pathways with at least three counts and $p < 0.05$ (Table S2). Most of the GO terms were related to "apoptosis", "proliferation", "cell migration", "cell cycle", and "angiogenesis", all processes playing an important role in cancer and shown to be affected by GIPR overexpression in RB cells. Nine out of the eighteen identified KEGG pathways were associated with cancer.

4. Discussion

We previously discovered that TFF1 overexpression in RB leads to anti-tumorigenic effects, suggesting a potential tumor suppressor role of TFF1 in this tumor entity [22,23]. Upon TFF1 overexpression, we found GIPR to be one of the highest differentially regulated genes and hypothesized that TFF1's effects on cell viability, growth, proliferation, apoptosis, and tumorigenicity in RB cells might be mediated via the GIPR signaling axis and that GIPR might as well be a receptor for TFF1. Most recently, TFF1 was also identified as an RB biomarker for a subset of more advanced RBs [7,23,24], being detectable in the aqueous humor of RB patients [25,26]. At a first glance, a potential tumor suppressor function of TFF1 and elevated expression levels in more advanced, higher-metastasizing RB tumors seem to be conflicting. However, the two facts are not necessarily contradictory, as various mechanisms potentially upregulate a tumor suppressor in advanced tumors. Possible scenarios are, e.g., cellular stress response to hypoxia and high reactive oxygen species (ROS) levels, frequently observed in more advanced tumor stages, or the activation of the immune system by inflammation, a key player in carcinogenesis. Fittingly, the ectopic expression of TFF1 during chronic inflammation processes and a role of TFF1 as an ROS scavenger have been previously described for various tissues (for review, see [18]). In addition, genetic alterations including mutations or altered epigenetic regulations are potential mechanisms explaining the discrepancy described above. Along this line, we could show that TFF1 is epigenetically regulated in RB [61], and others observed a correlation

between cancer progression and mutations/polymorphisms in the TFF1 gene [62–66]. To gain a deeper understanding of the molecular mechanisms underlying the dual tumor suppressor and biomarker function of TFF1, it is important to gain a deeper insight into its signaling pathways.

Thus, we investigated the general function of GIPR signaling in RB and its correlation with TFF1. In the study presented, we observed significantly elevated GIPR levels in Weri and Y79 RB cells compared to healthy human retina. In a pathological context, human and rat medullary thyroid cancers display high GIPR expression levels compared to normal tissue, and massive overexpression of GIPR was described for neoplastic C cells of both rats and humans [41]. Moreover, GIPR is significantly overexpressed in various neuroendocrine tumors (NETs) compared to normal tissue [67,68]. Particularly, pancreatic, illeal, and bronchial NETs display very high GIPR expression [39]. Moreover, while TFF1-negative RB tumor cells displayed similar GIPR levels to healthy human retina, significantly increased GIPR expression levels were detected in TFF1-positive primary tumor cells, representing the subset of more advanced RBs with TFF1 as an indicating biomarker [7,24]. Additionally, we verified the upregulation of GIPR's levels upon TFF1 overexpression in Weri and Y79 cells at the RNA and protein level, indicating a possible functional correlation of both proteins. In neuroendocrine neoplasms (NENs), high GIPR expression likewise correlates with a high tumor grade. In these tumor entities, GIPR levels gradually increase in a subset of insulinomas and non-functioning pancreatic NENs [40]. Furthermore, increased GIPR expression has been correlated with liver metastasis [69]. Further along this line, Costa et al. observed significantly higher GIPR mRNA levels in malignant adrenocortical carcinomas than in benign adenomas in both pediatric and adult patients [70]. Moreover, the presence of GIPR was demonstrated in advanced colorectal cancer (CRC) and MC-26 and HT29 cells, two CRC cell lines [43]. Interestingly, neither epithelial and stromal gastrointestinal (GI) tumors and GI stromal tumors nor lung adenocarcinomas express GIPR, except for a subgroup of pancreatic adenocarcinomas [39]. Our data support the hypothesis that TFF1 and GIPR, both expressed in higher-grade RB tumors, may be involved in the same signaling pathways.

To further study the functional role of GIPR in RB, we overexpressed GIPR in Weri and Y79 retinoblastoma cells. Increased GIPR expression resulted in significantly reduced cell viability, cell growth, and proliferation, and significantly smaller tumors were formed in in vivo CAM assays as well as significantly increased caspase-3-dependent cell death levels in vitro, mirroring the effects previously seen after TFF1 overexpression [22] and indicating a role of this protein as a tumor suppressor. In previous studies, GIPR signaling was instead mainly linked to the survival of pancreatic ß cells [45]. Contrasting our findings, Campbell et al. demonstrated that pancreatic ß cells from $Gipr^{-/-\text{ßCell}}$ mice with a selective ablation of GIPR displayed a significantly higher sensitivity to apoptosis [45]. Further along this line, in vitro studies in ß-insulin (INS) cells showed that GIP stimulation protected these cells against streptozotocin-induced apoptosis [46]. Moreover, GIP has been shown to promote ß-(INS) cell survival [47] and stimulate the proliferation of MC-26 and HT29 CRC cells expressing the GIPR [43], contradicting the findings of our study, where high GIPR levels after GIPR overexpression reduced cell viability and growth. This discrepancy might be explained in terms of comparing the effects of metabolic signaling along the GIP/GIPR axis with the pathological conditions of a cancer cell line. Otherwise, the effects might be tissue-dependent, as very high GIPR levels in neuroendocrine tumors have been observed to either increase or decrease raised proliferation levels, depending on the tumor site [39,40].

Next, we set out to investigate how GIPR expression is regulated in RB tumor cells. In non-small-cell lung cancer (NSCLC), GIPR has been described as 1 of 457 potential target genes of miR-542-5p [60]. Moreover, it has been shown that pristimerin, a natural-occurring quinone methide triterpenoid with anticancer effects, inhibits glioblastoma progression by targeting two receptors, the protein tyrosine phosphatase, non-receptor type 1 (PTPN1), and Argonaute 2 (AGO2) via miR-542-5p [71]. Target scans confirmed GIPR

as a potential target of this miR, but it has not been experimentally proven so far. In the study presented in this paper, we observed an opposing expression pattern of miR-542-5p and GIPR expression, with GIPR expression being significantly higher in Weri and Y79 RB cells and miR-542-5p levels being significantly lower compared to those in healthy human retina. Upon miR-542-5p overexpression, the GIPR significantly decreased, suggesting that miR-542-5p plays a role in regulating GIPR expression in RB cells. To further address this hypothesis, we performed luciferase binding studies and were able to prove the direct binding of miR-542-5p to the 3′-UTR of the *GIPR* gene. Thus, GIPR expression in RB cells is most likely at least partially regulated by miR-542-5p, without the involvement of TFF1.

A TFF receptor remained unknown for a long time, until, in 2009, the chemokine receptor type 4 (CXCR4), which belongs to the G protein-coupled receptor family (GPCR), was described as a low-affinity receptor for TFF2 [30]. Moreover, Dieckow et al. could show that CXCR4 and CXCR7 are involved in the TFF3-dependent activation of cell migration [31]. Therefore, GPCRs like GIPR, involved in various diseases and, consequently, targets of over 40% of drugs currently on the market [72,73], are potential mediators of TFF signaling. To address the question of whether GIPR is involved in TFF1 signaling as a direct TFF1 receptor, in the study hereby presented, we performed GIPR inhibitor experiments and stimulated the cells with recombinant TFF1 (rTFF1). We could show that the effects of GIPR overexpression are specific, since the reduction in cell viability seen in GIPR-overexpressing cells was reversed upon the administration of the GIPR inhibitor. However, the reduced cell viability in GIPR-overexpressing cells induced by rTFF1 could not be reversed by inhibiting GIPR, indicating that this effect is not GIPR-dependent and, thus, that GIPR is most likely not a direct TFF1 receptor.

Subsequently, we investigated the downstream targets of GIPR signaling in RB cells via a human oncology array, revealing p53 as one of the upregulated proteins in Weri and Y79 RB cells. The tumor suppressor gene *TP53* is, for instance, involved in the regulation of cell cycle arrest and apoptosis [74–76]. Our group already demonstrated that TFF1 induces apoptosis and decreases proliferation and tumor growth in human retinoblastoma cell lines in a p53-dependent manner [22]. Thus, upregulated p53 levels following GIPR overexpression would support the hypothesis that TFF1′s effects are mediated via GIPR signaling. Since it has been shown that p53 induces cell death via the transcriptional activation of the pro-apoptotic protein Bax [77] or direct binding to Bcl2 and Bcl$_{XL}$ [78], we also investigated the expression of these proteins. In our Western blot analyses, we did not observe any significant changes in the protein expression levels of Bax and Bcl2 following GIPR overexpression in Weri and Y79 cells. Bcl$_{XL}$, on one hand, was found to be upregulated by GIPR overexpression in Weri and Y79 cells. In our setting, increased levels of the anti-apoptotic protein Bcl$_{xL}$ at a first glance did not correlate with increased apoptosis levels following GIPR overexpression in RB cells. However, since p53 was also upregulated after GIPR overexpression, a possible scenario fitting our effects could be a direct induction of mitochondrial outer-membrane permeabilization (MOMP) via interaction with anti-apoptotic Bcl$_{xL}$, which, in turn, would lead to caspase-dependent apoptosis [78]. This would confirm our previously shown results, according to which TFF1 induces the apoptosis of human RB cell lines in a caspase-dependent manner [22]. Fittingly, in the study hereby presented, the increase in apoptosis seen after GIPR overexpression in RB tumor cells was likewise caspase-3-dependent. In addition, it has been demonstrated that the GIP-mediated suppression of apoptosis in a pancreatic ß-insulin cell line is caspase-3-dependent [42,46]. Moreover, "regulation of apoptosis" was a significantly enriched GO term in GIPR-overexpressing Weri RB cells, and "apoptosis" was one of the enriched KEGG pathways.

In conjunction with apoptosis regulation, we found survivin, an anti-apoptotic family member of the inhibitor of apoptosis proteins (IAPs; for review, see [79]), to be upregulated in GIPR-overexpressing Weri cells. Survivin is overexpressed in various tumor entities, and its overexpression frequently correlates with cancer progression and recurrence [79]. Increased levels of survivin, however, do not correlate with increased apoptosis levels and

reduced tumorigenicity following GIPR overexpression in Weri RB cells. These discrepancies might be explained in terms of the counter-regulatory mechanisms induced by the pro-apoptotic effects seen after GIPR overexpression.

In the study hereby presented, fibroblast growth factor 2 (FGF2/FGFb) was likewise upregulated upon GIPR overexpression in RB cells. FGFs are known as key factors in tissue homeostasis and cancer. FGFb regulates the self-renewal of multiple stem cell types and plays a pivotal role in brain tumors, particularly in malignant glioma [80]. Downstream signaling involves the FGF receptor family, PI3K/AKT, and RAS/RAF/MAPK, which also exert pro-proliferative and anti-apoptotic effects during metabolic signaling along the GIP/GIPR axis [42–44,81]. Therefore, we analyzed the phosphorylation status of Akt and the MAP kinase ERK1/2 after GIPR overexpression in Weri and Y79 RB cells; however, we observed no obvious changes in phosphorylation. In line with these findings, in medullary thyroid cancer, the cell effects of GIPR receptor stimulation on the downstream PI3K-Akt and MAPK-ERK1/2 signaling axis were likewise only marginal [34]. How upregulated FGFb expression fits into these signaling pathways and the GIPR-mediated effects seen in RB cells remains to be further investigated.

In summary, we identified GIPR as a potential key player involved in TFF1 signaling, triggering tumor-suppressing effects in RB, most likely with the involvement of miR-542-5p and p53 as up- and downstream mediators.

5. Conclusions

In the study hereby presented, the stable overexpression of the G protein-coupled transmembrane receptor GIPR, shown to be upregulated following the overexpression of TFF1, resulted in significantly increased apoptosis levels and a concomitant decrease in cell viability, growth, and proliferation in vitro as well as tumor growth in vivo, suggesting a tumor suppressor role of GIPR in RB. Although our data indicate that GIPR is not a receptor for TFF1, TFF1 and GIPR seem to be involved in the same signaling cascades, and up- and downstream signaling mediators like miR-542-5p and p53 are potential targets for new retinoblastoma treatment approaches. In future experiments, these novel treatment and adjuvant therapy options, e.g., modified nanoparticles, should be tested using in ovo and in vivo rodent models in order to optimize future RB treatment.

Supplementary Materials: The following supporting information can be downloaded at https://www.mdpi.com/article/10.3390/cancers16091656/s1, Figure S1: Verification of human oncology array data via Real-Time PCR; Figure S2: Uncropped Western blots shown in Figure 2c; Figure S3: Uncropped Western blots shown in Figure 4b; Figure S4: Hypothetical TFF1-miR-542-5p or miR-542-5p-TFF1 signaling axis; Figure S5: Uncropped human oncology array shown in Figure 10; Table S1: Significantly enriched GO terms of genes differentially expressed after GIPR overexpression in Weri RB cells; Table S2: Significantly enriched KEGG pathways of genes differentially expressed after GIPR overexpression in Weri RB cells.

Author Contributions: Conceptualization, M.A.B. and N.D.; methodology, A.H. and M.A.B.; validation, M.A.B. and A.H.; formal analysis, A.H.; investigation, A.H., E.A., F.Y. and D.V.M.; data curation, A.H. and M.A.B.; writing—original draft preparation, N.D., M.A.B. and A.H.; writing—review and editing, N.D. and M.A.B.; visualization, A.H.; supervision, M.A.B. and N.D.; project administration, N.D. and M.A.B. All authors have read and agreed to the published version of the manuscript.

Institutional Review Board Statement: This study was conducted according to the guidelines of the Declaration of Helsinki, and approval for the use of human retinal tissue (approval no. 06-30214) and RB samples (approval no. 14-5836-BO) was granted by the Ethics Committee of the Medical Faculty at the University Hospital Essen, University of Duisburg-Essen.

Informed Consent Statement: Informed consent was obtained from all the subjects involved in this study.

References

1. Byroju, V.V.; Nadukkandy, A.S.; Cordani, M.; Kumar, L.D. Retinoblastoma: Present scenario and future challenges. *Cell Commun. Signal.* **2023**, *21*, 226. [CrossRef]
2. Bouchoucha, Y.; Matet, A.; Berger, A.; Carcaboso, A.M.; Gerrish, A.; Moll, A.; Jenkinson, H.; Ketteler, P.; Dorsman, J.C.; Chantada, G.; et al. Retinoblastoma: From genes to patient care. *Eur. J. Med. Genet.* **2023**, *66*, 104674. [CrossRef] [PubMed]
3. Bornfeld, N.; Lohmann, D.; Bechrakis, N.E.; Biewald, E. [Retinoblastoma]. *Der Ophthalmol.* **2020**, *117*, 389–402. [CrossRef] [PubMed]
4. Roy, S.; Kaliki, S. Retinoblastoma: A Major Review. *Mymensingh Med. J. MMJ* **2021**, *30*, 881–895. [PubMed]
5. Dimaras, H.; Corson, T.W. Retinoblastoma, the visible CNS tumor: A review. *J. Neurosci. Res.* **2019**, *97*, 29–44. [CrossRef] [PubMed]
6. Rathore, S.; Verma, A.; Ratna, R.; Marwa, N.; Ghiya, Y.; Honavar, S.G.; Tiwari, A.; Das, S.; Varshney, A. Retinoblastoma: A review of the molecular basis of tumor development and its clinical correlation in shaping future targeted treatment strategies. *Indian J. Ophthalmol.* **2023**, *71*, 2662. [CrossRef] [PubMed]
7. Liu, J.; Ottaviani, D.; Sefta, M.; Desbrousses, C.; Chapeaublanc, E.; Aschero, R.; Sirab, N.; Lubieniecki, F.; Lamas, G.; Tonon, L.; et al. A high-risk retinoblastoma subtype with stemness features, dedifferentiated cone states and neuronal/ganglion cell gene expression. *Nat. Commun.* **2021**, *12*, 5578. [CrossRef]
8. Chronopoulos, A.; Babst, N.; Schiemenz, C.; Schutz, J.S.; Heindl, L.M.; Ranjbar, M.; Kakkassery, V. A Narrative Review—Therapy Options and Therapy Failure in Retinoblastoma. *Neurosignals* **2022**, *30*, 39–58. [PubMed]
9. Shields, C.L.; Bas, Z.; Laiton, A.; Silva, A.M.V.; Sheikh, A.; Lally, S.E.; Shields, J.A. Retinoblastoma: Emerging concepts in genetics, global disease burden, chemotherapy outcomes, and psychological impact. *Eye* **2023**, *37*, 815–822. [CrossRef] [PubMed]
10. Kaewkhaw, R.; Rojanaporn, D. Retinoblastoma: Etiology, Modeling, and Treatment. *Cancers* **2020**, *12*, 2304. [CrossRef]
11. Munier, F.L.; Beck-Popovic, M.; Chantada, G.L.; Cobrinik, D.; Kivelä, T.T.; Lohmann, D.; Maeder, P.; Moll, A.C.; Carcaboso, A.M.; Moulin, A.; et al. Conservative management of retinoblastoma: Challenging orthodoxy without compromising the state of metastatic grace. "Alive, with good vision and no comorbidity". *Prog. Retin. Eye Res.* **2019**, *73*, 100764. [CrossRef] [PubMed]
12. Manjandavida, F.P.; Shields, C.L. The role of intravitreal chemotherapy for retinoblastoma. *Indian J. Ophthalmol.* **2015**, *63*, 141–145. [CrossRef] [PubMed]
13. Francis, J.H.; Abramson, D.H.; Ji, X.; Shields, C.L.; Teixeira, L.F.; Schefler, A.C.; Cassoux, N.; Hadjistilianou, D.; Berry, J.L.; Frenkel, S.; et al. Risk of Extraocular Extension in Eyes With Retinoblastoma Receiving Intravitreous Chemotherapy. *JAMA Ophthalmol.* **2017**, *135*, 1426. [CrossRef] [PubMed]
14. Shields, C.L.; Manjandavida, F.P.; Arepalli, S.; Kaliki, S.; Lally, S.E.; Shields, J.A. Intravitreal Melphalan for Persistent or Recurrent Retinoblastoma Vitreous Seeds: Preliminary Results. *JAMA Ophthalmol.* **2014**, *132*, 319. [CrossRef] [PubMed]
15. Shields, C.L.; Douglass, A.M.; Beggache, M.; Say, E.A.T.; Shields, J.A. Intravitreous Chemotherapy For Active Vitreous Seeding From Retinoblastoma. *Retina* **2016**, *36*, 1184–1190. [CrossRef] [PubMed]
16. Temming, P.; Arendt, M.; Viehmann, A.; Eisele, L.; Le Guin, C.H.D.; Schündeln, M.M.; Biewald, E.; Astrahantseff, K.; Wieland, R.; Bornfeld, N.; et al. Incidence of second cancers after radiotherapy and systemic chemotherapy in heritable retinoblastoma survivors: A report from the German reference center. *Pediatr. Blood Cancer* **2017**, *64*, 71–80. [CrossRef] [PubMed]
17. Zhang, M.G.; Kuznetsoff, J.N.; Owens, D.A.; Gallo, R.A.; Kalahasty, K.; Cruz, A.M.; Kurtenbach, S.; Correa, Z.M.; Pelaez, D.; Harbour, J.W. Early Mechanisms of Chemoresistance in Retinoblastoma. *Cancers* **2022**, *14*, 4966. [CrossRef] [PubMed]
18. Hoffmann, W. Trefoil Factor Family (TFF) Peptides and Their Links to Inflammation: A Re-evaluation and New Medical Perspectives. *Int. J. Mol. Sci.* **2021**, *22*, 4909. [CrossRef] [PubMed]
19. Hoffmann, W. Trefoil Factor Family (TFF) Peptides and Their Diverse Molecular Functions in Mucus Barrier Protection and More: Changing the Paradigm. *Int. J. Mol. Sci.* **2020**, *21*, 4535. [CrossRef] [PubMed]
20. Jahan, R.; Shah, A.; Kisling, S.G.; Macha, M.A.; Thayer, S.; Batra, S.K.; Kaur, S. Odyssey of trefoil factors in cancer: Diagnostic and therapeutic implications. *Biochim. Et Biophys. Acta (BBA)-Rev. Cancer* **2020**, *1873*, 188362. [CrossRef]
21. Busch, M.; Dünker, N. Trefoil factor family peptides—Friends or foes? *Biomol. Concepts* **2015**, *6*, 343–359. [CrossRef] [PubMed]
22. Busch, M.; Große-Kreul, J.; Wirtz, J.J.; Beier, M.; Stephan, H.; Royer-Pokora, B.; Metz, K.; Dünker, N. Reduction of the tumorigenic potential of human retinoblastoma cell lines by TFF1 overexpression involves p53/caspase signaling and miR-18a regulation. *Int. J. Cancer* **2017**, *141*, 549–560. [CrossRef] [PubMed]
23. Busch, M.; Metz, K.; Beier, M.; Biewald, E.; Dünker, N. Trefoil Factor Family 1 Expression Correlates with Clinical Outcome in Patients with Retinoblastoma. *Retina* **2018**, *38*, 2422. [CrossRef] [PubMed]

24. Aschero, R.; Ganiewich, D.; Lamas, G.; Restrepo-Perdomo, C.A.; Ottaviani, D.; Zugbi, S.; Camarero, S.; Néspoli, E.; Vilanova, M.C.; Perez-Jaume, S.; et al. Immunohistochemical expression of TFF1 is a marker of poor prognosis in retinoblastoma. *Pediatr. Blood Cancer* **2024**, *71*, e30717. [CrossRef] [PubMed]

25. Busch, M.A.; Haase, A.; Miroschnikov, N.; Doege, A.; Biewald, E.; Bechrakis, N.E.; Beier, M.; Kanber, D.; Lohmann, D.; Metz, K.; et al. TFF1 in Aqueous Humor—A Potential New Biomarker for Retinoblastoma. *Cancers* **2022**, *14*, 677. [CrossRef]

26. Busch, M.A.; Haase, A.; Alefeld, E.; Biewald, E.; Jabbarli, L.; Dünker, N. Trefoil Family Factor Peptide 1—A New Biomarker in Liquid Biopsies of Retinoblastoma under Therapy. *Cancers* **2023**, *15*, 4828. [CrossRef] [PubMed]

27. Yamada, Y.; Hayami, T.; Nakamura, K.; Kaisaki, P.J.; Someya, Y.; Wang, C.-Z.; Seino, S.; Seino, Y. Human Gastric Inhibitory Polypeptide Receptor: Cloning of the Gene (GIPR) and cDNA. *Genomics* **1995**, *29*, 773–776. [CrossRef] [PubMed]

28. Gremlich, S.; Porret, A.; Hani, E.H.; Cherif, D.; Vionnet, N.; Froguel, P.; Thorens, B. Cloning, functional expression, and chromosomal localization of the human pancreatic islet glucose-dependent insulinotropic polypeptide receptor. *Diabetes* **1995**, *44*, 1202–1208. [CrossRef] [PubMed]

29. Volz, A.; Göke, R.; Lankat-Buttgereit, B.; Fehmann, H.-C.; Bode, H.P.; Göke, B. Molecular cloning, functional expression, and signal transduction of the GIP-receptor cloned from a human insulinoma. *FEBS Lett.* **1995**, *373*, 23–29. [CrossRef]

30. Dubeykovskaya, Z.; Dubeykovskiy, A.; Solal-Cohen, J.; Wang, T.C. Secreted Trefoil Factor 2 Activates the CXCR4 Receptor in Epithelial and Lymphocytic Cancer Cell Lines. *J. Biol. Chem.* **2009**, *284*, 3650–3662. [CrossRef]

31. Dieckow, J.; Brandt, W.; Hattermann, K.; Schob, S.; Schulze, U.; Mentlein, R.; Ackermann, P.; Sel, S.; Paulsen, F.P. CXCR4 and CXCR7 Mediate TFF3-Induced Cell Migration Independently From the ERK1/2 Signaling Pathway. *Investig. Ophthalmol. Vis. Sci.* **2016**, *57*, 56. [CrossRef] [PubMed]

32. Dupre, J.; Ross, S.A.; Watson, D.; Brown, J.C. Stimulation Of Insulin Secretion By Gastric Inhibitory Polypeptide In Man. *J. Clin. Endocrinol. Metab.* **1973**, *37*, 826–828. [CrossRef] [PubMed]

33. Regazzo, D.; Barbot, M.; Scaroni, C.; Albiger, N.; Occhi, G. The pathogenic role of the GIP/GIPR axis in human endocrine tumors: Emerging clinical mechanisms beyond diabetes. *Rev. Endocr. Metab. Disord.* **2020**, *21*, 165–183. [CrossRef] [PubMed]

34. Regazzo, D.; Bertazza, L.; Galletta, E.; Barollo, S.; Mondin, A.; Zovato, S.; Iacobone, M.; Zilio, E.; Scaroni, C.; Radu, C.M.; et al. The GIP/GIPR axis in medullary thyroid cancer: Clinical and molecular findings. *Endocr.-Relat. Cancer* **2022**, *29*, 273–284. [CrossRef] [PubMed]

35. Usdin, T.B.; Mezey, V.; Button, C.; Brownstein, J.; Bonner, T.I. Gastric Inhibitory Polypeptide Receptor, a Member of the Secretin-Vasoactive Intestinal Peptide Receptor Family, Is Widely Distributed in Peripheral Organs and the Brain. *Endocrinology* **1993**, *133*, 2861–2870. [CrossRef] [PubMed]

36. Singh, A.N.; Basu, D.; Skoblenick, K.J.; Castellano, J.M.; Pontoriero, G.; Thomas, N. Mapping Of Human Brain For Glucose-Dependent Insulinotropic Polypeptide (Gip) And Gip Receptors Expression: Implications In Schizophrenia. *Schizophr. Res.* **2010**, *2–3*, 528. [CrossRef]

37. Verma, M.K.; Goel, R.; Krishnadas, N.; Nemmani, K.V.S. Targeting glucose-dependent insulinotropic polypeptide receptor for neurodegenerative disorders. *Expert Opin. Ther. Targets* **2018**, *22*, 615–628. [CrossRef] [PubMed]

38. Samms, R.J.; Sloop, K.W.; Gribble, F.M.; Reimann, F.; Adriaenssens, A.E. GIPR Function in the Central Nervous System: Implications and Novel Perspectives for GIP-Based Therapies in Treating Metabolic Disorders. *Diabetes* **2021**, *70*, 1938–1944. [CrossRef]

39. Waser, B.; Rehmann, R.; Sanchez, C.; Fourmy, D.; Reubi, J.C. Glucose-Dependent Insulinotropic Polypeptide Receptors in Most Gastroenteropancreatic and Bronchial Neuroendocrine Tumors. *J. Clin. Endocrinol. Metab.* **2012**, *97*, 482–488. [CrossRef] [PubMed]

40. Körner, M.; Waser, B.; Reubi, J.C. Does Somatostatin or Gastric Inhibitory Peptide Receptor Expression Correlate with Tumor Grade and Stage in Gut Neuroendocrine Tumors? *Neuroendocrinology* **2015**, *101*, 45–57. [CrossRef] [PubMed]

41. Waser, B.; Beetschen, K.; Pellegata, N.S.; Reubi, J.C. Incretin Receptors in Non-Neoplastic and Neoplastic Thyroid C Cells in Rodents and Humans: Relevance for Incretin-Based Diabetes Therapy. *Neuroendocrinology* **2011**, *94*, 291–301. [CrossRef]

42. Widenmaier, S.B.; Ao, Z.; Kim, S.-J.; Warnock, G.; McIntosh, C.H. Suppression of p38 MAPK and JNK via Akt-mediated Inhibition of Apoptosis Signal-regulating Kinase 1 Constitutes a Core Component of the β-Cell Pro-survival Effects of Glucose-dependent Insulinotropic Polypeptide. *J. Biol. Chem.* **2009**, *284*, 30372–30382. [CrossRef] [PubMed]

43. Prabakaran, D.; Wang, B.; Feuerstein, J.D.; Sinclair, J.A.; Bijpuria, P.; Jepeal, L.I.; Wolfe, M.M. Glucose-dependent insulinotropic polypeptide stimulates the proliferation of colorectal cancer cells. *Regul. Pept.* **2010**, *163*, 74–80. [CrossRef] [PubMed]

44. Yabe, D.; Seino, Y. Two incretin hormones GLP-1 and GIP: Comparison of their actions in insulin secretion and β cell preservation. *Prog. Biophys. Mol. Biol.* **2011**, *107*, 248–256. [CrossRef] [PubMed]

45. Campbell, J.E.; Drucker, D.J. Islet α cells and glucagon—Critical regulators of energy homeostasis. *Nat. Rev. Endocrinol.* **2015**, *11*, 329–338. [CrossRef] [PubMed]

46. Pospisilik, J.A.; Martin, J.; Doty, T.; Ehses, J.A.; Pamir, N.; Lynn, F.C.; Piteau, S.; Demuth, H.-U.; McIntosh, C.H.S.; Pederson, R.A. Dipeptidyl peptidase IV inhibitor treatment stimulates β-cell survival and islet neogenesis in streptozotocin-induced diabetic rats. *Diabetes* **2003**, *52*, 741–750. [CrossRef] [PubMed]

47. Ehses, J.A.; Casilla, V.R.; Doty, T.; Pospisilik, J.A.; Winter, K.D.; Demuth, H.-U.; Pederson, R.A.; McIntosh, C.H.S. Glucose-Dependent Insulinotropic Polypeptide Promotes β-(INS-1) Cell Survival via Cyclic Adenosine Monophosphate-Mediated Caspase-3 Inhibition and Regulation of p38 Mitogen-Activated Protein Kinase. *Endocrinology* **2003**, *144*, 4433–4445. [CrossRef] [PubMed]

48. McFall, R.C.; Sery, T.W.; Makadon, M. Characterization of a New Continuous Cell Line Derived from a Human Retinoblastoma. *Cancer Res.* **1977**, *37*, 1003–1010. [PubMed]

49. Reid, T.W.; Albert, D.M.; Rabson, A.S.; Russell, P.; Craft, J.; Chu, E.W.; Tralka, T.S.; Wilcox, J.L. Characteristics of an Established Cell Line of Retinoblastoma2. *JNCI J. Natl. Cancer Inst.* **1974**, *53*, 347–360. [CrossRef]

50. Busch, M.; Philippeit, C.; Weise, A.; Dünker, N. Re-characterization of established human retinoblastoma cell lines. *Histochem. Cell Biol.* **2015**, *143*, 325–338. [CrossRef]

51. Campeau, E.; Ruhl, V.E.; Rodier, F.; Smith, C.L.; Rahmberg, B.L.; Fuss, J.O.; Campisi, J.; Yaswen, P.; Cooper, P.K.; Kaufman, P.D. A Versatile Viral System for Expression and Depletion of Proteins in Mammalian Cells. *PLoS ONE* **2009**, *4*, e6529. [CrossRef] [PubMed]

52. Imig, J.; Motsch, N.; Zhu, J.Y.; Barth, S.; Okoniewski, M.; Reineke, T.; Tinguely, M.; Faggioni, A.; Trivedi, P.; Meister, G.; et al. microRNA profiling in Epstein–Barr virus-associated B-cell lymphoma. *Nucleic Acids Res.* **2011**, *39*, 1880–1893. [CrossRef] [PubMed]

53. Pietschmann, T.; Heinkelein, M.; Heldmann, M.; Zentgraf, H.; Rethwilm, A.; Lindemann, D. Foamy Virus Capsids Require the Cognate Envelope Protein for Particle Export. *J. Virol.* **1999**, *73*, 2613–2621. [CrossRef] [PubMed]

54. Mochizuki, H.; Schwartz, J.P.; Tanaka, K.; Brady, R.O.; Reiser, J. High-Titer Human Immunodeficiency Virus Type 1-Based Vector Systems for Gene Delivery into Nondividing Cells. *J. Virol.* **1998**, *72*, 8873–8883. [CrossRef] [PubMed]

55. Zijlstra, A.; Mellor, R.; Panzarella, G.; Aimes, R.T.; Hooper, J.D.; Marchenko, N.D.; Quigley, J.P. A Quantitative Analysis of Rate-limiting Steps in the Metastatic Cascade Using Human-specific Real-Time Polymerase Chain Reaction1. *Cancer Res.* **2002**, *62*, 7083–7092. [PubMed]

56. Palmer, T.D.; Lewis, J.; Zijlstra, A. Quantitative Analysis of Cancer Metastasis using an Avian Embryo Model. *JoVE (J. Vis. Exp.)* **2011**, *51*, e2815. [CrossRef] [PubMed]

57. Busch, M.; Papior, D.; Stephan, H.; Dünker, N. Characterization of etoposide- and cisplatin-chemoresistant retinoblastoma cell lines. *Oncol. Rep.* **2018**, *39*, 160–172. [CrossRef] [PubMed]

58. Busch, M.; Klein, S.; Große-Kreul, J.; Scheiner, O.; Metz, K.; Stephan, H.; Dünker, N. p53, miR-34a and EMP1—Newly Identified Targets of TFF3 Signaling in Y79 Retinoblastoma Cells. *Int. J. Mol. Sci.* **2019**, *20*, 4129. [CrossRef] [PubMed]

59. Dennis, G.; Sherman, B.T.; Hosack, D.A.; Yang, J.; Gao, W.; Lane, H.C.; Lempicki, R.A. DAVID: Database for Annotation, Visualization, and Integrated Discovery. *Genome Biol.* **2003**, *4*, R60. [CrossRef]

60. He, R.; Li, X.; Liang, L.; Xie, Y.; Luo, D.; Ma, J.; Peng, Z.; Hu, X.; Chen, G. The suppressive role of miR-542-5p in NSCLC: The evidence from clinical data and in vivo validation using a chick chorioallantoic membrane model. *BMC Cancer* **2017**, *17*, 655. [CrossRef] [PubMed]

61. Philippeit, C.; Busch, M.; Dünker, N. Epigenetic Control of Trefoil Factor Family (TFF) Peptide Expression in Human Retinoblastoma Cell Lines. *Cell. Physiol. Biochem.* **2014**, *34*, 1001–1014. [CrossRef] [PubMed]

62. Huang, Y.-G.; Li, Y.-F.; Pan, B.-L.; Wang, L.-P.; Zhang, Y.; Lee, W.-H.; Zhang, Y. Trefoil factor 1 gene alternations and expression in colorectal carcinomas. *Tumori J.* **2013**, *99*, 702–707. [CrossRef] [PubMed]

63. Park, W.S.; Oh, R.R.; Park, J.Y.; Lee, J.H.; Shin, M.S.; Kim, H.S.; Lee, H.K.; Kim, Y.S.; Kim, S.Y.; Lee, S.H.; et al. Somatic mutations of the trefoil factor family 1 gene in gastric cancer. *Gastroenterology* **2000**, *119*, 691–698. [CrossRef] [PubMed]

64. Shekarriz, R.; Kochaki, N.; Eslami-Jouibari, M.; Omrani-Nava, V.; Ahmadi, M.; Alizadeh-Navaei, R. TFF1 gene single nucleotide polymorphism (rs3761376) and colorectal cancer risk. *Mol. Biol. Rep.* **2022**, *49*, 10127–10131. [CrossRef] [PubMed]

65. Wang, W.; Li, Z.; Wang, J.; Du, M.; Li, B.; Zhang, L.; Li, Q.; Xu, J.; Wang, L.; Li, F.; et al. A functional polymorphism in TFF1 promoter is associated with the risk and prognosis of gastric cancer. *Int. J. Cancer* **2018**, *142*, 1805–1816. [CrossRef]

66. Yio, X.; Diamond, M.; Zhang, J.-Y.; Weinstein, H.; Wang, L.-H.; Werther, L.; Itzkowitz, S. Trefoil Factor Family-1 Mutations Enhance Gastric Cancer Cell Invasion Through Distinct Signaling Pathways. *Gastroenterology* **2006**, *130*, 1696–1706. [CrossRef] [PubMed]

67. Reubi, J.C.; Fourmy, D.; Cordomi, A.; Tikhonova, I.G.; Gigoux, V. GIP receptor: Expression in neuroendocrine tumours, internalization, signalling from endosomes and structure-function relationship studies. *Peptides* **2020**, *125*, 170229. [CrossRef] [PubMed]

68. Sherman, S.K.; Maxwell, J.E.; Carr, J.C.; Wang, D.; O'Dorisio, M.S.; O'Dorisio, T.M.; Howe, J.R. GIPR expression in gastric and duodenal neuroendocrine tumors. *J. Surg. Res.* **2014**, *190*, 587–593. [CrossRef] [PubMed]

69. Karpathakis, A.; Dibra, H.; Pipinikas, C.; Feber, A.; Morris, T.; Francis, J.; Oukrif, D.; Mandair, D.; Pericleous, M.; Mohmaduvesh, M.; et al. Prognostic Impact of Novel Molecular Subtypes of Small Intestinal Neuroendocrine Tumor. *Clin. Cancer Res.* **2016**, *22*, 250–258. [CrossRef]

70. Costa, M.H.S.; Latronico, A.C.; Martin, R.M.; Barbosa, A.S.; Almeida, M.Q.; Lotfi, C.F.P.; Valassi, H.P.L.; Nishi, M.Y.; Lucon, A.M.; Siqueira, S.A.; et al. Expression profiles of the glucose-dependent insulinotropic peptide receptor and LHCGR in sporadic adrenocortical tumors. *J. Endocrinol.* **2009**, *200*, 167–175. [CrossRef] [PubMed]

71. Li, Z.; Hu, C.; Zhen, Y.; Pang, B.; Yi, H.; Chen, X. Pristimerin inhibits glioma progression by targeting AGO2 and PTPN1 expression via miR-542-5p. *Biosci. Rep.* **2019**, *39*, BSR20182389. [CrossRef] [PubMed]

72. Bachelerie, F.; Ben-Baruch, A.; Burkhardt, A.M.; Combadiere, C.; Farber, J.M.; Graham, G.J.; Horuk, R.; Sparre-Ulrich, A.H.; Locati, M.; Luster, A.D.; et al. International Union of Basic and Clinical Pharmacology. LXXXIX. Update on the Extended Family of Chemokine Receptors and Introducing a New Nomenclature for Atypical Chemokine Receptors. *Pharmacol. Rev.* **2014**, *66*, 1–79. [CrossRef] [PubMed]

73. Hauser, A.S.; Attwood, M.M.; Rask-Andersen, M.; Schiöth, H.B.; Gloriam, D.E. Trends in GPCR drug discovery: New agents, targets and indications. *Nat. Rev. Drug Discov.* **2017**, *16*, 829–842. [CrossRef] [PubMed]

74. Kastenhuber, E.R.; Lowe, S.W. Putting p53 in Context. *Cell* **2017**, *170*, 1062–1078. [CrossRef] [PubMed]

75. Levine, A.J. p53: 800 million years of evolution and 40 years of discovery. *Nat. Rev. Cancer* **2020**, *20*, 471–480. [CrossRef] [PubMed]

76. Wang, H.; Guo, M.; Wei, H.; Chen, Y. Targeting p53 pathways: Mechanisms, structures, and advances in therapy. *Signal Transduct. Target. Ther.* **2023**, *8*, 92. [CrossRef] [PubMed]

77. Chen, Y.; Zhang, X.; Dantas Machado, A.C.; Ding, Y.; Chen, Z.; Qin, P.Z.; Rohs, R.; Chen, L. Structure of p53 binding to the BAX response element reveals DNA unwinding and compression to accommodate base-pair insertion. *Nucleic Acids Res.* **2013**, *41*, 8368–8376. [CrossRef] [PubMed]

78. Wei, H.; Qu, L.; Dai, S.; Li, Y.; Wang, H.; Feng, Y.; Chen, X.; Jiang, L.; Guo, M.; Li, J.; et al. Structural insight into the molecular mechanism of p53-mediated mitochondrial apoptosis. *Nat. Commun.* **2021**, *12*, 2280. [CrossRef] [PubMed]

79. Kondapuram, S.K.; Ramachandran, H.K.; Arya, H.; Coumar, M.S. Targeting survivin for cancer therapy: Strategies, small molecule inhibitors and vaccine based therapeutics in development. *Life Sci.* **2023**, *335*, 122260. [CrossRef] [PubMed]

80. Jimenez-Pascual, A.; Mitchell, K.; Siebzehnrubl, F.A.; Lathia, J.D. FGF2: A novel druggable target for glioblastoma? *Expert Opin. Ther. Targets* **2020**, *24*, 311–318. [CrossRef] [PubMed]

81. Chandarana, R.; D'Souza, J.S.; Coutinho, E.C. Glucose-Dependent Insulinotropic Polypeptide Receptor (GIPR). In *Encyclopedia of Signaling Molecules*; Springer: Berlin/Heidelberg, Germany, 2012; pp. 773–779.

3) Fatty acid conjugated EPI-X4 derivatives with increased activity and *in vivo* stability

Cumulative Thesis/Extent of Contribution

Cumulative thesis of M.Sc. André Haase

Author contributions

Fatty acid conjugated EPI-X4 derivatives with increased activity and *in vivo* stability

M. Harms, **A. Haase**, A. Rodriguez-Alfonso, J. Löffler, Y. Almeida-Hernández, Y. Ruiz-Blanco, D. Albers, A. Gilg, F. von Bank, F. Zech, M. Datta, J. Jaikishan, B. Draphoen, M. Habib, L. Ständker, S. Wiese, M. Lindén, G. Winter, V. Rasche, A. Beer, H. Jumaa, A. Abadi, F. Kirchhoff, M. Busch, N. Dünker, E. Sanchez-Garcia and J. Münch

Status: published in Journal of Controlled Release (2024)

DOI: 10.1016/j.jconrel.2024.07.049

Impact factor at submission: 10.8 (2022)

André Haase contributions (**co-authorship**):

- **Conception: 80% of retinoblastoma part:** Study design, planning the analysis workflow, literature research.
- **Experimental work: 95% of retinoblastoma part:** Performance of WB, CXCR4 inhibitor studies, cell viability assays, cell proliferation assay and CAM assays.
- **Data analysis: 100% of retinoblastoma part:** Data evaluation, processing, formal analysis, and visualization of data.
- **Statistical analysis**: **100% of retinoblastoma part:** Data interpretation, integration and performance of various statistical tests.
- **Writing the manuscript: 50% of retinoblastoma part:** Writing of Material and Methods, Results, figure design and legends.
- **Revising the manuscript**: **40% of retinoblastoma part:** Revising Abstract, Results, Discussion, Material and Methods, Figures and supplementary materials.

_____

Signature André Haase

_____

Signature Prof. Dr. Nicole Dünker

Fatty acid conjugated EPI-X4 derivatives with increased activity and *in vivo* stability

Mirja Harms[1,*], André Haase[2], Armando Rodriguez-Alfonso[3,4], Jessica Löffler[5], Yasser Almeida-Hernández[6], Yasser B. Ruiz-Blanco[6], Dan Albers[1], Andrea Gilg[1], Franziska von Bank[1], Fabian Zech[1], Rüdiger Groß[1], Moumita Datta[7], Janeni Jaikishan[7], Bastian Draphoen[8], Monica Habib[9,10], Ludger Ständker[3], Sebastian Wiese[4], Mika Lindén[8], Gordon Winter[5], Volker Rasche[11], Ambros J. Beer[5], Hassan Jumaa[7], Ashraf H Abadi[9], Frank Kirchhoff[1], Maike Busch[2], Nicole Dünker[2], Elsa Sanchez-Garcia[6], Jan Münch[1,*]

[1] Institute of Molecular Virology, Ulm University Medical Center, Ulm, 89081, Germany

[2] Institute for Anatomy II, Department of Neuroanatomy, Center for Translational Neuro- and Behavioral Sciences (C-TNBS), Medical Faculty, University of Duisburg-Essen, 45147 Essen, Germany

[3] Core Facility Functional Peptidomics, Ulm University Medical Center, Ulm, 89081, Germany

[4] Core Unit Mass Spectrometry and Proteomics, Ulm University Medical Center, Ulm, 89081, Germany

[5] Department of Nuclear Medicine, Ulm University Medical Center, Ulm, 89081, Germany

[6] Computational Bioengineering, Department of Biochemical and Chemical Engineering, Emil-Figge Str. 66, 44227 Dortmund, Germany

[7] Institute of Immunology, Ulm University Medical Center, Ulm, 89081, Germany

[8] Institute for Inorganic Chemistry II, Albert Einsten-Allee 11, 89081 Ulm

[9] Department of Pharmaceutical Chemistry, Faculty of Pharmacy and Biotechnology, German University in Cairo, Cairo, 11835, Egypt

[10] Pharmaceutical Chemistry Department, School of Life and Medical Sciences, University of Hertfordshire Hosted by Global Academic Foundation, Cairo, Egypt

[11] Experimental Cardiovascular Imaging (ExCaVI), Ulm University Medical Center, Ulm, 89081, Germany

*Corresponding authors Mirja.Harms@uni-ulm.de, Jan.Münch@uni-ulm.de

Highlights

- Lipidated derivatives of EPI-X4 exhibit increased affinity and antagonistic activity towards the CXCR4 receptor
- Lipidated EPI-X4 derivatives exhibit a half-life of more than 8 hours in both blood and plasma
- The lipidated EPI-X4 JM#198 displays a circulation half-life of nearly 4 hours in mice
- EPI-X4 JM#198 inhibits retinoblastoma tumor formation *in vitro* and *in ovo*

Abstract

Dysregulation of the CXCL12/CXCR4 axis is implicated in autoimmune, inflammatory, and oncogenic diseases, positioning CXCR4 as a pivotal therapeutic target. We evaluated optimized variants of the specific endogenous CXCR4 antagonist, EPI-X4, addressing existing challenges in stability and potency. Our structure-activity relationship study investigates the conjugation of EPI-X4 derivatives with long-chain fatty acids, enhancing serum albumin interaction and receptor affinity. Molecular dynamic simulations revealed that the lipid moieties stabilize the peptide-receptor interaction through hydrophobic contacts at the receptor's N-terminus, anchoring the lipopeptide within the CXCR4 binding pocket and maintaining essential receptor interactions. Accordingly, lipidation resulted in increased receptor affinities and antagonistic activities. Additionally, by interacting with human serum albumin lipidated EPI-X4 derivatives displayed sustained stability in human plasma and extended circulation times *in vivo*. Selected candidates showed significant therapeutic potential in human retinoblastoma cells *in vitro* and *in ovo*, with our lead derivative exhibiting higher efficacies compared to its non-lipidated counterpart. This study not only elucidates the optimization trajectory for EPI-X4 derivatives but also underscores the intricate interplay between stability and efficacy, crucial for delineating their translational potential in clinical applications.

Graphical Astract
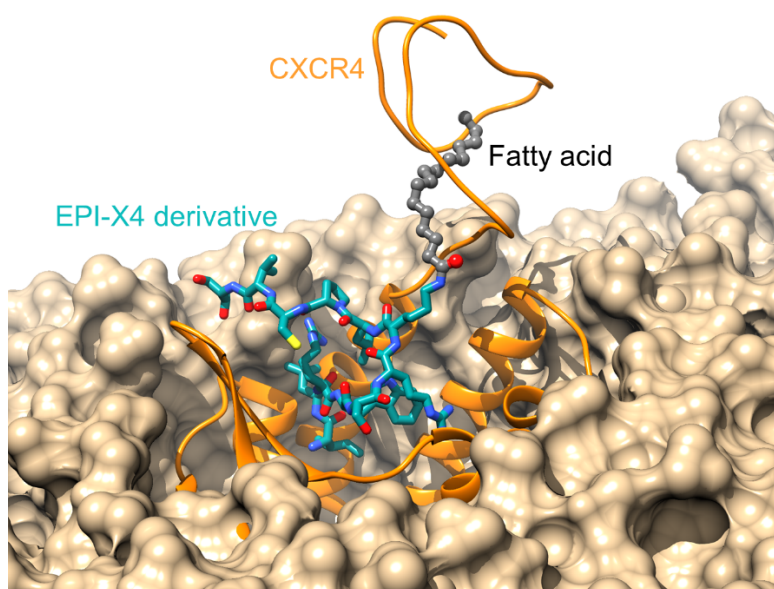
Keywords (6)

EPI-X4, CXCR4, serum albumin, lipidation, retinoblastoma

Introduction

The Endogenous Peptide Inhibitor of CXCR4 (EPI-X4), a 16-mer peptide, exhibits selective binding to the C-X-C chemokine receptor type 4 (CXCR4), a transmembrane protein expressed by a variety of cells, including immune and cancer cells [1], [2]. The peptide is generated via the proteolytic cleavage of human serum albumin (HSA) under acidic conditions, facilitated by acidic aspartic proteases such as Cathepsin D and E, commonly present in blood plasma and cellular lysosomes [2], [3], [4]. Comprising residues 408-423 of HSA, EPI-X4 specifically interacts with CXCR4 through its initial seven amino acid residues [5]. These key amino acids primarily engage with the receptor's minor binding pocket, impeding the binding of CXCL12, the canonical chemokine ligand of CXCR4 [5]. Consequently, EPI-X4 acts as an endogenous antagonist, inhibiting CXCL12-induced receptor signaling [2], [6]. Additionally, EPI-X4 functions as an inverse agonist by reducing basal CXCR4 signaling in the absence of CXCL12 [2].

Dysregulation or overexpression of CXCL12 and/or CXCR4 is associated with autoimmune, inflammatory, and cancer diseases, including tumor progression and metastasis [1], [7], [8], making CXCR4 an appealing therapeutic target for various chronic inflammatory diseases and cancers [9]. Presently, the only FDA-approved CXCR4 antagonists are AMD3100 - primarily used for peripheral blood stem cell transplantation due to limitations in its pharmacokinetics and adverse effects upon prolonged administration [10], [11], and BL-8040, which recently received FDA-approval for autologues stem cell transplantation [12]. Still, there is a crucial need for novel agents targeting CXCR4-related diseases. Retinoblastoma (RB) is a rare intraocular tumor, occurring mainly in young children [13], [14], [15]. Early-stage RB has a high cure rate, with over 90% of children surviving and maintaining vision in at least one eye. However, outcomes are often less favorable if the cancer has spread outside the eye or if diagnosis and treatment are delayed. Also, secondary tumors or chemotherapy resistances associated with current treatments can potentially develop [16], [17]. Thus, there is still a demand for new or adjuvant therapies. CXCR4 is expressed in RB and may represent a useful target for the therapy of retinoblastoma [8].

EPI-X4 emerged as a promising candidate for clinical development due to its high receptor specificity, low mitochondrial cytotoxicity, and dual antagonistic and inverse agonist activities [2], [3]. However, its initial inhibitory potency against CXCR4, with an IC_{50} value in the two-digit micromolar range, is insufficient for therapeutic applications [2], [18]. To enhance its effectiveness, quantitative structure-activity relationship (QSAR) studies identified two 12-mer derivatives, WSC02 and JM#21, exhibiting increased antagonistic efficacy in the nanomolar range [2], [6]. Mouse model studies with EPI-X4 JM#21 demonstrated its efficacy in preventing airway inflammation and atopic dermatitis through topical administration into the lungs or skin, respectively [6]. However, despite these advancements, both optimized EPI-X4 derivatives exhibit low stability in human plasma due to enzymatic degradation at the N-terminus, with half-lives of less than 10 minutes [2], [6], [19]. Efforts to enhance stability for systemic administration have explored strategies such as incorporating unnatural amino acids or larger polymer derivatization [20], [21]. However, while these novel derivatives showed increased resistance against enzymatic degradation in blood plasma, they suffered from decreased efficacy, hindering their advancement in preclinical studies. Increasing both, stability and therapeutic potency remains a critical challenge in optimizing EPI-X4 derivatives for future clinical applications.

One approach to augment the *in vivo* half-life of peptides involves coupling them with long-chain fatty acids. This modification, known as lipidation, can enhance peptide stability by shielding them from enzymatic degradation and facilitating their interaction with serum albumin [22]. Conjugating peptides to fatty acids, such as palmitic acid, can increase their resistance to enzymatic breakdown and result prolonged circulation times [22]. This strategy holds promise for improving the pharmacokinetic profile of peptide drugs, potentially resulting in clinical applicability by extending their duration of action and therapeutic benefits [23]. In a structure-activity-relationship (SAR) study, we here designed EPI-X4

derivatives conjugated to fatty acids of different lengths. We assessed their CXCR4 antagonistic activity and plasma stability. Additionally, we evaluated the *in vivo* circulation time of selected candidates and tested their potential therapeutic value for the treatment of retinoblastoma in *vitro*.

Material and Methods

Reagents and peptide synthesis. Peptides and peptides conjugated with fatty acids were synthesized by standard Fmoc solid-phase peptide synthesis using a Liberty Blue microwave synthesizer (CEM, USA) as previously described [6]. All chemicals were used as provided by the manufacturers. Amino acids were purchased from Novabiochem (Merck KGaA, Darmstadt, Germany). N,N-dimethylformamide (DMF), 20% (v/v) piperidine in DMF, O-benzotriazole-N,N,N′,N′-tetramethyluronium-hexafluoro-phosphate (HBTU) and trifluoroacetic acid (TFA) were purchased from Merck Millipore (Merck KGaA). Triisopropylsilane (TIS), diisopropylethylamine (DIEA) were purchased from Sigma–Aldrich (Sigma–Aldrich Chemie GmbH Munich, Germany). Acetonitrile was purchased from JT.Baker (Avantor Performance Materials B.V. 7418 AM Deventer Netherlands). The peptides were synthesized automatically on a 0.10 mmol scale using standard Fmoc solid phase peptide synthesis techniques with the microwave synthesizer (Liberty blue; CEM). A preloaded resin was used and provided in the reactor. The resin was washed with DMF. The Fmoc protecting group was removed with 3 mL 20% (v/v) piperidine in DMF and initialized with microwave followed by washing with DMF. An amount of five equivalents of amino acids was added to the reactor, and then 5 equiv of HBTU was dosed into the amino acid solution. Subsequently, an amount of 10 equiv of DIEA was added to the resin. The coupling reaction proceeded with microwaves for a few minutes, and then the resin was washed in DMF. These steps were repeated for every amino acid in the sequence. The last amino acid was deprotected Once the synthesis was completed, the peptide was cleaved in 95% (*v/v*) TFA, 2.5% (*v/v*) TIS, and 2.5% (*v/v*) H_2O for 1 h. The peptide residue was precipitated and washed with cold diethyl ether (DEE) by centrifugation. The peptide precipitate was then allowed to dry under airflow to remove residual ether. The synthetic peptides were purified by reversed-phase high-performance liquid chromatography (Waters, USA) employing an acetonitrile/water gradient under acidic conditions on a Phenomenex C18 Luna column (particle size 5 µm, pore size 100 Å) and then lyophilized on a freeze-dryer (Labconco, USA). The molecular mass of the pure peptides was verified by liquid chromatography-mass spectrometry (LC-MS; Waters).

For the synthesis of the conjugates, the same protocol was followed. Commercial Fmoc-Lys(palmitoyl)-OH and Fmoc-Lys(stearic)-OH (Sigma-Aldrich, USA, or Bachem, CH) were used to obtain the peptide specifically modified with palmitic and stearic chains in the Lysine residue (with or without a glutamic acid linker), respectively. Purity data (HPLC) and MS data (LC-MS) of peptides used in the *in vivo* studies (JM#21 and JM#21-fatty acid conjugates: JM#143, JM#192, JM#194, JM#198, JM#204, JM#255, and JM#257) are reported in supplement 2. Underivatized peptides were dissolved in phosphate-buffered saline (PBS), and the lipopeptides were dissolved in dimethyl sulfoxide (DMSO) at a stock concentration of 3 mM and further diluted in PBS (for *in vitro* experiments) or saline (for *in vivo* experiments) before usage. AMD3100 octahydrochloride hydrate was purchased from Sigma-Aldrich (#A5602) and dissolved in H_2O. Human and mouse CXCL12 were purchased from Peprotech (#300-28A, #250-20A) and dissolved at a concentration of 100 mg/mL in H_2O.

Dynamic light scattering (DLS). 50 mM TRIS-buffer was adjusted to a pH of 7.4. Peptide was dissolved in DMSO (50 mM) and incubated for 1h at 37 °C. For each concentration, 10 µL of the pre-incubated stock solution, adjusted to the relevant concentration, was added into 1 mL of pre-incubated (1 h) TRIS-Buffer at 37 °C, giving the desired concentrations of 500 - 1 µM. After an overnight (16h) incubation at 37°C in enclosed cuvettes the solutions were measured by dynamic light scattering (DLS). DLS was measured using a Zetasizer NanoZS Zen3600 (Malvern Panalytical, Germany).

Commassie staining and bicinchoninic acid assay (BCA). Peptide stocks were serially diluted in PBS and immediately separated on a 4-12% Bis-Tris SDS-PAGE and stained with colloidal Coomassie.

Alternatively, samples were analyzed by BCA assay (BCA Gold, Thermo Fisher). Optical density (OD) values were determined after 5 min of incubation with the BCA reagent at 480 nm using a plate reader.

Western blot. For Western blot protein quantification, cells were washed with PBS and lysed in RIPA buffer supplemented according to a previously described protocol [24]. After an incubation period of 30 min, lysates were centrifuged at 10,000 g at 4 °C for 30 min. The quantification of protein concentration was executed through a bicinchoninic acid assay (BCA; Thermo Scientific, Oberhausen, Germany) according to the manufacturer's protocol. Subsequently, equivalent quantities of protein lysats were separated on a 12% SDS/PAGE matrix (Bio-Rad, Hercules, CA, USA) and transferred onto nitrocellulose membranes. Thereafter blocking was performed in 5% milk powder (Roth, Karlsruhe, Germany) in TBS supplemented with 0,1% triton X-100 (TBS-T; Sigma, St. Louis, USA) for 1 h. Incubation of the primary antibody against CXCR4 (1:1000; cat. #704015, Invitrogen, Darmstadt, Germany) and β-actin (1:1000; cat. #4967; Cell Signaling Technology, Danvers, USA) in 5% BSA (Roth, Karlsruhe, Germany) in TBS-T took place overnight at 4 °C. HRP conjugated secondary antibodies (goat anti-rabbit; P0448, Agilent, Santa Clara, CA, USA) were applied at a dilution of 1:10.000 at room temperature for 1 hour. The HRP signal was visualized using Western Bright Chemiluminescence Reagent (Advansta, San Jose, CA, USA) and detected using a Celvin S reader (Biostep, Burkhardtsdorf, Germany).

Cell culture. TZM-bl HIV-1 reporter cells stably expressing CD4, CXCR4, and CCR5 and harboring the lacZ reporter genes under the control of the HIV LTR promoter were obtained through the NIH AIDS Reagent Program, Division of AIDS, NIAID, NIH: TZM-bl cells (Cat#8129) from Dr. John C. Kappes, and Dr. Xiaoyun Wu. TZM-bl cells and HEK293T cells were cultured in DMEM supplemented with 10% fetal calf serum (FCS), 100 units/mL penicillin, 100 mg/mL streptomycin, and 2 mmol/L L-glutamine (Gibco). SupT1 cells were cultured in RPMI supplemented with 10% FCS, 100 units/mL penicillin, 100 mg/mL streptomycin, 2 mmol/L L- glutamine and 1 mmol/L HEPES (Gibco). The BCR-ABL cell line was generated, introducing the BCR-ABL expression vector into bone marrow-derived wild type pro/pre B cells. Cells were cultured in Iscove's basal medium supplemented with 10% FCS, 100 units/mL penicillin, 100 units/mL streptomycin, 2 mmol/L L- glutamine and 50 mmol/L b-mercaptoethanol. Human CD14−CD4+ T cells from healthy male and female blood donors were prepared by negative selection using the RosetteSep CD4+ T cell enrichment cocktail according to the manufacturer's instructions and subsequent Ficoll density centrifugation and cultured in RPMI 1640 medium (Gibco) containing 10% FCS, penicillin (100 U/ml), streptomycin (100 µg/ml), 2 mM l-glutamine. The murine T cell line BW5147 derived from the thymus of a mouse with lymphoma (ATCC TIB-47™, kindly provided by H Hengel, Freiburg) was incubated in RPMI-1640 supplemented with 10% FCS, 1 mM sodium pyruvate, 100 units/mL penicillin, 100 µg/mL streptomycin and 50 µM β-mercaptoethanol. Retinoblastoma (RB) cell lines Weri-Rb1 [25] and Y79 [26], originally purchased from the Leibniz Institute DSMZ (German Collection of Microorganisms and Cell Cultures), were supplied by Dr. H. Stephan. The cultivation of the cells was carried out as described previously [27].

Hemolysis assay. Fresh human blood, collected by venipuncture, was centrifuged (10 min, 1000 x g, 4°C) to pellet erythrocytes, which were then washed three times and resuspended (1:10) in DPBS. Peptides were serially diluted in a 96-well plate in DPBS. To 90 µL of peptides, 10 µL of erythrocyte suspension was added. Following a 1-hour incubation at 37°C, while shaking at 500 rpm, the plates were centrifuged (5 min, 1000 x g, 4°C). Supernatant was transferred to transparent 96-well plates for absorbance measurement at λ=405 nm, with full erythrocyte lysis indicated by the Triton-X control.

Antibody competition. The antibody competition assay was performed as described before [19]. Briefly, SupT1 cells plated in 96-well plates (50.000 c/well). Medium was removed and plates precooled at 4°C. Compounds were serially diluted in cold PBS and added to the cells together with a single concentration of the fluorescently labelled antibodies clone 12G5-APC (Cat# 555976, BD Pharmingen) or clone 1D9-PE (Cat# 551510, BD Pharmingen) diluted in PBS supplemented with 1%

FCSfor 2 hours at 4°C. Afterwards, the unbound antibody was removed, and cells were analyzed by flow cytometry.

HIV-1 inhibition. To obtain viral stocks of CXCR4-tropic NL4-3 HEK293T cells were transiently transfected with proviral DNA, as described before [28]. Virus-containing supernatants were harvested after after 3 days and stored at -80°C in 1 ml aliquots. For the inhibition assay, TZM-bl reporter cells were plated in 96-well plates. The next day medium was changed to 70 µl growth medium supplemented with 2.5% FCS and cells pretreated with serially diluted (PBS) inhibitors for 15 min at 37 °C before virus was added. Infection rates were determined after 3 days using the Gal-Screen system (Applied Biosystems).

Akt or Erk phosphorylation. Phosphorylation of Akt and Erk was determined by phosphoflow. For this, cells were plated in 96-well plates and starved for 2 hours in medium containing 1% FCS at 37°C. Afterwards, compounds diluted in PBS were added for 10 min before cells were stimulated with 100 ng/ml CXCL12 for 2 min at 37°C. The reaction was stopped by adding 1% (w/v) paraformaldehyde (PFA). Cells were then permeabilized using methanol and stained with phospho-p44/ 42 MAPK (ERK1) (Tyr204)/(ERK2) (Tyr187) (D1H6G) mouse mAb (Cell Signaling, #5726) and phospho-AKT (Ser473) (193H12) rabbit mAb (Cell Signaling, #4058) and adequate sec- ondary antibodies for flow cytometry. Signal in the unstimulated control without inhibitor was defined as background and set to 0%. CXCL12 induced signal without inhibitor was set 100%.

Ca^{2+} signaling. Ca^{2+} signaling was analyzed as described previously [6]. Briefly, a murine cell line expressing the fusion protein BCR-ABL was loaded with Indo-1 AM (Invitrogen) and 0.5 mg/mL of pluronic F-127 (Invitrogen) in Iscove's medium supplemented with 1% FCS (Pan Biotech) at 37°C for 45 min, then washed and treated with the inhibitors diluted in PBS for 10 min at 37°C. CXCR4-dependent calcium signaling was determined by stimulating with 100 ng/mL of mouse CXCL12 using flow cytometry. The area under the curve (AUC) of each calcium flux plot was determined using FlowJo. In order to allow for inter-experimental comparison, the AUC was calculated after baseline subtraction for each single plot.

β-arrestin recruitment. Inhibition of CXCL12-induced recruitment of β-arrestin-2 to CXCR4 was determined using the NanoBiT protein-protein-interaction assay (Promega) in a modified antagonistic protocol as described before. [20]. Briefly, HEK293T cells were transiently transfected with SmBiT-β-arrestin-2 plasmid and CXCR4-LgBiT plasmid (generously provided by Jong-Ik Hwang). The next day, medium was changed to serum-free Opti-MEM before 25 µL of the NanoGlo Live Cell Assay System (Promega) was added to the cells. Compounds were titrated in PBS and added for 10 min before cells were stimulated with 30 nM CXCL12. The luminescence was recorded for 2 h. Area under the curves (AUC) of the signal over time was calculated for each treatment. The signal in the buffer control without inhibitor was defined as the background and set to 0%. CXCL12-induced signal without an inhibitor was set to 100%.

Chemotaxis. Chemotaxis was determined using 96-well transwell assay plates (Corning Incorporated, Kennebunk, ME, USA) with 5 µm polycarbonate filters. 75.000 cells were seeded into the upper chamber in RPMI-1640 supplemented with 2 mM L-glutamine, 100 units/ml penicillin, 100 µg/ml streptomycin and 0.1 % (w/v) bovine serum albumin (BSA) in the presence or absence of the compound diluted in PBS and allowed to settle for 15 min. Then, assay buffer supplemented with or without 100 ng/mL CXCL12 as well as compounds was filled into a 96-well-V plate (lower chamber) before the filter plates containing the cells was placed on top. Cells were allowed to migrate for 4 h at 37 °C (5% CO2). Cells migrated to the lower compartments were analyzed by the CellTiter-Glo assay (Promega).

Cell viability assay (WST-1). To investigate the cell viability of the retinoblastoma cell lines, sextuplicates of 4×10^4 cells were seeded in 200 µL DMEM based medium in a 96 well plate. The compounds were reconstituted with sterile-filtered H_2O at a stock solution concentration of 500 µM and

then added to a final concentration of 0.1 µM or 1 µM.. Subsequent to a 48, 72, 96 or 120-hour incubation period, 20 µL of a water-soluble tetrazolium (WST-1) solution (Sigma-Aldrich, St.Louis, USA) was added to each well, and the cells were incubated at 37 °C for another 2 hours. The formazan product generated by viable cells was quantified using a microplate reader (Agilent BioTek, Santa Clara, CA, USA) at an absorbance wavelength of 450 nm.

Cell proliferation assay (BrdU). The RB cell lines were first treated with the compounds (stock solution concentration 500 µM diluted in H_2O) to reach a final concentration of 0.1 µM or 1 µM. After 48-120 hours, the proliferation of the RB cell lines could be evaluated by adding 5 µM BrdU (5-bromo-2′-deoxyuridine; Sigma-Aldrich, Steinheim, Germany) to the cell culture growth medium.. Subsequently, 8×10^4 cells were seeded on Poly-D-Lysin (Sigma, St.Louis, USA) coated coverslips and incubated for 4 hours at 37°C with 10% CO_2. The cells were fixed in 4% paraformaldehyde (PFA; Sigma, St.Louis, USA) and permeabilized using 1% Triton X-100 (Sigma, St.Louis, USA) in PBS for 30 minutes. The DNA was denatured with 2 N HCl (Sigma, St.Louis, USA) for 1 hour. The solution was neutralized by adding 0.05 M boric acid (Sigma, St.Louis, USA) and 0.01 M sodium borate (Sigma, St.Louis, USA) dissolved in H_2O for 15 min. To minimize nonspecific binding, the cells were blocked in 5% BSA (bovine serum albumin; Sigma, St.Louis, USA) and 5% NGS (normal goat serum; Dako, Santa Clara, USA) in PBS containing 0.3 % Triton X-100. Subsequently, the blocking solution was exchanged to rat anti-BrdU primary antibody (1:1000; cat. # ab6326; Abcam, Cambridge, UK) diluted in 0.1 % Triton X-100 with 4% BSA and 1% NGS. The cells were incubated overnight at 4°C. The following day, the cells were washed (3x 5 min with PBS) and incubated with an Alexa Fluor 594-labeled goat anti-rat secondary antibody (1:1000 in PBS; cat. # A-1007, Molecular Probes, Eugene, OR, USA). Quantification of proliferating cells was performed by manual counting.

CAM assay. To evaluate the effects of the different inhibitors investigated on retinoblastoma (RB) cells on tumor formation potential and angiogenesis *in vivo*, 1×10^6 of Weri-Rb1 or Y79 RB cells were treated with either 1 µM of a mock control peptide, AMD3100, JM#21, or JM#198, dissolved in 50 µl PBS and subsequently grafted onto the chicken chorioallantoic membrane (CAM) *in ovo*. Therefore, a total of twenty fertilized eggs per treatment setting, preincubated to embryonic development day 10 (EDD10) were used in three independent experiments, in which the RB cells were grafted onto the CAM according to the protocol described previously by our group [27]. The modified protocol is based on the protocol established by Zijlstra and Palmer [29], [30]. On EDD17, the embryos were sacrificed and the tumors were excised, measured and photographed as described in previous studies [31], [32], [33]. Angiogenesis was evaluated in terms of total vessel area, vessel length, thickness and branching points by analyzing *in situ* images of the CAM tumors using the IKOSA online software (KLM Vision, Graz, Austria).

Stability of peptides in body fluids by antibody competition assay. Blood from healthy donors was collected in EDTA containing blood collection tubes. To obtain plasma, tubes were centrifuged at 2,500 x g for 15 min and the plasma phase collected. Plasma from 6 donors was pooled and immediately aliquoted and stored at -80°C. The stability of peptides in body fluids was determined by the antibody competition assay previously described [19]. Briefly, 20 µM of the peptides were spiked into 100% of the body fluid and incubated at 37°C on a shaker. Aliquots were taken and stored at -80°C before retained activity was determined using the antibody competition assay described above. For analyzing whole blood samples, an erythrocyte 1-Step fix lysis solution was added after removal of unbound antibody according to the manufacturer's instructions (eBioscience).

Estimation of the half-life in human plasma by mass spectrometry. Human plasma was spiked with 20 µM of the peptide and incubated at 37°C. Aliquots (10 µL) were separated at 0, 15, 30, 60, 120, 180, 240, 360, and 1440 min and mixed with 90 µL of a solution composed of 6 M GuHCl + 50 mM NH_4HCO_3 + 10 mM DTT. The samples were incubated for 20 min at room temperature. Every sample was loaded onto SPE HLB Oasis RP cartridges (Waters, USA), which were sequentially washed with

0.1% TFA/5% acetonitrile and 0.1%TFA/40%acetonitrile; the peptide was then eluted with 0.1%TFA/60% acetonitrile. The experiment was performed in triplicate. Samples were analyzed by an Axima Confidence MALDI-TOF MS (Shimadzu, Japan) in positive linear mode on a 384-spot stainless-steel sample plate. Spots were coated with 1 µL 5 mg/mL CHCA previously dissolved in matrix diluent (Shimadzu, Japan), and the solvent was allowed to air dry. Then 0.5 µL sample or standard was applied onto the dry pre-coated well and immediately mixed with 0.5 µL matrix; the solvent was allowed to air dry. Positive ions were accelerated at 20 kV, and laser shots (50 Hz and 50% of its full power) were automatically done following a regular circular raster of a diameter of 2000 µm and spacing of 200 µm on every well; 100 profiles were acquired per sample, and 20 shots were accumulated per profile. The samples from the three experiments in human plasma were measured in triplicate (81 measurements in total). The measurement and MS data processing (peak area calculation) were controlled by MALDI-MS Application Shimadzu Biotech Launchpad 2.9.8.1 (Shimadzu, Japan). Half-lives were calculated using GradPath Prism 9.3.1 (GradPath Software, LLC).

***In vivo* circulation time.** 3.5 mg/kg (70 µg/mouse) of compound in 100 µL of 0.9% NaCl was intravenously injected in the tail vein of male or female C57BL/6NCrl (BL6) mice. After the indicated times, mice were sacrificed by cervical dislocation. Blood was collected by heart punctation and 19:1 diluted with 0.16 M NaEDTA and then centrifuged at 2000g for 20 min at 4 °C to obtain plasma. Plasma was stored at −80 °C before the remaining peptide activity in the plasma was determined by antibody-competition assay as described above.

Estimation of the concentration in mouse plasma by mass spectrometry. Peptide standards were prepared in PBS at the following concentrations: 20, 100, 250, 500, 1250, and 2500 µM. A 1 µL-aliquot of each standard was added to 10 µL mouse plasma for a final concentration of 1.8, 9.1, 22.7, 45.4, 113.6, and 227.3 µM, respectively. A 10 µL-aliquot of sample or standard (in mouse plasma) was mixed with 90 µL of a solution composed of 6M GuHCl + 50mM NH_4HCO_3 + 10 mM DTT. The samples were incubated for 20 min at room temperature. Every sample was loaded onto SPE HLB Oasis RP cartridges (Waters, USA), which were sequentially washed with 0.1% TFA/5% acetonitrile and 0.1%TFA/40%acetonitrile; the peptide was then eluted with 0.1%TFA/60% acetonitrile. Samples and standards in mouse plasma were analyzed by an Axima Confidence MALDI-TOF MS (Shimadzu, Japan) in positive linear mode on a 384-spot stainless-steel sample plate, as described above, after spotting them in triplicate. A calibration curve of (spectral) peak area vs. peptide concentration in mouse plasma was constructed. Concentrations of the peptide in mouse plasma were estimated by interpolation of the spectral peak area of the mouse plasma sample (unknown concentration) within the calibration curve. GradPath Prism 9.3.1 (GradPath Software, LLC) was used to construct the calibration curve and calculate the peptide concentration in mouse plasma. For determining dedgradation products of the peptides in plasma MS/MS spectra of JM#198/JM#143 and their respective degradation products were analyzed by PEAKs11 [34] processing of raw data from LC-MS/MS analysis performed as previously described [35].

Molecular modeling. For CXCR4, we used the structure previously modeled by us that includes both, the CXCR4 transmembrane domain (PDB ID: 3ODU) [36] and the N-terminal loop (PDB ID: 2K04) [37]. The JM#143 lipopeptide was built taking the binding pose of JM#21 bound to CXCR4 previously reported by Sokkar et al. [5] and manually linked to a palmitic acid (16:0 hexadecanoic acid) moiety. The lipopeptide was parametrized with the *Ligand Reader and Modeler* tools [38] for the CHARMM General Force Field (CGenFF) [39] in the CHARMM-GUI web server [40].

The CXCR4-JM#143 complex was embedded in a 100 x 100 Å 1-palmitoyl-2-oleoyl-sn-glycero-3-phosphocholine (POPC) bilayer, composed of 252 lipid molecules using the CHARMM-GUI *Membrane Builder* tool. The system was solvated with TIP3P [41] water molecules and 50 mM KCl were added. The system was energy-minimized and equilibrated in 6 steps of 500 ps, applying harmonic position restraints with a starting force constant of 10 kcal/mol·$Å^2$ on the atoms of the protein and the

lipid heads, and gradually reduced to zero. The Particle Mesh Ewald method [42] was used for the computation of long-range electrostatics. Short-range Lennard-Jones and electrostatic interactions were calculated with a switching function between 10 Å and a cutoff value of 12 Å. Langevin dynamics [43] was used to maintain the temperature at 300 K and a Nose-Hoover piston [44] was used for maintaining the pressure at 1 atm. After the equilibration steps, 50 ns classical molecular dynamics simulation was performed with 2 fs of integration time, releasing all the restraints, except for the z coordinate of the center of mass of the phosphate group of all lipids, subjected to harmonic restraints of 50 kcal/mol per $Å^2$ to avoid translation of the membrane along the z axis.

Dual-boost Gaussian Accelerated Molecular Dynamics simulations (GaMD) [45], [46] were performed applying boost potentials on the total energy of the system and the dihedrals angles. The biasing potentials were equilibrated in two steps: first, 8 ns of classical MDs in which the potential energy distribution of the system is monitored. Thereafter, the biasing potential was equilibrated during 50 ns by setting the threshold value to the maximum potential energy sampled during the previous equilibration step and successively updating this value after every step of the simulation. A maximum value of 6 kT was employed to control the standard deviation of the biasing potential. Five replicas of 350 ns each of GaMD simulations were performed for a total sampling of ~1 μs. All the simulations were performed with NAMD (v2.13) [47] employing the CHARMM36m force field [48].

RMSF and temperature B-factor calculations were performed with the *gmx rmsf* tool of the GROMACS suite [49]. The contacts analysis was done with in house scripts in VMD [50], using a distance cutoff between heavy atoms of 5 Å. VMD and UCSF Chimera [51] were used for visualization of the structures.

Statistics. IC_{50} values were determined by nonlinear regression curve fit using GraphPad Prism (version 9.3.1). Correlations were performed by Pearson correlation with a two-tailed P value and confidence interval of 95%.

Ethics. The study was conducted in accordance with the declaration of Helsinki and approved by the Ethics Committee of Ulm University. Informed consent was obtained from all of the subjects involved in the study. The animal studies were approved (ethical approval code 1375) by the Regional Council (Regierungspräsidium Tübingen, Baden-Württemberg, Germany) in compliance with the German laboratory animal experimentation act, and study procedures were in accordance with the European Communities Council Directive of September 22, 2010 (2010/63/ EU). All applicable institutional and national guidelines for the care and use of animals were followed.

Results

Design and characterization of fatty acid coupled EPI-X4 derivatives

Long chain fatty acids C14 (myristic acid), C16 (palmitic acid), and C18 (stearic acid) were conjugated to ε-amino side chains of lysines in the peptides EPI-X4 WSC02 or JM#21, either directly or via a glutamic acid linker. The coupling involved lysine residues already existing in the peptide sequences (at position 6 and 7 for WSC02, and position 7 for JM#21), or those that were newly introduced (in JM#145 and JM#202). In addition, to enhance stability, variants were designed with D-amino acids at the N-terminus [20], or other modifications such as C-terminal truncations combined with C-terminal amidation (Table 1).

Table 1: Overview of all compounds used in the study

Compound	Sequence	IC$_{50}$ (nM ± SEM)		Apparent activity (% ± SEM)[c]	
		12G5[a]	HIV-1[b]	2 hours	8 hours
AMD3100	-	577 ± 57	23 ± 3	na	na
EPI-X4	LVRYTKKVPQVSTPTL	2008 ± 183	39222 ± 10673	23 ± 2	14 ± 3
Alb409-423	VRYTKKVPQVSTPTL	nd	nd	na	na
WSC02	IVRWSKKVPCVS	349 ± 71	424 ± 45	12 ± 2	7 ± 2
JM#21	ILRWSRKLPCVS	193 ± 22	123 ± 12	6 ± 2	3 ± 1
JM#21-Ac	ILRWSR(K-Ac)LPCVS	237 ± 34	172 ± 32	16 ± 2	4 ± 0.3
JM#201	ILKWSRK-NH2	3110 ± 576	na	na	na
C14 JM#21 analogues					
JM#204	ILRWSR(K-Glu-Myr)LPCVS	35 ± 2	469 ± 127	37 ± 2	36 ± 4
JM#216	ILRWSR(K-Myr)LPCVS	43 ± 7	110 ± 23	25 ± 2	29 ± 4
JM#262	ILRWSR(K-Myr)-NH2	15 ± 2	66 ± 6	96 ± 7	105 ± 1
JM#263	ILRWSR(K-Glu-Myr)-NH2	22 ± 2	28 ± 3	76 ± 15	80 ± 4
JM#261	(d-L)LRWSR(K-Myr)-NH2	44 ± 4	nd	84 ± 7	92 ± 6
JM#260	(d-L)LRWSR(K-Glu-Myr)-NH2	42 ± 8	26 ± 8	105 ± 7	130 ± 10
JM#202	IL(K-Glu-Pal)WSRK-NH2	2536 ± 1099	na	na	na
C16 WSC02 analogues					
JM#168	IVRWS(K-Pal)KVPCVS	969 ± 192	330 ± 100	21 ± 4	28 ± 3
JM#169	IVRWSK(K-Pal)VPCVS	5 ± 2	18 ± 4	37 ± 3	39 ± 3
JM#164	IVRWS(K-Pal)K-NH2	2801 ± 173	nd	na	na
JM#165	IVRWSK(K-Pal)-NH2	2864 ± 603	nd	na	na
JM#166	IVRWS(K-Pal)KVP-NH2	11 ± 8	780 ± 752	103 ± 14	101 ± 16
JM#167	IVRWSK(K-Pal)VP-NH2	5 ± 2	43 ± 14	104 ± 11	104 ± 10
C16 JM#21 analogues					
JM#143	ILRWSR(K-Glu-Pal)LPCVS	164 ± 65	317 ± 84	103 ± 12	116 ± 9
JM#144	ILRWSR(K-Pal)LPCVS	115 ± 22	207 ± 75	131 ± 20	125 ± 16
JM#145	ILRWSRKLPC(K-Glu-Pal)S	100 ± 22	1394 ± 1180	156 ± 25	163 ± 21
JM#149	ILRWSR(K-Pal)MPCLS	371 ± 41	145 ± 44	199 ± 43	186 ± 8
JM#140	(d-L)LRWSR(K-Pal-Glu)MPCVS	300 ± 82	181 ± 122	67 ± 9	57 ± 11
JM#141	(d-L)LRWSR(K-Pal)MPCVS	190 ± 38	23 ± 2	20 ± 4	23 ± 5
JM#177	M(d-L)RWSR(K-Pal)LPCVS	214 ± 50	nd	45 ± 4	59 ± 7
JM#170	ILRWSR(K-Pal)-NH2	9 ± 1	48 ± 16	126 ± 22	123 ± 5
JM#171	ILRWSR(K-Pal)LP-NH2	4 ± 1	20 ± 7	98 ± 6	98 ± 14
JM#172	ILRWSR(K-Pal)L-NH2	6 ± 2	69 ± 50	122 ± 17	118 ± 16
JM#191	ILRWSRK(K-Glu-Pal)-NH2	3 ± 0.3	31 ± 4	102 ± 4	103 ± 9
JM#192	ILRWSR(K-Glu-Pal)-NH2	11 ± 3	5 ± 1	99 ± 5	105 ± 11
JM#193	ILRWSRKL(K-Glu-Pal)-NH2	3 ± 0.4	19 ± 2	94 ± 14	99 ± 8
JM#194	(d-L)MRWSR(K-Glu-Pal)-NH2	14 ± 5	6 ± 2	101 ± 9	118 ± 11
JM#180	(d-L)LRWSR(K-Pal)-NH2	19 ± 4	144 ± 71	131 ± 7	151 ± 29
JM#235	(d-L)LRWSR(K-Glu-Pal)-NH2	24 ± 6	10 ± 3	108 ± 10	112 ± 5
JM#236	(d-L)LRWSR(K-Pal)-NH2	57 ± 13	nd	130 ± 19	134 ± 21
JM#237	(d-I)LRWSR(K-Pal)-NH2	94 ± 14	158 ± 64	200 ± 17	192 ± 16
JM#238	(d-I)LRWSR(K-Glu-Pal)-NH2	19 ± 1	5 ± 2	120 ± 10	119 ± 17
C18 JM#21 analogues					
JM#198	ILRWSR(K-Glu-Ste)LPCVS	3 ± 1	79 ± 22	109 ± 9	132 ± 30
JM#182	ILRWSR(K-Ste)LPCVS	24 ± 2	189 ± 80	61 ± 2	58 ± 4
JM#254	ILRWSR(K-Ste)-NH2	66 ± 8	28 ± 8	105 ± 13	100 ± 15

JM#255	ILRWSR(K-Glu-Ste)-NH2	35 ± 7	3 ± 1	144 ± 16	132 ± 14
JM#256	(d-L)LRWSR(K-Ste)-NH2	443 ± 196	134 ± 65	397 ± 43	431 ± 51
JM#257	(d-L)LRWSR(K-Glu-Ste)-NH2	119 ± 38	7 ± 3	143 ± 15	167 ± 9

[a] Competition with the CXCR4 antibody clone 12G5. [b] Inhibition of CXCR4-tropic HIV-1. [c] Apparent activity in human plasma after 2 or 8 hours of incubation compared to t = 0 hours control. na = not analyzed, nd = not detectable

In an antibody competition assay, the binding affinities of of the various lipopeptides to CXCR4 were assessed. The fluorescently labelled antibody clone 12G5, which binds close to the binding pocket of CXCR4, was dose-dependently replaced by the small molecule AMD3100 (IC_{50} = 577 nM), and the wild-type peptide EPI-X4 (IC_{50} = 2 µM), but not the N-terminally truncated ALB409-423, as expected from previous data[19]. Unconjugated EPI-X4 WSC02 as well as JM#21 replaced the antibody with IC_{50} values of 349 nM and 193 nM, confirming previous results (Figure S1a, Table 1) [6], [19]. Acetylation of the lysine residue at position 7 only marginally reduced activity (JM#21-Ac, IC_{50} = 237 nM), however replacement of the leucine at position 2, or acetylation of this position reduced binding affinity (Figure S1b). This was expected since the N-terminus of the peptide is required for receptor interaction [5]. All lipopeptides with derivatization at position 6, 7, or 11 replaced the antibody with IC_{50} values between 3 and 2864 nM (Figure 1a, Figure S1c, Table 1). The weakest binders were the WSC02 derivatives (JM#164, JM#165, JM#168) with IC_{50} values above 900 nM. Lipopeptides with the highest affinity were C-terminally truncated and palmitoylated JM#21 variants (JM#170-172, JM#191-193, IC_{50} values between 3 nM and 11 nM), as well as the 12-aa JM#21 derivative JM#198 (IC_{50} = 3 nM), in which a stearic acid was conjugated via a glutamic acid to lysine at position 7. In general, most fatty acid derivatives were more active than their precursor peptides, with versions having the N-terminus replaced by d-amino acids being about 2-fold less active than variants with isoleucine at position 1 (Figure 1a, Figure S1c, Table 1). Importantly, the fatty acid derivatives did not displace the CXCR4-specific antibody clone 1D9, which interacts with the receptor N-terminus, indicating specificity in the binding interactions (Figure S2). Notably, JM#198, the most potent derivative in the 12G5-antibody competition assay, was as detectable as the precursor JM#21 in buffered solution (Figure S3a, b). However for JM#198b we noted the formation of superstructures with 100-200 nm size in aqueous solution, which may play a role for activity or stability (Figure S4a-d).

Fatty acid EPI-X4 derivatives inhibit CXCR4-tropic HIV-1 infection

The human immunodeficiency virus type1 (HIV-1) infects target cells via intitial binding to CD4 and subsequent interactions with a co-receptor, either CCR5 or CXCR4 [52]. EPI-X4 was initially discovered as an inhibitor for CXCR4-tropic HIV-1, and the optimized derivatives EPI-X4 WSC02 and JM#21 have been reported to specifically inhibit CXCR4- but not CCR5-tropic HIV-1 [2], [6]. To test whether fatty acid derivatives also inhibit CXCR4-tropic HIV infection, we pretreated TZM-bl reporter cells with the test compounds and inoculated the cells with virus afterwards. AMD3100 inhibited viral infection with an IC_{50} of 23 nM, confirming previous results [53]. The inactive control (ALB409-423) was not active at concentrations up to 100 µM (Figure S5a). However, EPI-X4 WSC02 and JM#21 inhibited HIV-1 infection with IC_{50} values of 424 nM and 123 nM, respectively, as expected [2], [6]. With a few exceptions, IC_{50} values obtained for HIV-1 inhibition correlated with data from the antibody competition assay (R^2 = 0.7440, P < 0.0001, Pearson correlation), with JM#192, JM#194, JM#238, JM#255 and JM#257 exhibiting IC_{50} values below 10 nM (Figure 1b, Figure S5a-d, Table 1). In contrast, none of the tested lipopeptides affected the infection with a CCR5-tropic HIV-1 strain (Figure S6).
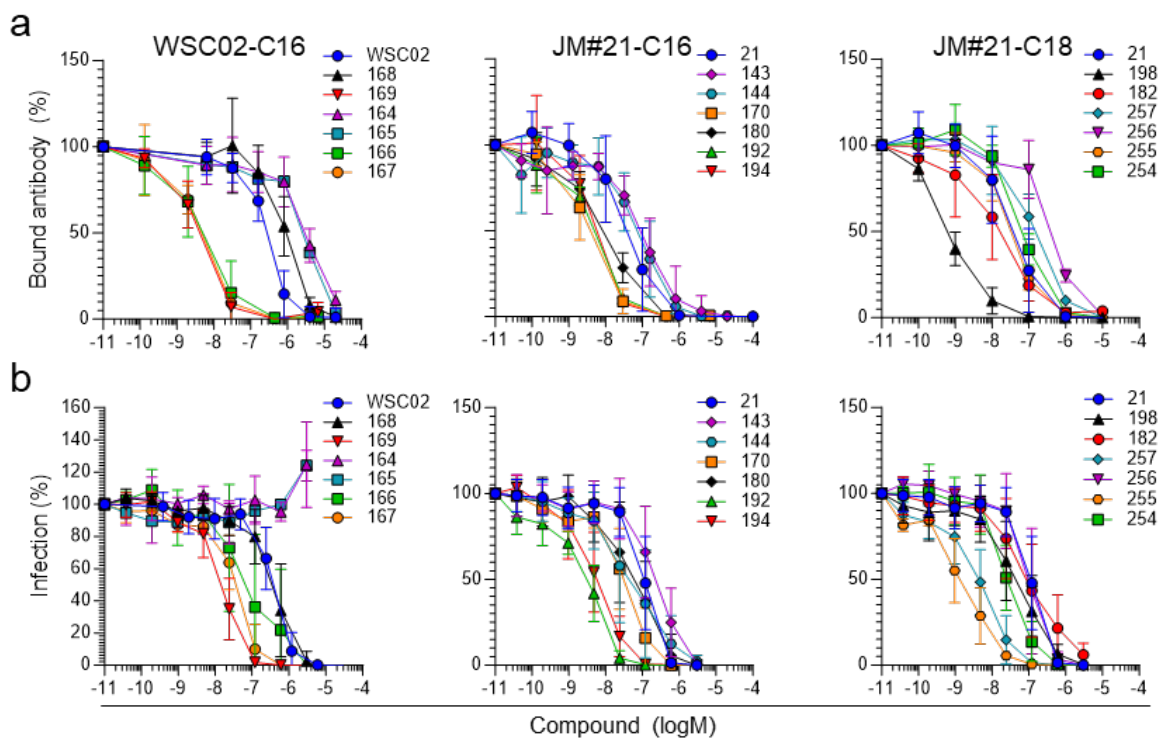
Figure 1. Fatty acid conjugates compete with CXCR4 antibody binding and inhibit CXCR4-tropic HIV-1 infection. a) Antibody competition: Serially-diluted compound was added to SupT1 cells together with a constant concentration of the CXCR4 antibody clone 12G5. After 2 hours of incubation at 4°C, the unbound antibody was removed, and cells were analyzed by flow cytometry. b) HIV-1 inhibition: TZM-bl reporter cells were pretreated with the compounds for 15 min before they were inoculated with CXCR4-tropic HIV-1. Infection rates were determined after 3 days by β-galactosidase assay. Shown are means derived from at least 3 individual experiments performed in singlicates (a) or triplicates (b) ± SD.

Computational modeling of EPI-X4-based lipopeptides interacting with CXCR4

To gain more insights into the binding of the lipopeptides to CXCR4, we selected JM#143, the palmitoylated derivative of JM#21, for Gaussian accelerated Molecular Dynamics (GaMD) simulations [51], [54], [55] (Figure 2). The simulations indicate that the fatty acid moiety does not interact with the binding site of the peptide and hence does alter the binding pose of the JM#143 pharmacophore to the CXCR4 pocket (Figure 2a). In fact, the binding is stabilized by interactions between the fatty acid's acyl chain and the N-terminal loop of CXCR4, while preserving positively charged residues in the N-terminal region, specifically Arg3 and Arg6, which are crucial for binding. Comparison with the published molecular dynamics simulations of the CXCR4-JM#21 complex [5] shows that the presence of the fatty acid decreases the flexibility of the peptide, particularly in the C-terminal region (residues 8 – 12). This is reflected in the lower temperature B-factor values computed from the fluctuations of the atoms of JM#21 and JM#143 during the simulations (Figure 2b) compared to the fluctuations of the receptor´s TM unit in each simulation. Furthermore, when compared to the CXCR4-JM#21 complex, in JM#143 the presence of the fatty acid results in a decrease of the flexibility of the N-terminal loop of CXCR4 (residues 1-30), especially residues 4-13, as indicated by the root-mean-squared fluctuations (RMSF) of the backbone of the loop (Figure 2c) compared to the fluctuations of the receptor´s TM unit in each simulation. This effect is related to the hydrophobic contacts between the fatty acid and residues in the N-terminal loop of CXCR4, in particular Y7, Y12, M16, Y21, M24, and F29 (Figure 2d, e). Despite the fact that the N-terminal loop is not a hydrophobic region, these contacts result in the N-terminal loop of the receptor wrapping the aliphatic chain of the fatty acid to shield it from the solvent, with the consequent loss of flexibility of the N-terminal loop of CXCR4. Interactions between methionine and hydrophobic residues have been previously reported to be involved in molecular recognition and folding stabilization [56], [57]. Furthermore, the plots of the RSMD values of the N-

12

terminal loop of CXCR4 and the acyl chain of fatty acid show two areas with a negative correlation. Altogether, while the RSMD of the N-terminal loop of CXCR4 increases (more mobility), the RMSD of the fatty acid decreases (less mobility) (Figure S7).
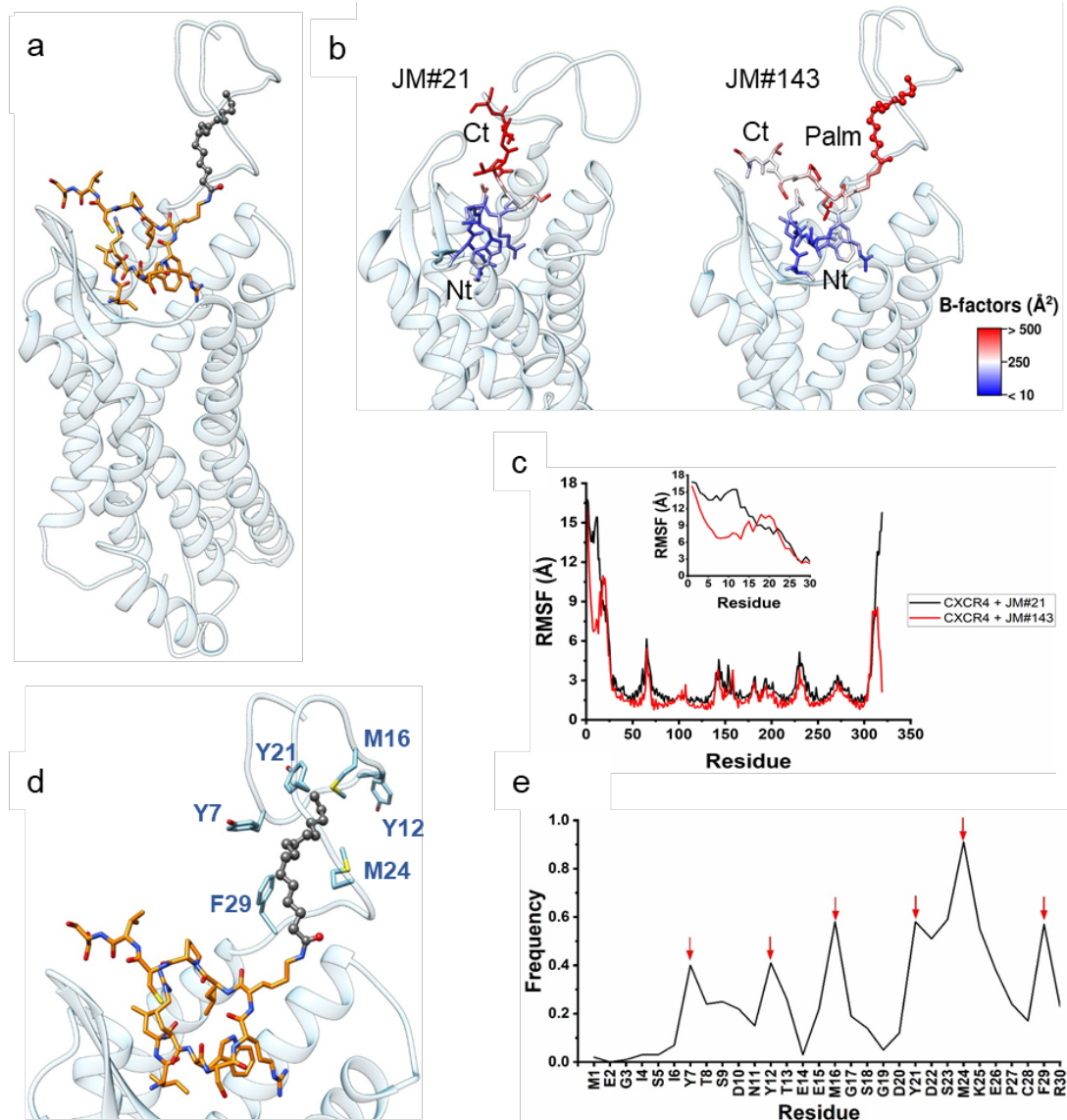
Figure 2: Interaction of JM#143 with CXCR4. a) Representative structure of the CXCR4-JM#143 complex from the GaMD simulations. Light blue ribbons: CXCR4; orange sticks: peptide moiety; dark gray balls: palmitic acid. b) Temperature B-factors of the heavy atoms of JM#21 and JM#143 (blue-red color scale). Sticks: N-terminal region of the peptide (Nt, residues 1-7) and C-terminal region (Ct, residues 8-12). Balls: palmitic acid moiety (Palm). C) RMSF of the backbone of CXCR4 bound to JM#21 and JM#143. The inset plot zooms on the region corresponding to the N-terminal loop of CXCR4 (residues 1-30). c) Contact frequency between the aliphatic chain of the fatty acid moiety and the N-terminal loop of CXCR4. The red arrows highlight the residues with the highest contact frequency. e) Residues of CXCR4's N-terminal loop (in light blue) with the highest contact frequency with the palmitic acid moiety.

EPI-X4 lipopeptides inhibit CXCL12-mediated signaling

Upon binding to CXCR4, CXCL12 activates several downstream pathways, including the phosphorylation of signaling proteins, such as Akt and Erk, and the release of calcium (Ca^{2+}) from intracellular stores, finally resulting in chemotaxis and migration following CXCL12 gradients. Under healthy conditions, CXCL12-mediated signaling is terminated by C-terminal phosphorylation of the receptor, leading to the recruitment of β-arrestin and receptor internalization. However, in several

diseases, including cancer, these signaling pathways may become overly active or dysfunctional due to accumulated mutations [1].

Here, we evaluated the potential of the lipopeptides to inhibit CXCL12-induced signaling pathways. Initially, we treated a T lymphoma cell line (SupT1) with the compounds, followed by CXCL12 stimulation for 2 min. Phosphorylation of Akt and Erk was subsequently analyzed by flow cytometry. AMD3100, EPI-X4, WSC02 and JM#21 all antagonized CXCL12-induced phosphorylation in a dose-dependent manner, with JM#21 showing the higher efficacies than the other non-lipid compounds (Figure 3a, b). Most tested lipopeptides outperformed their respective precursors in activity, some of them more than 100-fold (JM#169, JM#143, JM#182, JM#192, JM#194, JM#198, JM#254-257). Generally, the activity of the peptides increased with longer fatty acid chain lengths (Figure 3a, b, Figure S8).

We also investigated whether the compounds inhibit recruitment of β-arrestin to CXCR4 in response to CXCL12. For this, we used the NanoBiT assay in which two subunits of a luciferase reporter construct (SmBiT and LgBiT) were fused to β-arrestin and CXCR4, respectively, and transiently transfected into 293T cells. Upon CXCL12-mediated recruitment of β-arrestin to CXCR4 the subunits form a functional enzyme that generates a luminescence signal. Both AMD3100 and JM#21 effectively blocked the CXCL12-induced signal at concentrations of 0.1 µM (83 % and 65 % inhibition) and higher, similar to the majority of the lipopeptides tested (Figure 3c). In this context, the stearic acid coupled JM#198 exhibited the least antagonistic activity (20 % and 79 % inhibition at 0.1 µM and 1 µM, respectively), while the shortened and palmitoylated JM#194 displayed the highest activity (complete inhibition at 0.1 µM) (Figure 3c). In addition, neither JM#21, nor the stearic acid variant JM#198 induced β-arrestin recruitment to any other GPCRs we tested (GPR15, CXCR3, CCR6, CCR5, ACKR3, CCR7, CCR2, CXCR1) and only significantly inhibited agonist-induced β-arrestin recruitment to CXCR4, indicating that the fatty acid conjugation does not alter specificity of the compounds (Figure S9a,b).

To assess if the compounds inhibit cell migration towards a CXCL12 gradient, we utilized a transwell assay. At the tested concentrations, AMD3100, EPI-X4 WSC02, and JM#21 marginally impeded the chemotaxis of SupT1 cells towards CXCL12 (Figure 3d, Figure S10). Conversely, all fatty acid derivatives demonstrated greater effectiveness than their precursors, with those conjugated to stearic acid showing the highest activity (> 100-fold increase compared to JM#21) (Figure 3d, Figure S10).

To further examine the function impact of the peptides on CXCR4 signaling, precursor B cells known for their robust Ca2+ release in response to CXCL12 were treated with selected compounds before CXCL12 stimulation, with subsequent monitoring of Ca2+ release via flow cytometry. AMD3100 blocked the signal already at a concentration of 0.1 µM, whereas JM#21 was about 10-fold less effective. Surprisingly, the myristic acid conjugate JM#204 had no effect on CXCL12-induced Ca^{2+} release. In contrast, all other lipopeptides tested led to a dose-dependent inhibition of the signal (Figure 3e).

The assays described above were performed in immortalized cell lines. Thus, antagonistic effects for selected derivatives were assessed on primary CD4+ cells isolated from human blood. EPI-X4 JM#21 inhibited Akt and Erk phosphorylation with IC_{50} values of 1.2 µM and 1.3 µM, respectively. AMD3100 inhibited signaling with slightly higher IC_{50} values of 1.7 µM and 3 µM, respectively (Figure S11a,b , Table S1). All tested fatty acid derivatives were more active, with the stearic acid conjugate JM#198 being the most active derivative (IC_{50} = 0.18 µM and 0.17 µM, respectively). Similarly, JM#21 and AMD3100 inhibited CXCL12-induced migration with IC_{50} values of 1.5 µM and 1.7 µM, respectively, whereas JM#198 was active with an IC_{50} value of 0.35 µM (Figure S11c Table S1). In contrast, all tested compounds were slightly less active on a mouse cell line (Figure S11d, Table S1). JM#21 and AMD3100 inhibited mouse CXCL12-mediated signaling with IC_{50} values of 8.3 µM and 2.7 µM, respectively. JM#198 was about 2-fold less active than on the human cells with an IC_{50} value of 0.7

μM. Interestingly, JM#194 showed no antagonistic activity on the mouse cell line (IC$_{50}$ value > 10 μM) (Figure S11d).
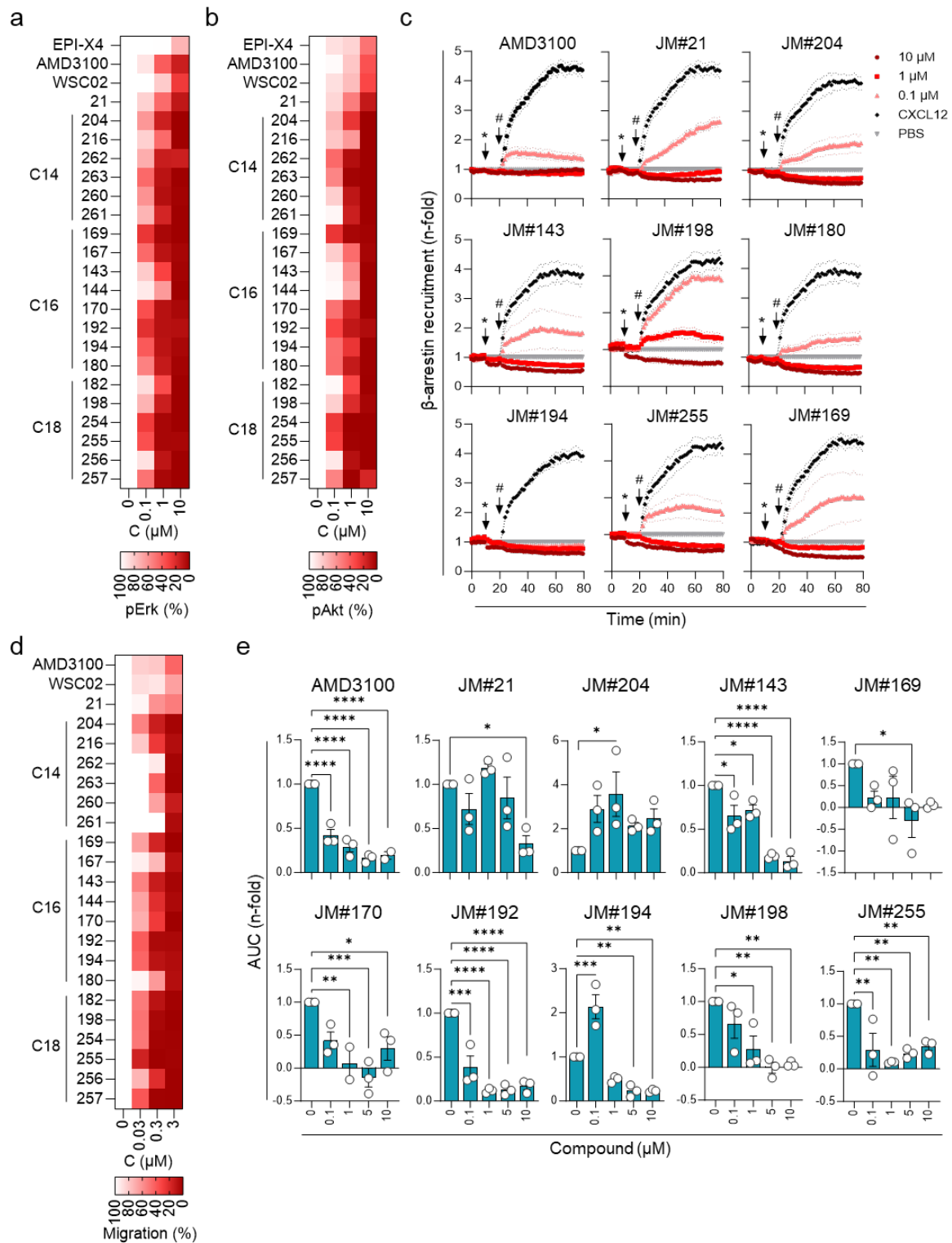

Figure 3. Fatty acid derivatization of peptides increases antagonistic activities. a-b) Inhibition of CXCL12-induced Erk (a) or Akt (b) phosphorylation. SupT1 cells were pretreated with compounds for 10 min and then stimulated with 100 ng/ml CXCL12 for 2 min. The reaction was stopped by adding 1 % PFA. Cells were then stained and analyzed by flow cytometry. unstimulated cells = 0 %, CXCL12 w/o compound = 100 %. See also Figure S8. c) Inhibition of CXCL12 induced β-arrestin recruitment. HEK293T cells were transfected with a plasmid containing β-arrestin-2 and a CXCR4 construct coupled to the two parts of the NanoBiT protein–protein interaction assay system. Cells were stimulated with 30 nM CXCL12 in the presence

15

of compounds, and the signal was determined over time. n = 3 ± SEM. d) Inhibition of CXCL12 mediated chemotaxis. SupT1 cells were allowed to migrate towards 100 ng/ml CXCL12 in the presence of compounds for 4 hours. unstimulated cells = 0 %, CXCL12 w/o compound = 100 %. See also Figure S10. e) Inhibition of CXCL12 induced Ca^{2+} release. BCR-ABL expressing murine pro/pre B cells were loaded with Indo-1 AM and incubated with inhibitors for 10 min. Baseline fluorescence signal was recorded for 30 s and calcium flux induced by stimulation with 100 ng/mL mCXCL12. Signal was recorded for additional 260 s. Areas under the curves (AUC) were calculated after baseline subtraction. Data. * $p \le 0.05$, ** $p \le 0.01$, *** $p \le 0.001$, **** $p \le 0.0001$ (one-way ANOVA). n = 3 ± SEM.

Fatty acid-coupled EPI-X4 derivatives are stable in human blood and plasma

We have previously shown, that EPI-X4 JM#21 is unstable in human blood plasma, exhibiting a half-life of only 6 minutes, leading to a rapid loss of activity [6], [35]. To investigate the protective role of long-chain fatty acids, we compared the stability of fatty acid conjugates with the unconjugated peptide. For this, compounds were added to 100% plasma and incubated at 37°C. Samples were collected immediately (t = 0), and after 2 and 8 hours, and then examined for their ability to compete with the 12G5 antibody for receptor binding (Figure 4a, b). IC_{50} values were normalized to t = 0 and presented as fold change or % retained activity as described previously [19] (Table 2).

The results showed that EPI-X4 JM#21 experienced a significant increase in IC_{50} values over time, with only 7% activity remaining after 2 hours and 4% after 8 hours (Figure 4a, Table 2) [6]. Acetylation (JM#21-Ac) only slightly improved stability (Figure 4a, Table 2). In contrast, fatty acid conjugates JM#143 and JM#198 demonstrated markedly increased stability in human plasma compared to the unconjugated peptide (Figure 4a, Table 2, Figure S12). Similarly, most lipidated EPI-X4 conjugates did not show any activity loss even after 8 hours of incubation in plasma, with a few exeptions (Figure 4b): C14 variants were generally less stable than C16 and C18 conjugated peptides (e.g. JM#204, JM#216). The palmitoylated WSC02 analogues (JM#168, JM#169) were less stable than the respective JM#21 analogue (JM#144), and the stearic acid conjugate JM#182 exhibited a lower stability than the derivative JM#198, in which the fatty acid was conjugated to the peptide backbone via a glutamic acid linker. Surprisingly, also lipidated JM#21 variants with modified N-termini (JM#140, JM#141, JM#177) exhibited a comparably low stability (Figure 4b). In contrast, all C16 and C18 conjugated truncated JM#21 and WSC02 variant showed no loss of activity after 8 hours of incubation in human plasma. Mass spectrometry data for the stearic acid-conjugated JM#198 confirmed the minimal change over time, supporting the hypothesis of increased stability through fatty acid conjugation (Figure 4c, d, Figure S13). Additionally, fatty acid conjugates showed superior stability compared to unconjugated peptides in whole human blood (Figure 4e, Figure S14), as determined for a representative panel of conjugates. Especially truncated palmitoylated variants and stearic acid derivatives maintained their activity throughout the testing period (Figure 4e).

Crucially, while JM#21 displayed only weak interaction with human serum albumin (HSA) (Figure S15a, c) [35], fatty acid derivatization significantly enhanced this interaction, which lead to an increased activity of lipopeptides in the presence of HSA (Figure S15b, d, e). We noticed, that some of the lipopeptides, rather than showing decreased activity after incubation in blood plasma, were more active after incubation, which is most likely attributed to this effect. The interaction with HSA is suggested to be the key to the enhanced stability of these conjugates in body fluids, providing protection against enzymatic degradation, which is lost in the absence of HSA (Figure S15f).
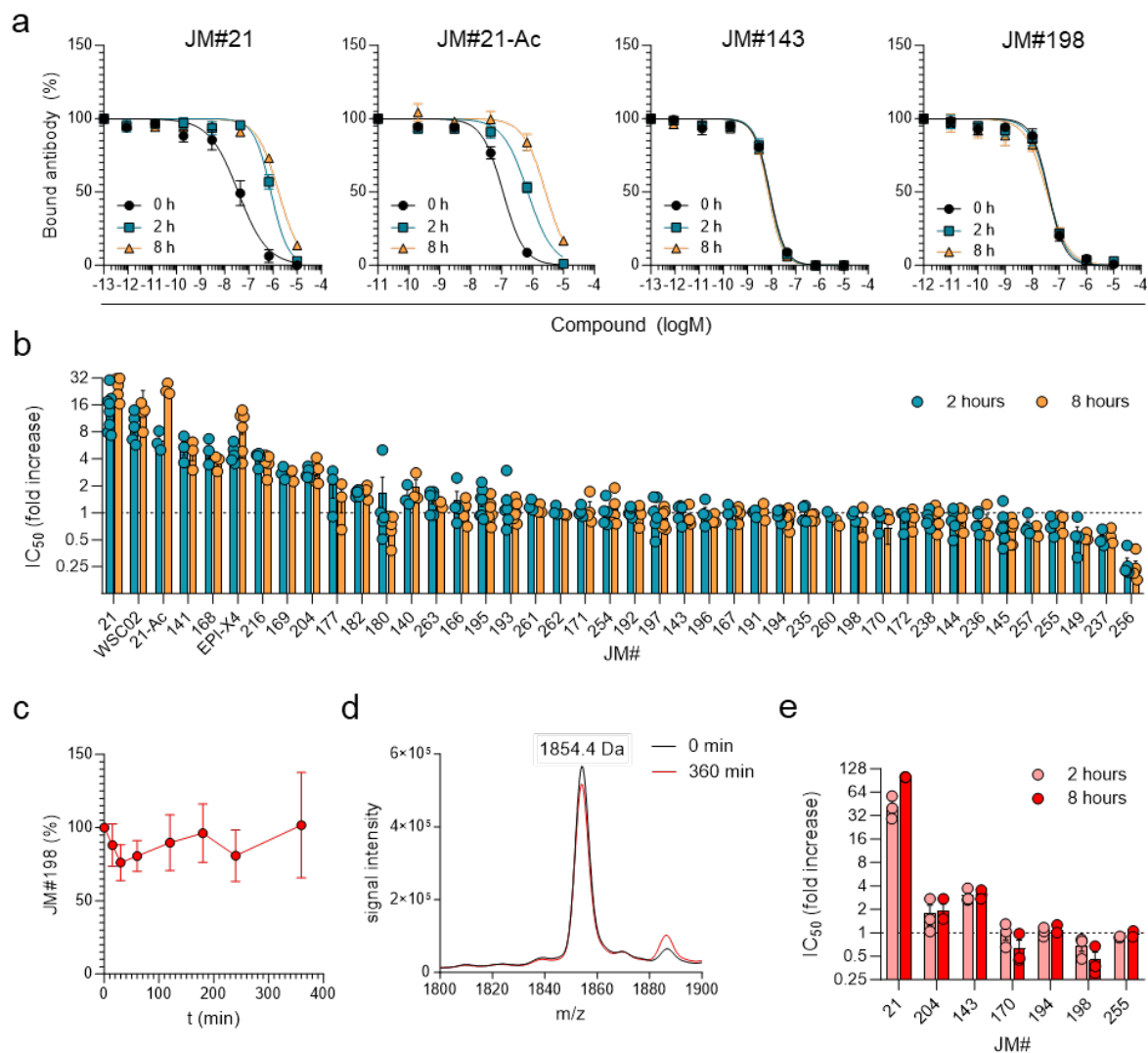
Figure 4. Fatty acid derivatization of peptides increases stability in human plasma and blood. a,b) 20 µM of the compounds was spiked into 100% of human plasma and incubated at 37°C. Aliquots were taken immediately (t = 0 hours), and after 2 and 8 hours and stored at -80°C. Aliquots were serially diluted and analyzed in parallel for 12G5 antibody competition to determine the remaining activities. a) Representative antibody competition curves. IC_{50} values were determined by non-linear regression. Shown are means of at least 3 individual rounds of incubation ± SEM. Fold changes were determined by IC_{50} (t) / IC_{50} (t = 0 hours). Apparent activity was determined by IC_{50} (t = 0) / IC_{50} (t) x 100. See also Table 2. b) Increase in IC_{50} values for all derivatives after 2 or 8 hours of plasma incubation compared to the t = 0 hours control. Shown are means of at least 3 individual rounds of incubation ± SEM. In the figure, derivatives are arrangend in descending order of stability after 2 h (see also Figure S12) c) The stability of JM#198 in human plasma was estimated by MS after incubation for 6. Signal intensity barely changed, as shown in the graph. d) Mass spectra overlay of JM#198 at 0 min and 360 min incubation in human plasma. (see also Figure S13). e) Stability of peptides in full human blood. 20 µM of the peptides were spiked in 100% human blood and incubated at 37°C. Retained activity of the peptides was determined by antibody competition assay as described in a. Shown are means of at least 3 individual rounds of incubation ± SEM. (see also Figure S14).

17

Table 2. Activities determined for EPI-X4 JM#21 and derivatives after incubation in human plasma

| | Time | IC$_{50}$ (nM) | Normalized | |
			Fold reduction of activity[a]	Apparent activity (%)[b]
JM#21	0 h	76 ± 23	1	100
	2 h	1002 ± 89	17 ± 4	7 ± 2
	8 h	1916 ± 203	33 ± 8	4 ± 1
JM#21-Ac	0 h	114 ± 17	1	100
	2 h	702 ± 57	6 ± 1	16 ± 2
	8 h	2805 ± 608	24 ± 2	4 ± 1
JM#143	0 h	9 ± 1	1	100
	2 h	9 ± 1	1 ± 0.1	103 ± 12
	8 h	7 ± 1	0.9 ± 0.1	116 ± 9
JM#198	0 h	50 ± 12	1	100
	2 h	48 ± 15	0.9 ± 0.1	109 ± 9
	8 h	40 ± 11	0.8 ± 0.2	134 ± 29

[a]Fold increase of IC$_{50}$ values determined by antibody competition assay. [b]Apparent activity of active peptide in sample was determined by IC$_{50}$ (t = 10 min) / IC$_{50}$ (t) x 100. Shown are means derived from at least 3 individual experiments ± SEM.

The fatty acid conjugates JM#143 and JM#198 have an increased *in vivo* half-life

Fatty acid derivatization enhances the circulation half-lives of lipopeptides, likely due to increased binding to endogenous serum albumin. Our previous results demonstrated rapid renal elimination of non-derivatized JM#21, resulting in a circulation time of less than 10 minutes [20]. Here, we evaluated the *in vivo* stability of pamitoylated JM#143 and stearoylated JM#198, which both displayed extended half-lives and maintained high activity in blood and plasma without causing hemolysis *in vitro* (Figure S16).

We administered 3.5 mg/kg of each peptide intravenously to mice and collected plasma after 10 min – 24 hours for activity assessment via the antibody competition assay. Determined activities were normalized to the 10 min time point (Table 3). Palmitoylated JM#143 retained over 90% activity one hour post-injection compared to the 10 min time point, decreasing to 37.7% at two hours and 7.8% at four hours (Figure 5a, Table 3). In comparison, stearoylated JM#198 showed 40% activity after four hours, maintaining 22% activity after eight hours, confirmed by liquid chromatography-mass spectrometry (LC-MS) analysis (Figure 5b, Table 3). Similar trends were observed with other fatty acid-conjugated derivatives, with the C14 version JM#204 being least active after 4 hours *in vivo*, and the truncated C16 and C18 versions (JM#194, JM#235, JM#257) being most active (Figure S17). Mass spectrometry identified N- and C-terminal truncations as primary degradation pathways for both JM#143 and JM#198 (Figure 5c, d , Figure S18, S19). Overall, stearic acid derivatization yielded the longest *in vivo* circulation times, with shorter fatty acids like myristic acid resulting in more rapid clearance. In our study, it is essential to acknowledge that the initial blood collection time point, set as the baseline representing 100% free peptide concentration in blood, may not fully capture the intricate dynamics such as biodistribution and biocompartmental behavior occurring within the initial 10-minute timeframe. Nevertheless, our findings demonstrate that lipid derivatization of optimized EPI-X4 extends circulation half-lives *in vivo,* depending on the length of the fatty acid chain.
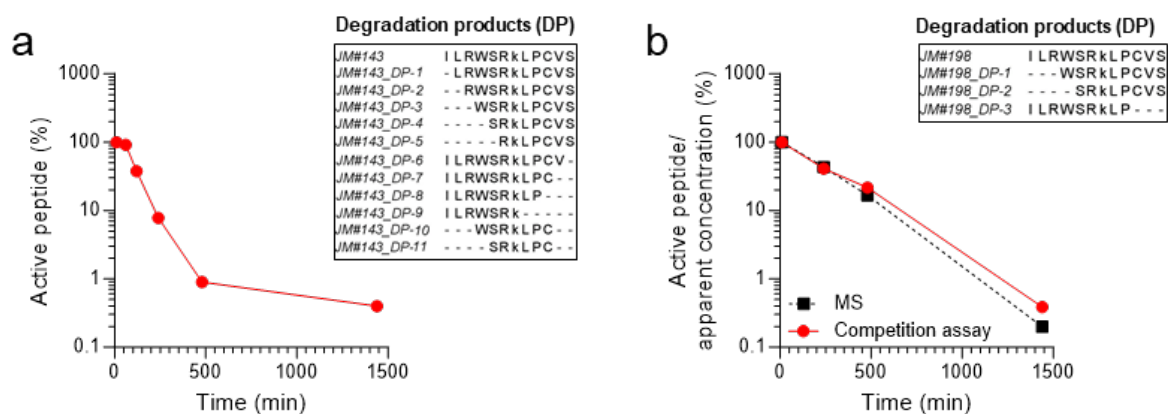
Figure 5. Bioavailability in mice. 3.5 mg/kg peptides JM#143 (a) or JM#198 (b) in saline were injected into the tail vein of C57BL/6 mice, blood was collected after given time points (Table 3), and the samples were centrifuged to obtain plasma. To evaluate the apparent activity of retained peptides in the plasma samples, they were serially diluted in PBS, and the antibody competition assay was performed, as described above. Shown are the data from 2 individuals analyzed in duplicates. Data for (b) were confirmed using LC-MS. Degradation products in the plasma samples were determined by mass spectrometry. k = the lysine residue modified by the glutamic acid linker and fatty acid (+395.304 for JM#198 and +367.272 for JM#198) (see also Figure S18 and S19).

Table 3. In vivo stability of EPI-X4 JM#143 and JM#198 [58]

Time point	EPI-X4 JM#143		EPI-X4 JM#198	
	Fold reduction of activity[a]	Apparent C (%)[b]	Fold reduction of activity[a]	Active peptide (%)[b]
10 min	1	100	1 (C = 6.9 μM)[c]	100 (100)
1 h	1.1	91.7	nd	nd
2 h	2.7	37.7	nd	nd
4 h	12.8	7.8	2.4 (C = 5.4 μM)	41.0 (43.4)
8 h	106.7	0.9	4.6 (C = 4.7 μM)	21.7 (16.7)
24 h	260.0	0.4	259.1 (C = 0.02 μM)	0.4 (0.2)

[a]Fold increase of IC_{50} values determined by antibody competition assay. [b]Active peptide in sample was determined by IC_{50} (t = 10 min) / IC_{50} (t) x 100. [c]Concentrations and percentages determined by LC-MS are shown in brackets.

Fatty acid derivative JM#198 inhibits tumor formation in an *in ovo* model of retinoblastoma

CXCR4 is expressed at high levels on retinoblastoma cells and might contribute to tumor progression and disease [58], [59], [60]. Thus, targeting CXCR4 signaling pathways may offer potential therapeutic strategies for retinoblastoma treatment. As a proof of principle, we used the two retinoblastoma cell lines Y79 and Weri-Rb1, which express high levels of CXCR4 (Figure S20) [61], and evaluated anti-cancer efficacies of EPI-X4 JM#21, the stearoylated variant JM#198, and the small molecule AMD3100 *in vitro* and *in ovo*.

For *in vitro* experiments cells were treated with the compounds for 48 – 120 hours (Figure 6 a-f, Figure S21). 0.1 μM AMD3100 reduced NADPH-dependend formazan production of Y79 cells by about 30% after 48 and 72 hours (Figure 6a) and concominantly significantly increased apoptosis levels, leading to an increase of trypan blue positive cells (Figure 6b). The effect was less pronounced in Weri-Rb1 cells (Figure 6d-e) and lost after 96 hours of incubation. Similarly, AMD3100 significantly inhibited proliferation of Y79 cells by about 40 % after 48 hours and 72 hours (Figure 6c). The EPI-X4 derivative JM#21 showed a similar trend but lower efficies than AMD3100 for the inhibition of cell NADPH-activity and proliferation (33% inhibition after 48 hours on Y79 cells), which was lost after 96 hours (Figure 6a-f,). Both compounds were less active at a 10-fold higher concentration of 1 μM. (Figure S21). The stabilized EPI-X4 variant JM#198 was as active as AMD3100 at a concentration of 0.1 μM

19

and more active than JM#21 in both, proliferation and apoptosis assays (Figure 6a-f). Additionally, effects on NADPH-activity lasted even after 96 hours and 120 hours of incubation, with 24 % less viable cancer cells after 120 hours compared to the negative control, highlighting its advantage over the unmodified JM#21 and the small molecule AMD3100 (Figure 6a-b, d-e).

For *in vivo* experiments *in ovo*, the retinoblastoma cell lines were treated with 1 µM of the compounds and subsequently grafted on the chorioallantoic membrane (CAM) of fertilized chicken embryos. After 7 days, tumor formation and vascularization were analyzed (Figure 6g-l, Figure S22). All CXCR4 inhibitors reduced tumor formation and size of the tumors formed by the grafted cells, suggesting a key role of CXCR4 in retinoblastoma tumorigenesis (Figure 6g-l). None of the tested compounds had a significant impact on angiogenesis in terms of changes in total vessel area, vessel length, thickness and branching points (Figure S22a, b). AMD3100 reduced Y79 and Weri-Rb1 tumor formation by 28 % and 37 %, respectively (Figure 6h, k). Compared to the negative control dissected CAM tumors were significantly smaller (Figure 6i, l). Similarly, EPI-X4 JM#21 reduced tumor formation by 37 % and 31 %, respectively, accompanied by reduced tumor size and weight (Figure 6h-i, k-l). EPI-X4 JM#198 was significantly more active than AMD3100 and EPI-X4 JM#21. The peptide reduced tumor formation by 55 % for Y79 and more than 70 % for Weri-Rb1 (Figure 6h, k). Growing tumors were significantly smaller compared to the control (Figure 6i, l).

Thus, our data indicate that targeting the CXCR4 receptor could be an effective approach for treating retinoblastoma. Furthermore, results clearly demonstrate that the stability and affinity optimized EPI-X4 JM#198 outperforms the unmodified JM#21 variant, highlighting the importance of molecular refinement in drug development.
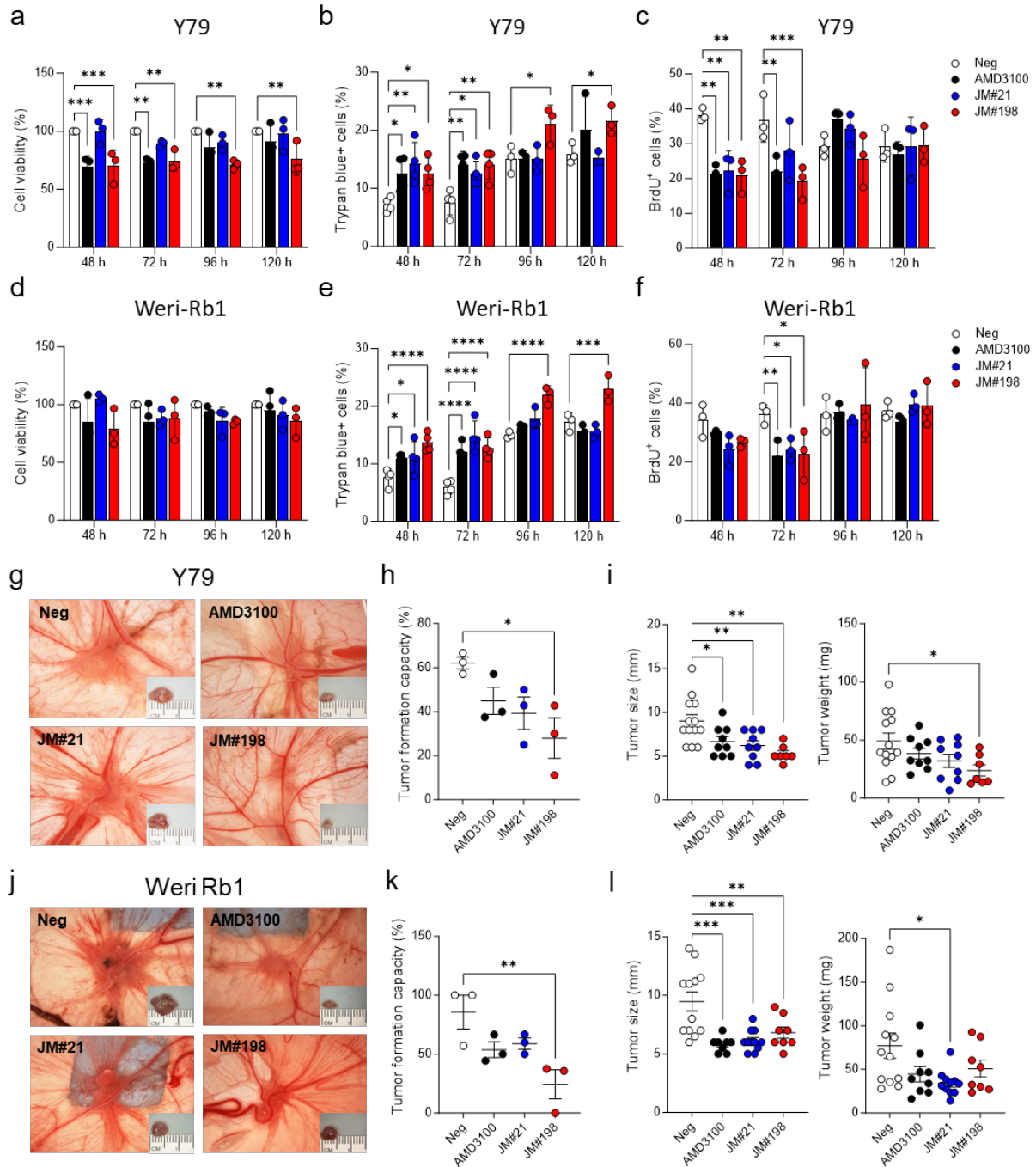
Figure 6. *In vitro* effects of CXCR4 inhibitors on retinoblastoma cells *in vitro* and *in ovo*. a-f) *in vitro*: Y79 or Weri-Rb1 cells were treated with 0.1 μM of the compounds for 48 – 120 hours. a,d) Cell viability was determined by water-soluble tetrazolium (WST-1) staining and values normalized to mock treated control. b,e) Dead cells were visualized by trypan blue staining and counted manually. c,f) Cell proliferation was determined by the addition of 5-Bromo-2′-deoxyuridine (BrdU). Values were normalized to mock treated controls. Values represent means ± SD. Significances were calculated by ordinary two-way ANOVA with Turkey's multiple comparisons test compared to the negative control. *p < 0.1; **p<0.01; ***p<0.001; ****p<0.0001. **g-l) *in ovo*:** 1x10^6 Y79 cells (g,h) or Weri-Rb1 cells (i,j) were treated with 1 μM of the compounds and subsequently grafted on the chicken chorioallantoic membrane (CAM). After 7 days, tumors were excised, measured and photographed. g,i) Representative *in situ* photographs of the vascularized CAM tumors developed from the grafted retinoblastoma cells and the excised tumors on a ruler (insets). h,k) Tumor formation capacity of all surviving embryos. Each point represents the % of tumor-harboring embryos ± SEM. i,l) Each point represents size or weight of a dissected tumor ± SEM. Significances were calculated by ordinary one-way ANOVA with Holm-Šidák's multiple comparisons test compared to the negative control. *p < 0.1; **p<0.01; ***p<0.001. Neg = inactive peptide Alb410-423 [2].

Discussion

The optimized EPI-X4 derivatives JM#21 and WSC02 have shown promising therapeutic effects in mouse models of inflammatory diseases and cancer [2], [6], [18]. However, they showed low stability in blood and rapid renal filtration [20]. To overcome these limitations, we here designed derivatives, which are conjugated to long-chain fatty acids. These fatty acids are well described binders of human serum albumin (HSA), an abundant protein in human blood plasma with a half-life of about 19 days. HSA harbors several fatty acid binding pockets, allowing the lipidated peptide cargo to interact with the protein, thereby avoiding release by the kidneys. In contrast to unmodified EPI-X4 JM#21, which only weakly interacts with HSA [35], we here showed that the lipidated peptide binds HSA, shielding the pharmacophore from degradation by enzymes in blood and plasma. Notably, albumin interaction not only increases peptide stability, but also antagonistic activities making lipidated EPI-X4 variants excellent candidates for further *in vivo* evaluation. Fatty acid derivatizes of JM#21 showed elevated half-lives in mice after intravenous administration, which was dependent on the alkyl chain length (C14 < C16 < C18). This confirms other studies showing that the albumin affinity correlates with the lengh of the fatty acid [62], [63]. Analysis of degradation products in blood plasma after i.v. injection revealed truncation of the lipopeptides at the N-terminus, as well as the C-terminus, suggesting further stabilization at these vulnerable sites by introduction of unnatural amino acids [5], [20] or amide bond surrogates [64]. In our study, we showed that the binding to serum albumin is responsible for resistance against enzymatic degradation. Neverthless, we have noted that fatty acid conjugation causes the formation of superstructures with 100-200 nm size in aqueous solution. Formation of these structures could protect the peptide from degradation or renal filtration and, thus, might further increase circulation half-lives. This has also been observed for other pharmaceutically used fatty acid peptides, e.g. for the diabetes drug Liraglutide, which forms oligomers at the injection side leading to delayed drug absorption and *in vivo* stability [65]. In addition, superstructure formation could be a reason for the observed enhanced anatagonistic activities mediated by multivalent interactions with CXCR4 [66].

The position of the fatty acid derivatization and the presence of residues at the C-terminal region of the peptide after the derivatization position are critical for the interaction with the receptor. Lipidation at position 2 or 6 leads to loss of activity (JM#202, JM#168), most likely by disrupting key interaction sites within the binding pocket or by steric effects [5]. As suggested by the results of the GaMD simulations, a lipid moiety close to the C-terminus provides additional stabilization to the complex via hydrophobic interactions between the N-terminal loop of CXCR4 and the acyl chain of the fatty acid. These interactions keep the lipopeptide anchored in the binding pocket while the interactions of the parent peptide with CXCR4 are preserved. In line with this, lipidation close to the peptide C-terminus preserved or increased CXCR4 binding and antagonistic effects of the compounds compared to the parental peptide. Lipidation at the lysine at position 7 resulted in most active compounds, contingent upon the length of the fatty acid chain (C14 < C16 < C18).

Despite retinoblastoma being a curable disease, frequent relapses and chemotherapy resistance pose significant challenges [13], [14], [15], [16], [17]. We show that the lipidated EPI-X4 derivative JM#198 reduces viability and proliferation of human retinoblastoma cells *in vitro* and reduces tumor formation and size in an *in ovo* disease model. Our findings not only highlight the superior activity of the optimized lipopeptide JM#198 over the unmodified JM#21, but - giving the observed high expression levels of CXCR4 in the retinoblastoma cells - also suggest a key role of the receptor during retinoblastoma tumor formation. This underscores the potential therapeutic value of optimized EPI-X4 derivatives, particularly JM#198, in mitigating retinoblastoma progression and resistance.

Although, we here showed that fatty monoacid derivatization leads to increased receptor binding activities and circulation half-lives *in vivo*, it will be interesting to compare the efficacy and stability of these compounds to derivatives conjugated to alternative fatty acid protractor moieties (e.g. fatty diacids), as suggested by Kurtzhals et al. [22]. The lead compound from our study, the stearic acid

conjugate EPI-X4 JM#198, was active with a half-life of almost 4 hours post intravenous administration in mice. Studies have shown that conjugation to fatty diacids harboring an extra carboxylic group at the ω-end of the alkyl chain further increases albumin interaction and solubility, and reduces unspecific interaction with cell membranes, which leads to higher half-lives compared to monoacid conjugates [22]. In addition, we have recently designed covalent HSA-peptide fusion constructs, which also showed protection against degradation in blood plasma and could also be excellent starting points for further optimization [35].

Conclusions

Lipidation significantly enhances the stability and in vivo circulation half-lives of optimized EPI-X4 derivatives. These lead compounds exhibit antagonistic activity in the low nanomolar range and maintain in vivo activity for several hours, making them promising candidates for further preclinical development aimed at treating cancer or chronic inflammatory diseases.

Author contributions

Mirja Harms: Conceptualization, Methodology, Formal analysis, Investigation, Writing – Original Draft, Visualization, Project administration; **André Haase:** Methodology, Formal analysis, Investigation, Wirting – Review & Editing; **Armando Rodriguez-Alfonso:** Methodology, Formal analysis, Investigation; **Jessica Löffler:** Investigation; **Yasser Almeida-Hernández:** Methodology, Investigation, Formal analysis, Data Curation, Wirting – Review & Editing; **Yasser B. Ruiz-Blanco:** Methodology, Investigation, Formal analysis, Data Curation; **Dan Albers:** Methodology, Investigation; **Andrea Gilg:** Investigation; **Franziska von Bank:** Investigation; **Fabian Zech:** Investigation; **Moumita Datta**: Investigation; **Janeni Jaikishan:** Investigation; **Bastian Draphoen:** Investigation; **Monica Habib:** Conceptualization, Investigation; **Ludger Ständker:** Project administration; **Sebastian Wiese:** Supervision; **Mika Lindén:** Supervision; **Gordon Winter:** Investigation, Supervision; **Volker Rasche:** Supervision; **Ambros J. Beer:** Supervision; **Hassan Jumaa:** Supervision; **Ashraf H Abade:** Supervision; **Frank Kirchhoff:** Supervision, Funding acquisition; **Maike Busch:** Wirting – Review & Editing, Supervision; **Nicole Dünker:** Wirting – Review & Editing, Supervision; **Elsa Sanchez-Garcia:** Wirting – Review & Editing, Supervision; **Jan Münch:** Conceptualization; Wirting – Review & Editing, Supervision, Project administration, Funding acquisition.

Declaration of competing interest

M.H, M.W.H.H., A.H.A., L.S., F.K., E.SG., and J.M. are coinventors of pending and issued patents that claim to use EPI-X4 (ALB408-423) and derivatives for the therapy of CXCR4-associated diseases.

Data availability

Primary data are available upon reasonable request.

Korea. The authors are grateful to Merve Karacan and Nico Preising (Core Facility of Functional Peptidomics) for the synthesis and purification of underivatized peptides; Ilayda Senel, Carolin Weiss, and Dana Weiss for their support in sample preparation and mass spectrometry.

Declaration of Generative AI and AI-assisted technologies in the writing process

During the preparation of this work the authors used ChatGPT version 3.5 in order to improve readability of the manuscript. After using this tool, the authors reviewed and edited the content as needed and take full responsibility for the content of the publication.

References

[1] T. Pozzobon, G. Goldoni, A. Viola, and B. Molon, "CXCR4 signaling in health and disease," *Immunol. Lett.*, vol. 177, pp. 6–15, Sep. 2016, doi: 10.1016/j.imlet.2016.06.006.

[2] O. Zirafi *et al.*, "Discovery and Characterization of an Endogenous CXCR4 Antagonist," *Cell Rep.*, vol. 11, no. 5, pp. 737–747, May 2015, doi: 10.1016/j.celrep.2015.03.061.

[3] O. Zirafi *et al.*, "Proteolytic processing of human serum albumin generates EPI-X4, an endogenous antagonist of CXCR4," *J. Leukoc. Biol.*, vol. 99, no. 6, pp. 863–868, Jun. 2016, doi: 10.1189/jlb.2MR1115-521RR.

[4] S. Patel, A. Homaei, H. R. El-Seedi, and N. Akhtar, "Cathepsins: Proteases that are vital for survival but can also be fatal," *Biomed. Pharmacother.*, vol. 105, pp. 526–532, Sep. 2018, doi: 10.1016/j.biopha.2018.05.148.

[5] P. Sokkar *et al.*, "Computational modeling and experimental validation of the EPI-X4/CXCR4 complex allows rational design of small peptide antagonists," *Commun. Biol.*, vol. 4, no. 1, p. 1113, Dec. 2021, doi: 10.1038/s42003-021-02638-5.

[6] M. Harms *et al.*, "An optimized derivative of an endogenous CXCR4 antagonist prevents atopic dermatitis and airway inflammation," *Acta Pharm. Sin. B*, vol. 11, no. 9, pp. 2694–2708, Sep. 2021, doi: 10.1016/j.apsb.2020.12.005.

[7] S. Chatterjee, B. Behnam Azad, S. Nimmagadda, B. B. Azad, S. Nimmagadda, and R. H. Morgan, "The Intricate Role of CXCR4 in Cancer," in *Advances in Cancer Research*, vol. 124, Academic Press Inc., 2014, pp. 31–82. doi: 10.1016/B978-0-12-411638-2.00002-1.

[8] K. Mortezaee, "CXCL12/CXCR4 axis in the microenvironment of solid tumors: A critical mediator of metastasis," *Life Sciences*, vol. 249. Pergamon, p. 117534, May 15, 2020. doi: 10.1016/j.lfs.2020.117534.

[9] Y. A. Tahirovic *et al.*, "Small molecule and peptide-based CXCR4 modulators as therapeutic agents. A patent review for the period from 2010 to 2018," *Expert Opin. Ther. Pat.*, vol. 30, no. 2, pp. 87–101, Feb. 2020, doi: 10.1080/13543776.2020.1707186.

[10] C. W. Hendrix *et al.*, "Safety, Pharmacokinetics, and Antiviral Activity of AMD3100, a Selective CXCR4 Receptor Inhibitor, in HIV-1 Infection," *JAIDS J. Acquir. Immune Defic. Syndr.*, vol. 37, no. 2, pp. 1253–1262, Oct. 2004, doi: 10.1097/01.qai.0000137371.80695.ef.

[11] E. De Clercq, "Mozobil® (Plerixafor, AMD3100), 10 years after its approval by the US Food and Drug Administration," *Antivir. Chem. Chemother.*, vol. 27, p. 204020661982938, Jan. 2019, doi: 10.1177/2040206619829382.

[12] S. M. Hoy, "Motixafortide: First Approval," *Drugs*, vol. 83, no. 17, pp. 1635–1643, Nov. 2023, doi: 10.1007/s40265-023-01962-w.

[13] Y. Bouchoucha *et al.*, "Retinoblastoma: From genes to patient care," *Eur. J. Med. Genet.*, vol. 66, no. 1, Jan. 2023, doi: 10.1016/j.ejmg.2022.104674.

[14] V. V. Byroju, A. S. Nadukkandy, M. Cordani, and L. D. Kumar, "Retinoblastoma: present scenario and future challenges," *Cell Communication and Signaling*, vol. 21, no. 1. BioMed Central, pp. 1–16, Sep. 04, 2023. doi: 10.1186/s12964-023-01223-z.

[15] N. Bornfeld, D. Lohmann, N. E. Bechrakis, and E. Biewald, "Retinoblastoma," *Ophthalmologe*, vol. 117, no. 4, pp. 389–402, Apr. 2020, doi: 10.1007/s00347-020-01081-x.

[16] M. G. Zhang *et al.*, "Early Mechanisms of Chemoresistance in Retinoblastoma," *Cancers*, vol. 14, no. 19, p. 4966, Oct. 2022, doi: 10.3390/cancers14194966.

[17] P. Temming *et al.*, "Incidence of second cancers after radiotherapy and systemic chemotherapy in heritable retinoblastoma survivors: A report from the German reference center," *Pediatr. Blood Cancer*, vol. 64, no. 1, pp. 71–80, Jan. 2017, doi: 10.1002/pbc.26193.

[18] L. M. Kaiser *et al.*, "Targeting of CXCR4 by the Naturally Occurring CXCR4 Antagonist EPI-X4 in Waldenström's Macroglobulinemia," *Cancers*, vol. 13, no. 4, p. 826, Feb. 2021, doi: 10.3390/cancers13040826.

[19] M. Harms *et al.*, "Microtiter plate-based antibody-competition assay to determine binding affinities and plasma/blood stability of CXCR4 ligands," *Sci. Rep.*, vol. 10, no. 1, p. 16036, Dec. 2020, doi: 10.1038/s41598-020-73012-4.

[20] M. Harms *et al.*, "Development of N-Terminally Modified Variants of the CXCR4-Antagonistic Peptide EPI-X4 for Enhanced Plasma Stability.," *J. Med. Chem.*, vol. 66, no. 22, pp. 15189–15204, Nov. 2023, doi: 10.1021/acs.jmedchem.3c01128.

[21] M. Harms *et al.*, "Dimerization of the peptide CXCR4-antagonist on macromolecular and supramolecular protraction arms affords increased potency and enhanced plasma stability," *Bioconjug. Chem.*, vol. 33, no. 4, pp. 594–607, Apr. 2022, doi: 10.1021/ACS.BIOCONJCHEM.2C00034.

[22] P. Kurtzhals, S. Østergaard, E. Nishimura, and T. Kjeldsen, "Derivatization with fatty acids in peptide and protein drug discovery.," *Nat. Rev. Drug Discov.*, vol. 22, no. 1, pp. 59–80, Jan. 2023, doi: 10.1038/s41573-022-00529-w.

[23] L. B. Knudsen and J. Lau, "The Discovery and Development of Liraglutide and Semaglutide," *Front. Endocrinol.*, vol. 10, no. APR, p. 155, Apr. 2019, doi: 10.3389/fendo.2019.00155.

[24] A. Weise and N. Dünker, "High trefoil factor 1 (TFF1) expression in human retinoblastoma cells correlates with low growth kinetics, increased cyclin-dependent kinase (CDK) inhibitor levels and a selective down-regulation of CDK6," *Histochem. Cell Biol.*, vol. 139, no. 2, pp. 323–338, Feb. 2013, doi: 10.1007/s00418-012-1028-y.

[25] R. C. McFall, T. W. Sery, and M. Makadon, "Characterization of a New Continuous Cell Line Derived from a Human Retinoblastoma," *Cancer Res.*, vol. 37, no. 4, pp. 1003–1010, 1976.

[26] T. W. Reid *et al.*, "Characteristics of an established cell line of retinoblastoma," *J. Natl. Cancer Inst.*, vol. 53, no. 2, pp. 347–360, 1974, doi: 10.1093/jnci/53.2.347.

[27] M. Busch, C. Philippeit, A. Weise, and N. Dünker, "Re-characterization of established human retinoblastoma cell lines," *Histochem. Cell Biol.*, vol. 143, no. 3, pp. 325–338, Mar. 2015, doi: 10.1007/s00418-014-1285-z.

[28] M. Harms *et al.*, "Spermine and spermidine bind CXCR4 and inhibit CXCR4- but not CCR5-tropic HIV-1 infection," *Sci. Adv.*, vol. 9, no. 27, p. eadf8251, Jul. 2023, doi: 10.1126/sciadv.adf8251.

[29] A. Zijlstra *et al.*, "A quantitative analysis of rate-limiting steps in the metastatic cascade using human-specific real-time polymerase chain reaction," *Cancer Res.*, vol. 62, no. 23, pp. 7083–7092, 2002.

[30] T. D. Palmer, J. Lewis, and A. Zijlstra, "Quantitative analysis of cancer metastasis using an avian embryo model.," *J. Vis. Exp. JoVE*, no. 51, p. e2815, May 2011, doi: 10.3791/2815.

[31] M. Busch *et al.*, "Reduction of the tumorigenic potential of human retinoblastoma cell lines by TFF1 overexpression involves p53/caspase signaling and miR-18a regulation," *Int. J. Cancer*, vol. 141, no. 3, pp. 549–560, Aug. 2017, doi: 10.1002/IJC.30768.

[32] M. Busch *et al.*, "p53, miR-34a and EMP1—Newly Identified Targets of TFF3 Signaling in Y79 Retinoblastoma Cells," *Int. J. Mol. Sci. 2019 Vol 20 Page 4129*, vol. 20, no. 17, p. 4129, Aug. 2019, doi: 10.3390/IJMS20174129.

[33] A. Haase *et al.*, "New retinoblastoma (RB) drug delivery approaches: anti-tumor effect of atrial natriuretic peptide (ANP)-conjugated hyaluronic-acid-coated gold nanoparticles for intraocular treatment of chemoresistant RB," *Mol. Oncol.*, 2024, doi: 10.1002/1878-0261.13587.

[34] N. H. Tran *et al.*, "Deep learning enables de novo peptide sequencing from data-independent-acquisition mass spectrometry," *Nat. Methods*, vol. 16, no. 1, pp. 63–66, Jan. 2019, doi: 10.1038/s41592-018-0260-3.

[35] A. Rodríguez-Alfonso *et al.*, "Advanced EPI-X4 Derivatives Covalently Bind Human Serum Albumin Resulting in Prolonged Plasma Stability.," *Int. J. Mol. Sci.*, vol. 23, no. 23, Nov. 2022, doi: 10.3390/ijms232315029.

[36] B. Wu *et al.*, "Structures of the CXCR4 Chemokine GPCR with Small-Molecule and Cyclic Peptide Antagonists," *Science*, vol. 330, no. 6007, pp. 1066–1071, Nov. 2010, doi: 10.1126/science.1194396.

[37] C. T. Veldkamp *et al.*, "Structural Basis of CXCR4 Sulfotyrosine Recognition by the Chemokine SDF-1/CXCL12," *Sci. Signal.*, vol. 1, no. 37, pp. ra4–ra4, Sep. 2008, doi: 10.1126/scisignal.1160755.

[38] S. Kim, J. Lee, S. Jo, C. L. Brooks, H. S. Lee, and W. Im, "CHARMM-GUI ligand reader and modeler for CHARMM force field generation of small molecules," *J. Comput. Chem.*, vol. 38, no. 21, pp. 1879–1886, Jun. 2017, doi: 10.1002/jcc.24829.

[39] K. Vanommeslaeghe *et al.*, "CHARMM general force field: A force field for drug-like molecules compatible with the CHARMM all-atom additive biological force fields," *J. Comput. Chem.*, vol. 31, no. 4, pp. 671–690, Mar. 2010, doi: 10.1002/jcc.21367.

[40] S. Jo, T. Kim, V. G. Iyer, and W. Im, "CHARMM-GUI: A web-based graphical user interface for CHARMM," *J. Comput. Chem.*, vol. 29, no. 11, pp. 1859–1865, Aug. 2008, doi: 10.1002/JCC.20945.

[41] W. L. Jorgensen, J. Chandrasekhar, J. D. Madura, R. W. Impey, and M. L. Klein, "Comparison of simple potential functions for simulating liquid water," *J. Chem. Phys.*, vol. 79, no. 2, pp. 926–935, Jul. 1983, doi: 10.1063/1.445869.

[42] T. Darden, D. York, and L. Pedersen, "Particle mesh Ewald: An N ·log(N) method for Ewald sums in large systems," *J. Chem. Phys.*, vol. 98, no. 12, pp. 10089–10092, Jun. 1993, doi: 10.1063/1.464397.

[43] J. A. Izaguirre, D. P. Catarello, J. M. Wozniak, and R. D. Skeel, "Langevin stabilization of molecular dynamics," *J. Chem. Phys.*, vol. 114, no. 5, pp. 2090–2098, Feb. 2001, doi: 10.1063/1.1332996.

[44] G. J. Martyna, D. J. Tobias, and M. L. Klein, "Constant pressure molecular dynamics algorithms," *J. Chem. Phys.*, vol. 101, no. 5, pp. 4177–4189, Sep. 1994, doi: 10.1063/1.467468.

[45] Y. Miao, V. A. Feher, and J. A. McCammon, "Gaussian Accelerated Molecular Dynamics: Unconstrained Enhanced Sampling and Free Energy Calculation," *J. Chem. Theory Comput.*, vol. 11, no. 8, pp. 3584–3595, Aug. 2015, doi: 10.1021/acs.jctc.5b00436.

[46] Y. Miao, W. Sinko, L. Pierce, D. Bucher, R. C. Walker, and J. A. McCammon, "Improved reweighting of accelerated molecular dynamics simulations for free energy calculation," *J. Chem. Theory Comput.*, vol. 10, no. 7, pp. 2677–2689, Jul. 2014, doi: 10.1021/ct500090q.

[47] J. C. Phillips *et al.*, "Scalable molecular dynamics with NAMD.," *J. Comput. Chem.*, vol. 26, no. 16, pp. 1781–802, Dec. 2005, doi: 10.1002/jcc.20289.

[48] J. Huang *et al.*, "CHARMM36m: an improved force field for folded and intrinsically disordered proteins.," *Nat. Methods*, vol. 14, no. 1, pp. 71–73, Dec. 2017, doi: 10.1038/nmeth.4067.

[49] M. J. Abraham *et al.*, "GROMACS: High performance molecular simulations through multi-level parallelism from laptops to supercomputers," *SoftwareX*, vol. 1–2, pp. 19–25, Sep. 2015.

[50] W. Humphrey, A. Dalke, and K. Schulten, "VMD: visual molecular dynamics.," *J. Mol. Graph.*, vol. 14, no. 1, pp. 33–8, 27–8, Feb. 1996, doi: 10.1016/0263-7855(96)00018-5.

[51] E. F. Pettersen *et al.*, "UCSF Chimera--a visualization system for exploratory research and analysis.," *J. Comput. Chem.*, vol. 25, no. 13, pp. 1605–12, Oct. 2004, doi: 10.1002/jcc.20084.

[52] C. B. Wilen, J. C. Tilton, and R. W. Doms, "HIV: cell binding and entry.," *Cold Spring Harb. Perspect. Med.*, vol. 2, no. 8, pp. 1–14, 2012, doi: 10.1101/cshperspect.a006866.

[53] G. A. Donzella *et al.*, "AMD3100, a small molecule inhibitor of HIV-1 entry via the CXCR4 co-receptor," *Nat. Med.*, vol. 4, no. 1, pp. 72–77, Jan. 1998, doi: 10.1038/nm0198-072.

[54] Y. Miao, V. A. Feher, and J. A. McCammon, "Gaussian Accelerated Molecular Dynamics: Unconstrained Enhanced Sampling and Free Energy Calculation," *J. Chem. Theory Comput.*, vol. 11, no. 8, pp. 3584–3595, Aug. 2015, doi: 10.1021/acs.jctc.5b00436.

[55] Y. Miao, W. Sinko, L. Pierce, D. Bucher, R. C. Walker, and J. A. McCammon, "Improved reweighting of accelerated molecular dynamics simulations for free energy calculation," *J. Chem. Theory Comput.*, vol. 10, no. 7, pp. 2677–2689, Jul. 2014, doi: 10.1021/ct500090q.

[56] D. S. Weber and J. J. Warren, "The interaction between methionine and two aromatic amino acids is an abundant and multifunctional motif in proteins," *Arch. Biochem. Biophys.*, vol. 672, p. 108053, Sep. 2019, doi: 10.1016/j.abb.2019.07.018.

[57] C. C. Valley *et al.*, "The methionine-aromatic motif plays a unique role in stabilizing protein structure," *J. Biol. Chem.*, vol. 287, no. 42, pp. 34979–34991, Oct. 2012, doi: 10.1074/jbc.M112.374504.

[58] R. M. Nair, M. M. S. Balla, I. Khan, R. K. R. Kalathur, P. Kondaiah, and G. K. Vemuganti, "In vitro characterization of CD133lo cancer stem cells in Retinoblastoma Y79 cell line," *BMC Cancer*, vol. 17, no. 1, pp. 1–12, Nov. 2017, doi: 10.1186/s12885-017-3750-2.

[59] N. Wu *et al.*, "Tetramethylpyrazine-mediated regulation of CXCR4 in retinoblastoma is sensitive to cell density," *Mol. Med. Rep.*, vol. 15, no. 5, pp. 2481–2488, 2017, doi: 10.3892/mmr.2017.6293.

[60] N. Wu *et al.*, "Tetramethylpyrazine downregulates transcription of the CXC receptor 4 (CXCR4) via nuclear respiratory factor-1 (Nrf-1) in WERI-Rb1 retinoblastoma cells," *Oncol. Rep.*, vol. 42, no. 3, pp. 1214–1224, Sep. 2019, doi: 10.3892/OR.2019.7233/HTML.

[61] R. Gao, R. N. Mitra, M. Zheng, K. Wang, J. C. Dahringer, and Z. Han, "Developing Nanoceria-Based pH-Dependent Cancer-Directed Drug Delivery System for Retinoblastoma," *Adv. Funct. Mater.*, vol. 28, no. 52, Dec. 2018, doi: 10.1002/adfm.201806248.

[62] J. Lau *et al.*, "Discovery of the Once-Weekly Glucagon-Like Peptide-1 (GLP-1) Analogue Semaglutide.," *J. Med. Chem.*, vol. 58, no. 18, pp. 7370–80, Sep. 2015, doi: 10.1021/acs.jmedchem.5b00726.

[63] S. Østergaard *et al.*, "The effect of fatty diacid acylation of human PYY3-36 on Y2 receptor potency and half-life in minipigs.," *Sci. Rep.*, vol. 11, no. 1, p. 21179, Oct. 2021, doi: 10.1038/s41598-021-00654-3.

[64] L. M. Rečnik, W. Kandioller, and T. L. Mindt, "1,4-disubstituted 1,2,3-triazoles as amide bond surrogates for the stabilisation of linear peptides with biological activity," *Molecules*, vol. 25, no. 16. Multidisciplinary Digital Publishing Institute (MDPI), Aug. 01, 2020. doi: 10.3390/molecules25163576.

[65] T. M. Frederiksen *et al.*, "Oligomerization of a Glucagon-like Peptide 1 Analog: Bridging Experiment and Simulations," *Biophys. J.*, vol. 109, no. 6, pp. 1202–1213, Sep. 2015, doi: 10.1016/j.bpj.2015.07.051.

[66] I. W. Hamley, "Lipopeptides: from self-assembly to bioactivity," *Chem. Commun.*, vol. 51, no. 41, pp. 8574–8583, May 2015, doi: 10.1039/C5CC01535A.

Supplementary Information

Table S1. IC$_{50}$ values on primary human CD4+ T cells and a mouse cell line.

Compound	Human			Mouse
	Migration[a]	pAkt[b]	pErk[c]	pErk[c]
	IC$_{50}$ (µM ± SEM)			
EPI-X4	> 100	> 100	> 100	>100
JM#21	1.46 ± 0.26	1.16 ± 0.28	1.28 ± 0.31	8.31 ± 2.47
JM#143	0.65 ± 0.48	0.23 ± 0.10	0.29 ± 0.22	0.69 ± 0.55
JM#194	0.03 ± 0.01	0.99 ± 0.03	0.11 ± 0.05	> 10
JM#198	0.35 ± 0.18	0.18 ± 0.02	0.17 ± 0.03	1.03 ± 0.4
AMD3100	1.74 ± 1.36	1.70 ± 0.77	3.00 ± 1.74	2.72 ± 0.46

[a] migration towards CXCL12 in transwell system, [b] inhibition of CXCL12 induced Akt phosphorylation, [c] inhibition of CXCL12 induced Erk phosphorylation
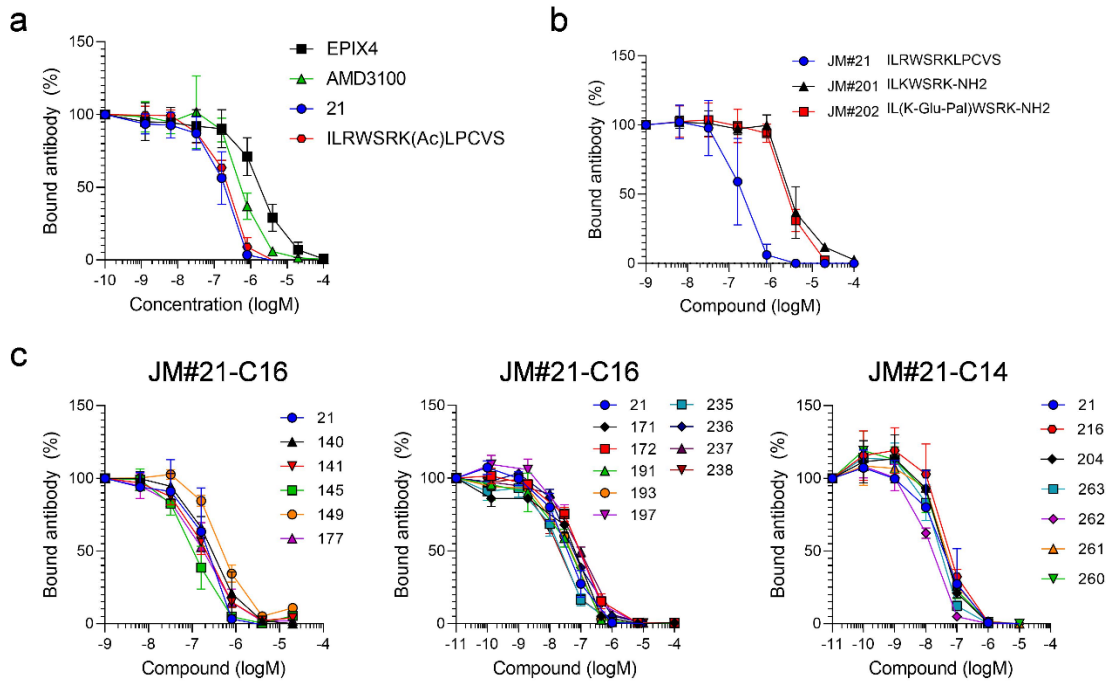
Figure S1. 12G5 CXCR4 antibody competition curves for all derivatives. Serially diluted compound was added to SupT1 cells together with a constant concentration of the antibody. After 2 hours, unbound antibody was removed, and cells were analyzed in flow cytometry. Shown are means derived from at least 3 individual experiments ± SD. a) Controls. b) Compounds with alternative fatty acid conjugation site. c) Fatty acid conjugates.
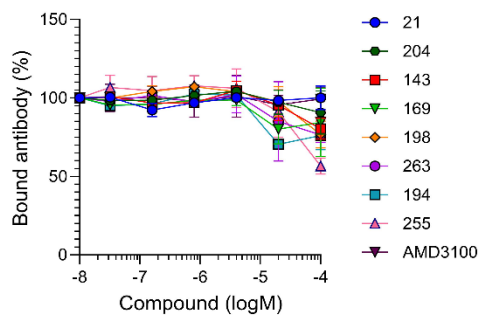
Figure S2: Fatty acid conjugates have no effect on 1D9 antibody binding. The peptides were serially diluted in PBS and added to SupT1 cells together with a constant concentration of the CXCR4 specific antibody clone 1D9 (binding to the receptor N-terminus). After 2 hours incubation at 4°C, unbound antibody was removed and cells were analyzed in flow cytometry. Shown are means derived from 3 individual experiments ± SEM.
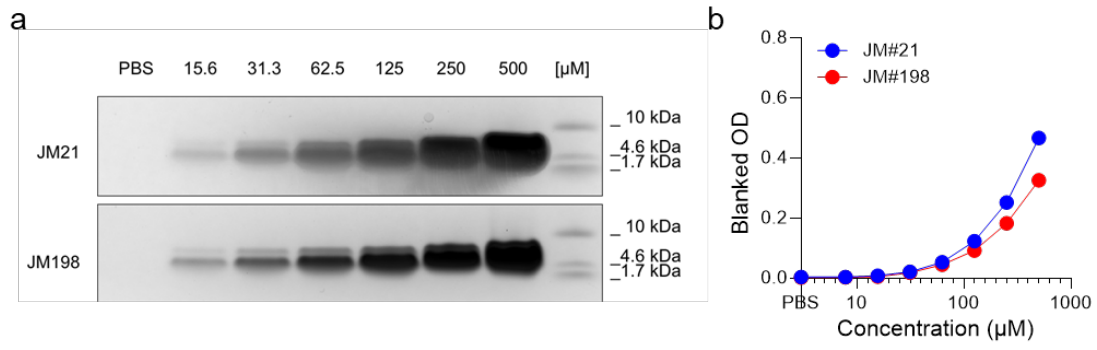
Figure S3. Solubility of JM#198 in a buffered solution. Peptides stocks were serially diluted in PBS and separated on SDS-PAGE before staining for total protein with colloidal Coomassie (a) or evaluated for protein content by BCA assay (BCA Gold, Thermo Fisher) (b). Shown is one representative experiment.
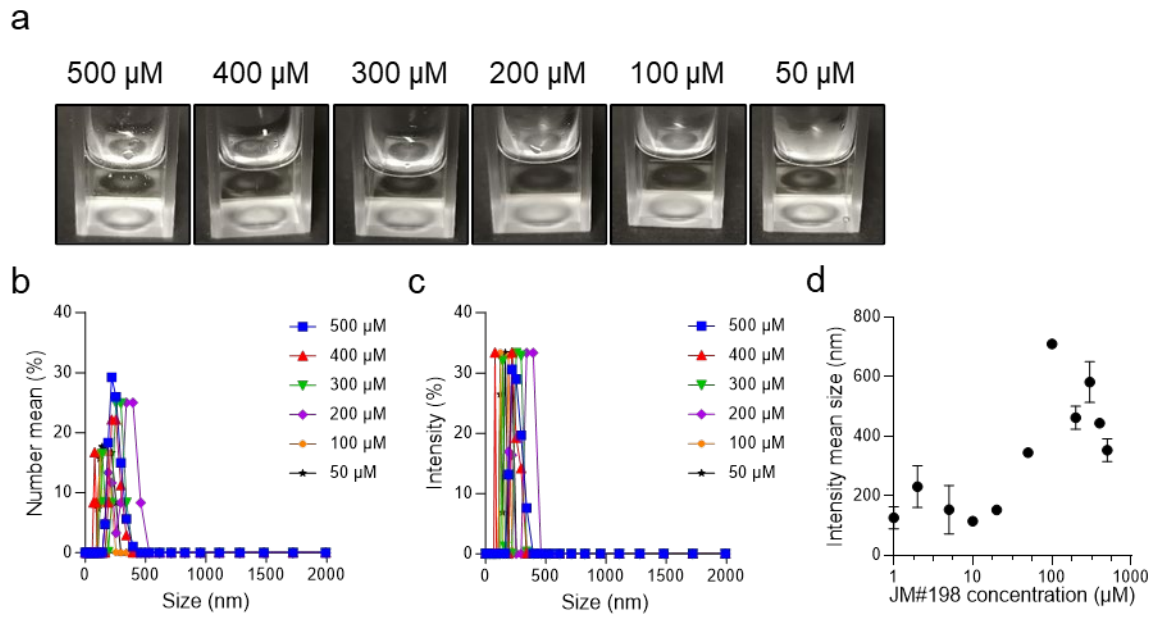
Figure S4. Formation of superstructures of JM#198 in a buffered solution. a-d) JM#198 was dissolved in DMSO at a concentration of 50 mM and then further diluted in warm Tris-buffer and then incubated at 37°C for 16 hours. a) Pictures were taken after 16 hours of incubation. b-d) DLS measurements of solutions after incubation representing (b) number weighted size distribution, and (c,d) intensity. It can be assumed that JM#198 forms small aggregates or nanogel like structures that are around 100 – 300 nm in size.
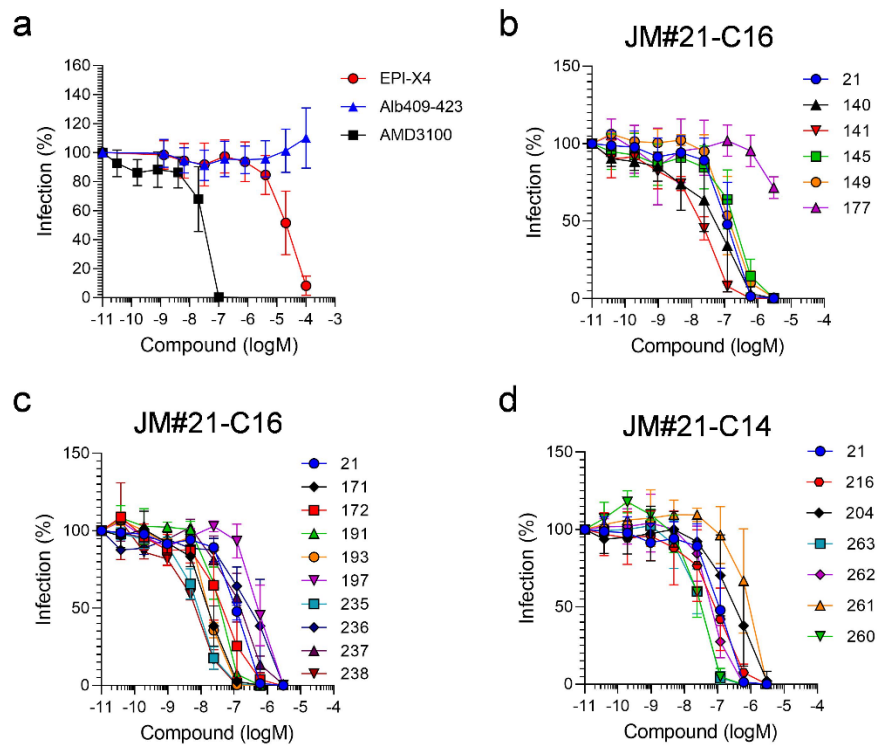
Figure S5. Fatty acid conjugates inhibit CXCR4-tropic HIV-1. TZM-bl reporter cells were pretreated with the compounds for 15 min before they were inoculated with CXCR4-tropic HIV-1. Infection rates were determined after 3 days by β-galactosidase assay. Shown are means derived from at least 3 individual experiments performed in triplicates ± SD. a) Controls. b) JM#21-C16 conjugates. c) Truncated JM#21-C16 conjugates. d) JM#21-C14 conjugates.
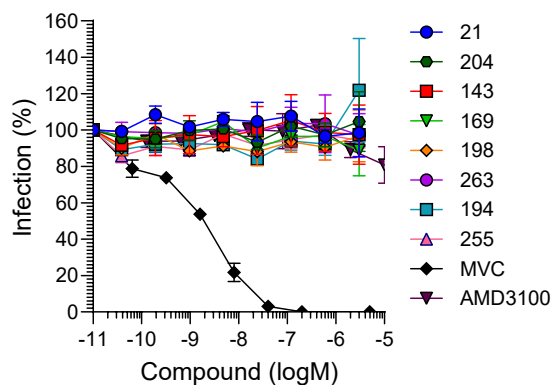
Figure S6. Fatty acid conjugates are not inhibiting CCR5-tropic HIV-1. TZM-bl reporter cells were pretreated with the compounds for 15 min before they were inoculated with CCR5-tropic HIV-1. Infection rates were determined after 3 days by β-galactosidase assay. Shown are means derived from at least 3 individual experiments performed in triplicates ± SD.
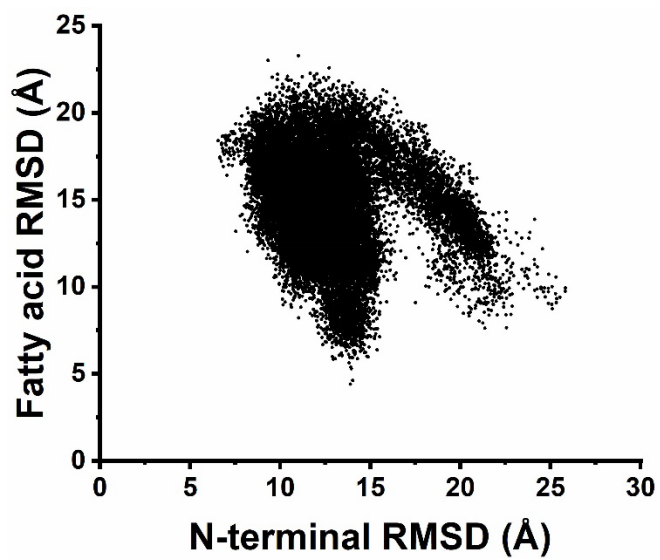
Figure S7: RMSD of the N-terminal loop of CXCR4 vs. RMSD of the fatty acid
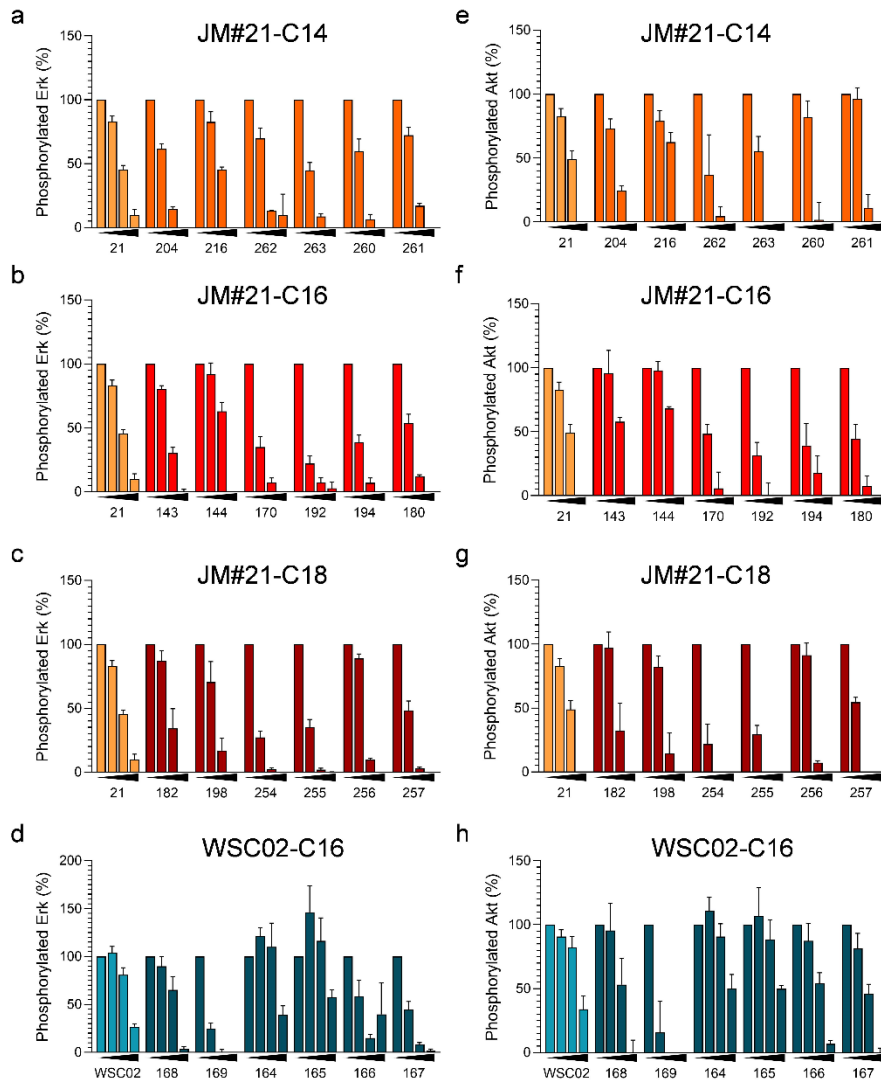
Figure S8. Compounds inhibit CXCL12-induced phosphorylation of Akt and Erk. SupT1 cells were pretreated with compounds for 10 min and then stimulated with 100 ng/ml CXCL12 for 2 min. The reaction was stopped by adding 1% PFA. Cells were then stained and analyzed by flow cytometry. Shown are normalized means derived from at least 4 individual experiments performed in singlicates ± SEM.
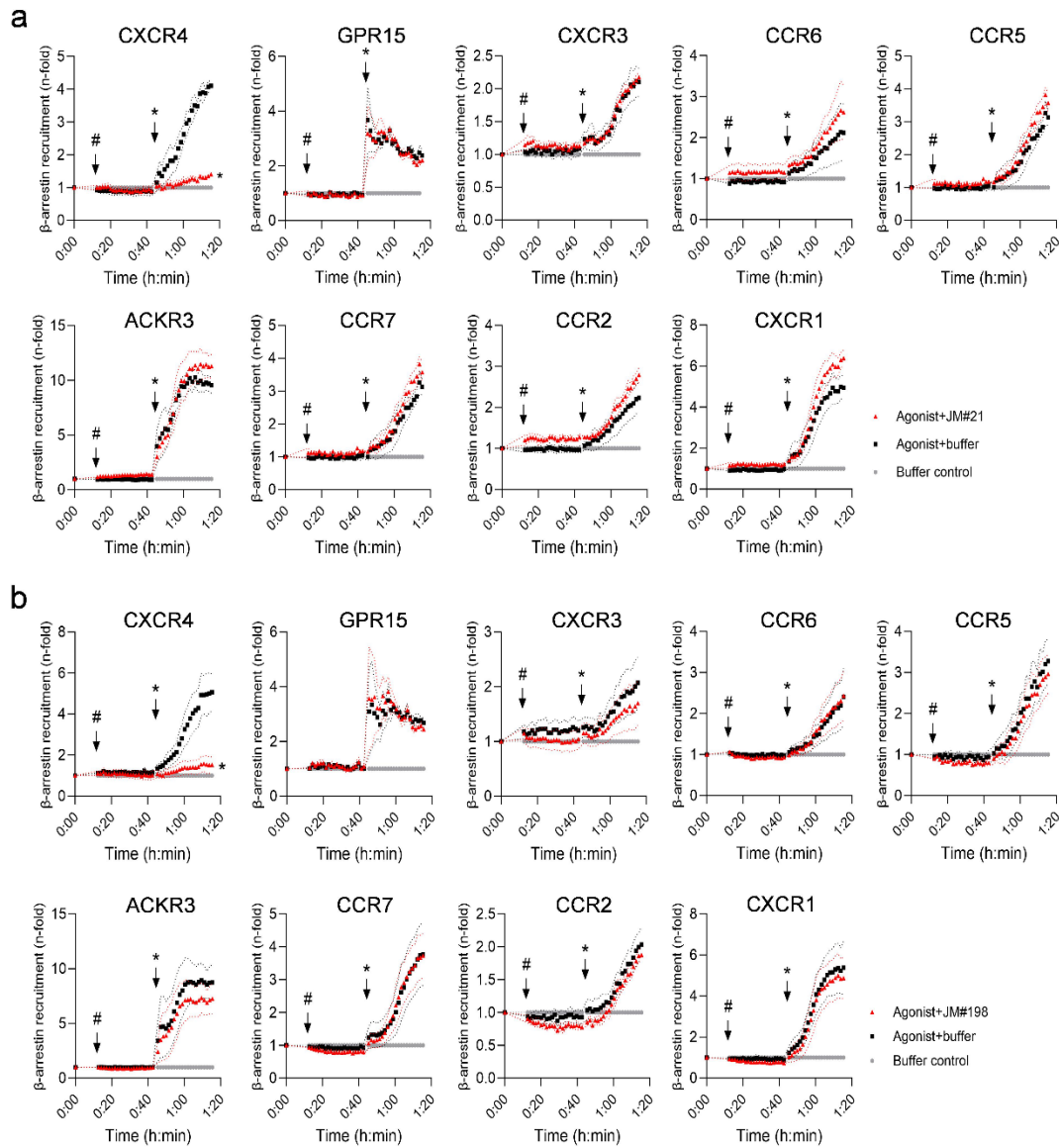
Figure S9. Inhibition of agonist-induced β-arrestin recruitment to a panel of GPCRs. HEK293T cells were transfected with a plasmid containing β-arrestin-2 and a GPCR construct coupled to the two parts of the NanoBiT protein−protein interaction assay system. Cells were stimulated the respective agonists in the presence of 1 μM JM#21 (a) or JM#198 (b), and the signal was determined over time. n = 3 ± SEM. CXCR4: 300 ng/ml CXCL12; GPR15: 1.5 μM GPR15LG; CXCR3: 40 nM CXCL11; CCR6: 50 nM CCL20; CCR5: 100 nM CCL5; ACKR3: 300 ng/ml CXCL12; CCR7: 50 nM CCL19; CCR2: 100 nM CCL8; CXCR1: 50 nM CXCL8.
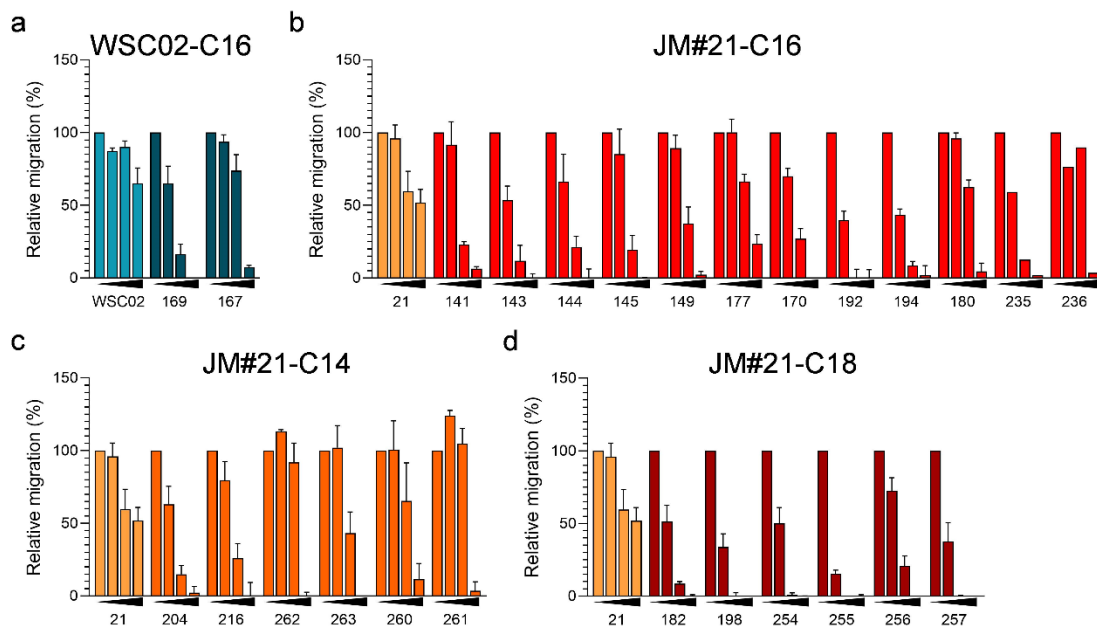
Figure S10. Compounds inhibit CXCL12-induced cell migration. The assay was performed using a transwell assay system (5 μm pore size) with 100 ng/mL CXCL12 as chemoattractant in the lower chamber. The number of migrated cells was determined by CellTiterGlo assay. Shown are means derived from at least three individual experiments performed in triplicates ± SEM.
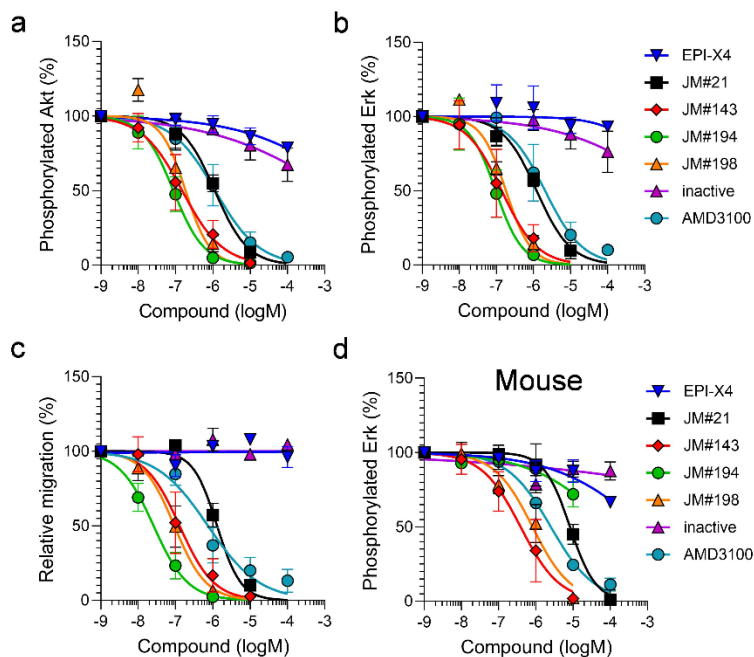
Figure S11. Compounds inhibit CXCL12-mediated signaling on primary human CD4+ T cells and mouse cells. a,b) Inhibition of CXCL12-induced Akt or Erk phosphorylation on primary human CD4+ T cells. Cells were preincubated with the compounds and stimulated with 100 ng/ml CXCL12 for 2 min. The reaction was stopped by adding 1% PFA. Cells were then stained and analyzed by flow cytometry. c) Compounds inhibit CXCL12-mediated migration of human CD4+ T cells. The assay was performed using a transwell assay system (5 μm pore size) with 100 ng/mL CXCL12 as chemoattractant in the lower chamber. The number of migrated cells was determined by CellTiterGlo assay. d) Inhibition of CXCL12-induced Erk phosphorylation on a murine T cell line. Shown are means derived from at least three individual experiments performed in triplicates ± SEM. IC$_{50}$ values were calculated by non-linear regression curve fit.
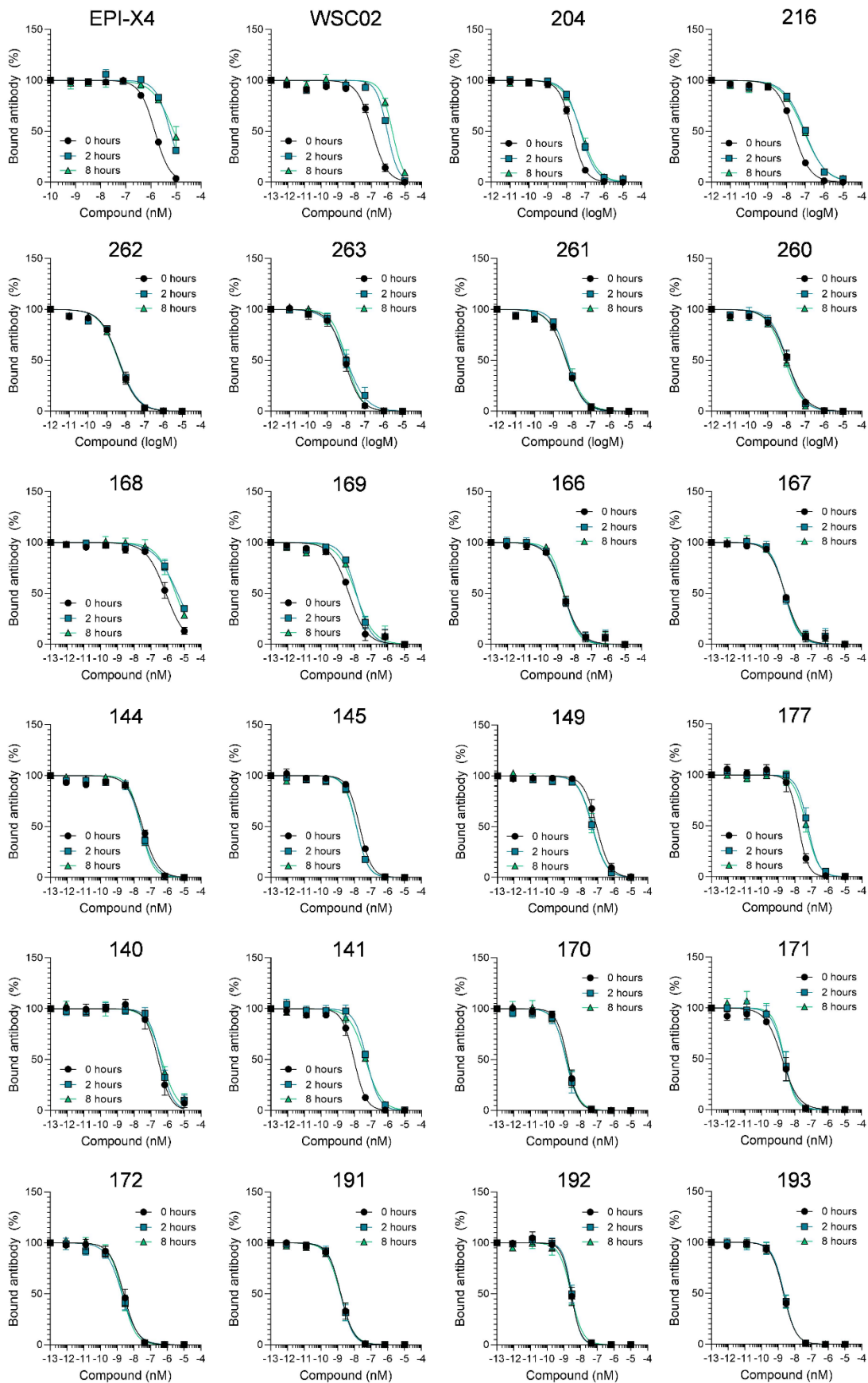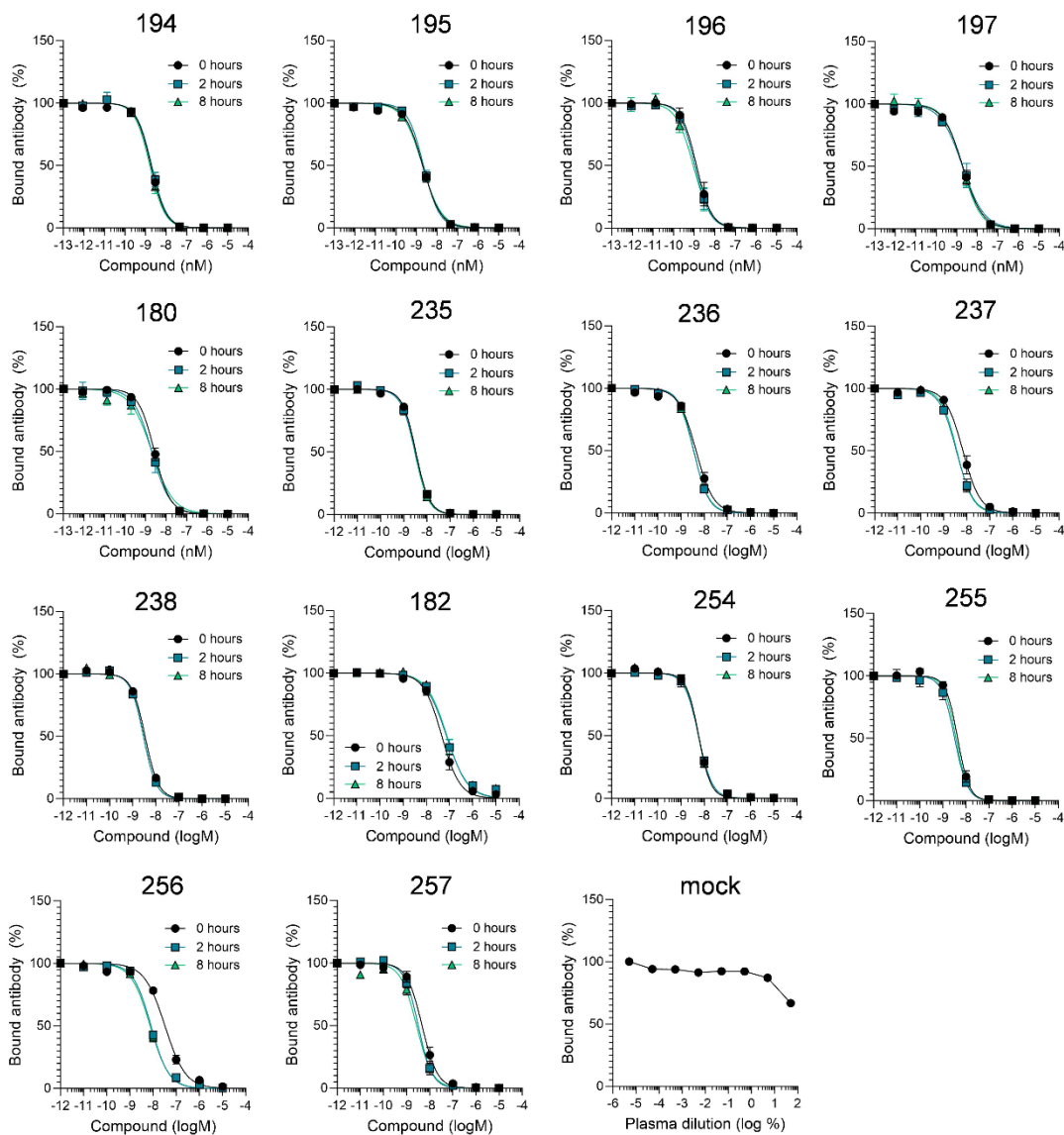
Figure S12. Activity curves of peptides before and after incubation in human plasma. 20 µM of the compounds was spiked into 100% of human plasma and incubated at 37°C. Aliquots were taken immediately (t = 0 hours), and after 2 and 8 hours and stored at -80°C. To determine remaining activities, aliquots were serially diluted and analyzed in parallel for 12G5 antibody competition. Shown are means of at least 3 individual rounds of incubation ± SEM.
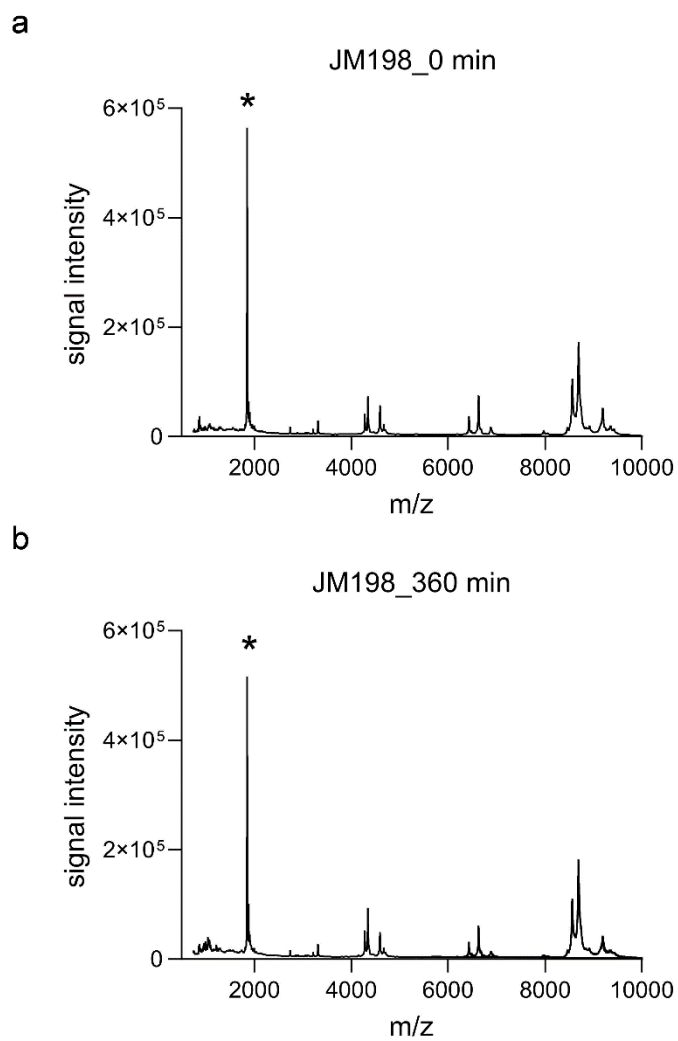
Figure S13. Spectra of JM#198 in human plasma (m/z) after incubation in human plasma for 0 and 360 min, respectively.
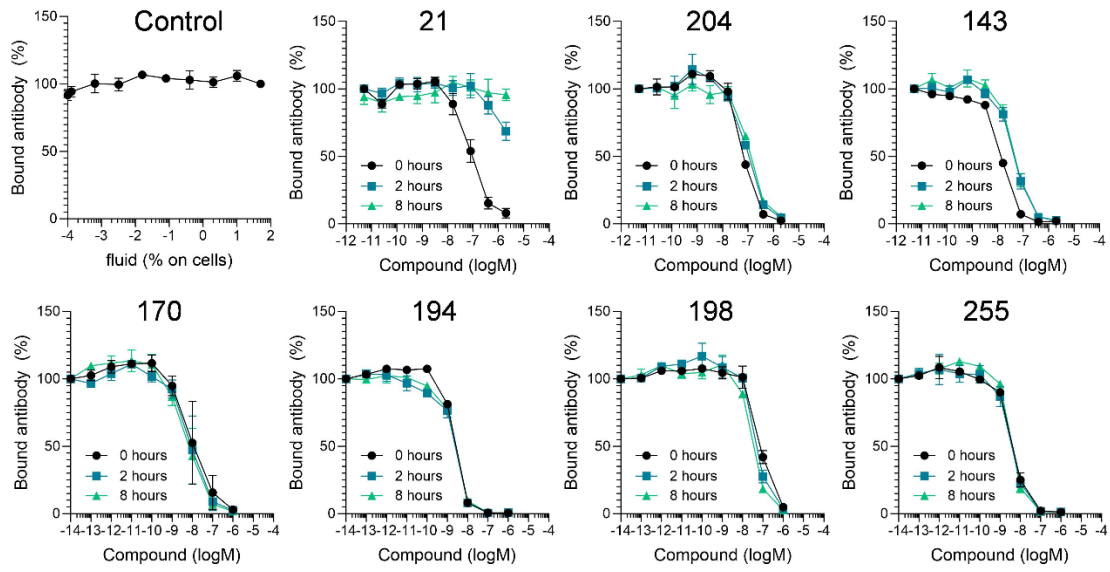
Figure S14. Activity curves of peptides before and after incubation in full human blood. 20 μM of the compounds was spiked into 100% of human plasma and incubated at 37°C. Aliquots were taken immediately (t = 0 hours), and after 2 and 8 hours and stored at -80°C. To determine remaining activities, aliquots were serially diluted and analyzed in parallel for 12G5 antibody competition. Shown are means of 3 individual rounds of incubation ± SEM.
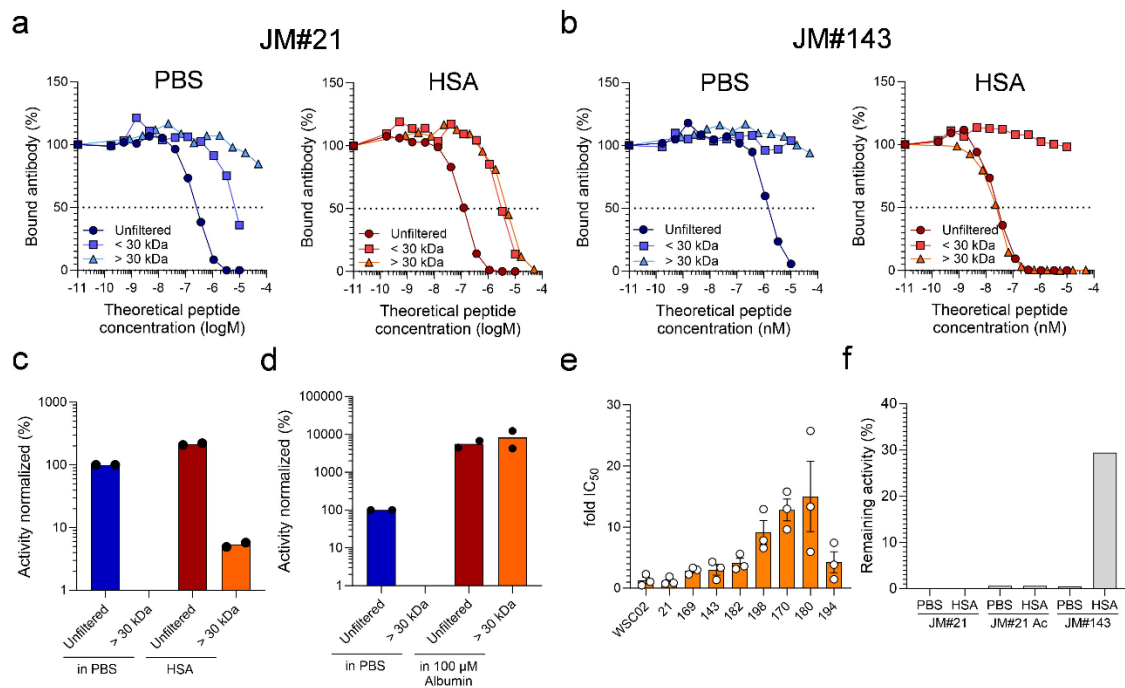
Figure S15. Enhanced stability of the fatty acid conjugate JM#143 is dependent on the presence of serum albumin. a-d) JM#143 shows stronger binding to albumin than JM#21. 20 μM of peptides were incubated with 100 μM human serum albumin (fatty acid free, Sigma Aldrich) or PBS for 10 min at 37°C. Afterwards samples were taken and stored at -80°C. The remaining mixture was applied to ultracentrifugation (Amicon Ultra MWCO 30 kDa) and centrifuged for 30 min at 14,000 x g. The >30 kDa fraction was collected and the volume restored to the previous volume. Both samples were stored at -80°C until they were applied to the antibody competition assay. IC_{50} values from each curve was determined by non-linear regression. Apparent activity of JM#21 (c) or JM#143 (d) was determined by IC_{50} (unfiltered in PBS)/IC_{50} x 100. n = 2. e) Activity enhancement of lipopeptides in the presence of albumin. 20 μM of peptides added to 50 mg/ml human serum albumin (fatty acid free, Sigma Aldrich) or PBS before the antibody competition assay was performed. n = 3 ± SEM. f) Albumin protects the fatty acid conjugate JM#143 from degradation by leucyl aminopeptidases (LAP). 20 μM of compounds in the presence of 100 μM HSA or PBS were incubated with 0.07 u LAPs for 3 h at 37°C. Activity was determined by antibody competition assay together with peptide not treated with LAPs. IC_{50} values were determined by non-linear regression and remaining activity calculated by IC_{50} (mock)/IC_{50} (LAP) x 100. Shown are data from one experiment.
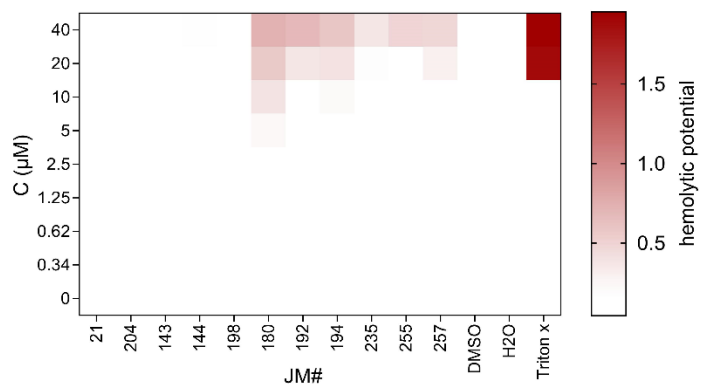
Figure S16. Analysis of hemolytic potential for selected compounds on human erythrocytes.
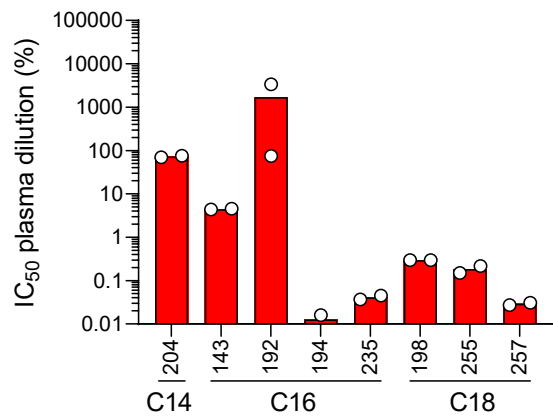
Figure S17. Apparent activity of mouse plasma 4 hours after peptide injection. 3.5 mg/kg peptide-conjugate in saline was injected into the tail vein of C57BL/6 mice (n = 2 per conjugate), and blood was taken after 4 h and centrifuged to obtain plasma. The remaining activity of peptides in plasma was determined by antibody competition. Each dot represents the mean of plasma derived from an individual analyzed in duplicates.
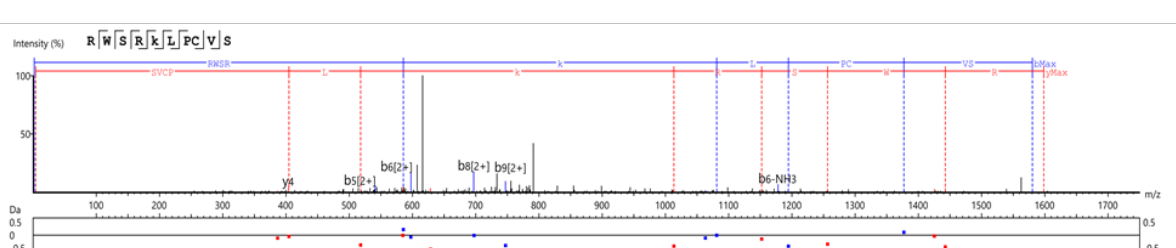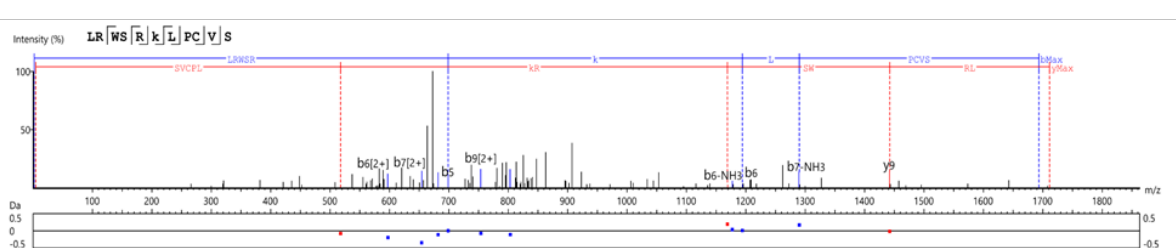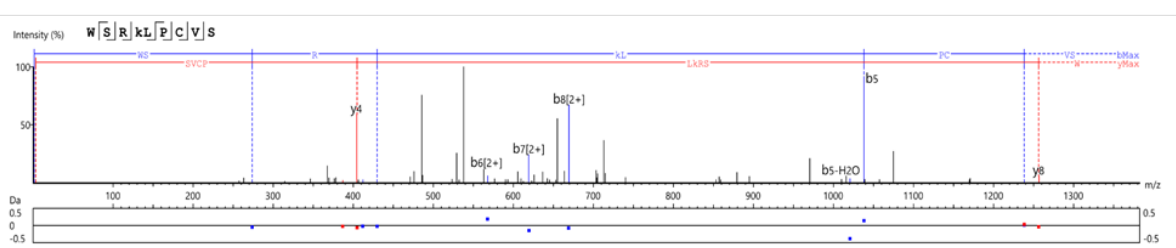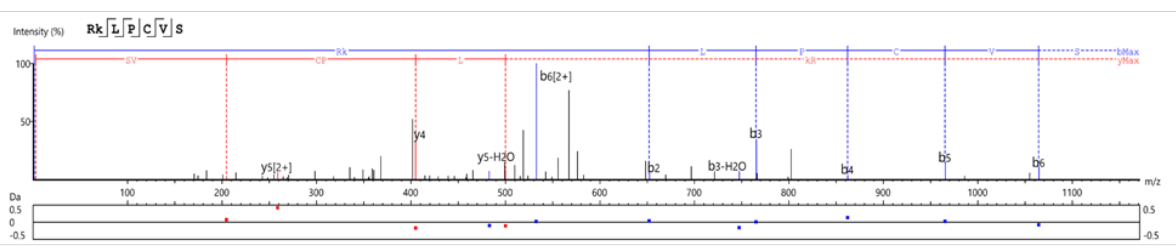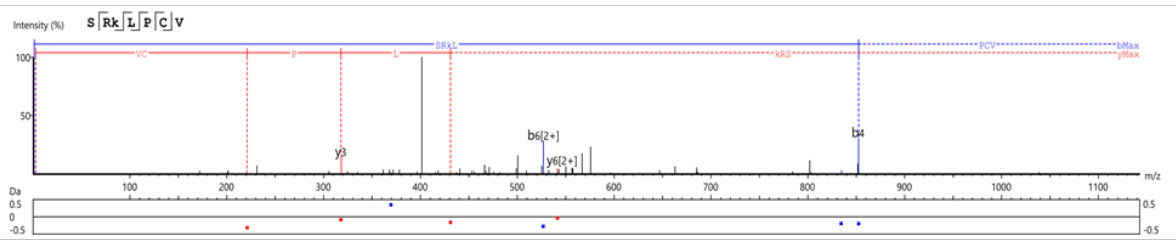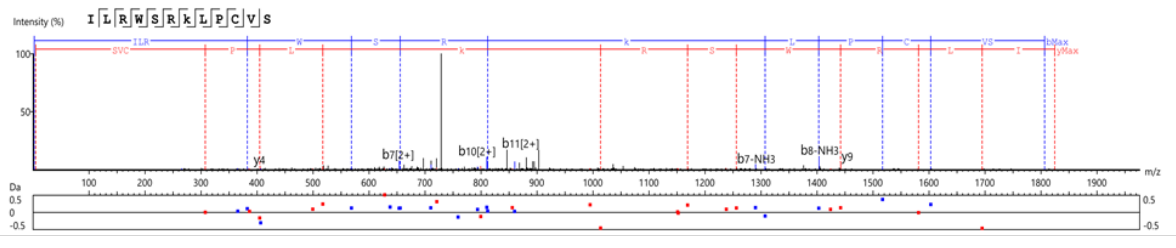
Continued on next page
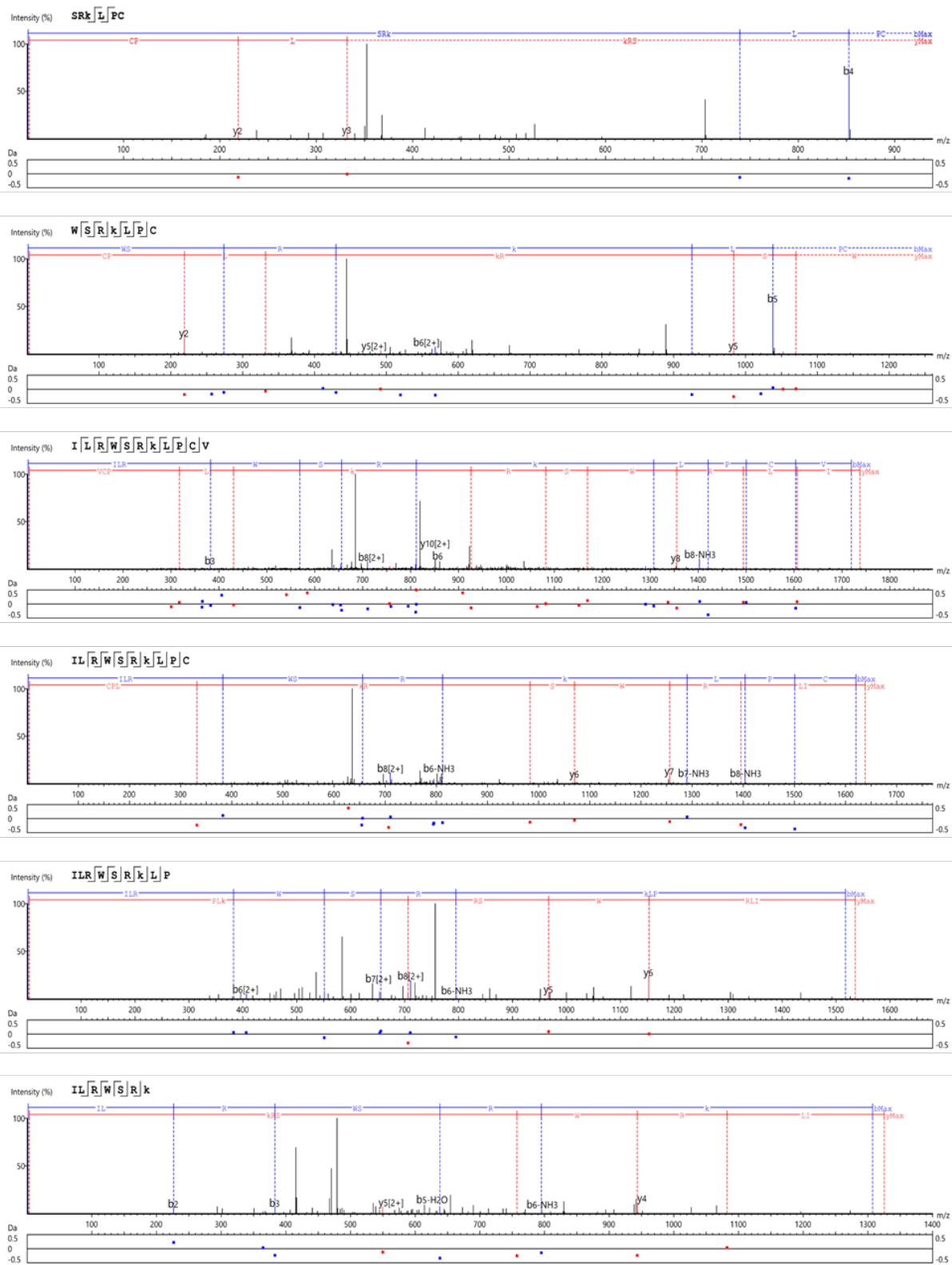
Figure S18. MS/MS spectra of JM#143 and the respective degradation products, found by PEAKs11 processing of raw data from LC-MS/MS analysis.
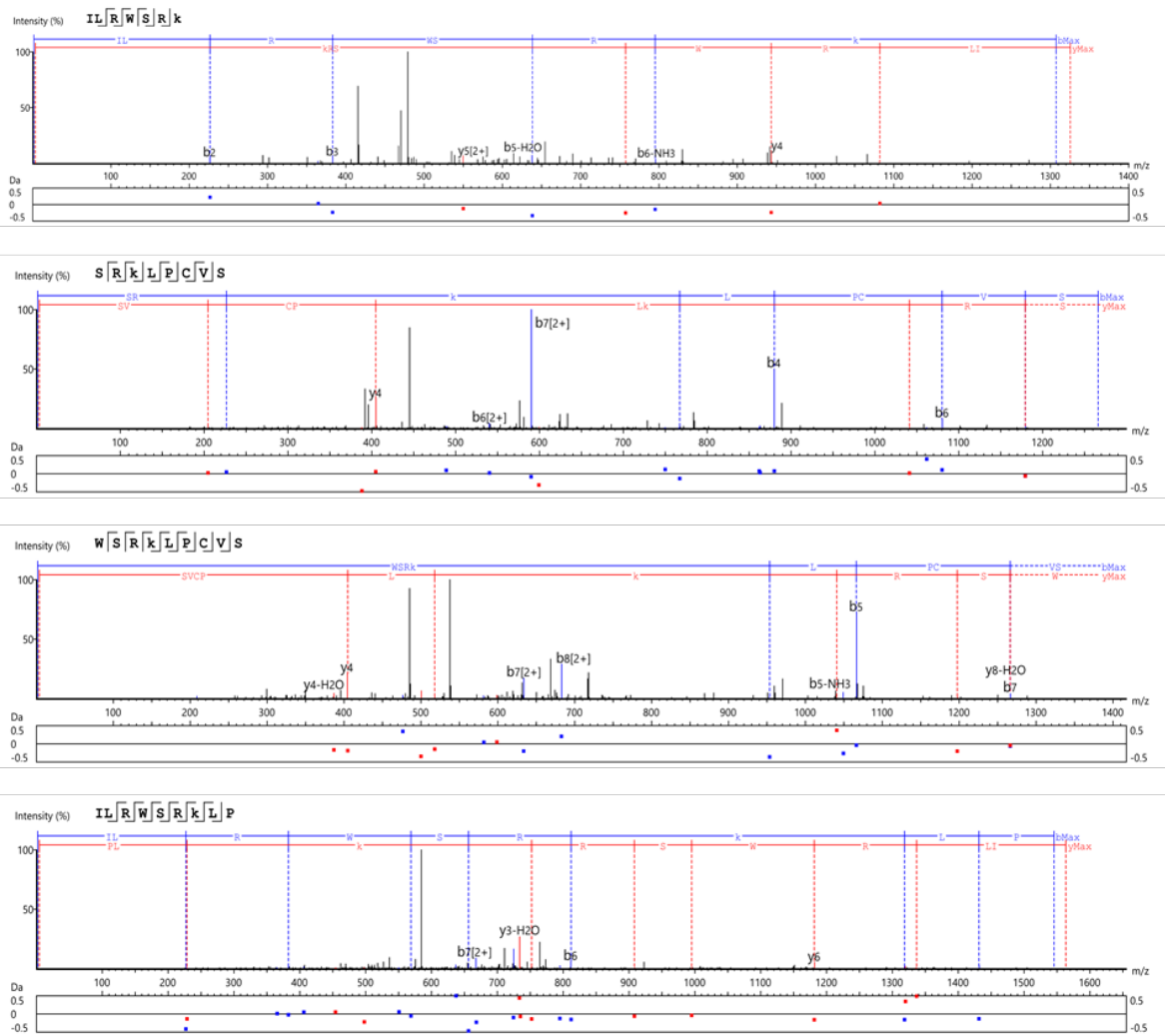
Figure S19. MS/MS spectra of JM#198 and the respective degradation products, found by PEAKs11 processing of raw data from LC-MS/MS analysis.
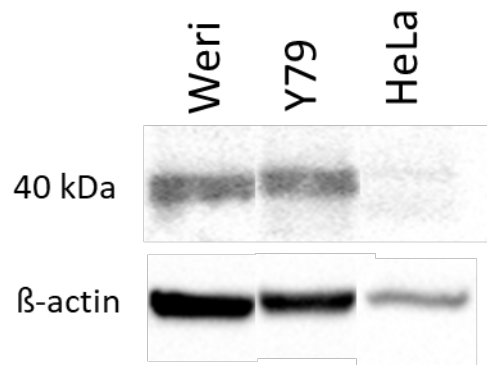
Figure S20. Western blot showing the CXCR4 expression in RB lysates compared to HeLa cells.
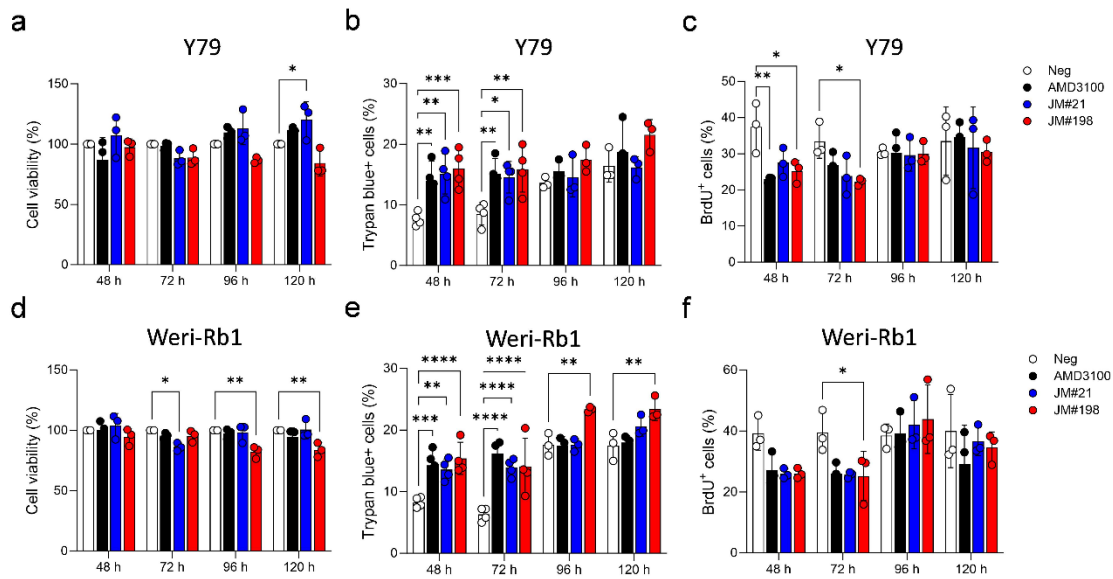
Figure S21. *In vitro* effects of CXCR4 inhibitors on retinoblastoma cells. Y79 (a-c) or Weri-Rb1 (d-f) cells were treated with 1 µM of the compounds or the negative control peptide for 48 – 120 hours. a,d) Cell viability was determined by water-soluble tetrazolium (WST-1) staining and values normalized to mock treated control. b,e) Dead cells were visualized by trypan blue staining. c,f) Cell proliferation was determined by the addition of 5-Bromo-2′-deoxyuridine (BrdU). Values were normalized to cells treated with negative controls. Values represent means ± SEM. Significances were calculated by ordinary two-way ANOVA with Turkey's multiple comparisons test. *p < 0.1; **p<0.01; ***p<0.001; ****p<0.0001.
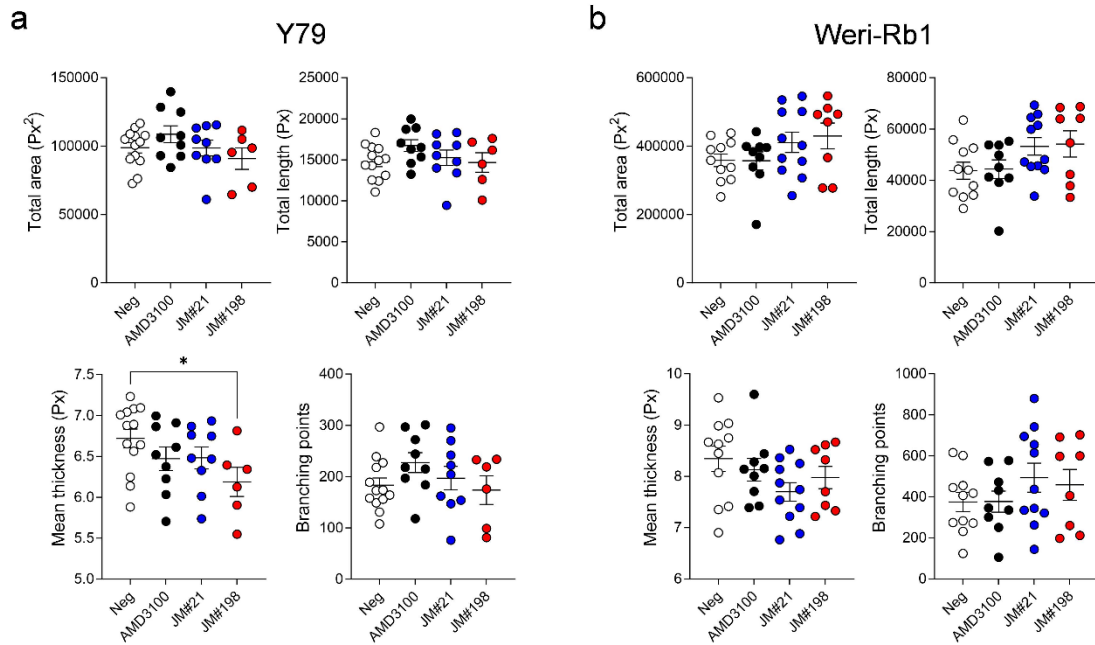
Figure S22. Analysis of angiogenesis in vascularized of chicken chorioallantoic membrane (CAM) tumors developing from inhibitor treated retinoblastoma cell lines. Y79 (a) or Weri-Rb1 human retinoblastoma cells (b) were treated with 50 µl of 1 µM compound and grafted onto the CAM of 10-day-old fertilized chiken embryos. Images of the vascularized CAM tumor formed by the grafted cells were taken after 7 days of incubation and analyzed for angiogenetic effects in terms of changes in total vascularized area, total vessel length, vessel thickness, and vessel branching points by IKOSA software. Shown are means for individual CAMs ± SEM

4) New retinoblastoma (RB) drug delivery approaches: anti-tumor effect of atrial natriuretic peptide (ANP)-conjugated hyaluronic-acid-coated gold nanoparticles for intraocular treatment of chemoresistant RB

Cumulative Thesis/Extent of Contribution

Cumulative thesis of M.Sc. André Haase

Author contributions

New retinoblastoma (RB) drug delivery approaches: anti-tumor effect of atrial natriuretic peptide (ANP)-conjugated hyaluronic-acid-coated gold nanoparticles for intraocular treatment of chemoresistant RB

A. Haase, N. Miroschnikov, S. Klein, A. Doege, N. Dünker, D. Van Meenen, A. Junker, A. Göpferich, P.S. Apaolaza, M. Busch

Status: published in Molecular Oncology (2024)

DOI: 10.1002/1878-0261.13587

Impact factor at submission: 6.6 (2022)

André Haase contributions (shared **first-authorship**):

- **Experimental work: 30% -** Conjugation of ANP-HA-GNPs, planning animal experiments, performing of intravitreal injection of luciferase tagged and etoposide resistant RB cells in newborn rat pups, *in vivo* luciferase measurements of rat pups, administration of ANP-HA-GNPs, part of CAM assays, IHC.

- **Data analysis: 40% -** Data evaluation, processing, formal analysis, and visualization.

- **Statistical analysis: 30% -** Data interpretation, integration and performance of various statistical tests.

- **Writing the manuscript: 10% -** Writing of parts of Material and Methods, Results, figure design and legends.

- **Revising the manuscript: 5% -** Revising Abstract, Introduction, Results, Discussion, Material and Methods, Figures.

_____

Signature André Haase

_____

Signature Prof. Dr. Nicole Dünker

New retinoblastoma (RB) drug delivery approaches: anti-tumor effect of atrial natriuretic peptide (ANP)-conjugated hyaluronic-acid-coated gold nanoparticles for intraocular treatment of chemoresistant RB

André Haase[1], Natalia Miroschnikov[1], Stefan Klein[1], Annika Doege[1], Nicole Dünker[1], Dario Van Meenen[1], Andreas Junker[2], Achim Göpferich[3], Paola Stephanie Apaolaza[4] and Maike Anna Busch[1] (iD)

1 Department of Neuroanatomy, Center for Translational Neuro- and Behavioral Sciences (C-TNBS), Institute for Anatomy II, University of Duisburg-Essen, Medical Faculty, Germany
2 Institute of Neuropathology, University of Duisburg-Essen, Medical Faculty, Germany
3 Department of Pharmaceutical Technology, University of Regensburg, Germany
4 Type 1 Diabetes Pathology Research Unit, Institute of Diabetes Research, Helmholtz Centre Munich, Germany

Intraocular drug delivery is a promising approach for treatment of ocular diseases. Chemotherapeutic drugs used in retinoblastoma (RB) treatment often lead to side effects and drug resistances. Therefore, new adjuvant therapies are needed to treat chemoresistant RBs. Biocompatible gold nanoparticles (GNPs) have unique antiangiogenic properties and can inhibit cancer progression. The combination of gold and low-molecular-weight hyaluronan (HA) enhances the stability of GNPs and promotes the distribution across ocular barriers. Attached to HA-GNPs, the atrial natriuretic peptide (ANP), which diminishes neovascularization in the eye, is a promising new therapeutic agent for RB treatment. In the study presented, we established ANP-coupled HA-GNPs and investigated their effect on the tumor formation potential of chemoresistant RB cells in an *in ovo* chicken chorioallantoic membrane model and an orthotopic *in vivo* RB rat eye model. Treatment of etoposide-resistant RB cells with ANP-HA-GNPs *in ovo* resulted in significantly reduced tumor growth and angiogenesis compared with controls. The antitumorigenic effect could be verified in the rat eye model, including a noninvasive application form via eye drops. Our data suggest that ANP-HA-GNPs represent a new minimally invasive, adjuvant treatment option for RB.

Abbreviations

ANP, atrial natriuretic peptide; ARPE-19, adult retinal pigment epithelial cell line; CAM, chorioallantoic membrane; CO_2, carbon dioxide; CRX, cone-rod homeobox; DAB, diaminobenzidin; DMEM, Dulbecco's modified Eagle medium; DNA, deoxyribonucleic acid; EDD, embryonic developmental day; etop, etoposide-resistant; FBS, fetal bovine serum; GFP, green fluorescent protein; GMP, guanosine monophosphate; GNP, gold nanoparticles; HA, hyaluronic acid; HA-SH, thiol-functionalized hyaluronic acid; HEK293T, human embryonic kidney cells; IHC, immunohistochemistry; IL-1β, interleukin-1β; LDV, laser Doppler velocimetry; NPRA, natriuretic peptide receptor A; NPRC, natriuretic peptide receptor C; NVG, neovascular glaucoma; PBS, phosphate-buffered saline; PCS, photon correlation spectroscopy; PDI, polydispersity index; PDR, proliferative diabetic retinopathy; PFA, paraformaldehyde; RB, retinoblastoma; RB1, retinoblastoma gene 1; RPE, retinal pigment epithelium cells; SEM, standard error of the mean; STR, short tandem repeat; TEM, transmission electron microscopy; TS, treatment setting; VEC, vincristine, etoposide, and carboplatin; VEGF, vascular epithelial growth factor; VEGFR2, vascular epithelial growth factor receptor 2; WERI, WERI-Rb1.

1. Introduction

Ocular drug delivery through noninvasive routes is challenging because of the anatomical structure and physiology of the eye, often resulting in low drug availability. Thus, for treatment of several retinal disorders, for example, proliferative diabetic retinopathy (PDR) [1], neovascular glaucoma (NVG) [2], and retinoblastoma intravitreal administration routes are currently used in order to reach the retina. Retinoblastoma (RB) is the predominant primary intraocular tumor found in children, occurring at a rate of 1 in 16 000 live births. It constitutes 2–4% of all childhood malignancies [3]. Retinoblastoma has an overall high survival rate, but further progressed tumors are often associated with high-risk characteristics such as dissemination [4] and chemotherapy resistances. Initially, enucleation was the primary successful therapeutic approach for retinoblastoma. However, the emergence of new drug delivery routes, such as intra-arterial, intravitreal, or intracameral, injections significantly increased ocular preservation rates and diminished the need for systemic chemotherapy [4,5]. Chemotherapy with chemotherapeutics such as vincristine, etoposide, or carboplatin, which are routinely used in a combined RB VEC-therapy often induce massive side effects and leads to drug resistances frequently limiting the treatment options of resistant tumors, which might cause relapses [6]. After therapy, 35% of retinoblastoma patients experience the development of secondary tumors, and among this group, 50% do not survive [7]. Emerging technologies, such as the utilization of nanoparticles as delivery systems for ocular drugs, small molecules, peptides, or nucleic acids, provide a noninvasive alternative treatment of retinoblastoma with increased accessibility, which is not only safe, but also long-lasting.

For biomedical applications, plasmonic materials such as gold nanoparticles (GNPs) have unique advantages as antioxidant and antiangiogenic agents [8]. It has been shown that GNPs can reduce the proliferation and migration of retinal pigment epithelium cells (RPE) induced by vascular epithelial growth factor (VEGF) or interleukin IL-1β [9]. Gold nanoparticles can be conjugated to different biomolecules [10] combing multiple advantages, including robust absorption and scattering of visible light, straightforward synthesis, manageable size and shape control, as well as high biocompatibility [11]. Following systemic administration, small-sized gold nanoparticles can traverse physiological and anatomical ocular barriers, such as the blood-retinal barrier. This expands the potential applications of GNPs as drug delivery systems through various administration routes [12]. We could recently

show that a combination of a gold core with a hyaluronic acid (HA) coat is a promising candidate nanocarrier for treatment of eye diseases [11]. Hyaluronic acid is a FDA-approved polymer commonly used in eye drops with the potential to enhance the delivery of anticancer drugs due to its CD44 receptor [13,14]. Several cells of the eye express the CD44 receptor endogenously and in disease conditions, for example, retinal pigmented epithelium (RPE), Müller glial, and ganglion cells [13,15]. Therefore, CD44 expressing cells have the capability to bind and internalize HA. Moreover, the composition of the ocular vitreous body contains not only 98% water and collagen but also hyaluronic acid (HA). The composition of this gel meshwork allows for a sustained release of drug molecules, extending the duration of their effect and enhancing bioavailability when administered in a solution [16]. Modifying the surface of GNPs with HA increases their mobility and permeability through ocular barriers, leading to antiangiogenic effects. This modification transforms GNPs into inhibitors of neovascularization [11]. In addition, HA enables larger nanoparticles to enter the cells as potential vehicles for the delivery of therapeutics to the posterior part of the eye via noninvasive application routes, for example, by eye drops [17].

The atrial natriuretic peptide (ANP), belonging to the family of atrial natriuretic peptides, plays an important role during stimulation of vasodilatation, natriuresis, and diuresis [18]. It has also been observed that ANP reduces choroidal neovascularization in the eye by inhibiting VEGF [19], likewise expressed in RB and correlated with increased RB malignancy [20]. Špiranec Spes et al. [21] recently demonstrated that ANP mitigates pathological retinal vascular regression and subsequent neovascularization through cyclic GMP signaling, protecting pericytes from apoptosis, and diminishing hypersecretion of VEGF from astrocytes. In addition, a combined treatment with glipizide, a second-generation sulfonylurea hypoglycemic agent, and ANP suppressed breast cancer growth and metastasis by the inhibition of angiogenesis via the VEGF/VEGFR2 signaling pathway [22].

Against the background that HA improves ocular tissue distribution and inhibition of neovascularization by ANP potentially reduces tumor growth, the goal of the study presented was to evaluate the applicability of ANP-conjugated, HA-coated gold nanoparticles (ANP-HA-GNPs) as promising candidate nanocarriers for the treatment of chemoresistant RB tumors *in vivo*. For this purpose, we investigated potential suppressive effects of ANP-HA-GNPs on tumor growth and angiogenesis of aggressive etoposide-resistant RB cell

lines in an *in ovo* chorioallantoic membrane (CAM) model as well as in a newly established orthotopic *in vivo* RB rat eye model.

2. Materials and methods

2.1. Synthesis and characterization of ANP coupled hyaluronan-modified gold nanoparticles

The synthesis of thiol-modified HA and GNPs used in this manuscript was described previously [11]. Briefly, thiol-functionalized HA (MW 5K; Lifecore™ Biomedical, Chaska, MN, USA) was cross-linked by carboxylic acid mainly following the protocol previously described by Oliveira et al [23]. Gold nanoparticles were synthesized based on the reduction and stabilization of the salt form of gold (HAuCl$_4$; Sigma-Aldrich, Munich, Germany) by trisodium citrate dehydrate salt (Sigma-Aldrich, Munich, Germany) by the Turkevich method [24]. The ratio of gold to citrate was 1 : 3.7 (w/w) to obtain GNPs with a 20 nm gold core. Thereafter, the ligand HA-SH was covalently bound to the surface of gold by interaction of the thiol group and molecular gold as described previously [11].

The concentration of HA-GNPs was determined by assessing the absorbance of the GNP core [25]. Gold nanoparticle surface modification with hyaluronic acid (HA) was identified by a shift in the maximum peak of the UV–visible spectrum. Measurements were conducted using a FLUOstar Omega microplate reader (BMG, Labtech, Ortenberg, Germany). The concentration of HA-SH covalently bound to GNPs was indirectly determined using the Ellman's method. The ANP was then bound by electrostatic interaction to the HA component of the nanoparticle surface. Complete binding of the ANP to the HA-GNPs was confirmed by SDS/PAGE electrophoresis (data not shown).

2.2. Size and zeta potential measurements

Particle size analysis of GNPs, HA-GNPs, and ANP-HA-GNPs was conducted through photon correlation spectroscopy (PCS), while zeta potentials were measured using Laser Doppler Velocimetry (LDV). Both analyses were performed on a Zetasizer Nanoseries-Nano ZS instrument (Malvern Instruments, Lappersdorf, Germany). All samples were appropriately diluted in Milli-Q™ (Merck, Darmstadt, Germany) water for the analyses.

2.3. Transmission electron microscopy

Transmission electron microscopy (TEM) was conducted using a Libra 120 electron microscope (Carl Zeiss,

Oberkochen, Germany). The procedures followed were consistent with protocols published previously [26,27].

2.4. Cell lines and culture

The human retinoblastoma (RB) cell lines Y79 [28] (RRID: CVCL_1893) and WERI [29] (RRID: CVCL_1792), originally purchased from the Leibniz Institute DSMZ (German Collection of Microorganisms and Cell Cultures) were placed to our disposal by H. Stephan along with the RB cell line RB355 [30] (RRID: CVCL_S611), initially provided by K. Heise, and the corresponding etoposide-resistant RB cell lines Y79-Etop, WERI-Etop, and RB355-Etop. The cultivation protocols for these cell lines, as well as for human embryonic kidney cells (HEK293T, RRID: CVCL_0063) kindly provided by B. Royer-Pokora and originally purchased from DSMZ, were comprehensively described in a prior publication [31].

All cell lines used were initially tested and authenticated by STR analysis. In the following, samples of all tested cells were frozen to insure access to tested cells in the course of all experiments. In addition, the RB cell lines were regularly analyzed for their individual *RB1* mutation status. The adult retinal pigment epithelial cell line ARPE-19 (RRID:CVCL_0145) was purchased from ATCC (Manassas, VA, USA) and maintained in DMEM/F12 medium supplemented with 1% penicillin streptomycin (10 000 U·mL^{-1}) and 10% inactivated FCS (GIBCO®, ThermoFisher Scientific, Darmstadt, Germany) at 37 °C in 5% CO$_2$ atmosphere. No ethics approval was required for work with the human cell lines. All cell lines were tested for mycoplasms on a regular basis.

2.5. Intracellular distribution of nanoparticles

ARPE-19 cells (65 000) were seeded on poly-L-lysine (0.1 mg·mL^{-1} for 30 min at 37 °C; GIBCO®, Thermo-Fisher Scientific) treated coverslips in a 24-well plate and incubated overnight. Thereafter, 25 μM GNPs or ANP-HA-GNPs were added to the cells. Following a 24-h incubation period, ARPE-19 cells were fixed using paraformaldehyde (PFA; 4% in PBS; pH 7.4). Incorporated particles were stained using a silver staining kit (Sigma-Aldrich, Munich, Germany) according to the manufacturer's protocol. Photomicrographs were captured using a Zeiss Axiovert 200 microscope (Zeiss, Jena, Germany).

2.6. *Ex vivo* vitreous humor diffusion and retinal explant studies

To get fresh vitreous humor and retinae, porcine eyes from a local slaughterhouse were enucleated after the

animals were sacrificed. The eyes were transported in cold (4 °C) CO_2-independent L-glutamine medium (GIBCO, ThermoFisher Scientific) until needed. The vitreous humor was separated from the retina and adjacent tissues and placed in a Petri-dish (25 cm^2; Corning, Kaiserslautern, Germany). To investigate the diffusion effect, 100 μL (0.5 mM) of ANP-HA-GNPs were injected into the vitreous body and monitored under a normal bright field camera (Nikon, Düsseldorf, Germany) for 24 h at room temperature.

In order to study the retinal distribution of ANP-HA-GNPs, conventional porcine retinal explants were dissected and cultured as described previously [32]. A trephine blade (ø 8 mm; Beaver Visitec, Waltham, MA, USA) was used to cut out a circular piece of retina from each eye with the inner limiting membrane (ILM) facing up. The retinal explants underwent treatment with 0.5 mM ANP-HA-GNPs. Neurobasal medium (GIBCO, ThermoFisher Scientific) was used for the dilution of the GNPs. Retinal cryosections (12 μm) were mounted on Superfrost Plus slides (ThermoFisher Scientific). Bright field microscopy visualization within the retinal tissue 24-h postadministration of the particles was performed utilizing a Zeiss Axiovert 200 microscope (Zeiss).

2.7. Generation of lentiviral particles for stable transduction

For the transduction of WERI and RB355 RB cell lines, lentiviral particles were generated. For this pupose, 6×10^6 human embryonic kidney cells (HEK293T) were transfected with 6 μg of each of the following plasmid DNAs: packaging vectors pczVSV-G [33] and pCD NL-BH [33], and pCL6LucEGwo (provided by H. Hanenberg). This transfection was carried out in DMEM medium in the presence of 45 μg polyethyleneimine (PEI, branched; Sigma-Aldrich, St. Louis, MO, USA). The lentiviral vector (pCL6LucEGwo) contained a fusion of the human codon usage-optimized luciferase (InvivoGen, San Diego, CA, USA) and an enhanced green fluorescent protein (EGFP; Clontech, Mountain View, CA, USA), driven by a modified spleen focus-forming virus (SFFV) retrovirus U3 promoter [34]. Twenty-four hours later, we exchanged the medium. After 72-h cultivation in Iscove's Modified Dulbecco's medium (IMDM; Pan-Biotech, Aidenbach, Germany) with 10% FBS and 1% penicillin/-streptomycin, viral supernatants were harvested, filtered (0.45 μm filter), and cryoconserved. In order to stably transfect RB cells with luciferase/GFP for in vivo tumor formation experiments, cells were seeded in DMEM medium at a concentration of 1.25×10^6. After 1 day, the medium was discarded and the WERI/WERI-Etop or RB355/RB355-Etop RB cells were transduced with the virus particles in the presence of polybrene (5 μL per ml lentivirus; H9268; Sigma-Aldrich, München, Germany). Dulbecco's modified eagle medium with supplements (twice the volume of the virus particles) was added after another 24 h, and additional 48 h later, the medium was changed completely.

2.8. In ovo tumor formation

To assess alterations in tumor formation, etoposide-resistant RB cells (Y79-Etop and WERI-Etop) and their respective control cells were grafted onto the chick chorio-allantoic membrane (CAM) mainly following the protocol of Zijlstra and Palmer [35,36] with modifications described previously [37]. Briefly, 1×10^6 RB cells per egg were directly grafted onto the CAM membrane at embryonic developmental day 10 (EDD10) without using silicone rings. After 24 h, at EDD11, the grafted eggs were treated by dropping 40 μL solution containing particles (at a concentration of 1 mM) and/or ANP (at a concentration of 0.06 μg·μL^{-1}) onto the CAM area, where the RB had previous been grafted. The different treatment conditions were as follows: (a) GNPs alone (1 mM stock), (b) HA-GNPs (0.9 mM stock), (c) ANP-HA-GNPs (0.865 mM stock), (d) ANP alone (1 mg·mL^{-1} stock), or (e) PBS (control). Five to seven eggs were grafted in at least three independent experiments for each condition. Seven days after grafting and 6 days after treatment (EDD17), tumors that formed from the grafted cells were excised, measured, and photographed as described previously [31,38,39]. The eggs were cooled down on ice for at least 15 min prior to preparation, and the chicken embryos were decapitated directly after opening of the eggs. Vessel formation was analyzed with regard to total vessel area, vessel length, thickness, and branching points based on CAM tumors photographed in situ using the IKOSA online software (KLM Vision, Graz, Austria).

2.9. In vivo orthotopic rat eye model

All experiments were approved by the state office for nature, environment, and consumer protection NRW (LANUV) under the reference numbers 81-02.04.2018.A003 and 81-02.04.2021.A015. The animals were anesthetized with isoflurane and euthanized by CO_2. Sex-independent Lewis rats (LEW/HanHsd) provided by the central animal laboratory of Essen (ZTL) were maintained on a 12-h light–dark cycle with ad libitum access to food and water. Before anesthesia, rats were weighed, and metamizol (100 mg·kg^{-1}) was administered orally for prophylactic pain prevention. Within the first 24 h of birth, newborn rat pups (P0)

were anesthetized with isoflurane (3.0% isoflurane at an Ø flow of 1.5 L·min^{-1}; Sigma Delta Vaporizer, Penlon, UK). The pups got an individual tattoo on their paws for identification during the experimental procedure and were transferred to a heated pad to ensure a body temperature of 37 °C. Maintenance of anesthesia (2.5% isoflurane at an O flow rate of 1.5 L·min^{-1}) was assured using a nosecone for rat pups under a microscope. A 33 G needle attached to a 5-μL Hamilton syringe was used bevel-up to inject the RB cells through the naturally closed eyelid into the vitreous of the rats' eyes. Each animal received a single injection of 1×10^5 luciferase-GFP labeled WERI ($n = 24$), WERI-Etop ($n = 21$), RB355 ($n = 18$), RB355-Etop ($n = 21$) cells or an injection of sterile phosphate-buffered saline (PBS control; $n = 3$) into the right eye. Injection of RB cells or PBS control (1 μL total volume for all injections) was done manually under a microscope. The RB cell suspension or PBS was injected slowly, and the needle remained in place for 30 s following injection to avoid reflux during extraction of the needle. The pups were returned to their mother in their home cage, and tumor formation was consecutively monitored by bioluminescence measurements over a time period of 9 weeks as described below. After 2 (P14), 4 (P28), or 9 weeks (P63), the rats were euthanized, and the right eye was removed and investigated immunhistochemically.

2.10. Bioluminescence imaging

Isoflurane anesthesia was performed as described above, following a subcutaneous injection of VivoGlo D-luciferin potassium salt (Promega, Fitchburg, MA, USA) from a 40 mg·mL^{-1} stock in PBS. The dosage was calculated after weighting the animals prior to imaging (150 mg luciferin per kg animal weight). On the indicated days after injection (P3, P7, P10, P14, P28, P42), the anesthetized animals were imaged under maintenance of anesthesia using a Caliper Lumina II system (PerkinElmer, Waltham, MA, USA). Animals were imaged with their right side up, three to five at a time using full-frame camera height. Images were gathered over 45 s each. Image visualization and quantification were performed using the LIVING IMAGE ANALYSIS software 4.7.4 (PerkinElmer).

2.11. Treatment of etoposide-resistant WERI cells with ANP-HA-GNPs in an orthotopic rat eye model

In order to investigate the effectiveness of a nanoparticle therapy on tumor development of etoposide

resistant RB cells, three different treatment regimen (Fig. 1) were investigated based on the cell line WERI-Etop labeled with luciferase and GFP (luc-GFP). In treatment setting I, 1×10^5 WERI-Etop cells in 1 μL ANP-HA-GNPs solution (0.865 mM stock) were injected into the right eye of P0 rat pubs (Fig. 1). Animals were imaged on the indicated days after injection (P3, P7, P10, P14, P21, and P28) in comparison with control cells (WERI-Etop) without treatment. In treatment setting II and III, RB tumors were allowed to grow 14 days prior to treatment. After 10 (P10) and 14 (P14) days, the animals were imaged. Those with detectable RB tumor growth were treated with 1 μL ANP-HA-GNPs solution (0.865 mM stock) via intravitreal injection on P14 and P21 in treatment setting II and with eye drops (1 μL ANP-HA-GNPs solution) on P14, P17, P21, and P24 in treatment setting III (Fig. 1). In treatment setting II and III, animals were imaged on the indicated days (P10, P14, P17, P21, P24, and P28) in comparison with control cells (WERI-Etop) injected or dropped with PBS as vehicle under the same schedule. After 4 weeks (P28), rats were euthanized, and the right eye was enucleated and investigated immunohistochemically.

2.12. Histological and immunohistological processing

Upon completion of the experimental protocols, animals were euthanized by CO_2 and eyes were enucleated. Whole P14, P28, and P63 eyes or CAM tumors were fixed in 4% paraformaldehyde overnight, dehydrated, paraffin-embedded, and 5 μm sections were obtained using a microtome. Sections were deparaffinized and rehydrated in an ethanol series of descending concentration. Subsequently, sections were stained using Mayer's hematoxylin. Besides, immunohistochemical detection was performed using a ready-to-use rabbit monoclonal antibody against Ki67 (clone 30-9; Roche Ventana, Basel, Switzerland) or CRX red (dilution 1 : 50; clone A-9; Santa Cruz Biotechnology, Heidelberg, Germany) with the OptiView DAB IHC detection kit (Thermo Fisher, Darmstadt, Germany) for visualization. Images were captured using a slide scanner (Leica, Wetzlar, Germany) and subsequently analyzed by am APERIO IMAGE SCOPE Software (Leica).

2.13. Statistical analysis

Statistical analyses were performed using GRAPHPAD PRISM 9 (GraphPad Software, Boston, MA, USA). Data represent means ± SEM, and results were analyzed by a Student's t-test and considered significantly different if
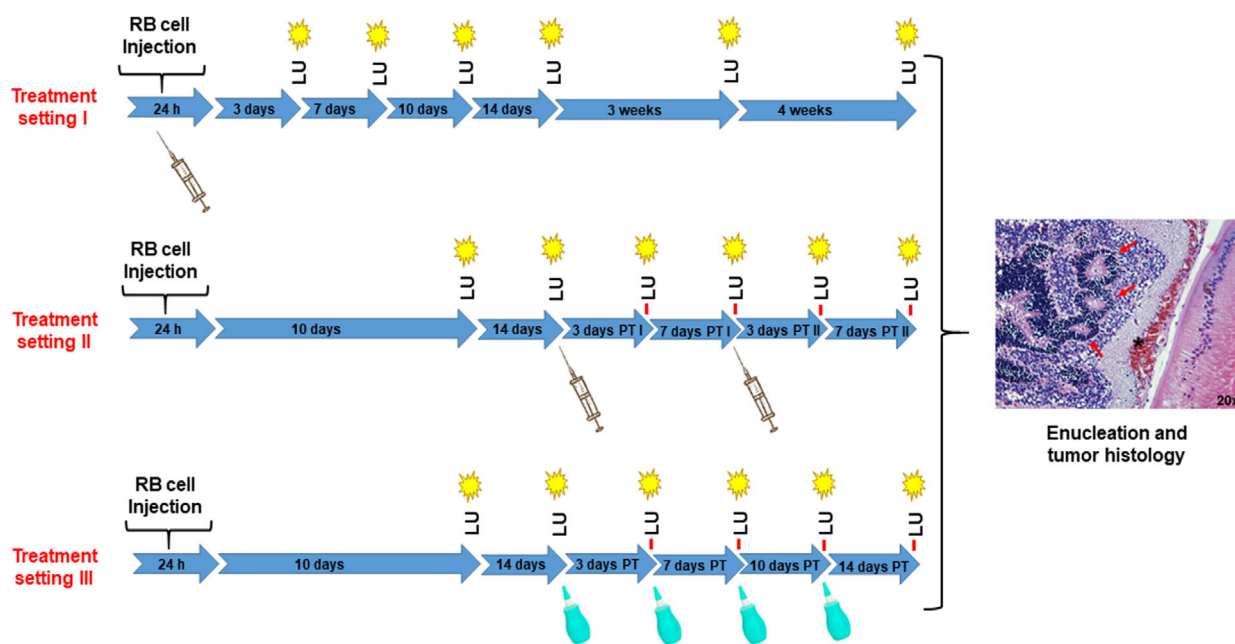
Fig. 1. Workflow of retinoblastoma (RB) tumor cell injection into the naturally closed eye of newborn rats (P0) and the detection of luciferase signals under nanoparticle treatment. Treatment setting I: $n = 12$ treated and $n = 10$ control animals; Treatment setting II: $n = 12$ treated and $n = 11$ control animals; Treatment setting III: $n = 12$ treated and $n = 12$ control animals; LU, luminescence measurement; PT, post-treatment; syringe: time point of nanoparticle treatment; green dropping bottle: time-point of topical nanoparticle treatment; red arrows in the tumor histology demarcate rosette like RB tumor structures.

P-value < 0.05 (*), P-value < 0.01 (**), or P-value < 0.001 (***). To quantify Ki67-positive cells, regions of interest were extracted from scanned slides and analyzed using IMAGEJ [40]. In a macro, hue, saturation and brightness were determined from the individual images and the threshold values for these parameters were adjusted to the needs of the "Analyze Particles" function in order to determine the percentage of Ki67-positive cells. Quantification of CAM vessel formation was performed with the IKOSA online software (KLM Vision, Graz, Austria; https://app.ikosa.ai/).

3. Results

3.1. Physical characterization of GNPs and ANP-HA-GNPs

Table 1 displays the particle size, zeta potential, and polydispersity index (PDI) of the GNPs, both with and without attached hyaluronic acid (HA) or ANP-HA. The attachment of HA or ANP-HA to the GNP surface resulted in a significant increase in both, size and zeta potential, with values more than doubling. The PDI, reflecting the uniformity of particle size distribution, remained around 0.2 for bare 20 nm gold core GNPs (GNPs 20), HA-GNPs, and ANP-HA-

Table 1. Particle size, zeta potential, and polydispersity index (PDI) of the gold nanoparticles (GNPs); $n \geq 6$; data represent mean $\pm$ standard deviation. ANP, atrial natriuretic peptide; ANP-HA-GNP, ANP coupled HA-GNPs; HA-GNP, hyaluronic acid coupled GNPs.

	SIZE (nm)	Zeta potential (mV)	PDI
GNPs	22.34 ± 0.54	−52.73 ± 7.30	0.292
HA-GNPs	57.01 ± 3.86	−17.33 ± 0.67	0.224
ANP-HA-GNPs	59.26 ± 1.72	−7.58 ± 1.40	0.282

GNPs, indicating a homogeneous distribution. TEM microscopy analysis of the GNPs and ANP-HA-GNPs revealed that a polymer HA corona surrounded the ANP-HA-GNPs (Fig. 2B,C), whereas GNPs (Fig. 2A) lacked a visible corona. The presence of this surface layer accounted for the augmentation in size noticed in the PCS measurements (Table 1). To investigate the interactions of bare GNPs in comparison with ANP coupled HA-coated GNPs (ANP-HA-GNPs), we analyzed the cellular nanoparticle uptake and distribution in ARPE-19 cells (Fig. 2E,F) and nontreated cells as negative controls (Fig. 2D). Bare GNPs shown in Fig. 2E formed large vesicular aggregates inside the cells, whereas modified ANP-HA-GNPs displayed as small individual particles throughout the cytoplasm
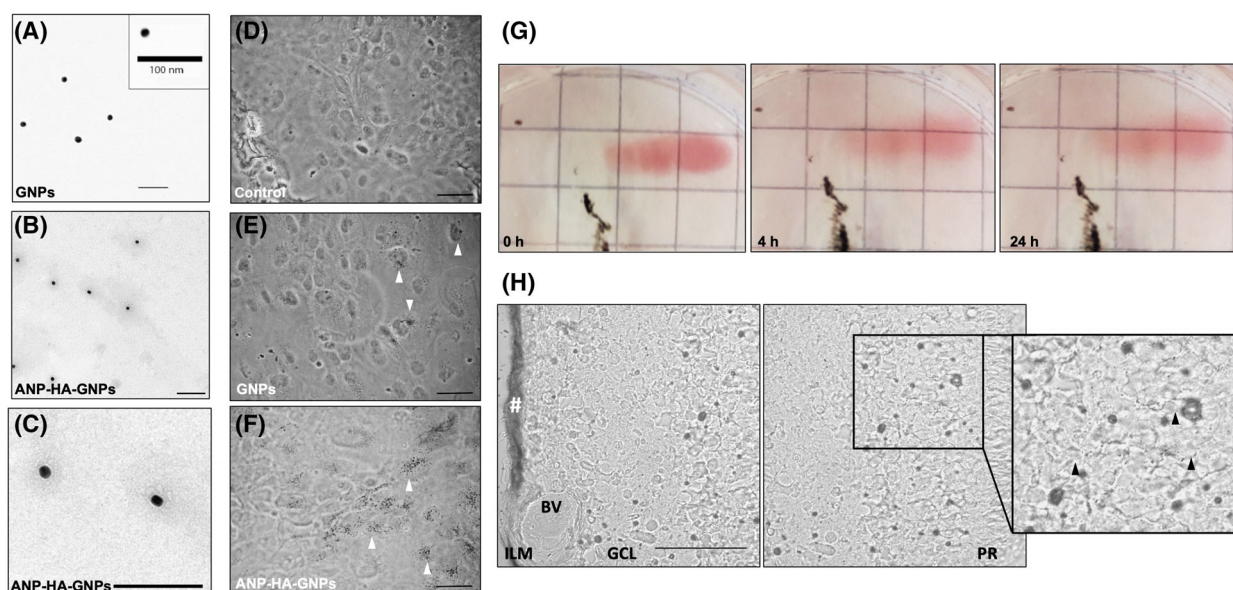
Fig. 2. Characterization of atrial natriuretic peptide coupled hyaluronic acid coated gold nanoparticles (ANP-HA-GNPs). (A–C) Transmission electron microscopy (TEM) microscopy pictures of bare GNPs with 20 nm gold core (A) and modified ANP-HA-GNPs (B, C). Scale bars: 100 nm. (D–F) Bright field images of ARPE-19 cells after silver staining for gold (black dots). Scale bars: 50 μm. Photographs were taken 24 h after treatment with 25 μM GNPs (E) or ANP-HA-GNPs (F) in comparison with nontreated control cells (D). White arrowheads exemplarily indicate some of the silver stained particles. (G) Photographs of porcine vitreous humor 0, 4 and 24 h after administration of 100 μL ANP-HA-GNPs. The black tissue represent remains of the retinal pigment epithelial layer. (H) Confocal bright field pictures of sequential cryosections of porcine retinal explants 24 h after administration of 0.5 mM ANP-HA-GNPs. Particles are visible as dotted black pattern within the tissues after silver staining. Accumulation/retention of ANP-HA-GNPs occurs at the administration side in the ILM and is marked by #. Black arrowheads indicate the location of the invaded particles. Scale bar: 50 μm. The experiments were performed in triplicates. ANP, atrial natriuretic peptide; ANP-HA-GNP, ANP coupled HA-GNPs; BV, blood vessel; GCL, ganglion cell layer; GNP, gold nanoparticles; HA, hyaluronic acid; ILM, inner limiting membrane; PR, photoreceptor layer.

(Fig. 2F). As a proof of principle, we additionally analyzed the cellular uptake of ANP-HA-GNPs in RB cells and observed an internalization of the particles into WERI-Etop cells (Fig. S1).

3.2. Vitreous humor diffusion and biodistribution in retinal explants

To analyze the diffusion of ANP-HA-GNPs into the vitreous humor, we utilized the visible red color of the GNPs as a qualitative indicator. The ANP-HA-GNP particles showed a good distribution in the vitreous humor after 4 and 24 h (Fig. 2G). In addition, the red color in the vitreous humor turned lighter 4 and 24 h after ANP-HA-GNP injection, supporting the notion of a proper diffusion capacity of the particles (Fig. 2G).

Analyzing the biodistribution of the ANP-HA-GNPs in retinal explants, administered particles were mainly observed in the photoreceptor layer of the retina (Fig. 2H). They were able to cross the inner limiting membrane and distributed from the ganglion cell layer to the photoreceptors. Nevertheless, there was a retention of ANP-HA-GNPs in the inner limiting membrane (Fig. 2H) due to the fact that the high particle volume used was not proportional to the explant size but was necessary to ascertain that the particles can penetrate and interact with the retinal tissue.

Taken together, (a) ANP-HA were successfully attached to gold core nanoparticles, (b) a good uptake and intracellular distribution of the GNPS was overserved in ARPE-19 cells and (c) good diffusion into the vitreous as well as *ex vivo* retinal biodistribution was verified. Thus, ANP-HA-GNPs have a promising potential to serve as antiangiogenic nanocarriers for the treatment of eye cancers like retinoblastoma.

3.3. *In ovo* tumor formation capacity of etoposide-resistant RB cells after ANP-HA-GNP treatment

A previous study by our group revealed that etoposide resistant RB cells display a significantly increased tumor formation potential compared with chemotherapy-

formation. By contrast, in ANP-HA-GNP-treated Y79-Etop CAM tumors significantly reduced mean vessel thickness was observed and WERI-Etop CAM tumors displayed a significantly reduced total vessel area, vessel length, and branching points.

Additionally, the tumor formation capacity of Y79-Etop (Fig. 4A) and WERI-Etop cells (Fig. 4D) was significantly reduced after treatment with ANP-HA-GNPs compared with control cells treated with PBS. Controls of the cell line Y79-Etop also displayed a significantly decreased tumor formation capacity and tumor size in comparison with cells treated with GNPs, HA-GNPs or ANP alone (Fig. 4A). Weight (Fig. 4B,E) and size (Fig. 4C,F) of CAM tumors developing from etoposide-resistant RB cells treated with ANP-HA-GNPs were significantly lower compared with tumors forming from control cells treated with PBS only.

3.4. *In vivo* tumor formation of etoposide-resistant RB cells in an orthotopic rat model

Next, we set out to establish an orthotopic *in vivo* rat eye model for treatment of chemoresistant retinoblastoma tumors. To validate our *in vitro* and *in ovo* findings,

suggesting that etoposide-resistant RBs exhibit a more aggressive behavior than their chemosensitive cells of origin, we conducted *in vivo* investigations. We therefore injected luciferase and GFP-labeled etoposide-resistant RB cells (WERI-Etop and RB355-Etop) into the right eye of newborn rats 24 h after birth. Tumor growth was monitored by detection of the luciferase signal (Fig. 5A) over a time period of 9 weeks and compared with signal intensities of corresponding chemosensitive RB cell (WERI and RB355) tumors. We could show a high luciferase signal reflecting a high tumor formation capacity in at least 80% of the RB cell lines tested and observed a constant tumor growth until Day 14 postinjection (Fig. 5B,C). After 2 weeks, the luciferase signal dropped down in all RB cells investigated, except for RB355-Etop cells (Fig. 5B,C). Nevertheless, we were able to verify our *in vitro* and *in ovo* data as WERI-Etop cells showed a significantly increased tumor growth reflected by an increased luciferase signal compared with chemosensitive WERI cells until Day 28 (Fig. 5B) and RB355-Etop cells displayed a slightly increased luciferase signal upon Day 14 reaching significance at Day 28 (Fig. 5C).

In order to analyze RB tumors grown *in vivo* histologically, enucleated rat eyes were embedded in
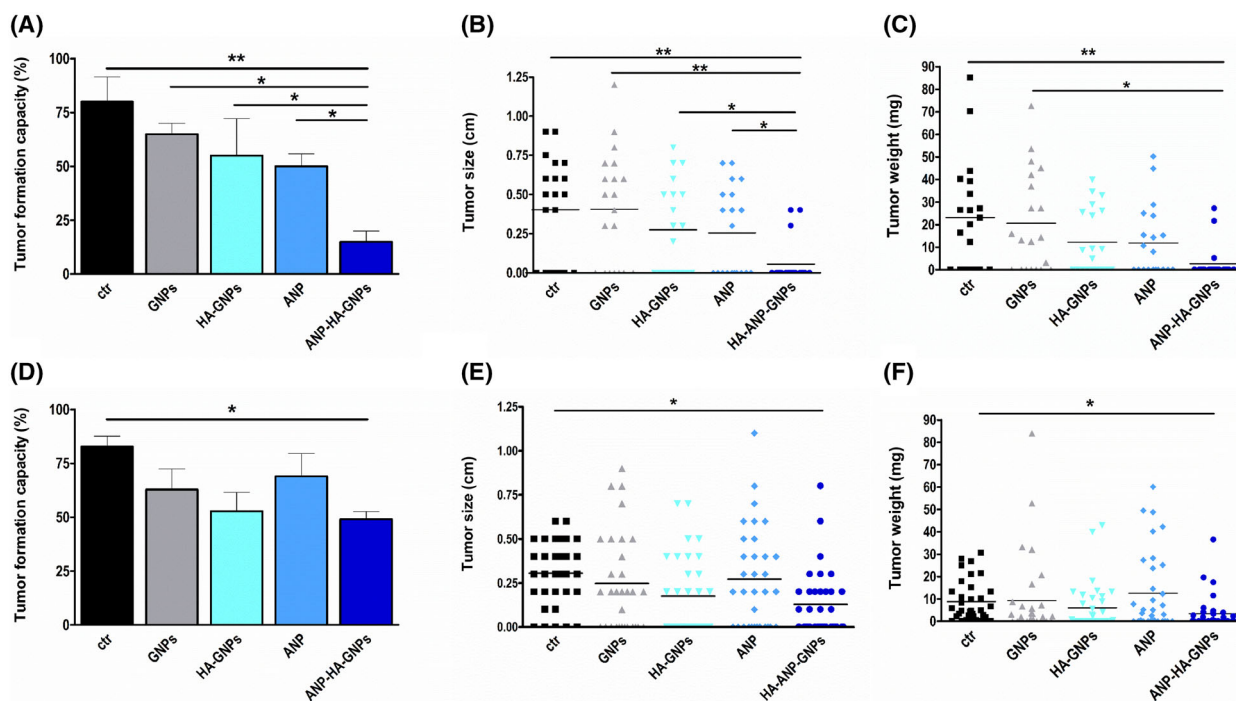
Fig. 4. Quantification of tumor formation from grafted retinoblastoma (RB) cells after gold nanoparticle treatment in chorioallantoic membrane (CAM) assays. Tumor formation capacity (A, B), CAM tumor weight (B, E) and CAM tumor size (C, F) of etoposide resistant RB cells was quantified after treatment with GNPs, HA-GNPs, ANP, or ANP-HA-GNPs. Upper row (A–C) shows the results for Y79-Etop cells and lower row (D–F) data for WERI-Etop cells. ANP, atrial natriuretic peptide; ANP-HA-GNP, ANP coupled HA-GNPs; ctr, PBS treated; GNP, gold nanoparticles; HA-GNP, hyaluronic acid coupled GNPs. Values are means of three independent experiments ± SEM. *$P < 0.05$; **$P < 0.01$ statistical differences compared to the control group calculated by one-way ANOVA with Newman–Keuls post-test.

Fig. 5. Luminescence signal (LU) of ocular tumors developing from chemosensitive and etoposide (−Etop) resistant WERI and RB355 RB cells injected into the eyes of newborn rats. (A) Pseudo-color images of two representative animals injected with luciferase and green fluorescent protein (luc-GFP) labeled sensitive and etoposide resistant RB355 cells at three time points (Day 3, 10, 28). Red color indicates highest luminescence intensity, dark blue color lowest luminescence signal. Quantification of luminescence signa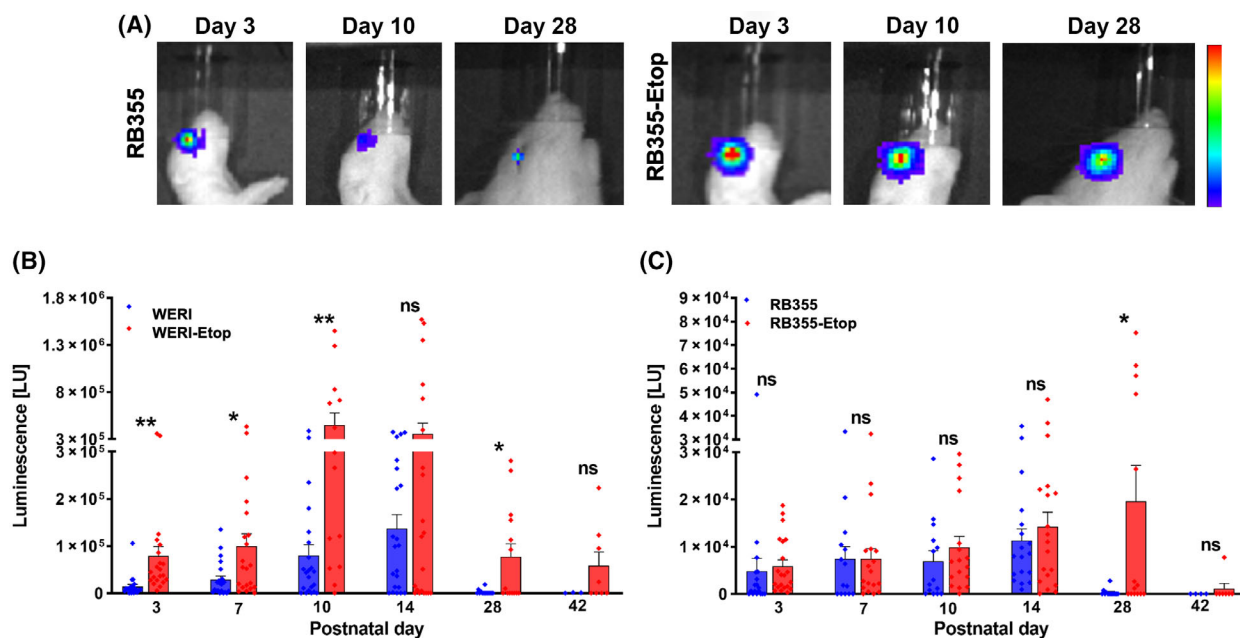l measurements revealed increased tumor growth for WERI-Etop (B) and RB355-Etop (C) cells (red columns) compared with their chemosensitive counterparts (blue columns). Values are means of independent animals injected with WERI cells ($n = 24$), WERI-Etop cells ($n = 21$), RB355 cells ($n = 18$), RB355-Etop cells ($n = 21$), and phosphate buffered saline (PBS control; $n = 3$). Error bars indicate the SEM. $^{ns}P > 0.05$; $*P < 0.05$; $**P < 0.01$ statistical differences compared to the control group (WERI or RB355) calculated by Student's t-test.

paraffin, cut and immunohistologically stained for CRX and Ki67 to verify the RB origin and proliferation potential of the tumor xenografts. Hematoxylin and eosin stains proved tumor development for every RB cell line investigated (Fig. 6) supporting our luminescence-based tumor data described above. In addition, we verified the RB origin of the tumors by CXR expression and were able to show proliferative activity of the tumor cells (Fig. 6). In the control eyes with PBS vehicle injection, no histological changes were visible upon 9 weeks of postinjection (Fig. 6).

Correlating with the observation that intraocular luciferase signals dropped down from Day 28 on, not all proven tumors were proliferative 9 weeks after injection. Therefore, experimental time line was shortened from 9 to 4 weeks for the following nanoparticle treatment approaches.

3.5. *In vivo* treatment effects of ANP-HA-GNPs on tumor formation of etoposide-resistant RB cells in an orthotopic rat model

We set out to test the effectiveness and potential application routes of ANP-HA-GNPs to treat etoposide-

resistant RB cells *in vivo*. As a proof of principle and to verify the *in ovo* effects of ANP-HA-GNPs on RB tumor growth, we injected WERI-Etop cells together with ANP-HA-GNPs into the rat eyes 24 h after birth (treatment setting I). We could show that in comparison with controls tumor growth of the treated WERI-Etop cells were significantly reduced 14 days upon injection (Fig. 7A). In treatment setting II and III, more closely resembling the actual conditions in RB patients, we let the tumor grow for 2 weeks prior to treatment with ANP-HA-GNPs. Thereupon, in treatment setting II, we injected the ANP-HA-GNPs into the rat eyes with RB tumor growth and used ANP-HA-GNP eye drops as topical treatment under treatment regimen III. As shown in Fig. 7B, the injection regimen of ANP-HA-GNPs in treatment setting II did not significantly reduce RB tumor growth in comparison to the controls, whereas topical administration of ANP-HA-GNPs eye drops led to a significant tumor reduction after the first treatment cycle at Day 17 and further, not yet significant, reduced tumor growth upon Day 24 (Fig. 7C).

After 4 weeks of RB tumor growth, we enucleated the rats eyes of all three treatment regimen and
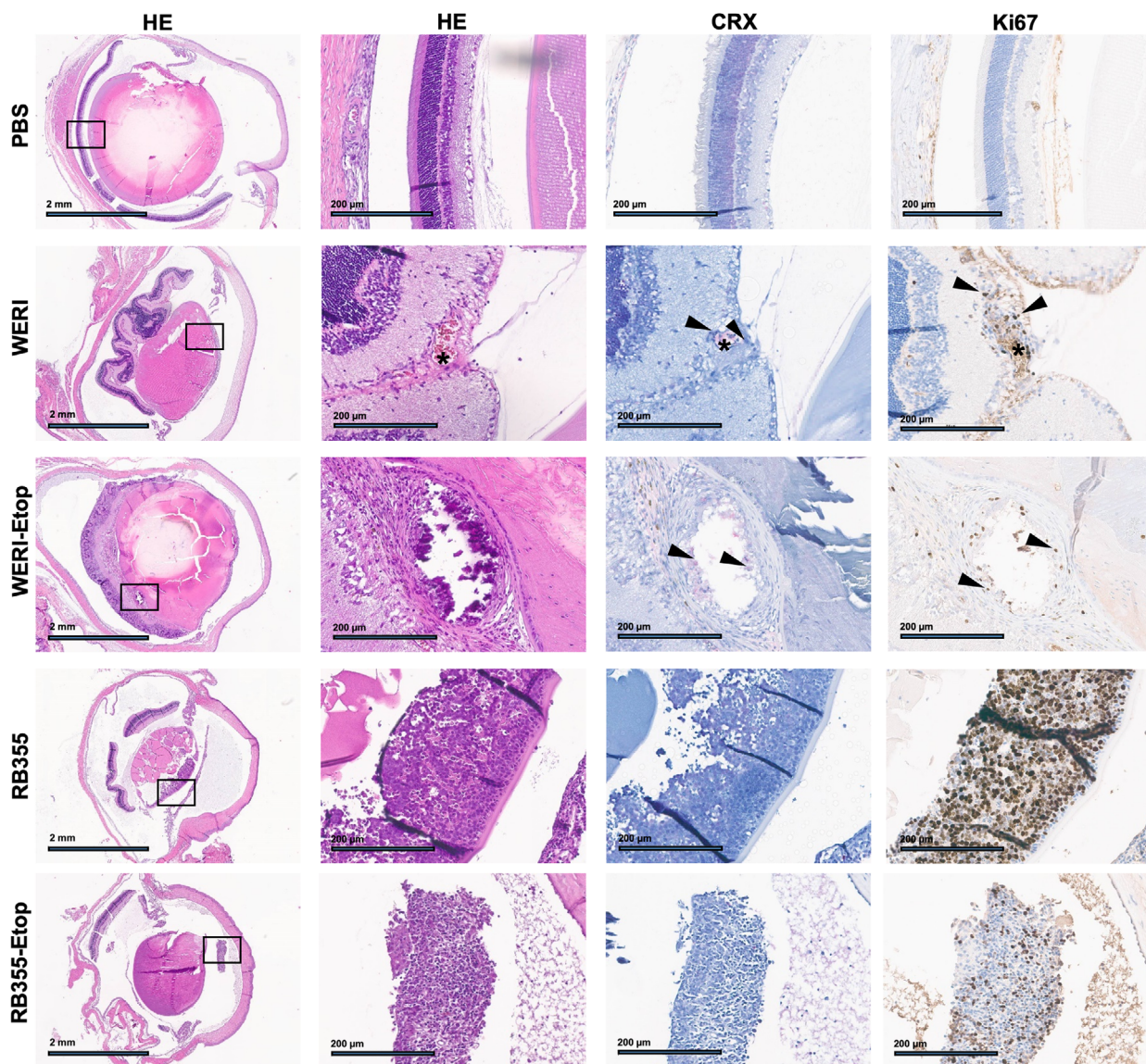
Fig. 6. Histologic analysis of rat eye tumors after injection of human retinoblastoma (RB) cells. Paraffin sections of rat eyes 9 weeks after injection of chemosensitive and etoposide (−Etop)-resistant WERI and RB355 RB cells revealed intravitreal tumors with CRX (light red signal) and Ki67 (brown signal) positive cells. PBS (upper row): control eye injected with PBS depicting normal retinal histology. HE: hematoxylin and eosin stains in two different magnifications (black boxes depict the zoom-in area shown in the adjacent columns), Scale bars: 2 mm at 4× magnification (HE) and 200 μm in the zoom-in area, CRX: retinal and RB marker, Ki67: proliferation marker, asterisk: blood vessel, arrowheads: RB tumor cells.

performed histological stainings for Ki67, CRX, and luciferase to verify the RB origin and the proliferation potential of the tumor xenografts (Fig. 8). Hematoxylin and eosin as well as luciferase stains revealed RB tumor development, while CRX positivity proved their RB tumor cell origin and Ki67 staining verified a positive proliferation status of the tumor. The majority of the RB tumors were positive for all markers analyzed. In treatment setting I and II, ANP-HA-GNP-treated

tumors showed a slightly reduced proliferation rate with less Ki67-positive RB tumor cells in comparison with the control group. This reduction did, however, not reach significance (Fig. 8).

In conclusion, we verified that ANP-HA-GNPs inhibit tumor growth *in vivo*, but a suitable treatment modality and the most effective treatment cycle need to be further elaborated. Generally, treatment with eye drops displayed to be effective in reducing tumor
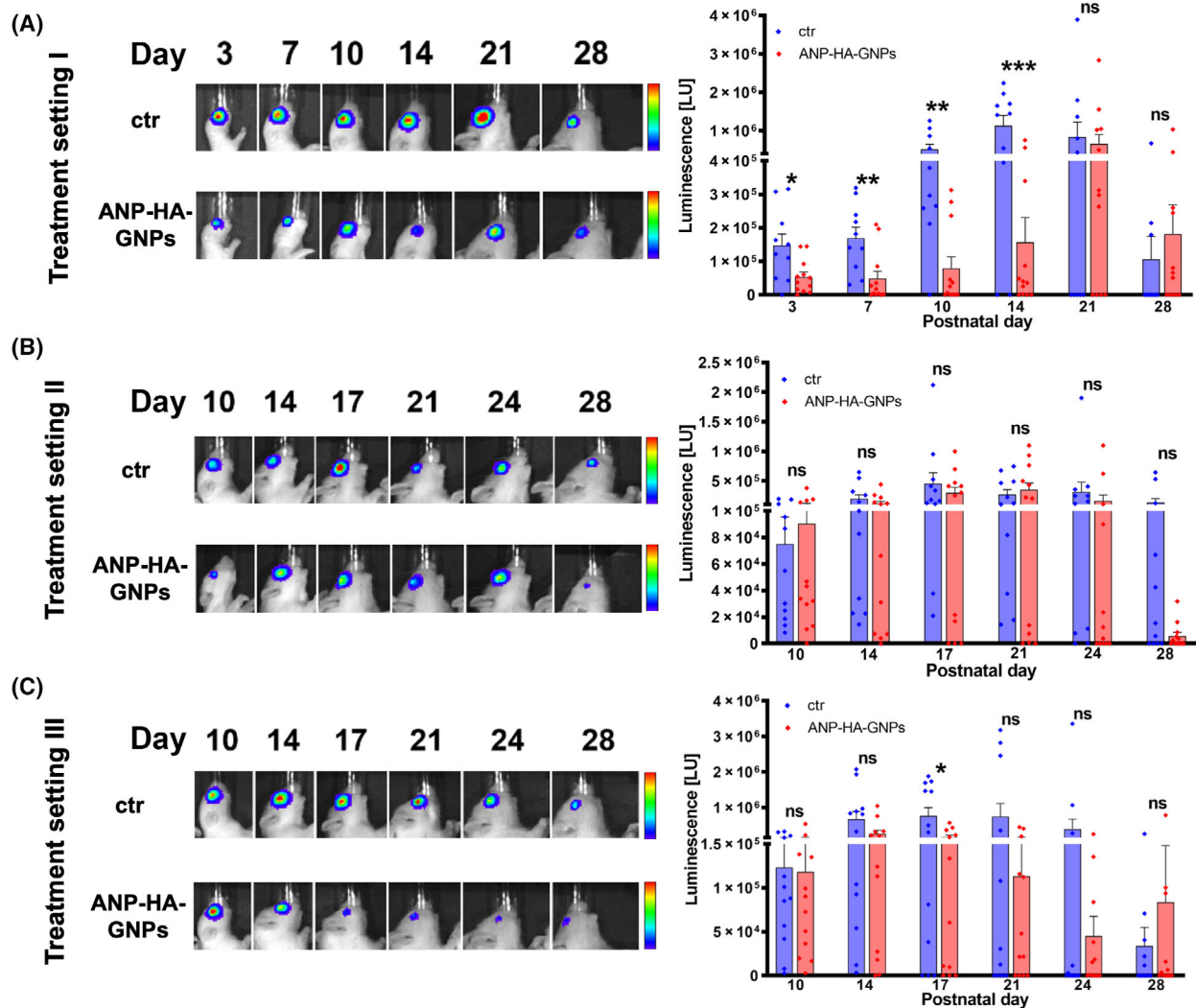
Fig. 7. Luminescence signal (LU) of ocular tumors developing from etoposide (−Etop) resistant WERI RB cells injected into the eyes of newborn rats. (A) Treatment setting I: WERI-Etop cells were injected into the right eye of P0 rat pups together with ANP-HA-GNPs (ctr: $n = 10$, ANP-HA-GNPs: $n = 12$). Treatment setting II and III: WERI-Etop cells were allowed to form tumors 14 days prior to treatment with intravitreal injections of ANP-HA-GNPs (ctr: $n = 11$, ANP-HA-GNPs: $n = 12$; B) or topical treatment via eye drops (ctr: $n = 12$, ANP-HA-GNPs: $n = 12$; C). (A–C) Pseudo-color images of representative animals injected with luciferase and green fluorescent protein (luc-GFP) labeled etoposide resistant WERI cells at six different time points (Day 3–28; left side). Red color indicates highest luminescence intensity, dark blue color lowest luminescence signal. Quantification of luminescence signal measurements (right side) revealed differences in tumor growth between ANP-HA-GNPs treated WERI-Etop cells (red columns) and untreated WERI-Etop control cells (blue columns). Values represent means of independent animals ± SEM; significances were calculated by unpaired Student's t-test. $^{ns}P > 0.05$; $*P < 0.05$; $**P < 0.01$; $***P < 0.001$.

growth, but it seems that the dose needs to be increased, for example, by more frequent administrations of the ANP-HA-GNPs.

4. Discussion

Retinoblastoma is an ophthalmological childhood cancer with serious consequences if left untreated, for

example, loss of vision, secondary cancers, and death [7,41]. Systemic or local chemotherapy treatment regimens effectively reduce tumor size, inhibit metastasis, and preserve vision [5,42,43]. Chemotherapy can, however, cause the development of resistant RB tumor cells. We recently demonstrated that compared with corresponding chemosensitive cells of origin etoposide-resistant RB cells are more aggressive in terms of
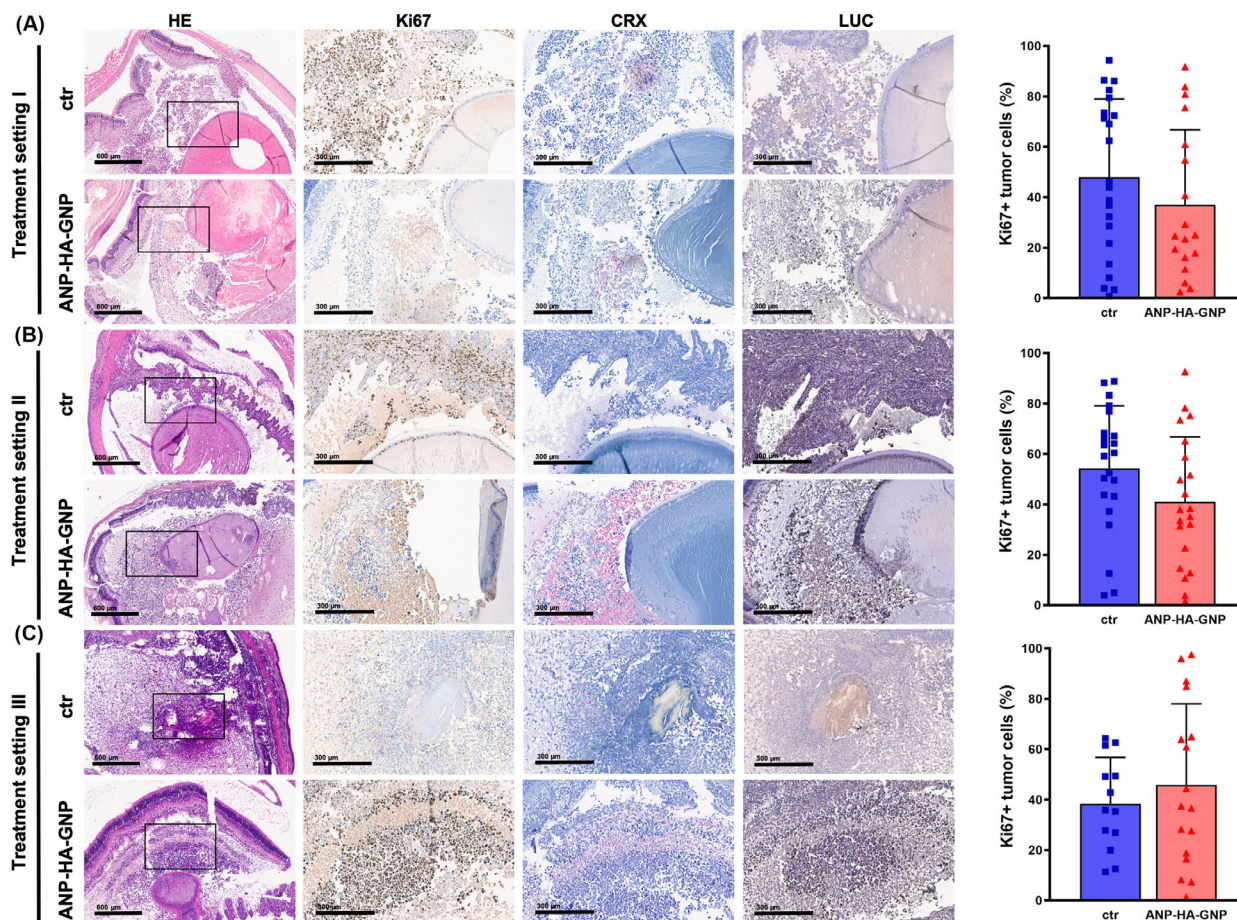
Fig. 8. Histological analysis of rat eye tumors after injection of human retinoblastoma (RB) cells and treatment with gold nanoparticles. Paraffin sections of rat eyes 4 weeks after different treatments setting. (A) Treatment setting I: Etoposide (−Etop)-resistant WERI-Etop cells were injected into rat pups eyes together with ANP-HA-GNPs (ctr: $n = 10$, ANP-HA-GNPs: $n = 12$). Treatment setting II and III: WERI-Etop cells were allowed to form tumors prior to treatment with intravitreal injections of ANP-HA-GNPs (ctr: $n = 11$, ANP-HA-GNPs: $n = 12$; (B) or topical treatment via eye drops (ctr: $n = 12$, ANP-HA-GNPs: $n = 12$; (C). Intravitreal tumors with CRX (light red signal), Ki67 (brown signal) and luciferase (LUC, brown signal)) positive cells. ctr (upper rows): control eyes treated with PBS, HE: Hematoxylin and eosin stains (black boxes depict the zoom-in area shown in the adjacent columns), CRX: retinal and RB marker, Ki67: proliferation marker, LUC: luciferase expressing cells, Scale bars: 600 µm at 4× magnification and 300 µm at 10× magnification Ki67 positive (Ki67+), proliferating tumor cells were quantified using IMAGEJ. ctr: PBS treated (blue bars). ANP, atrial natriuretic peptide; ANP-HA-GNP, ANP coupled HA-GNPs (red bars); GNP, gold nanoparticles; HA, hyaluronic acid. Values represent means of independent animals ± SEM.

increased proliferation and tumor formation *in ovo* [39]. Therefore, new additional treatment approaches are needed to either prevent tumor growth from residual resistant RB cells developing upon chemotherapy or even treat resistant RB cells after recurrence. Nowadays, the development of new diagnostic and treatment approaches, also in the context of retinoblastoma, focusses on multifunctionalized nanocarriers (for review see Ref. [44]). These nanocarriers can be used to effectively transport drugs, peptides, or nucleic acids to tumor sites [45]. For RB, feasible ocular application routes comprise systemic, topical, periocular, intravitreal, and suprachoroidal approaches [46]. A

noninvasive topical administration via eye drops would be the most convenient and desirable treatment option for children. Up to now all nanocarrier systems including organic polymers and inorganic nanoparticles loaded with different drugs displayed an increased bioavailability and reduced side effects compared with application of coupled anticancer agents alone [44].

Inorganic gold nanoparticles (GNPs) have naturally antioxidant and antiangiogenic properties [8] and the potential to reduce proliferation and migration of retinal pigment epithelium (RPE) cells [9]. Besides, most recent studies demonstrated that GNPs can either be combined with ultrasonic hypothermia [47] or laser

therapy [48] to enhance RB cell death. Small sized GNPs are able to pass anatomical barriers of the eye [12], a property augmented by combining a gold core with a hyaluronic acid (HA) coat, allowing for binding to the CD44 surface receptor expressed by several cells of the eye [11,13,15]. We recently demonstrated an increased mobility and permeability of HA-GNPs through ocular barriers resulting in antiangiogenic effects via inhibition of neovascularization [11]. These previous data are in good accordance with effects seen in the study presented, in which HA-GNP treatment of etoposide-resistant cells reduced RB tumor growth in an *in ovo* CAM assay.

It has been demonstrated that the atrial natriuretic peptide (ANP) reduces choroidal neovascularization by inhibiting the vascular endothelial growth factor (VEGF) [19], shown to be expressed in RB and to correlate with increased malignancy [20]. Besides, combined treatment with glipizide and ANP not only inhibited angiogenesis but also effectively suppressed breast cancer growth and metastasis via the VEGFR signaling axis [22]. Against this background, we set out to attach ANP to HA-GNPs in order to create a nanocarrier combining two properties: a high ocular delivery rate due to a HA coat and antitumorigenic qualities due to attached ANP to effectively reduce RB tumor growth. In the study presented, we successfully coupled ANP to HA-GNPs and showed that these nanoparticles are internalized by ARPE-19 cells and display a homogenous distribution. In addition, an efficient diffusion of ANP-HA-GNPs into the vitreous humor of *ex vivo* retina explants was observed, and the nanoparticles were able to cross the inner limiting membrane and ganglion cell layer of the retina to reach the photoreceptors. Thus, the basic conditions for treatment applications were fulfilled. Next, testing antitumorigenic and antiangiogenic effects of the GNPs on etoposide-resistant RB cells *in ovo*, we revealed that the tumor-repressive effect of HA-GNPs treatment on RB tumor growth significantly increased upon coupling of ANP to the nanoparticles. Besides, it significantly affected vessel development. These results are in good accordance with previous studies showing that ANP induces various antitumor effects in different cancer entities (for review see Ref. [49]). Moreover, an ANP-derived peptide (KTH-22) inhibited pancreatic cancer cells more effectively than gemcitabine [50]. ANP mainly signals through two specific plasma membrane receptors, the natriuretic peptide receptor A (NPRA) and the natriuretic peptide receptor C (NPRC), and modulates expression and signaling of different molecules including the Ras-MEK1/2-ERK1/2 kinase cascade, the Wnt-β-catenin pathway, VEGF,

and JNK/JAK/STAT signaling, ultimately leading to anticancer effects [49,51].

Based on previous published work by Corson et al. [34], in the study presented, we established an orthotopic rat eye model system to test different RB treatment approaches in an ocular *in vivo* situation. In this model, we observed significantly increased tumor growth of etoposide-resistant WERI and RB355 cells *in vivo*, verifying our previous *in vitro* findings that etoposide-resistant RB cells behave more aggressively compared to their chemosensitive counterparts [39]. Besides, we investigated three different application routes for the ANP-HA-GNPs in order to find the most effective ocular drug delivery route to reduce RB tumor growth. As a proof of principle, we injected etoposide-resistant WERI cells together with ANP-HA-GNPs into newborn rat eyes and observed significantly decreased tumor growth 14 days after treatment. To investigate the properties of ANP-HA-GNPs in a more clinical setting, we treated already developed RB tumors in rat eyes via injection or topical administration of nanoparticles via eye drops. Topical administration reduced tumor growth of resistant RB cells, whereas the injection therapy approach did not change the tumor formation capacity compared with control cells. Thus, the effect of ANP-HA-GNP eye drops is promising, nevertheless, should be optimized by increased dose rates and/or more frequent administrations.

Next to intracellular effects on several signaling molecules described above, ANP has been shown to modulate inflammation, a hallmark of cancer known to promote tumor progression, metastasis and drug resistance [52,53]. Along this line, it could be demonstrated that lung cancer patients treated with ANPs had longer 2-year relapse-free survival time [54] and reduced inflammatory responses [55,56]. These effects are possibly trigged via the ANP-NPRA signaling axis [54], which also plays a role in tumor–stroma interactions [57], rendering it a potential therapy target in the context of inflammation-associated tumorigenesis [49]. Interestingly, previous studies also showed prophylactic effects on recurrence of lung cancer after ANP therapy [49] and protection from cisplatin induced renal dysfunction and renal tubular necrosis, a major toxicity after cisplatin therapy [58]. Thus, ANP is a highly attractive candidate for future cancer therapies as it mediates antiproliferative and anti-inflammatory effects and offers the potential to circumvent cytotoxic side effects of conventionally used chemotherapeutics such as cisplatin, also used in RB therapy.

Taken together, we established functionally active GNPs with a hyaluronic acid coat leading to increased ocular accessibility. Additional coupling of ANP to these effective nanocarriers reduced angiogenesis and

further increased the antitumorigenic effect on resistant RB cells *in vivo*. Therefore, ANP-HA-GNPs are a promising new adjuvant therapy option to treat RB tumors via non-invasive eye drops and/or for use as prophylactic agents to prevent recurrence upon the development of chemoresistance. Nevertheless, downstream signaling effectors of the ANP-HA-GNPs need to be investigated in more detail in future experiments.

5. Conclusion

In the study presented, we demonstrated that compared with parental chemosensitive tumor cells etoposide-resistant RB tumor cells exhibit a more aggressive growth behavior in an established *in vivo* orthotopic rat model. To treat these resistant cells, we established ANP-coupled, HA-coated gold nanoparticles, which displayed a good ocular biodistribution. *In ovo* CAM experiments demonstrated for the first time a RB tumor reducing effect of ANP-HA GNPs, which was confirmed in the *in vivo* orthotopic rat model. To identify an optimal application route for a potential future clinical RB therapy approach, ANP-HA GNPs were injected into RB tumor bearing rat eyes as well as administered by eye drops. The less invasive treatment method via eye drops seems to be the most effective administration strategy, however, this finding needs to be further evaluated. Overall, we demonstrated that the synthesized ANP-HA GNPs effectively reduce RB tumor growth *in ovo* and *in vivo* and administered as eye drops might potentially serve as a useful adjunct to standard RB therapy.

Acknowledgements

Conflict of interest

The authors declare no conflict of interest.

Author contributions

MAB and PSA conceptualized the study. AH, NM, SK, AD, DVM, AJ, AG, and PSA performed the methodology. AH, NM, SK, AD, PSA, and MAB involved in investigation. MAB, PSA, and ND curated the data. MAB, PSA, ND, and AH wrote the original draft preparation. MAB and ND reviewed, and edited the manuscript. MAB, PSA, AH, and NM visualized the data. MAB supervised the study. ND and AG involved in project administration. All authors have read and agreed to the published version of the manuscript.

Data accessibility

The data that support the findings of this study are available from the corresponding author (maike.busch@uk-essen.de) upon reasonable request.

References

1 Ting DSW, Cheung GCM, Wong TY. Diabetic retinopathy: global prevalence, major risk factors, screening practices and public health challenges: a review. *Clin Exp Ophthalmol*. 2016;**44**(4):260–77. https://doi.org/10.1111/ceo.12696

2 Netland PA. The Ahmed glaucoma valve in neovascular glaucoma (an AOS thesis). *Trans Am Ophthalmol Soc*. 2009;**107**:325–42.

3 Dimaras H, Kimani K, Dimba EAO, Gronsdahl P, White A, Chan HSL, et al. Retinoblastoma. *Lancet*. 2012;**379**(9824):1436–46. https://doi.org/10.1016/S0140-6736(11)61137-9

4 Kaewkhaw R, Rojanaporn D. Retinoblastoma: etiology, modeling, and treatment. *Cancer*. 2020;**12**(8):2304. https://doi.org/10.3390/cancers12082304

5 Munier FL, Beck-Popovic M, Chantada GL, Cobrinik D, Kivelä TT, Lohmann D, et al. Conservative management of retinoblastoma: challenging orthodoxy without compromising the state of metastatic grace. "Alive, with good vision and no comorbidity". *Prog Retin Eye Res*. 2019;**73**:100764. https://doi.org/10.1016/j.preteyeres.2019.05.005

6 Thangavel R, Bhaskaran S, Demirei H. Chemofailure and chemoresistance in retinoblastoma. *IP Int J Ocul Oncol Oculoplasty*. 2017;**3**(1):2–7. https://doi.org/10.18231/2455-8478

7 Temming P, Arendt M, Viehmann A, Eisele L, le Guin CH, Schündeln MM, et al. Incidence of second cancers after radiotherapy and systemic chemotherapy in heritable retinoblastoma survivors. A report from the German reference center. *Pediatr Blood Cancer*. 2017;**64**(1):71–80. https://doi.org/10.1002/pbc.26193

8 Barathmanikanth S, Kalishwaralal K, Sriram M, Pandian SRK, Youn H-S, Eom S, et al. Anti-oxidant effect of gold nanoparticles restrains hyperglycemic conditions in diabetic mice. *J Nanobiotechnol*. 2010;**8**:16. https://doi.org/10.1186/1477-3155-8-16

9 Karthikeyan B, Kalishwaralal K, Sheikpranbabu S, Deepak V, Haribalaganesh R, Gurunathan S. Gold nanoparticles downregulate VEGF-and IL-1β-induced cell proliferation through Src kinase in retinal pigment epithelial cells. *Exp Eye Res*. 2010;**91**(5):769–78. https://doi.org/10.1016/j.exer.2010.09.003

10 Gao J, Huang X, Liu H, Zan F, Ren J. Colloidal stability of gold nanoparticles modified with thiol compounds. Bioconjugation and application in cancer cell imaging. *Langmuir*. 2012;**28**(9):4464–71. https://doi.org/10.1021/la204289k

11 Apaolaza PS, Busch M, Asin-Prieto E, Peynshaert K, Rathod R, Remaut K, et al. Hyaluronic acid coating of gold nanoparticles for intraocular drug delivery: evaluation of the surface properties and effect on their distribution. *Exp Eye Res*. 2020;**198**:108151. https://doi.org/10.1016/j.exer.2020.108151

12 Kim JH, Kim JH, Kim K-W, Kim MH, Yu YS. Intravenously administered gold nanoparticles pass through the blood-retinal barrier depending on the particle size, and induce no retinal toxicity. *Nanotechnology*. 2009;**20**(50):505101. https://doi.org/10.1088/0957-4484/20/50/505101

13 Martens TF, Peynshaert K, Nascimento TL, Fattal E, Karlstetter M, Langmann T, et al. Effect of hyaluronic acid-binding to lipoplexes on intravitreal drug delivery for retinal gene therapy. *Eur J Pharm Sci*. 2017;**103**:27–35. https://doi.org/10.1016/j.ejps.2017.02.027

14 Kim JH, Moon MJ, Kim DY, Heo S, Jeong Y. Hyaluronic acid-based nanomaterials for cancer therapy. *Polymers*. 2018;**10**(10):1133. https://doi.org/10.3390/polym10101133

15 Apaolaza PS, Delgado D, del Pozo-Rodríguez A, Gascón AR, Solinís MÁ. A novel gene therapy vector based on hyaluronic acid and solid lipid nanoparticles for ocular diseases. *Int J Pharm*. 2014;**465**(1–2):413–26. https://doi.org/10.1016/j.ijpharm.2014.02.038

16 Xu Q, Boylan NJ, Suk JS, Wang YY, Nance EA, Yang JC, et al. Nanoparticle diffusion in, and microrheology of, the bovine vitreous ex vivo. *J Control Release*. 2013;**167**(1):76–84. https://doi.org/10.1016/j.jconrel.2013.01.018

17 Laradji A, Karakocak BB, Kolesnikov AV, Kefalov VJ, Ravi N. Hyaluronic acid-based gold nanoparticles for the topical delivery of therapeutics to the retina and the retinal pigment epithelium. *Polymers*. 2021;**13**(19):3324. https://doi.org/10.3390/polym13193324

18 Hansen LH, Madsen TD, Goth CK, Clausen H, Chen Y, Dzoyashvili N, et al. Correction: discovery of O-glycans on atrial natriuretic peptide (ANP) that affect both its proteolytic degradation and potency at its cognate receptor. *J Biol Chem*. 2019;**294**(48):18516. https://doi.org/10.1074/jbc.AAC119.011661

19 Lara-Castillo N, Zandi S, Nakao S, Ito Y, Noda K, She H, et al. Atrial natriuretic peptide reduces vascular leakage and choroidal neovascularization. *Am J Pathol*. 2009;**175**(6):2343–50. https://doi.org/10.2353/ajpath.2009.090439

20 Zhu J, Zhang X, Ai L, Yuan R, Ye J. Clinicohistopathological implications of MMP/VEGF expression in retinoblastoma: a combined meta-analysis and bioinformatics analysis. *J Transl Med*. 2019;**17**(1):226. https://doi.org/10.1186/s12967-019-1975-3

21 Špiranec Spes K, Hupp S, Werner F, Koch F, Völker K, Krebes L, et al. Natriuretic peptides attenuate retinal pathological neovascularization via cyclic guanosine monophosphate signaling in pericytes and astrocytes. *Arterioscler Thromb Vasc Biol*. 2020;**40**(1):159–74. https://doi.org/10.1161/ATVBAHA.119.313400

22 Mao G, Zheng S, Li J, Liu X, Zhou Q, Cao J, et al. Glipizide combined with ANP suppresses breast cancer growth and metastasis by inhibiting angiogenesis through VEGF/VEGFR2 signaling. *Anticancer Agents Med Chem*. 2022;**22**(9):1735–41. https://doi.org/10.2174/1871520621666210910085733

23 Oliveira AV, Marcelo A, da Costa AMR, Silva GA. Evaluation of cystamine-modified hyaluronic acid/chitosan polyplex as retinal gene vector. *Mater Sci Eng C Mater Biol Appl*. 2016;**58**:264–72. https://doi.org/10.1016/j.msec.2015.08.047

24 Turkevich J, Stevenson PC, Hillier J. A study of the nucleation and growth processes in the synthesis of colloidal gold. *Discuss Faraday Soc*. 1951;**11**:55. https://doi.org/10.1039/df9511100055

25 Cho EC, Zhang Q, Xia Y. The effect of sedimentation and diffusion on cellular uptake of gold nanoparticles. *Nat Nanotechnol*. 2011;**6**(6):385–91. https://doi.org/10.1038/nnano.2011.58

26 Braunger BM, Leimbeck SV, Schlecht A, Volz C, Jägle H, Tamm ER. Deletion of ocular transforming growth factor β signaling mimics essential characteristics of diabetic retinopathy. *Am J Pathol*. 2015;**185**(6):1749–68. https://doi.org/10.1016/j.ajpath.2015.02.007

27 Seitz R, Hackl S, Seibuchner T, Tamm ER, Ohlmann A. Norrin mediates neuroprotective effects on retinal ganglion cells via activation of the Wnt/beta-catenin signaling pathway and the induction of neuroprotective growth factors in Muller cells. *J Neurosci*. 2010;**30**(17):5998–6010. https://doi.org/10.1523/JNEUROSCI.0730-10.2010

28 Reid TW, Albert DM, Rabson AS, Russell P, Craft J, Chu EW, et al. Characteristics of an established cell line of retinoblastoma. *J Nat Cancer Inst*. 1974;**53**(2):347–60.

29 McFall RC, Sery TW, Makadon M. Characterization of a new continuous cell line derived from a human retinoblastoma. *Cancer Res*. 1977;**37**(4):1003–10.

30 Griegel S, Hong C, Frötschl R, Hülser DF, Greger V, Horsthemke B, et al. Newly established human retinoblastoma cell lines exhibit an "immortalized" but not an invasive phenotype in vitro. *Int J Cancer*. 1990;**46**(1):125–32. https://doi.org/10.1002/ijc.2910460123

31 Busch M, Grosse-Kreul J, Wirtz JJ, Beier M, Stephan H, Royer-Pokora B, et al. Reduction of the tumorigenic potential of human retinoblastoma cell lines by TFF1 overexpression involves p53/caspase signaling and miR-18a regulation. *Int J Cancer*. 2017;**141**:549–60. https://doi.org/10.1002/ijc.30768

32 Peynshaert K, Devoldere J, Forster V, Picaud S, Vanhove C, de Smedt SC, et al. Toward smart design of retinal drug carriers: a novel bovine retinal explant model to study the barrier role of the vitreoretinal interface. *Drug Deliv*. 2017;**24**(1):1384–94. https://doi.org/10.1080/10717544.2017.1375578

33 Hartmann L, Neveling K, Borkens S, Schneider H, Freund M, Grassman E, et al. Correct mRNA processing at a mutant TT splice donor in FANCC ameliorates the clinical phenotype in patients and is enhanced by delivery of suppressor U1 snRNAs. *Am J Hum Genet*. 2010;**87**:480–93. https://doi.org/10.1016/j.ajhg.2010.08.016

34 Corson TW, Samuels BC, Wenzel AA, Geary AJ, Riley AA, McCarthy BP, et al. Multimodality imaging methods for assessing retinoblastoma orthotopic xenograft growth and development. *PLoS One*. 2014;**9**:e99036.

35 Zijlstra A, Mellor R, Panzarella G, Aimes RT, Hooper JD, Marchenko ND, et al. A quantitative analysis of rate-limiting steps in the metastatic cascade using human-specific real-time polymerase chain reaction. *Cancer Res*. 2002;**62**(23):7083–92.

36 Palmer TD, Lewis J, Zijlstra A. Quantitative analysis of cancer metastasis using an avian embryo model. *J Vis Exp*. 2011;**51**:2815. https://doi.org/10.3791/2815

37 Busch M, Philippeit C, Weise A, Dünker N. Re-characterization of established human retinoblastoma cell lines. *Histochem Cell Biol*. 2015;**143**(3):325–38. https://doi.org/10.1007/s00418-014-1285-z

38 Busch M, Klein S, Große-Kreul J, Scheiner O, Metz K, Stephan H, et al. p53, miR-34a and EMP1-newly identified targets of TFF3 signaling in Y79 retinoblastoma cells. *Int J Mol Sci*. 2019;**20**(17):4129. https://doi.org/10.3390/ijms20174129

39 Busch M, Papior D, Stephan H, Dünker N. Characterization of etoposide- and cisplatin-chemoresistant retinoblastoma cell lines. *Oncol Rep*. 2018;**39**(1):160–72. https://doi.org/10.3892/or.2017.6100

40 Schindelin J, Rueden CT, Hiner MC, Eliceiri KW. The ImageJ ecosystem: an open platform for biomedical image analysis. *Mol Reprod Dev*. 2015;**82**(7–8):518–29. https://doi.org/10.1002/mrd.22489

41 Liu J, Ottaviani D, Sefta M, Desbrousses C, Chapeaublanc E, Aschero R, et al. A high-risk retinoblastoma subtype with stemness features, dedifferentiated cone states and neuronal/ganglion cell gene expression. *Nat Commun*. 2021;**12**(1):5578. https://doi.org/10.1038/s41467-021-25792-0

42 Munier FL, Gaillard M-C, Balmer A, Beck-Popovic M. Intravitreal chemotherapy for vitreous seeding in retinoblastoma: recent advances and perspectives. *Saudi J Ophthalmol*. 2013;**27**(3):147–50. https://doi.org/10.1016/j.sjopt.2013.06.003

43 Roy SR, Kaliki S. Retinoblastoma: a major review. *Mymensingh Med J*. 2021;**30**(3):881–95.

44 Russo E, Spallarossa A, Tasso B, Villa C, Brullo C. Nanotechnology for pediatric retinoblastoma therapy. *Pharmaceuticals*. 2022;**15**(9):1087. https://doi.org/10.3390/ph15091087

45 Zahin N, Anwar R, Tewari D, Kabir MT, Sajid A, Mathew B, et al. Nanoparticles and its biomedical applications in health and diseases: special focus on drug delivery. *Environ Sci Pollut Res Int*. 2020;**27**(16):19151–68. https://doi.org/10.1007/s11356-019-05211-0

46 Arshad R, Barani M, Rahdar A, Sargazi S, Cucchiarini M, Pandey S, et al. Multi-functionalized nanomaterials and nanoparticles for diagnosis and treatment of retinoblastoma. *Biosensors*. 2021;**11**(4):97. https://doi.org/10.3390/bios11040097

47 Moradi S, Mokhtari-Dizaji M, Ghassemi F, Sheibani S, Amoli FA. The effect of ultrasound hyperthermia with gold nanoparticles on retinoblastoma Y79 cells. *Gold Bull*. 2020;**53**(2):111–20. https://doi.org/10.1007/s13404-020-00279-w

48 Darviot C, Hardy P, Meunier M. Laser-induced plasmon-mediated treatment of retinoblastoma in viscous vitreous phantom. *J Biophotonics*. 2019;**12**(11):e201900193. https://doi.org/10.1002/jbio.201900193

49 Fu H, Zhang J, Cai Q, He Y, Yang D. Pleiotropic roles of atrial natriuretic peptide in anti-inflammation and anti-cancer activity. *Cancer*. 2022;**14**(16):3981. https://doi.org/10.3390/cancers14163981

50 Kozlowski MR, Kozlowski RE. A novel, small peptide with activity against human pancreatic cancer. *Am J Cancer Res*. 2020;**10**(5):1356–65.

51 Zhang X, Wang Q, Jia C, Li D, Lv Z, Yang J. Role of atrial natriuretic peptide receptor in inhibition of laterally spreading tumors via Wnt/β-catenin signaling. *Arch Med Sci Atheroscler Dis*. 2022;**7**:e104–8. https://doi.org/10.5114/amsad/151928

52 Hanahan D, Weinberg RA. Hallmarks of cancer: the next generation. *Cell*. 2011;**144**(5):646–74. https://doi.org/10.1016/j.cell.2011.02.013

53 Grivennikov SI, Greten FR, Karin M. Immunity, inflammation, and cancer. *Cell*. 2010;**140**(6):883–99. https://doi.org/10.1016/j.cell.2010.01.025

54 Nojiri T, Arai M, Suzuki Y, Kumazoe M, Tokudome T, Miura K, et al. Retraction: transcriptome analysis reveals a role for the endothelial ANP-GC-A signaling in interfering with pre-metastatic niche formation by solid cancers. *Oncotarget*. 2022;**13**:551–2. https://doi.org/10.18632/oncotarget.28223

55 Nojiri T, Inoue M, Yamamoto K, Maeda H, Takeuchi Y, Funakoshi Y, et al. Effects of low-dose human atrial natriuretic peptide for preventing post-operative cardiopulmonary complications in elderly patients undergoing pulmonary resection for lung cancer. *Eur J Cardiothorac Surg*. 2012;**41**(6):1330–4. https://doi.org/10.1093/ejcts/ezr202

56 Nojiri T, Yamamoto K, Maeda H, Takeuchi Y, Funakoshi Y, Inoue M, et al. Effect of low-dose human atrial natriuretic peptide on postoperative atrial fibrillation in patients undergoing pulmonary resection for lung cancer: a double-blind, placebo-controlled study. *J Thorac Cardiovasc Surg*. 2012;**143**(2):488–94. https://doi.org/10.1016/j.jtcvs.2011.09.003

57 Mallela J, Ravi S, Jean Louis F, Mulaney B, Cheung M, Sree Garapati U, et al. Natriuretic peptide receptor A signaling regulates stem cell recruitment and angiogenesis: a model to study linkage between inflammation and tumorigenesis. *Stem Cells*. 2013;**31**(7):1321–9. https://doi.org/10.1002/stem.1376

58 Nojiri T, Hosoda H, Kimura T, Miura K, Ishikane S, Tokudome T, et al. Atrial natriuretic peptide protects against cisplatin-induced acute kidney injury. *Cancer Chemother Pharmacol*. 2015;**75**(1):123–9. https://doi.org/10.1007/s00280-014-2624-4

Supporting information

Additional supporting information may be found online in the Supporting Information section at the end of the article.

Fig. S1. Transmission electron microscopy (TEM) of a retinoblastoma (RB) cell after gold nanoparticle uptake.

Discussion

TFF1 as a new subtype II RB biomarker

The results of this project were incorporated into two publications in Cancers:

1. TFF1 in Aqueous Humor - A Potential New Biomarker for Retinoblastoma by M. Busch, **A. Haase**, N. Miroschnikov, A. Doege, E. Biewald, N. Bechrakis, M. Beier, D. Kanber, D. Lohmann, K. Metz and N. Dünker
2. Trefoil Family Factor Peptide 1 - A New Biomarker in Liquid Biopsies of Retinoblastoma under Therapy by M. Busch, **A. Haase**, E. Alefeld, E. Biewald, L. Jabbarli and N. Dünker.

Aqueous humor (AH) paracentesis offers new opportunities for the management of ocular tumor entities such as RB, since it provides access to biomarkers before and during therapy that may correlate with tumor characteristics and have diagnostic and prognostic value. We were able to demonstrate that liquid biopsy of AH allows the identification of tumor biomarkers in the eye without the need for an intraocular biopsy or even enucleation. AH paracentesis is part of the routine protocol for IVC treatment of RB patients, and the risk of extraocular spread is considered extremely low (Munier *et al.*, 2013, Smith and Smith, 2013, Ghassemi *et al.*, 2014, Lawson *et al.*, 2014, Smith *et al.*, 2014, Francis *et al.*, 2017).

TFF1 is the most upregulated gene in the more advanced and metastasis-associated subtype II RB (Busch *et al.*, 2018, Liu *et al.*, 2021). TFF1 has also been described as a functional biomarker in several other tumor entities (Gonzaga *et al.*, 2017, Schulten *et al.*, 2017, Shimura *et al.*, 2020, Yi *et al.*, 2020). Moreover, TFF1 has also been identified as an liquid biopsy (LB) biomarker in a study of breast cancer patients, where high TFF1 levels correlated with increased metastatic activity in blood samples (Elnagdy *et al.*, 2018).

Here, we examined the AH of RB patients to discover whether TFF1 is also detectable in the AH. Initially, we demonstrated that TFF1 levels can be detected in the AH of RB subtype II patients using TFF1 ELISA in a cohort of enucleated RB eyes. Immunohistochemical staining of the corresponding tumors revealed that all TFF1-positive AH samples originated from tumors expressing TFF1. However, some RB tumors expressed TFF1 without secreting it into the AH, suggesting that not all TFF1-expressing tumors can be identified by examining AH. This may be because there are fewer TFF1-secreting cells within the tumor, resulting in TFF1 levels in AH below the

detection limit. This is consistent with the fact that we identified both TFF1-positive and TFF1-negative areas in the immunohistochemical staining of group II RB tumors.

We also investigated whether TFF1 is expressed and secreted by tumor or stromal cells. For this purpose, we used primary RB tumors from enucleated eyes to establish a primary cell culture of RB tumor cells and RB tumor-associated stromal cells. Our analyses showed that only RB tumor cells expressed and secreted TFF1; RB-derived stromal cells did not express and secrete TFF1. Thus, we provide evidence for the specificity of TFF1 as a biomarker for RB tumor cells (Busch *et al.*, 2022, 2023).

In a cohort of three patients with subtype II RB, two patients exhibited a decline in TFF1 levels in the AH below the detection limit following successful melphalan-IVC therapy. The third patient did not show a persistent response to melphalan-IVC therapy and quickly developed a relapse, which was consistent with a constant TFF1 level in the AH (Busch *et al.*, 2023). New and unpublished data from a fourth RB subtype II patient confirm that TFF1 levels in AH decrease during treatment if therapy is successful. In this case, we were even able to detect the differences in TFF1 levels by Western blotting, which has a lower sensitivity than ELISA.

A possible explanation for the decrease in TFF1 concentrations during successful therapy is the death of tumor cells. Thus, our method enables the detection of TFF1-secreting tumor cells that have survived therapy, thereby conferring important feedback on therapeutic strategies with high prognostic value.

Furthermore, we were able to show that an ELISA assay is a reliable method for TFF1 diagnostics of AH, since it is very sensitive (lower limit of TFF1 level <10 pg/mL), and the amount routinely collected by AH paracentesis is sufficient for diagnostics. In addition, the TFF1 ELISA is fast, inexpensive, easy to perform, and does not require complex equipment. This makes TFF1 a practical diagnostic and prognostic tool not only in high-income countries.

GIPR overexpression decreases tumorigenic potential in RB cells

The results of this project were published in Cancers:

Gastric Inhibitory Polypeptide Receptor (GIPR) Overexpression Reduces the Tumorigenic Potential of Retinoblastoma Cells by **A. Haase**, E. Alefeld, F. Yalinci, D. Van Meenen, M. Busch and N. Dünker.

TFF1 has an ambiguous role in RB although it has been described as a marker for a more aggressive and metastatic RB subtype and as a tumor suppressor. TFF1 overexpression leads to antitumor effects in human RB cells (Busch *et al.*, 2017), and gene expression analyses showed that GIPR is one of the most strongly upregulated genes upon TFF1 overexpression. Therefore, one can hypothesize that TFF1 and GIPR overlap in their signaling cascade or possibly have a ligand/receptor relationship. However, this ambiguous role of TFF1 is not necessarily contradictory, since different mechanisms may upregulate a tumor suppressor in advanced tumors.

TFF1 has been described as a reactive oxygen species (ROS) scavenger in various tissues and its expression levels are favored by inflammatory processes (reviewed in: Hoffmann, 2021). A possible cellular stress response to hypoxia in the tumor, which is associated with increased levels of ROS, could be an explanation. The increased expression of TFF1 could be a compensatory response of the tumor cells to eliminate high levels of ROS. Another explanation could be activation of the immune system by inflammatory reactions during tumor progression, since ectopic expression of TFF1 was described in chronic inflammatory processes (reviewed in: Hoffmann, 2021). In addition, genetic mutations could explain the described discrepancy, since evidence already exists for a correlation between cancer progression and mutations/polymorphisms in the TFF1 gene (Park *et al.*, 2000, Yio *et al.*, 2006, Huang *et al.*, 2013, Wang *et al.*, 2018, Shekarriz *et al.*, 2022). Epigenetic alterations could also be a possible explanation for the ambiguity described above, since our research group has previously shown that TFFs are epigenetically regulated in RB cells (Philippeit *et al.*, 2014).

To better understand the role of TFF1 in RB, we investigated the role of GIPR, which as mentioned above is also upregulated after TFF1 overexpression in RB cells. As with TFF1, increased GIPR expression levels were associated with different non-RB tumor entities and higher TNM stages (Costa *et al.*, 2009, Waser *et al.*, 2012, Sherman *et al.*, 2014, Karpathakis *et al.*, 2016, Reubi *et al.*, 2020). We observed a correlation between GIPR and TFF1 expression in primary RB tumor-derived cells and RB tumors. TFF1 positive primary RB tumor-derived cells and RB tumors showed significantly increased GIPR expression compared to TFF1 negatives (Haase *et al.*, 2024 A).

To study the GIPR axis in more detail, we overexpressed GIPR in Weri and Y79 RB cell lines and performed functional *in vitro* and *in ovo* CAM assays. Lentiviral-induced

GIPR overexpression resulted in significantly decreased cell viability, cell growth and proliferation, and significantly increased caspase-3-dependent cell death. We could show that addition of MK0893 inhibitor reversed highly specifically GIPR-induced effects on cell viability, proliferation and cell death.

In the CAM assay, tumors were significantly smaller and significantly reduced in weight. These effects are similar to those observed after TFF1 overexpression.

In addition, we investigated the regulation of GIPR in RB cells. Studies by He *et al.* described GIPR as a potential target gene of miR-542-5p (He *et al.*, 2017). We now provide the first experimental evidence for regulation of GIPR by miR-542-5p by showing reciprocal expression of miR-542-5p and GIPR in RB cells, as well as binding of miR-542-5p to the potential miR-binding site in the 3'UTR of the GIPR gene. However, we could not find a direct link between TFF1 and miR-542-5p regulation.

Our working hypothesis that GIPR is a potential receptor for TFF1 was not confirmed by our experiments. Nevertheless, many of the facts discussed above suggest that parts of the GIPR and TFF1 signaling cascades overlap and influence each other. This is evidenced by the fact that p53, a known tumor suppressor, is upregulated after both TFF1 and GIPR overexpression (Busch *et al.*, 2017, Haase *et al.*, 2024 A).

Optimized CXCR4 inhibitors reduce tumorigenic potential of RB cells

The results of this project were submitted to Journal of Controlled Release:

Fatty acid conjugated EPI-X4 derivatives with increased activity and *in vivo* stability by M. Harms, **A. Haase**, A. Rodriguez-Alfonso, J. Löffler, Y. Almeida-Hernández, Y. Ruiz-Blanco, D. Albers, A. Gilg, F. von Bank, F. Zech, M. Datta, J. Jaikishan, B. Draphoen, M. Habib, L. Ständker, S. Wiese, M. Lindén, G. Winter, V. Rasche, A. Beer, H. Jumaa, A. Abadi, F. Kirchhoff, M. Busch, N. Dünker, E. Sanchez-Garcia and J. Münch.

Inhibition of the CXCR4 receptor has been discussed as a potential therapeutic target in inflammatory diseases and cancer. However, existing CXCR4 inhibitor candidates are subject to rapid degradation and maximized renal excretion (Harms *et al.*, 2023). To circumvent this problem, we used lipidated EPI-X4 derivatives with long chain fatty acids, which allows interaction with human serum albumins, thereby increasing stability and providing enhanced antagonist activity. We were able to demonstrate that the lipidated EPI-X4 derivative JM#198 reduces cell viability and proliferation of RB cells

while increasing cell death. *In ovo* studies revealed that the lipidated JM#198 had a stronger effect on RB cell tumor growth than the unmodified JM#21 or the established CXCR4 Inhibitor AMD3100. RB cells treated with JM#198 formed significantly smaller and lighter tumors than the control groups. In addition, tumor formation capacity was significantly reduced, suggesting an important role for CXCR4 in RB.

CXCR4 has been shown to be a target of the tumor suppressor RB1. Studies by Tang *et al.* have demonstrated that RB1 inhibits the CXCL12/CXCR4 signaling pathway, suggesting the existence of a mechanistic axis that could also regulate expression of CXCR4 directly through RB1 (Tang *et al.*, 2021). Since the RB1 gene is frequently mutated and defective in RB tumor cells, it is possible that the mutated protein is unable to influence CXCR4 inhibition or regulation. This could explain the strong expression and activity of CXCR4 in RB tumors. Further research is necessary to elucidate the exact mechanism.

CXCR4 is also very interesting in the context of RB because it is one of the few described receptors for TFF2 (reviewed in: Hoffmann, 2009), which belongs to the same protein family as TFF1, the new biomarker described here for subtype II RB. To clarify whether CXCR4 could also be a receptor for TFF1, we performed ß-arrestin assays (data not included in the publication). No TFF1-induced intracellular effect was found, indicating no receptor-ligand relationship. Since the specific relationship between TFFs and CXCR4 remains unclear, further investigations should be carried out to gain a deeper understanding of the signaling pathways.

Targeted gold nanoparticles tackle resistant RB cells

The results of this project were published in Molecular Oncology:

New retinoblastoma (RB) drug delivery approaches: anti-tumor effect of atrial natriuretic peptide (ANP)-conjugated hyaluronic-acid-coated gold nanoparticles for intraocular treatment of chemoresistant RB by **A. Haase**, N. Miroschnikov, S. Klein, A. Doege, N. Dünker, D. Van Meenen, A. Junker, A. Göpferich, P.S. Apaolaza, M. Busch.

New therapeutic approaches are needed to provide an alternative to chemotherapy or to treat resistant RB cells after relapse (reviewed in: Bromma and Chithrani, 2020). The development of new multifunctional nanocarriers such as GNPs, which can be used as drug carriers, has become a major focus in recent years (reviewed in: Arshad

et al., 2021, Russo *et al.*, 2022; Zahin *et al.*, 2020). We functionalized GNPs with (i) HA, allowing improved and more targeted delivery to CD44 receptor-expressing, retinal cells (Apaolaza *et al.*, 2014, 2020, Martens *et al.*, 2017), and (ii) ANP, which was previously described to reduce ocular neovascularization (Lara-Castillo *et al.*, 2009).

We showed that the administration of ANP-HA-GNPs in the *in ovo* CAM model reduced tumor size, weight and tumor formation capacity of aggressive etoposide-resistant RB cells (Busch *et al.*, 2018, Haase *et al.*, 2024 B). In addition, the total area, total length, mean thickness and number of branching points of blood vessels nurturing the CAM tumor formed from the grafted RB cells were all significantly reduced.

We used an orthotopic rat eye model system that allows *in vitro* visualization of the growing RB tumor. We tested three different application routes for the ANP-HA-GNPs in order to find an effective ocular administration route. Administration of ANP-HA-GNPs significantly reduced tumor growth *in vivo* in this setup. Interestingly, topical administration via eye drops, which could be a clinically highly interesting treatment method, also showed reduced tumor growth of resistant RB cells. In the long term, such an application method using eye drops would enable simple, minimally invasive treatment that could be applied by non-medical personnel.

These *in vivo* effects are probably mainly due to reduced angiogenesis under ANP-HA-GNP treatment conditions. This results in a reduced blood supply to the tumor and the onset of hypoxia could reduce tumor growth (reviewed in: Harris, 2002, Pouysségur *et al.*, 2006). Neoangiogenesis is a fundamental biological process necessary for tumor growth, and by inhibiting this process, tumor progression can be effectively inhibited (reviewed in: Ferrara and Kerbel, 2005, Jain, 2005). GNPs are already used in cancer therapy and show an intrinsic inhibition of neoangiogenesis, this effect could be further enhanced by functionalizing with ANP and thus also enable the therapy of other tumor entities (reviewed in: Şen *et al.*, 2021, Ali *et al.*, 2022).

However, it should be noted that both pathologic and non-pathologic neoangiogenesis is impaired by ANP-HA-GNPs. Therefore, the limitations of this treatment restrict it to organs that do not require efficient neoangiogenesis (e.g. the eye).

Conclusions and outlook

We showed that TFF1 is detectable in AH of RB patients and is therefore a candidate biomarker for advanced subtype II RB. Moreover, detecting the presence of TFF1 in the AH of patients with RB symptoms excludes diseases such as Coats disease. Thus, a simple AH examination could facilitate the diagnosis of RB.

It should also be investigated whether the precursor of RB, retinoma, expresses TFF1 and whether TFF1 could be used as a retinoma/retinoblastoma demarcation marker. In addition, we have shown that the levels of TFF1 reflect the treatment success. This opens new possibilities for the management of RB patients, since information on the subtype status of RB can be obtained prior to enucleation. This would make it possible to optimize the treatment according to the RB subtype from the very beginning.

Although the approaches are very promising, the quantity of data concerning TFF1-AH-LB should be further expanded. Despite the connection to the RB Center in Essen, where RB patients from all over Europe are treated, we were only able to monitor the AH of seven RB patients during IVC treatment. Therefore, large-scale, multi-center and possibly worldwide studies are needed to improve the data obtained for this rare tumor. In the long term, it would be desirable to include AH paracentesis with subsequent TFF1 testing in standard RB diagnostic protocols, as well as in monitoring treatment responses via TFF1 ELISA to improve early detection of residual tumor cells at follow-up. Already today, all enucleated eyes of RB patients are analyzed for TFF1 expression by immunohistochemical stainings at the reference pathology department of University Hospital Essen.

GIPR appears to play a similarly diverse role as TFF1 in RB. While GIPR *in vitro* and *in vivo* experiments suggest a tumor suppressor role, GIPR expression is detectable in predominantly TFF1-positive tumors and thus advanced subtype II tumors. We were able to demonstrate a correlation between TFF1 and GIPR in RB, but we were not able to find the exact mechanism that regulates TFF1 and GIPR expression, or other overlaps in their signaling cascade. Furthermore, our studies showed that GIPR does not appear to be a potential receptor for TFF1. However, overexpression of TFF1 or GIPR shows the same effects in functional experiments in RB cells, suggesting that there must be an overlap in the downstream signaling cascades. Further research in this area may shed light on the exact relationship between GIPR and TFF1. To confirm

the tumor suppressor role GIPR in RB, GIPR knockout studies could be performed to see if GIPR$^{(-/-)}$ cells gain a survival advantage. This could potentially reveal further overlap in TFF1 and GIPR signaling and finally provide an explanation for the diverse roles of TFF1 and GIPR.

We also demonstrated for the first time the regulation of GIPR expression by miR-542-5p. Since GIPR and TFF1 are both overexpressed in the same tumors, it would be interesting to further investigate the role of miR-542-5p as a potential therapeutic target. To this end, overexpression and knockout studies of miR-542-5p could be performed to investigate their influence on RB cell viability, proliferation and apoptosis.

The new and optimized CXCR4 inhibitor #JM198 showed improved antagonistic activity and stability in *in vitro* and *in vivo* experiments with RB cells. Thus, CXCR4 inhibition is a potentially therapeutically important treatment option and should be further explored. The CXCR4 inhibitors already approved for human use were less effective at inhibiting CXCR4 than the optimized CXCR4 inhibitors in our experiments. Since bringing improved CXCR4 inhibitors into clinical use may provide better treatment for patients, it would make sense to pursue human use in the long term. However, this would require many more *in vivo* studies with JM#198, and for a first step our newly established orthotopic rat eye model seems to be a good and feasible option. It may also be possible to consider non-invasive therapeutic applications for treatment with CXCR4 inhibitors. Hyaluronic acid-coated GNPs could be functionalized with the new optimized JM#198, which would allow the CXCR4 inhibitor to easily cross the ocular barrier and treatment could be administered by eye drops.

In addition, further investigation of CXCR4 inhibition in chemotherapy-resistant RB cells would be of interest, since our own analyses have shown that some etoposide-resistant RB cells exhibit increased CXCR4 expression (unpublished data). In the long term, CXCR4 inhibitors could be administered in combination with chemotherapy, or represent an important additional treatment option for tumors that are already resistant.

ANP-HA-GNPs reduced tumor size, weight and tumor formation capacity in various *in vivo* models and significantly reduced neoangiogenesis in *in ovo* experiments. Strongly reduced RB tumor growth was also shown in our newly established rat eye model. Topical administration of functionalized GNPs is an interesting method as it would be

very easy to implement for clinical applications. Since this method of application is non-invasive, significantly fewer risks and side effects are to be expected.

Initially, the positive approaches should be confirmed by further animal studies. The frequency of topical application should be maximized (e.g. daily instead of 2 times a week) which could potentially improve the efficacy of the treatment.

In addition, GNPs could be functionalized with other substances to further improve and individualize treatment options. For instance, GNPs could be functionalized with rTFF1, which has been shown to decreases cell viability and proliferation (Weise and Dünker, 2013).

GNPs could also be used as potential radiosensitizers in radiation therapy such as proton beam therapy (PBT; Senavirathna *et al.*, 2013, Peukert *et al.*, 2020). HA functionalized GNPs would provide precise targeting of CD44 expressing cells, and indeed RB tumors strongly express CD44 (Soebagjo *et al.*, 2019). Such GNPs could make a therapy even more effective or help achieve the same effects with lower doses. For instance, cell culture studies have shown that PBT therapy with the addition of GNPs increases cell death by up to 44% compared to the control group (Cunningham *et al.*, 2021). In addition, recent studies by Lo *et al.* showed that GNP-treated tumor cells exhibited increased ROS levels after PBT therapy, where the cytoskeleton and mitochondria were more severely damaged than in the control group that received proton irradiation only (Lo *et al.*, 2023).

In conclusion, this study used a multifaceted approach to discover new biomarkers, unravel potential molecular mechanisms, and identify potential targets to pave the way towards targeted therapies with alternative application routes using a new animal model. Together these could facilitate early, accurate and fast diagnosis, monitoring of tumor progression, as well as providing prognostic value, to improve the treatment of RB in both high- and low-income countries.

References

Abramson, D. H., Ji, X., Francis, J. H., Catalanotti, F., Brodie, S. E., Habib, L., 2019. Intravitreal chemotherapy in retinoblastoma: expanded use beyond intravitreal seeds, *British Journal of Ophthalmology*, BMJ Publishing Group Ltd, 103, 4, 488–493. doi: 10.1136/bjophthalmol-2018-312037.

Aerts, I., Lumbroso-Le Rouic, L., Gauthier-Villars, M., Brisse, H., Doz, F., Desjardins, L., 2006. Retinoblastoma, *Orphanet Journal of Rare Diseases*, 1, 1, 31. doi: 10.1186/1750-1172-1-31.

Ali, A. A., Abuwatfa, W. H., Al-Sayah, M. H., Husseini, G. A., 2022. Gold-Nanoparticle Hybrid Nanostructures for Multimodal Cancer Therapy, *Nanomaterials*, Multidisciplinary Digital Publishing Institute, 12, 20, 3706. doi: 10.3390/nano12203706.

Amiry, N., Kong, X., Muniraj, N., Kannan, N., Grandison, P. M., Lin, J., Yang, Y., Vouyovitch, C. M., Borges, S., Perry, J. K., Mertani, H. C., Zhu, T., Liu, D., Lobie, P. E., 2009. Trefoil Factor-1 (TFF1) Enhances Oncogenicity of Mammary Carcinoma Cells, *Endocrinology*, 150, 10, 4473–4483. doi: 10.1210/en.2009-0066.

Ancona-Lezama, D., Dalvin, L. A., Shields, C. L., 2020. Modern treatment of retinoblastoma: A 2020 review, *Indian Journal of Ophthalmology*, 68, 11, 2356. doi: 10.4103/ijo.IJO_721_20.

Apaolaza, P. S., Busch, M., Asin-Prieto, E., Peynshaert, K., Rathod, R., Remaut, K., Dünker, N., Göpferich, A., 2020. Hyaluronic acid coating of gold nanoparticles for intraocular drug delivery: Evaluation of the surface properties and effect on their distribution, *Experimental Eye Research*, 198, 108151. doi: 10.1016/j.exer.2020.108151.

Apaolaza, P. S., Delgado, D., Pozo-Rodríguez, A. del, Gascón, A. R., Solinís, M. Á., 2014. A novel gene therapy vector based on hyaluronic acid and solid lipid nanoparticles for ocular diseases, *International Journal of Pharmaceutics*, 465, 1, 413–426. doi: 10.1016/j.ijpharm.2014.02.038.

Arshad, R., Barani, M., Rahdar, A., Sargazi, S., Cucchiarini, M., Pandey, S., Kang, M., 2021. Multi-Functionalized Nanomaterials and Nanoparticles for Diagnosis and Treatment of Retinoblastoma, *Biosensors*, Multidisciplinary Digital Publishing Institute, 11, 4, 97. doi: 10.3390/bios11040097.

Bai, X., Wang, Y., Song, Z., Feng, Y., Chen, Y., Zhang, D., Feng, L., 2020. The Basic Properties of Gold Nanoparticles and their Applications in Tumor Diagnosis and Treatment, *International Journal of Molecular Sciences*, Multidisciplinary Digital Publishing Institute, 21, 7, 2480. doi: 10.3390/ijms21072480.

BarathManiKanth, S., Kalishwaralal, K., Sriram, M., Pandian, S. R. K., Youn, H., Eom, S., Gurunathan, S., 2010. Anti-oxidant effect of gold nanoparticles restrains hyperglycemic conditions in diabetic mice, *Journal of Nanobiotechnology*, 8, 1, 16. doi: 10.1186/1477-3155-8-16.

Berry, J. L., Xu, L., Polski, A., Jubran, R., Kuhn, P., Kim, J. W., Hicks, J., 2020. Aqueous Humor Is Superior to Blood as a Liquid Biopsy for Retinoblastoma, *Ophthalmology*, Elsevier, 127, 4, 552–554. doi: 10.1016/j.ophtha.2019.10.026.

Biewald, E., Kiefer, T., Geismar, D., Schlüter, S., Manthey, A., Westekemper, H., Wulff, J., Timmermann, B., Ketteler, P., Schönberger, S., Metz, K. A., Ting, S., Göricke, S., Bechrakis, N. E., Bornfeld, N., 2021. Feasibility of Proton Beam Therapy as a Rescue Therapy in Heavily Pre-Treated Retinoblastoma Eyes, *Cancers*, 13, 8, 1862. doi: 10.3390/cancers13081862.

Bornfeld, N., Lohmann, D., Bechrakis, N. E., Biewald, E., 2020. [Retinoblastoma], *Der Ophthalmologe*, 117, 4, 389–402. doi: 10.1007/s00347-020-01081-x.

Bossenmeyer-Pourié, C., Kannan, R., Ribieras, S., Wendling, C., Stoll, I., Thim, L., Tomasetto, C., Rio, M.-C., 2002. The trefoil factor 1 participates in gastrointestinal cell

differentiation by delaying G1-S phase transition and reducing apoptosis, *Journal of Cell Biology*, 157, 5, 761–770. doi: 10.1083/jcb200108056.

Bouchoucha, Y., Matet, A., Berger, A., Carcaboso, A. M., Gerrish, A., Moll, A., Jenkinson, H., Ketteler, P., Dorsman, J. C., Chantada, G., Beck-Popovic, M., Munier, F., Aerts, I., Doz, F., Golmard, L., European Retinoblastoma Group EuRbG, 2023. Retinoblastoma: From genes to patient care, *European Journal of Medical Genetics*, 66, 1, 104674. doi: 10.1016/j.ejmg.2022.104674.

Braga Emidio, N., Brierley, S. M., Schroeder, C. I., Muttenthaler, M., 2020. Structure, Function, and Therapeutic Potential of the Trefoil Factor Family in the Gastrointestinal Tract, *ACS Pharmacology & Translational Science*, 3, 4, 583–597. doi: 10.1021/acsptsci.0c00023.

Bromma, K., Chithrani, D. B., 2020. Advances in Gold Nanoparticle-Based Combined Cancer Therapy, *Nanomaterials*, Multidisciplinary Digital Publishing Institute, 10, 9, 1671. doi: 10.3390/nano10091671.

Bukowski, K., Kciuk, M., Kontek, R., 2020. Mechanisms of Multidrug Resistance in Cancer Chemotherapy, *International Journal of Molecular Sciences*, Multidisciplinary Digital Publishing Institute, 21, 9, 3233. doi: 10.3390/ijms21093233.

Busch, M. A., Haase, A., Alefeld, E., Biewald, E., Jabbarli, L., Dünker, N., 2023. Trefoil Family Factor Peptide 1—A New Biomarker in Liquid Biopsies of Retinoblastoma under Therapy, *Cancers*, Multidisciplinary Digital Publishing Institute, 15, 19, 4828. doi: 10.3390/cancers15194828.

Busch, M. A., Haase, A., Miroschnikov, N., Doege, A., Biewald, E., Bechrakis, N. E., Beier, M., Kanber, D., Lohmann, D., Metz, K., Dünker, N., 2022. TFF1 in Aqueous Humor—A Potential New Biomarker for Retinoblastoma, *Cancers*, Multidisciplinary Digital Publishing Institute, 14, 3, 677. doi: 10.3390/cancers14030677.

Busch, M., Große-Kreul, J., Wirtz, J. J., Beier, M., Stephan, H., Royer-Pokora, B., Metz, K., Dünker, N., 2017. Reduction of the tumorigenic potential of human retinoblastoma cell lines by TFF1 overexpression involves p53/caspase signaling and miR-18a regulation, *International Journal of Cancer*, 141, 3, 549–560. doi: 10.1002/ijc.30768.

Busch, M., Metz, K., Beier, M., Biewald, E., Dünker, N., 2018. TREFOIL FACTOR FAMILY 1 EXPRESSION CORRELATES WITH CLINICAL OUTCOME IN PATIENTS WITH RETINOBLASTOMA, *RETINA*, 38, 12, 2422. doi: 10.1097/IAE.0000000000001881.

Busch, M., Papior, D., Stephan, H., Dünker, N., 2018. Characterization of etoposide- and cisplatin-chemoresistant retinoblastoma cell lines, *Oncology Reports*, Spandidos Publications, 39, 1, 160–172. doi: 10.3892/or.2017.6100.

Buske, C., Kirchhoff, F., Münch, J., 2015. EPI-X4, a novel endogenous antagonist of CXCR4, *Oncotarget*, 6, 34, 35137–35138. doi: 10.18632/oncotarget.6037.

Byroju, V. V., Nadukkandy, A. S., Cordani, M., Kumar, L. D., 2023. Retinoblastoma: present scenario and future challenges, *Cell Communication and Signaling*, 21, 1, 226. doi: 10.1186/s12964-023-01223-z.

Calnan, D. P., Westley, B. R., May, F. E. B., Floyd, D. N., Marchbank, T., Playford, R. J., 1999. The trefoil peptide TFF1 inhibits the growth of the human gastric adenocarcinoma cell line AGS, *The Journal of Pathology*, 188, 3, 312–317. doi: 10.1002/(SICI)1096-9896(199907)188:3<312::AID-PATH360>3.0.CO;2-P.

Castela, G., Providência, J., Monteiro, M., Oliveiros, B., Silva, S., Brito, M., Machado, E., Neto Murta, J., Castelo-Branco, M., Correa, Z., 2023. Effectiveness of Intra-Arterial Chemotherapy for the Treatment of Intraocular Retinoblastoma: Relevance of a Multidisciplinary Setting, *Clinical Ophthalmology*, Dove Medical Press, 17, 487–496. doi: 10.2147/OPTH.S398488.

Chatterjee, S., Behnam Azad, B., Nimmagadda, S., 2014. The Intricate Role of CXCR4 in

Cancer, in, *Advances in Cancer Research*, Elsevier, pp. 31–82. doi: 10.1016/B978-0-12-411638-2.00002-1.

Cobrinik, D., 2005. Pocket proteins and cell cycle control, *Oncogene*, Nature Publishing Group, 24, 17, 2796–2809. doi: 10.1038/sj.onc.1208619.

Cobrinik, D., 2024. Retinoblastoma Origins and Destinations, *New England Journal of Medicine*, Edited by D. L. Longo, 390, 15, 1408–1419. doi: 10.1056/NEJMra1803083.

Comings, D. E., 1973. A General Theory of Carcinogenesis, *Proceedings of the National Academy of Sciences*, Proceedings of the National Academy of Sciences, 70, 12, 3324–3328. doi: 10.1073/pnas.70.12.3324.

Corson, T. W., Samuels, B. C., Wenzel, A. A., Geary, A. J., Riley, A. A., McCarthy, B. P., Hanenberg, H., Bailey, B. J., Rogers, P. I., Pollok, K. E., Rajashekhar, G., Territo, P. R., 2014. Multimodality Imaging Methods for Assessing Retinoblastoma Orthotopic Xenograft Growth and Development, *PLOS ONE*, Public Library of Science, 9, 6, e99036. doi: 10.1371/journal.pone.0099036.

Costa, M. H. S., Latronico, A. C., Martin, R. M., Barbosa, A. S., Almeida, M. Q., Lotfi, C. F. P., Valassi, H. P. L., Nishi, M. Y., Lucon, A. M., Siqueira, S. A., Zerbini, M. C. N., Carvalho, L. R., Mendonca, B. B., Fragoso, M. C. B. V., 2009. Expression profiles of the glucose-dependent insulinotropic peptide receptor and LHCGR in sporadic adrenocortical tumors, *The Journal of Endocrinology*, 200, 2, 167–175. doi: 10.1677/JOE-08-0395.

Cunningham, C., de Kock, M., Engelbrecht, M., Miles, X., Slabbert, J., Vandevoorde, C., 2021. Radiosensitization Effect of Gold Nanoparticles in Proton Therapy, *Frontiers in Public Health*, Frontiers, 9. doi: 10.3389/fpubh.2021.699822.

De Clercq, E., 2009. The AMD3100 story: The path to the discovery of a stem cell mobilizer (Mozobil), *Biochemical Pharmacology*, 77, 11, 1655–1664. doi: 10.1016/j.bcp.2008.12.014.

De Jong, M. C., Van Der Meer, F. J. S., Göricke, S. L., Brisse, H. J., Galluzzi, P., Maeder, P., Sirin, S., De Francesco, S., Sastre-Garau, X., Metz, K. A., Cerase, A., Noij, D. P., Van Der Valk, P., Moll, A. C., Castelijns, J. A., De Graaf, P., For the European Retinoblastoma Imaging Collaboration, 2016. Diagnostic Accuracy of Intraocular Tumor Size Measured with MR Imaging in the Prediction of Postlaminar Optic Nerve Invasion and Massive Choroidal Invasion of Retinoblastoma, *Radiology*, 279, 3, 817–826. doi: 10.1148/radiol.2015151213.

Dieckow, J., Brandt, W., Hattermann, K., Schob, S., Schulze, U., Mentlein, R., Ackermann, P., Sel, S., Paulsen, F. P., 2016. CXCR4 and CXCR7 Mediate TFF3-Induced Cell Migration Independently From the ERK1/2 Signaling Pathway, *Investigative Opthalmology & Visual Science*, 57, 1, 56. doi: 10.1167/iovs.15-18129.

Dimaras, H., Khetan, V., Halliday, W., Orlic, M., Prigoda, N. L., Piovesan, B., Marrano, P., Corson, T. W., Eagle, R. C., Jr, Squire, J. A., Gallie, B. L., 2008. Loss of RB1 induces non-proliferative retinoma: increasing genomic instability correlates with progression to retinoblastoma, *Human Molecular Genetics*, 17, 10, 1363–1372. doi: 10.1093/hmg/ddn024.

Dimaras, H., Kimani, K., Dimba, E. A., Gronsdahl, P., White, A., Chan, H. S., Gallie, B. L., 2012. Retinoblastoma, *The Lancet*, Elsevier, 379, 9824, 1436–1446. doi: 10.1016/S0140-6736(11)61137-9.

Domanska, U. M., Timmer-Bosscha, H., Nagengast, W. B., Oude Munnink, T. H., Kruizinga, R. C., Ananias, H. J. K., Kliphuis, N. M., Huls, G., De Vries, E. G. E., de Jong, I. J., Walenkamp, A. M. E., 2012. CXCR4 Inhibition with AMD3100 Sensitizes Prostate Cancer to Docetaxel Chemotherapy, *Neoplasia*, 14, 8, 709–718. doi: 10.1593/neo.12324.

Dommering, C. J., Mol, B. M., Moll, A. C., Burton, M., Cloos, J., Dorsman, J. C., Meijers-Heijboer, H., van der Hout, A. H., 2014. RB1 mutation spectrum in a comprehensive nationwide cohort of retinoblastoma patients, *Journal of Medical Genetics*, 51, 6, 366–374.

doi: 10.1136/jmedgenet-2014-102264.

Dubeykovskaya, Z., Dubeykovskiy, A., Solal-Cohen, J., Wang, T. C., 2009. Secreted Trefoil Factor 2 Activates the CXCR4 Receptor in Epithelial and Lymphocytic Cancer Cell Lines *, *Journal of Biological Chemistry*, Elsevier, 284, 6, 3650–3662. doi: 10.1074/jbc.M804935200.

Dupre, J., Ross, S. A., Watson, D., Brown, J. C., 1973. STIMULATION OF INSULIN SECRETION BY GASTRIC INHIBITORY POLYPEPTIDE IN MAN. [1], *The Journal of Clinical Endocrinology & Metabolism*, 37, 5, 826–828. doi: 10.1210/jcem-37-5-826.

Dyson, N. J., 2016. RB1: a prototype tumor suppressor and an enigma, *Genes & Development*, 30, 13, 1492–1502. doi: 10.1101/gad.282145.116.

Elnagdy, M. H., Farouk, O., Seleem, A. K., Nada, H. A., 2018. *TFF1* and *TFF3* mRNAs Are Higher in Blood from Breast Cancer Patients with Metastatic Disease than Those without, *Journal of Oncology*, 2018, 1–8. doi: 10.1155/2018/4793498.

Emidio, N. B., Hoffmann, W., Brierley, S. M., Muttenthaler, M., 2019. Trefoil Factor Family: Unresolved Questions and Clinical Perspectives, *Trends in Biochemical Sciences*, Elsevier, 44, 5, 387–390. doi: 10.1016/j.tibs.2019.01.004.

Escudero, L., Martínez-Ricarte, F., Seoane, J., 2021. ctDNA-Based Liquid Biopsy of Cerebrospinal Fluid in Brain Cancer, *Cancers*, Multidisciplinary Digital Publishing Institute, 13, 9, 1989. doi: 10.3390/cancers13091989.

Fabian, I. D., Johnson, K. P., Stacey, A. W., Sagoo, M. S., Reddy, M. A., 2017. Focal laser treatment in addition to chemotherapy for retinoblastoma, *Cochrane Database of Systematic Reviews*, Edited by Cochrane Eyes and Vision Group, 2017, 6. doi: 10.1002/14651858.CD012366.pub2.

Feng, Y., Broder, C. C., Kennedy, P. E., Berger, E. A., 1996. HIV-1 Entry Cofactor: Functional cDNA Cloning of a Seven-Transmembrane, G Protein-Coupled Receptor, *Science*, American Association for the Advancement of Science, 272, 5263, 872–877. doi: 10.1126/science.272.5263.872.

Ferrara, N., Kerbel, R. S., 2005. Angiogenesis as a therapeutic target, *Nature*, Nature Publishing Group, 438, 7070, 967–974. doi: 10.1038/nature04483.

Francis, J. H., Abramson, D. H., Ji, X., Shields, C. L., Teixeira, L. F., Schefler, A. C., Cassoux, N., Hadjistilianou, D., Berry, J. L., Frenkel, S., Munier, F. L., 2017. Risk of Extraocular Extension in Eyes With Retinoblastoma Receiving Intravitreous Chemotherapy, *JAMA Ophthalmology*, 135, 12, 1426. doi: 10.1001/jamaophthalmol.2017.4600.

Francis, J. H., Brodie, S. E., Marr, B., Zabor, E. C., Mondesire-Crump, I., Abramson, D. H., 2017. Efficacy and Toxicity of Intravitreous Chemotherapy for Retinoblastoma: Four-Year Experience, *Ophthalmology*, 124, 4, 488–495. doi: 10.1016/j.ophtha.2016.12.015.

Friend, S. H., Bernards, R., Rogelj, S., Weinberg, R. A., Rapaport, J. M., Albert, D. M., Dryja, T. P., 1986. A human DNA segment with properties of the gene that predisposes to retinoblastoma and osteosarcoma, *Nature*, Nature Publishing Group, 323, 6089, 643–646. doi: 10.1038/323643a0.

Gaillard, M.-C., Houghton, S., Stathopoulos, C., Munier, F. L., 2018. OCT-guided management of subclinical recurrent retinoblastoma, *Ophthalmic Genetics*, Taylor & Francis, 39, 3, 338–343. doi: 10.1080/13816810.2018.1436183.

Galardi, A., Stathopoulos, C., Colletti, M., Lavarello, C., Russo, I., Cozza, R., Romanzo, A., Carcaboso, A. M., Locatelli, F., Petretto, A., Munier, F. L., Di Giannatale, A., 2022. Proteomics of Aqueous Humor as a Source of Disease Biomarkers in Retinoblastoma, *International Journal of Molecular Sciences*, Multidisciplinary Digital Publishing Institute, 23, 21, 13458. doi: 10.3390/ijms232113458.

Gallie, B. L., Ellsworth, R. M., Abramson, D. H., Phillips, R. A., 1982. Retinoma: Spontaneous regression of retinoblastoma or benign manifestation of the mutation?, *British Journal of Cancer*, 45, 4, 513–521. doi: 10.1038/bjc.1982.87.

Ganju, R. K., Brubaker, S. A., Meyer, J., Dutt, P., Yang, Y., Qin, S., Newman, W., Groopman, J. E., 1998. The α-Chemokine, Stromal Cell-derived Factor-1α, Binds to the Transmembrane G-protein-coupled CXCR-4 Receptor and Activates Multiple Signal Transduction Pathways *, *Journal of Biological Chemistry*, Elsevier, 273, 36, 23169–23175. doi: 10.1074/jbc.273.36.23169.

Gao, J., Huang, X., Liu, H., Zan, F., Ren, J., 2012. Colloidal Stability of Gold Nanoparticles Modified with Thiol Compounds: Bioconjugation and Application in Cancer Cell Imaging, *Langmuir*, American Chemical Society, 28, 9, 4464–4471. doi: 10.1021/la204289k.

Ghassemi, F., Shields, C. L., Ghadimi, H., Khodabandeh, A., Roohipoor, R., 2014. Combined Intravitreal Melphalan and Topotecan for Refractory or Recurrent Vitreous Seeding From Retinoblastoma, *JAMA Ophthalmology*, 132, 8, 936–941. doi: 10.1001/jamaophthalmol.2014.414.

Ghiam, B. K., Xu, L., Berry, J. L., 2019. Aqueous Humor Markers in Retinoblastoma, a Review, *Translational Vision Science & Technology*, 8, 2, 13. doi: 10.1167/tvst.8.2.13.

Goel, M., Picciani, R. G., Lee, R. K., Bhattacharya, S. K., 2010. Aqueous Humor Dynamics: A Review, *The Open Ophthalmology Journal*, 4, 52–59. doi: 10.2174/1874364101004010052.

Gonzaga, I. M., Soares Lima, S. C., Nicolau, M. C., Nicolau-Neto, P., da Costa, N. M., de Almeida Simão, T., Hernandez-Vargas, H., Herceg, Z., Ribeiro Pinto, L. F., 2017. TFF1 hypermethylation and decreased expression in esophageal squamous cell carcinoma and histologically normal tumor surrounding esophageal cells, *Clinical Epigenetics*, 9, 1, 130. doi: 10.1186/s13148-017-0429-0.

Gremlich, S., Porret, A., Hani, E. H., Cherif, D., Vionnet, N., Froguel, P., Thorens, B., 1995. Cloning, functional expression, and chromosomal localization of the human pancreatic islet glucose-dependent insulinotropic polypeptide receptor, *Diabetes*, 44, 10, 1202–1208. doi: 10.2337/diab.44.10.1202.

Griepentrog, T., Bauer, M., Hornstein, C., Sauer, H., Jirikowski, G. F., 2000. Coexistence of Intestinal Trefoil Factor (hITF) and Oxytocin in Magnocellular Neurons in the Human Hypothalamus, *Hormone and Metabolic Research*, © Georg Thieme Verlag Stuttgart · New York, 32, 04, 121–124. doi: 10.1055/s-2007-978604.

Haase, A., Alefeld, E., Yalinci, F., Meenen, D. V., Busch, M. A., Dünker, N., 2024 **A**. Gastric Inhibitory Polypeptide Receptor (GIPR) Overexpression Reduces the Tumorigenic Potential of Retinoblastoma Cells, *Cancers*, 16, 9, 1656. doi: 10.3390/cancers16091656.

Haase, A., Miroschnikov, N., Klein, S., Doege, A., Dünker, N., Van Meenen, D., Junker, A., Göpferich, A., Apaolaza, P. S., Busch, M. A., 2024 **B**. New retinoblastoma (RB) drug delivery approaches: anti-tumor effect of atrial natriuretic peptide (ANP)-conjugated hyaluronic-acid-coated gold nanoparticles for intraocular treatment of chemoresistant RB, *Molecular Oncology*, 18, 4, 832–849. doi: 10.1002/1878-0261.13587.

Hang, Y., Wang, A., Wu, N., 2024. Plasmonic silver and gold nanoparticles: shape- and structure-modulated plasmonic functionality for point-of-caring sensing, bio-imaging and medical therapy, *Chemical Society Reviews*, Royal Society of Chemistry, 53, 6, 2932–2971. doi: 10.1039/D3CS00793F.

Harms, M., Fabech Hansson, R., Gilg, A., Almeida-Hernández, Y., Löffler, J., Rodríguez-Alfonso, A., Habib, M. M. W., Albers, D., Ahmed, N. S., Abadi, A. H., Winter, G., Rasche, V., Beer, A. J., Weidinger, G., Preising, N., Ständker, L., Wiese, S., Sanchez-Garcia, E., Zelikin, A. N., Münch, J., 2023. Development of N-Terminally Modified Variants of the CXCR4-

Antagonistic Peptide EPI-X4 for Enhanced Plasma Stability, *Journal of Medicinal Chemistry*, American Chemical Society, 66, 22, 15189–15204. doi: 10.1021/acs.jmedchem.3c01128.

Harris, A. L., 2002. Hypoxia — a key regulatory factor in tumour growth, *Nature Reviews Cancer*, Nature Publishing Group, 2, 1, 38–47. doi: 10.1038/nrc704.

He, R., Li, X., Liang, L., Xie, Y., Luo, D., Ma, J., Peng, Z., Hu, X., Chen, G., 2017. The suppressive role of miR-542-5p in NSCLC: the evidence from clinical data and in vivo validation using a chick chorioallantoic membrane model, *BMC Cancer*, 17, 1, 655. doi: 10.1186/s12885-017-3646-1.

Heitzer, E., Haque, I. S., Roberts, C. E. S., Speicher, M. R., 2019. Current and future perspectives of liquid biopsies in genomics-driven oncology, *Nature Reviews Genetics*, 20, 2, 71–88. doi: 10.1038/s41576-018-0071-5.

Henley, S. A., Dick, F. A., 2012. The retinoblastoma family of proteins and their regulatory functions in the mammalian cell division cycle, *Cell Division*, 7, 1, 10. doi: 10.1186/1747-1028-7-10.

Ho, T. K., Shiwen, X., Abraham, D., Tsui, J., Baker, D., 2012. Stromal-Cell-Derived Factor-1 (SDF-1)/CXCL12 as Potential Target of Therapeutic Angiogenesis in Critical Leg Ischaemia, *Cardiology Research and Practice*, Hindawi, 2012, e143209. doi: 10.1155/2012/143209.

Hoffmann, W., 2009. Trefoil Factor Family (TFF) Peptides and Chemokine Receptors: A Promising Relationship, *Journal of Medicinal Chemistry*, 52, 21, 6505–6510. doi: 10.1021/jm9008136.

Hoffmann, W., 2020. Trefoil Factor Family (TFF) Peptides and Their Diverse Molecular Functions in Mucus Barrier Protection and More: Changing the Paradigm, *International Journal of Molecular Sciences*, 21, 12, 4535. doi: 10.3390/ijms21124535.

Hoffmann, W., 2021. Trefoil Factor Family (TFF) Peptides and Their Links to Inflammation: A Re-evaluation and New Medical Perspectives, *International Journal of Molecular Sciences*, 22, 9, 4909. doi: 10.3390/ijms22094909.

Hoffmann, W., Jagla, W., 2002. Cell Type Specific Expression of Secretory TFF Peptides: Colocalization with Mucins and Synthesis in the Brain, in Jeon, K. W. (Ed.), *International Review of Cytology*, Academic Press (A Survey of Cell Biology), pp. 147–188e. doi: 10.1016/S0074-7696(02)13014-2.

Hoffmann, W., Jagla, W., Wiede, A., 2001. Molecular medicine of TFF-peptides: from gut to brain, *Histology and Histopathology*, 16, 1, 319–334. doi: no DOI available.

Holash, J. A., Soans, C., Chong, L. D., Shao, H., Dixit, V. M., Pasquale, E. B., 1997. Reciprocal Expression of the Eph Receptor Cek5 and Its Ligand(s) in the Early Retina, *Developmental Biology*, 182, 2, 256–269. doi: 10.1006/dbio.1996.8496.

Huang, Y.-G., Li, Y.-F., Pan, B.-L., Wang, L.-P., Zhang, Yong, Lee, W.-H., Zhang, Yun, 2013. Trefoil factor 1 gene alternations and expression in colorectal carcinomas, *Tumori Journal*, 99, 6, 702–707. doi: 10.1177/030089161309900610.

Jain, R. K., 2005. Normalization of Tumor Vasculature: An Emerging Concept in Antiangiogenic Therapy, *Science*, 307, 5706, 58–62. doi: 10.1126/science.1104819.

Janowski, M., 2009. Functional diversity of SDF-1 splicing variants, *Cell Adhesion & Migration*, Taylor & Francis, 3, 3, 243–249. doi: 10.4161/cam.3.3.8260.

Kaewkhaw, R., Rojanaporn, D., 2020. Retinoblastoma: Etiology, Modeling, and Treatment, *Cancers*, Multidisciplinary Digital Publishing Institute, 12, 8, 2304. doi: 10.3390/cancers12082304.

Karpathakis, A., Dibra, H., Pipinikas, C., Feber, A., Morris, T., Francis, J., Oukrif, D., Mandair, D., Pericleous, M., Mohmaduvesh, M., Serra, S., Ogunbiyi, O., Novelli, M., Luong, T., Asa, S.

L., Kulke, M., Toumpanakis, C., Meyer, T., Caplin, M., Meyerson, M., Beck, S., Thirlwell, C., 2016. Prognostic Impact of Novel Molecular Subtypes of Small Intestinal Neuroendocrine Tumor, *Clinical Cancer Research*, 22, 1, 250–258. doi: 10.1158/1078-0432.CCR-15-0373.

Katoh, M., 2003. Trefoil factors and human gastric cancer (Review), *International Journal of Molecular Medicine*, Spandidos Publications, 12, 1, 3–9. doi: 10.3892/ijmm.12.1.3.

Kim, J. H., Moon, M. J., Kim, D. Y., Heo, S. H., Jeong, Y. Y., 2018. Hyaluronic Acid-Based Nanomaterials for Cancer Therapy, *Polymers*, Multidisciplinary Digital Publishing Institute, 10, 10, 1133. doi: 10.3390/polym10101133.

Kim, J. W., Ngai, L. K., Sadda, S., Murakami, Y., Lee, D. K., Murphree, A. L., 2014. Retcam fluorescein angiography findings in eyes with advanced retinoblastoma, *British Journal of Ophthalmology*, BMJ Publishing Group Ltd, 98, 12, 1666–1671. doi: 10.1136/bjophthalmol-2014-305180.

Kivelä, T., 2009. The epidemiological challenge of the most frequent eye cancer: retinoblastoma, an issue of birth and death, *British Journal of Ophthalmology*, BMJ Publishing Group Ltd, 93, 9, 1129–1131. doi: 10.1136/bjo.2008.150292.

Kjellev, S., 2009. The trefoil factor family – small peptides with multiple functionalities, *Cellular and Molecular Life Sciences*, 66, 8, 1350–1369. doi: 10.1007/s00018-008-8646-5.

Kleinerman, R. A., Schonfeld, S. J., Tucker, M. A., 2012. Sarcomas in hereditary retinoblastoma, *Clinical Sarcoma Research*, 2, 1, 15. doi: 10.1186/2045-3329-2-15.

Kleinerman, R., Tucker, M., Tarone, R., Abramson, D., Seddon, J., Stovall, M., Li, F., Fraumeni, J., 2005. Risk of New Cancers After Radiotherapy in Long-Term Survivors of Retinoblastoma: An Extended Follow-Up, *Journal of clinical oncology : official journal of the American Society of Clinical Oncology*, 23, 2272–9. doi: 10.1200/JCO.2005.05.054.

Knudson, A. G., 1971. Mutation and Cancer: Statistical Study of Retinoblastoma, *Proceedings of the National Academy of Sciences*, Proceedings of the National Academy of Sciences, 68, 4, 820–823. doi: 10.1073/pnas.68.4.820.

Körner, M., Waser, B., Reubi, J. C., 2015. Does Somatostatin or Gastric Inhibitory Peptide Receptor Expression Correlate with Tumor Grade and Stage in Gut Neuroendocrine Tumors?, *Neuroendocrinology*, 101, 1, 45–57. doi: 10.1159/000371804.

Kritfuangfoo, T., Rojanaporn, D., 2024. Update on chemotherapy modalities for retinoblastoma: Progress and challenges, *Asia-Pacific Journal of Ophthalmology*, 13, 2, 100061. doi: 10.1016/j.apjo.2024.100061.

Kucia, M., Reca, R., Miekus, K., Wanzeck, J., Wojakowski, W., Janowska-Wieczorek, A., Ratajczak, J., Ratajczak, M. Z., 2005. Trafficking of Normal Stem Cells and Metastasis of Cancer Stem Cells Involve Similar Mechanisms: Pivotal Role of the SDF-1–CXCR4 Axis, *Stem Cells*, 23, 7, 879–894. doi: 10.1634/stemcells.2004-0342.

Kumar, P., Gupta, S., Das, B. C., 2024. Saliva as a potential non-invasive liquid biopsy for early and easy diagnosis/prognosis of head and neck cancer, *Translational Oncology*, 40, 101827. doi: 10.1016/j.tranon.2023.101827.

Lara-Castillo, N., Zandi, S., Nakao, S., Ito, Y., Noda, K., She, H., Ahmed, M., Frimmel, S., Ablonczy, Z., Hafezi-Moghadam, A., 2009. Atrial Natriuretic Peptide Reduces Vascular Leakage and Choroidal Neovascularization, *The American Journal of Pathology*, Elsevier, 175, 6, 2343–2350. doi: 10.2353/ajpath.2009.090439.

Lavasidis, G., Strongylis, M., Tzamalis, A., Tsinopoulos, I., Ntzani, E. E., 2024. Safety of intravitreal chemotherapy in the management of retinoblastoma: A systematic review of the literature, *Critical Reviews in Oncology/Hematology*, 200, 104423. doi: 10.1016/j.critrevonc.2024.104423.

Lawson, B. M., Saktanasate, J., Say, E. A. T., Shields, C. L., 2014. Intravitreal chemotherapy provides control for massive vitreous seeding from retinoblastoma, *Journal of Pediatric Ophthalmology and Strabismus*, 51 Online, e92-94. doi: 10.3928/01913913-20141203-05.

Leal-Leal, C., Flores-Rojo, M., Medina-Sansón, A., Cerecedo-Díaz, F., Sánchez-Félix, S., González-Ramella, O., Pérez-Pérez, F., Gómez-Martínez, R., Quero-Hernández, A., Altamirano-Álvarez, E., Alejo-González, F., Figueroa-Carbajal, J., Ellis-Irigoyen, A., Tejocote-Romero, I., Cervantes-Paz, R., Pantoja-Guillén, F., Vega-Vega, L., Carrete-Ramírez, F., 2004. A multicentre report from the Mexican Retinoblastoma Group, *British Journal of Ophthalmology*, BMJ Publishing Group Ltd, 88, 8, 1074–1077. doi: 10.1136/bjo.2003.035642.

Lefebvre, O., Chenard, M.-P., Masson, R., Linares, J., Dierich, A., LeMeur, M., Wendling, C., Tomasetto, C., Chambon, P., Rio, M.-C., 1996. Gastric Mucosa Abnormalities and Tumorigenesis in Mice Lacking the pS2 Trefoil Protein, *Science*, 274, 5285, 259–262. doi: 10.1126/science.274.5285.259.

Little, M. P., Kleinerman, R. A., Stiller, C. A., Li, G., Kroll, M. E., Murphy, M. F. G., 2012. Analysis of retinoblastoma age incidence data using a fully stochastic cancer model, *International Journal of Cancer*, 130, 3, 631–640. doi: 10.1002/ijc.26039.

Liu, J., Ottaviani, D., Sefta, M., Desbrousses, C., Chapeaublanc, E., Aschero, R., Sirab, N., Lubieniecki, F., Lamas, G., Tonon, L., Dehainault, C., Hua, C., Fréneaux, P., Reichman, S., Karboul, N., Biton, A., Mirabal-Ortega, L., Larcher, M., Brulard, C., Arrufat, S., Nicolas, A., Elarouci, N., Popova, T., Némati, F., Decaudin, D., Gentien, D., Baulande, S., Mariani, O., Dufour, F., Guibert, S., Vallot, C., Rouic, L. L.-L., Matet, A., Desjardins, L., Pascual-Pasto, G., Suñol, M., Catala-Mora, J., Llano, G. C., Couturier, J., Barillot, E., Schaiquevich, P., Gauthier-Villars, M., Stoppa-Lyonnet, D., Golmard, L., Houdayer, C., Brisse, H., Bernard-Pierrot, I., Letouzé, E., Viari, A., Saule, S., Sastre-Garau, X., Doz, F., Carcaboso, A. M., Cassoux, N., Pouponnot, C., Goureau, O., Chantada, G., De Reyniès, A., Aerts, I., Radvanyi, F., 2021. A high-risk retinoblastoma subtype with stemness features, dedifferentiated cone states and neuronal/ganglion cell gene expression, *Nature Communications*, 12, 1, 5578. doi: 10.1038/s41467-021-25792-0.

Lo, C.-Y., Tsai, S.-W., Niu, H., Chen, F.-H., Hwang, H.-C., Chao, T.-C., Hsiao, I.-T., Liaw, J.-W., 2023. Gold-Nanoparticles-Enhanced Production of Reactive Oxygen Species in Cells at Spread-Out Bragg Peak under Proton Beam Radiation, *ACS Omega*, American Chemical Society, 8, 20, 17922–17931. doi: 10.1021/acsomega.3c01025.

Lu, J. E., Francis, J. H., Dunkel, I. J., Shields, C. L., Yu, M. D., Berry, J. L., Kogachi, K., Skalet, A. H., Miller, A. K., Santapuram, P. R., Daniels, A. B., Abramson, D. H., 2019. Metastases and death rates after primary enucleation of unilateral retinoblastoma in the USA 2007–2017, *British Journal of Ophthalmology*, BMJ Publishing Group Ltd, 103, 9, 1272–1277. doi: 10.1136/bjophthalmol-2018-312915.

MacCarthy, A., Draper, G. J., Steliarova-Foucher, E., Kingston, J. E., 2006. Retinoblastoma incidence and survival in European children (1978–1997). Report from the Automated Childhood Cancer Information System project, *European Journal of Cancer*, (Cancer in Children and Adolescents in Europe), 42, 13, 2092–2102. doi: 10.1016/j.ejca.2006.06.003.

Madsen, J., Nielsen, O., Tornøe, I., Thim, L., Holmskov, U., 2007. Tissue Localization of Human Trefoil Factors 1, 2, and 3, *Journal of Histochemistry & Cytochemistry*, 55, 5, 505–513. doi: 10.1369/jhc.6A7100.2007.

Marees, T., Moll, A. C., Imhof, S. M., De Boer, M. R., Ringens, P. J., Van Leeuwen, F. E., 2008. Risk of Second Malignancies in Survivors of Retinoblastoma: More Than 40 Years of Follow-up, *JNCI: Journal of the National Cancer Institute*, 100, 24, 1771–1779. doi: 10.1093/jnci/djn394.

Marković, L., Bukovac, A., Varošanec, A. M., Šlaus, N., Pećina-Šlaus, N., 2023. Genetics in ophthalmology: molecular blueprints of retinoblastoma, *Human Genomics*, 17, 1, 82. doi:

10.1186/s40246-023-00529-w.

Martens, T. F., Peynshaert, K., Nascimento, T. L., Fattal, E., Karlstetter, M., Langmann, T., Picaud, S., Demeester, J., De Smedt, S. C., Remaut, K., Braeckmans, K., 2017. Effect of hyaluronic acid-binding to lipoplexes on intravitreal drug delivery for retinal gene therapy, *European Journal of Pharmaceutical Sciences*, (30 years of Drug Delivery; - In Honour of 60th Anniversary of Arto Urtti), 103, 27–35. doi: 10.1016/j.ejps.2017.02.027.

McDermott David H., Pastrana Diana V., Calvo Katherine R., Pittaluga Stefania, Velez Daniel, Cho Elena, Liu Qian, Trout Hugh H., Neves João F., Gardner Pamela J., Bianchi David A., Blair Elizabeth A., Landon Emily M., Silva Susana L., Buck Christopher B., Murphy Philip M., 2019. Plerixafor for the Treatment of WHIM Syndrome, *New England Journal of Medicine*, Massachusetts Medical Society, 380, 2, 163–170. doi: 10.1056/NEJMoa1808575.

Meel, R., Kashyap, S., Bakhshi, S., Singh Bajaj, M., Wadhwani, M., 2020. Retinoblastoma in Children Older than 6 Years of Age, *Ocular Oncology and Pathology*, 6, 6, 395–404. doi: 10.1159/000509040.

Mendoza, P. R., Grossniklaus, H. E., 2015. Chapter Thirty - The Biology of Retinoblastoma, in Hejtmancik, J. F. and Nickerson, J. M. (Eds.), *Progress in Molecular Biology and Translational Science*, Academic Press (Molecular Biology of Eye Disease), pp. 503–516. doi: 10.1016/bs.pmbts.2015.06.012.

Morel, Y., Schiano de Colella, J.-M., Harrop, J., Deen, K. C., Holmes, S. D., Wattam, T. A., Khandekar, S. S., Truneh, A., Sweet, R. W., Gastaut, J.-A., Olive, D., Costello, R. T., 2000. Reciprocal Expression of the TNF Family Receptor Herpes Virus Entry Mediator and Its Ligand LIGHT on Activated T Cells: LIGHT Down-Regulates Its Own Receptor1, *The Journal of Immunology*, 165, 8, 4397–4404. doi: 10.4049/jimmunol.165.8.4397.

Mortezaee, K., 2020. CXCL12/CXCR4 axis in the microenvironment of solid tumors: A critical mediator of metastasis, *Life Sciences*, 249, 117534. doi: 10.1016/j.lfs.2020.117534.

Moulin, A. P., Gaillard, M.-C., Balmer, A., Munier, F. L., 2012. Ultrasound biomicroscopy evaluation of anterior extension in retinoblastoma: a clinicopathological study, *British Journal of Ophthalmology*, BMJ Publishing Group Ltd, 96, 3, 337–340. doi: 10.1136/bjophthalmol-2011-300051.

Mouw, K. W., Sethi, R. V., Yeap, B. Y., MacDonald, S. M., Chen, Y.-L. E., Tarbell, N. J., Yock, T. I., Munzenrider, J. E., Adams, J., Grabowski, E., Mukai, S., Shih, H. A., 2014. Proton Radiation Therapy for the Treatment of Retinoblastoma, *International Journal of Radiation Oncology*Biology*Physics*, 90, 4, 863–869. doi: 10.1016/j.ijrobp.2014.07.031.

Müller, A., Homey, B., Soto, H., Ge, N., Catron, D., Buchanan, M. E., McClanahan, T., Murphy, E., Yuan, W., Wagner, S. N., Barrera, J. L., Mohar, A., Verástegui, E., Zlotnik, A., 2001. Involvement of chemokine receptors in breast cancer metastasis, *Nature*, 410, 6824, 50–56. doi: 10.1038/35065016.

Munier, F. L., Beck-Popovic, M., Chantada, G. L., Cobrinik, D., Kivelä, T. T., Lohmann, D., Maeder, P., Moll, A. C., Carcaboso, A. M., Moulin, A., Schaiquevich, P., Bergin, C., Dyson, P. J., Houghton, S., Puccinelli, F., Vial, Y., Gaillard, M.-C., Stathopoulos, C., 2019. Conservative management of retinoblastoma: Challenging orthodoxy without compromising the state of metastatic grace. 'Alive, with good vision and no comorbidity', *Progress in Retinal and Eye Research*, 73, 100764. doi: 10.1016/j.preteyeres.2019.05.005.

Munier, F. L., Gaillard, M.-C., Balmer, A., Beck-Popovic, M., 2013. Intravitreal chemotherapy for vitreous seeding in retinoblastoma: Recent advances and perspectives, *Saudi Journal of Ophthalmology: Official Journal of the Saudi Ophthalmological Society*, 27, 3, 147–150. doi: 10.1016/j.sjopt.2013.06.003.

Munier, F. L., Soliman, S., Moulin, A. P., Gaillard, M.-C., Balmer, A., Beck-Popovic, M., 2012. Profiling safety of intravitreal injections for retinoblastoma using an anti-reflux procedure and

sterilisation of the needle track, *British Journal of Ophthalmology*, 96, 8, 1084–1087. doi: 10.1136/bjophthalmol-2011-301016.

Naseripour, M., Mirshahi, R., Kasraei, H., Sedaghat, A., Azimi, F., 2022. Spotlight on Targeted Chemotherapy in Retinoblastoma: Safety, Efficacy, and Patient Outcomes, *OncoTargets and Therapy*, Dove Press, 15, 1545. doi: 10.2147/OTT.S370878.

Nyamori, J. M., Kimani, K., Njuguna, M. W., Dimaras, H., 2012. The incidence and distribution of retinoblastoma in Kenya, *British Journal of Ophthalmology*, BMJ Publishing Group Ltd, 96, 1, 141–143. doi: 10.1136/bjophthalmol-2011-300739.

Oshi, M., Murthy, V., Takahashi, H., Huyser, M., Okano, M., Tokumaru, Y., Rashid, O. M., Matsuyama, R., Endo, I., Takabe, K., 2021. Urine as a Source of Liquid Biopsy for Cancer, *Cancers*, Multidisciplinary Digital Publishing Institute, 13, 11, 2652. doi: 10.3390/cancers13112652.

Park, W. S., Oh, R. R., Park, J. Y., Lee, J. H., Shin, M. S., Kim, H. S., Lee, H. K., Kim, Y. S., Kim, S. Y., Lee, S. H., Yoo, N. J., Lee, J. Y., 2000. Somatic mutations of the trefoil factor family 1 gene in gastric cancer, *Gastroenterology*, 119, 3, 691–698. doi: 10.1053/gast.2000.16483.

Perry, J. K., Kannan, N., Grandison, P. M., Mitchell, M. D., Lobie, P. E., 2008. Are trefoil factors oncogenic?, *Trends in Endocrinology & Metabolism*, 19, 2, 74–81. doi: 10.1016/j.tem.2007.10.003.

Peukert, D., Kempson, I., Douglass, M., Bezak, E., 2020. Gold nanoparticle enhanced proton therapy: A Monte Carlo simulation of the effects of proton energy, nanoparticle size, coating material, and coating thickness on dose and radiolysis yield, *Medical Physics*, 47, 2, 651–661. doi: 10.1002/mp.13923.

Philippeit, C., Busch, M., Dünker, N., 2014. Epigenetic Control of Trefoil Factor Family (TFF) Peptide Expression in Human Retinoblastoma Cell Lines, *Cellular Physiology and Biochemistry*, 34, 3, 1001–1014. doi: 10.1159/000366316.

Pouysségur, J., Dayan, F., Mazure, N. M., 2006. Hypoxia signalling in cancer and approaches to enforce tumour regression, *Nature*, 441, 7092, 437–443. doi: 10.1038/nature04871.

Pozzobon, T., Goldoni, G., Viola, A., Molon, B., 2016. CXCR4 signaling in health and disease, *Immunology Letters*, 177, 6–15. doi: 10.1016/j.imlet.2016.06.006.

Probst, J. C., Zetzsche, T., Weber, M., Theilemann, P., Skutella, T., Landgraf, R., Jirikowskt, G. F., 1996. Human intestinal trefoil factor is expressed in human hypothalamus and pituitary: evidence for a novel neuropeptide, *The FASEB Journal*, 10, 13, 1518–1523. doi: 10.1096/fasebj.10.13.8940297.

Regazzo, D., Barbot, M., Scaroni, C., Albiger, N., Occhi, G., 2020. The pathogenic role of the GIP/GIPR axis in human endocrine tumors: emerging clinical mechanisms beyond diabetes, *Reviews in Endocrine and Metabolic Disorders*, 21, 1, 165–183. doi: 10.1007/s11154-019-09536-6.

Regazzo, D., Bertazza, L., Galletta, E., Barollo, S., Mondin, A., Zovato, S., Iacobone, M., Zilio, E., Scaroni, C., Radu, C. M., Di Benedetto, G., Mian, C., Lefkimmiatis, K., Occhi, G., 2022. The GIP/GIPR axis in medullary thyroid cancer: clinical and molecular findings, *Endocrine-Related Cancer*, 29, 5, 273–284. doi: 10.1530/ERC-21-0258.

Reubi, J. C., Fourmy, D., Cordomi, A., Tikhonova, I. G., Gigoux, V., 2020. GIP receptor: Expression in neuroendocrine tumours, internalization, signalling from endosomes and structure-function relationship studies, *Peptides*, (Glucose-dependent insulinotropic polypeptide (GIP)), 125, 170229. doi: 10.1016/j.peptides.2019.170229.

Rinnert, M., Hinz, M., Buhtz, P., Reiher, F., Lessel, W., Hoffmann, W., 2010. Synthesis and localization of trefoil factor family (TFF) peptides in the human urinary tract and TFF2

excretion into the urine, *Cell and Tissue Research*, 339, 3, 639–647. doi: 10.1007/s00441-009-0913-8.

Rushlow, D. E., Mol, B. M., Kennett, J. Y., Yee, S., Pajovic, S., Thériault, B. L., Prigoda-Lee, N. L., Spencer, C., Dimaras, H., Corson, T. W., Pang, R., Massey, C., Godbout, R., Jiang, Z., Zacksenhaus, E., Paton, K., Moll, A. C., Houdayer, C., Raizis, A., Halliday, W., Lam, W. L., Boutros, P. C., Lohmann, D., Dorsman, J. C., Gallie, B. L., 2013. Characterisation of retinoblastomas without RB1 mutations: genomic, gene expression, and clinical studies, *The Lancet Oncology*, Elsevier, 14, 4, 327–334. doi: 10.1016/S1470-2045(13)70045-7.

Russano, M., Napolitano, A., Ribelli, G., Iuliani, M., Simonetti, S., Citarella, F., Pantano, F., Dell'Aquila, E., Anesi, C., Silvestris, N., Argentiero, A., Solimando, A. G., Vincenzi, B., Tonini, G., Santini, D., 2020. Liquid biopsy and tumor heterogeneity in metastatic solid tumors: the potentiality of blood samples, *Journal of Experimental & Clinical Cancer Research*, 39, 1, 95. doi: 10.1186/s13046-020-01601-2.

Russo, E., Spallarossa, A., Tasso, B., Villa, C., Brullo, C., 2022. Nanotechnology for Pediatric Retinoblastoma Therapy, *Pharmaceuticals*, Multidisciplinary Digital Publishing Institute, 15, 9, 1087. doi: 10.3390/ph15091087.

Schulten, H.-J., Bangash, M., Karim, S., Dallol, A., Hussein, D., Merdad, A., Al-Thoubaity, F. K., Al-Maghrabi, J., Jamal, A., Al-Ghamdi, F., Choudhry, H., Baeesa, S. S., Chaudhary, A. G., Al-Qahtani, M. H., 2017. Comprehensive molecular biomarker identification in breast cancer brain metastases, *Journal of Translational Medicine*, 15, 1, 269. doi: 10.1186/s12967-017-1370-x.

Şen, Ö., Emanet, M., Ciofani, G., 2021. Nanotechnology-Based Strategies to Evaluate and Counteract Cancer Metastasis and Neoangiogenesis, *Advanced Healthcare Materials*, 10, 10, 2002163. doi: 10.1002/adhm.202002163.

Senavirathna, L. K., Fernando, R., Maples, D., Zheng, Y., Polf, J. C., Ranjan, A., 2013. Tumor Spheroids as an In Vitro Model for Determining the Therapeutic Response to Proton Beam Radiotherapy and Thermally Sensitive Nanocarriers, *Theranostics*, 3, 9, 687–691. doi: 10.7150/thno.6381.

Shekarriz, R., Kochaki, N., Eslami-Jouibari, M., Omrani-Nava, V., Ahmadi, M., Alizadeh-Navaei, R., 2022. TFF1 gene single nucleotide polymorphism (rs3761376) and colorectal cancer risk, *Molecular Biology Reports*, 49, 10, 10127–10131. doi: 10.1007/s11033-022-07828-w.

Sherman, S. K., Maxwell, J. E., Carr, J. C., Wang, D., O'Dorisio, M. S., O'Dorisio, T. M., Howe, J. R., 2014. GIPR expression in gastric and duodenal neuroendocrine tumors, *Journal of Surgical Research*, 190, 2, 587–593. doi: 10.1016/j.jss.2014.01.044.

Shields, C. L., Douglass, A. M., Beggache, M., Say, E. A. T., Shields, J. A., 2016. INTRAVITREOUS CHEMOTHERAPY FOR ACTIVE VITREOUS SEEDING FROM RETINOBLASTOMA, *Retina*, 36, 6, 1184–1190. doi: 10.1097/IAE.0000000000000903.

Shimura, T., Dayde, D., Wang, H., Okuda, Y., Iwasaki, H., Ebi, M., Kitagawa, M., Yamada, Tamaki, Yamada, Tomonori, Hanash, S. M., Taguchi, A., Kataoka, H., 2020. Novel urinary protein biomarker panel for early diagnosis of gastric cancer, *British Journal of Cancer*, Nature Publishing Group, 123, 11, 1656–1664. doi: 10.1038/s41416-020-01063-5.

Singh, A. N., Basu, D., Skoblenick, K. J., Castellano, J. M., Pontoriero, G., Thomas, N., 2010. MAPPING OF HUMAN BRAIN FOR GLUCOSE-DEPENDENT INSULINOTROPIC POLYPEPTIDE (GIP) AND GIP RECEPTORS EXPRESSION: IMPLICATIONS IN SCHIZOPHRENIA, *Schizophrenia Research*, 2–3, 117, 528. doi: 10.1016/j.schres.2010.02.1018.

Smith, S. J., Smith, B. D., 2013. Evaluating the risk of extraocular tumour spread following intravitreal injection therapy for retinoblastoma: a systematic review, *The British Journal of*

Ophthalmology, 97, 10, 1231–1236. doi: 10.1136/bjophthalmol-2013-303188.

Smith, S. J., Smith, B. D., Mohney, B. G., 2014. Ocular side effects following intravitreal injection therapy for retinoblastoma: a systematic review, *The British Journal of Ophthalmology*, 98, 3, 292–297. doi: 10.1136/bjophthalmol-2013-303885.

Soebagjo, H., Komaratih, E., Fatmariyanti, S., Nurwasis, N., Aulanniam, A., 2019. Expression of MMP-14 and CD44 associated with proliferation of retinoblastoma cells, *Medicine Science | International Medical Journal*, 0, 1. doi: 10.5455/medscience.2018.07.8958.

Suzuki, S., Kaneko, A., 2004. Management of intraocular retinoblastoma and ocular prognosis, *International Journal of Clinical Oncology*, 9, 1, 1–6. doi: 10.1007/s10147-003-0366-0.

Sztandera, K., Gorzkiewicz, M., Klajnert-Maculewicz, B., 2019. Gold Nanoparticles in Cancer Treatment, *Molecular Pharmaceutics*, American Chemical Society, 16, 1, 1–23. doi: 10.1021/acs.molpharmaceut.8b00810.

Tang, H., Long, Q., Zhuang, K., Han, K., Zhang, X., Guo, H., Lu, X., 2021. Retinoblastoma tumor suppressor gene 1 enhances 5-Fluorouracil chemosensitivity through SDF-1/CXCR4 axis by regulating autophagy in gastric cancer, *Pathology - Research and Practice*, 224, 153532. doi: 10.1016/j.prp.2021.153532.

Temming, P., Arendt, M., Viehmann, A., Eisele, L., Le Guin, C. H. D., Schündeln, M. M., Biewald, E., Astrahantseff, K., Wieland, R., Bornfeld, N., Sauerwein, W., Eggert, A., Jöckel, K.-H., Lohmann, D. R., 2017. Incidence of second cancers after radiotherapy and systemic chemotherapy in heritable retinoblastoma survivors: A report from the German reference center, *Pediatric Blood & Cancer*, 64, 1, 71–80. doi: 10.1002/pbc.26193.

Thomas, H., Timmermann, B., 2020. Paediatric proton therapy, *British Journal of Radiology*, 93, 1107, 20190601. doi: 10.1259/bjr.20190601.

Tolušić Levak, M., Mihalj, M., Koprivčić, I., Novak, S., Bijelić, N., Baus Lončar, M., Belovari, T., Kralik, K., Pauzar, B., 2018. Differential Expression of TFF Genes and Proteins in Breast Tumors, *Acta clinica Croatica*, Klinički bolnički centar Sestre milosrdnice, 57., 2., 264–277. doi: 10.20471/acc.2018.57.02.06.

Tomar, A. S., Finger, P. T., Gallie, B., Mallipatna, A., Kivelä, T. T., Zhang, C., Zhao, J., Wilson, M. W., Kim, J., Khetan, V., Ganesan, S., Yarovoy, A., Yarovaya, V., Kotova, E., Yousef, Y. A., Nummi, K., Ushakova, T. L., Yugay, O. V., Polyakov, V. G., Ramirez-Ortiz, M. A., Esparza-Aguiar, E., Chantada, G., Schaiquevich, P., Fandino, A., Yam, J. C., Lau, W. W., Lam, C. P., Sharwood, P., Moorthy, S., Long, Q. B., Essuman, V. A., Renner, L. A., Català, J., Correa-Llano, G., 2020. A Multicenter, International Collaborative Study for American Joint Committee on Cancer Staging of Retinoblastoma, *Ophthalmology*, 127, 12, 1719–1732. doi: 10.1016/j.ophtha.2020.05.050.

Trujillo, B., Wu, A., Wetterskog, D., Attard, G., 2022. Blood-based liquid biopsies for prostate cancer: clinical opportunities and challenges, *British Journal of Cancer*, Nature Publishing Group, 127, 8, 1394–1402. doi: 10.1038/s41416-022-01881-9.

Usdin, T. B., Mezey, E., Button, D. C., Brownstein, M. J., Bonner, T. I., 1993. Gastric inhibitory polypeptide receptor, a member of the secretin-vasoactive intestinal peptide receptor family, is widely distributed in peripheral organs and the brain, *Endocrinology*, 133, 6, 2861–2870. doi: 10.1210/en.133.6.2861.

Vempuluru, V. S., Maniar, A., Bakal, K., Kaliki, S., 2024. Role of MYCN in retinoblastoma: A review of current literature, *Survey of Ophthalmology*. doi: 10.1016/j.survophthal.2024.05.009.

Venesio, T., Siravegna, G., Bardelli, A., Sapino, A., 2018. Liquid Biopsies for Monitoring Temporal Genomic Heterogeneity in Breast and Colon Cancers, *Pathobiology*, 85, 1–2, 146–

154. doi: 10.1159/000473882.

Volz, A., Göke, R., Lankat-Buttgereit, B., Fehmann, H.-C., Bode, H. P., Göke, B., 1995. Molecular cloning, functional expression, and signal transduction of the GIP-receptor cloned from a human insulinoma, *FEBS Letters*, 373, 1, 23–29. doi: 10.1016/0014-5793(95)01006-Z.

Wang, K., Wang, X., Pan, Q., Zhao, B., 2023. Liquid biopsy techniques and pancreatic cancer: diagnosis, monitoring, and evaluation, *Molecular Cancer*, 22, 1, 167. doi: 10.1186/s12943-023-01870-3.

Wang, W., Li, Z., Wang, J., Du, M., Li, B., Zhang, L., Li, Q., Xu, J., Wang, L., Li, F., Zhang, D., Xu, H., Yang, L., Gong, W., Qiang, F., Zhang, Z., Xu, Z., 2018. A functional polymorphism in TFF1 promoter is associated with the risk and prognosis of gastric cancer, *International Journal of Cancer*, 142, 9, 1805–1816. doi: 10.1002/ijc.31197.

Waser, B., Rehmann, R., Sanchez, C., Fourmy, D., Reubi, J. C., 2012. Glucose-Dependent Insulinotropic Polypeptide Receptors in Most Gastroenteropancreatic and Bronchial Neuroendocrine Tumors, *The Journal of Clinical Endocrinology & Metabolism*, 97, 2, 482–488. doi: 10.1210/jc.2011-2454.

Weise, A., Dünker, N., 2013. High trefoil factor 1 (TFF1) expression in human retinoblastoma cells correlates with low growth kinetics, increased cyclin-dependent kinase (CDK) inhibitor levels and a selective down-regulation of CDK6, *Histochemistry and Cell Biology*, 139, 2, 323–338. doi: 10.1007/s00418-012-1028-y.

Wu, J., Qian, D., Sun, X., 2020. Long noncoding RNAs as potential biomarkers in retinoblastoma: a systematic review and meta-analysis, *Cancer Cell International*, 20, 1, 201. doi: 10.1186/s12935-020-01281-0.

Wu, N., Yang, Y., Yu, N., Wu, Y., Han, X., Chen, S., Zhang, J., Chen, X., Wu, C., Yang, M., Qiu, J., Ge, J., Yu, K., Zhuang, J., 2019. Tetramethylpyrazine downregulates transcription of the CXC receptor 4 (CXCR4) via nuclear respiratory factor-1 (Nrf-1) in WERI-Rb1 retinoblastoma cells, *Oncology Reports*. doi: 10.3892/or.2019.7233.

Xu, X. L., Fang, Y., Lee, T. C., Forrest, D., Gregory-Evans, C., Almeida, D., Liu, A., Jhanwar, S. C., Abramson, D. H., Cobrinik, D., 2009. Retinoblastoma Has Properties of a Cone Precursor Tumor and Depends Upon Cone-Specific MDM2 Signaling, *Cell*, Elsevier, 137, 6, 1018–1031. doi: 10.1016/j.cell.2009.03.051.

Xu, X. L., Singh, H. P., Wang, L., Qi, D.-L., Poulos, B. K., Abramson, D. H., Jhanwar, S. C., Cobrinik, D., 2014. Rb suppresses human cone-precursor-derived retinoblastoma tumours, *Nature*, 514, 7522, 385–388. doi: 10.1038/nature13813.

Yamada, Y., Hayami, T., Nakamura, K., Kaisaki, P. J., Someya, Y., Wang, C.-Z., Seino, S., Seino, Y., 1995. Human Gastric Inhibitory Polypeptide Receptor: Cloning of the Gene (GIPR) and cDNA, *Genomics*, 29, 3, 773–776. doi: 10.1006/geno.1995.9937.

Yamanaka, R., Hayano, A., Takashima, Y., 2019. Trilateral retinoblastoma: A systematic review of 211 cases, *Neurosurgical Review*, 42, 1, 39–48. doi: 10.1007/s10143-017-0890-4.

Yang, D., Qu, F., Cai, H., Chuang, C.-H., Lim, J. S., Jahchan, N., Grüner, B. M., S Kuo, C., Kong, C., Oudin, M. J., Winslow, M. M., Sage, J., 2019. Axon-like protrusions promote small cell lung cancer migration and metastasis, *eLife*, 8, e50616. doi: 10.7554/eLife.50616.

Yi, J., Ren, L., Li, D., Wu, J., Li, W., Du, G., Wang, J., 2020. Trefoil factor 1 (TFF1) is a potential prognostic biomarker with functional significance in breast cancers, *Biomedicine & Pharmacotherapy = Biomedecine & Pharmacotherapie*, 124, 109827. doi: 10.1016/j.biopha.2020.109827.

Yio, X., Diamond, M., Zhang, J., Weinstein, H., Wang, L., Werther, L., Itzkowitz, S., 2006. Trefoil Factor Family-1 Mutations Enhance Gastric Cancer Cell Invasion Through Distinct

Signaling Pathways, *Gastroenterology*, 130, 6, 1696–1706. doi: 10.1053/j.gastro.2006.01.040.

Yu, L., Cecil, J., Peng, S.-B., Schrementi, J., Kovacevic, S., Paul, D., Su, E. W., Wang, J., 2006. Identification and expression of novel isoforms of human stromal cell-derived factor 1, *Gene*, 374, 174–179. doi: 10.1016/j.gene.2006.02.001.

Zahin, N., Anwar, R., Tewari, D., Kabir, Md. T., Sajid, A., Mathew, B., Uddin, Md. S., Aleya, L., Abdel-Daim, M. M., 2020. Nanoparticles and its biomedical applications in health and diseases: special focus on drug delivery, *Environmental Science and Pollution Research*, 27, 16, 19151–19168. doi: 10.1007/s11356-019-05211-0.

Zhou, C., Wen, X., Ding, Y., Ding, J., Jin, M., Liu, Z., Wang, S., Han, M., Yuan, H., Xiao, Y., Wu, L., Wang, J., Li, Y., Yu, J., Wen, Y., Ye, J., Liu, R., Chen, Z., Xue, S., Lu, W., Liao, H., Cui, J., Zhu, D., Lu, F., Tang, S., Wu, Y., Yangkyi, T., Zhang, G., Wubuli, M., Guo, H., Wang, X., He, Y., Sheng, X., Wang, Q., Luo, Y., Fan, J., Qi, J., Yu, Z., Tan, J., Liang, J., Sun, X., Jin, L., Yang, X., Zhang, J., Ji, X., Zhao, J., Jia, R., Fan, X., 2022. Eye-Preserving Therapies for Advanced Retinoblastoma: A Multicenter Cohort of 1678 Patients in China, *Ophthalmology*, 129, 2, 209–219. doi: 10.1016/j.ophtha.2021.09.002.

Zhu, J., Zhang, X., Ai, L., Yuan, R., Ye, J., 2019. Clinicohistopathological implications of MMP/VEGF expression in retinoblastoma: a combined meta-analysis and bioinformatics analysis, *Journal of Translational Medicine*, 17, 1, 226. doi: 10.1186/s12967-019-1975-3.

Zirafi, O., Kim, K.-A., Ständker, L., Mohr, K. B., Sauter, D., Heigele, A., Kluge, S. F., Wiercinska, E., Chudziak, D., Richter, R., Moepps, B., Gierschik, P., Vas, V., Geiger, H., Lamla, M., Weil, T., Burster, T., Zgraja, A., Daubeuf, F., Frossard, N., Hachet-Haas, M., Heunisch, F., Reichetzeder, C., Galzi, J.-L., Pérez-Castells, J., Canales-Mayordomo, A., Jiménez-Barbero, J., Giménez-Gallego, G., Schneider, M., Shorter, J., Telenti, A., Hocher, B., Forssmann, W.-G., Bonig, H., Kirchhoff, F., Münch, J., 2015. Discovery and Characterization of an Endogenous CXCR4 Antagonist, *Cell Reports*, Elsevier, 11, 5, 737–747. doi: 10.1016/j.celrep.2015.03.061.

Zou, Y.-R., Kottmann, A. H., Kuroda, M., Taniuchi, I., Littman, D. R., 1998. Function of the chemokine receptor CXCR4 in haematopoiesis and in cerebellar development, *Nature*, Nature Publishing Group, 393, 6685, 595–599. doi: 10.1038/31269.

Acknowledgements (German)

Die Wissenschaft fängt eigentlich erst da an,

interessant zu werden, wo sie aufhört.

Justus von Liebig

Curriculum vitae

Der Lebenslauf ist in der Online-Version aus Gründen des Datenschutzes nicht enthalten.

Curriculum vitae

Der Lebenslauf ist in der Online-Version aus Gründen des Datenschutzes nicht enthalten.

Declarations (German)

Erklärung:

Hiermit erkläre ich, gem. § 6 Abs. (2) g) der Promotionsordnung der Fakultät für Biologie zur Erlangung der Dr. rer. nat., dass ich das Arbeitsgebiet, dem das Thema „Trefoil factor family peptide 1 (TFF1) as a biomarker, its possible receptors, signaling pathways and prospective application strategies in retinoblastoma therapy" zuzuordnen ist, in Forschung und Lehre vertrete und den Antrag von André Marcel Haase befürworte und die Betreuung auch im Falle eines Weggangs, wenn nicht wichtige Gründe dem entgegenstehen, weiterführen werde.
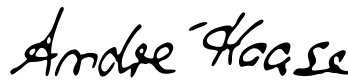
Essen, den 24.07.2024

Prof. Dr. Nicole Dünker

Erklärung:

Hiermit erkläre ich, gem. § 7 Abs. (2) d) + f) der Promotionsordnung der Fakultät für Biologie zur Erlangung des Dr. rer. nat., dass ich die vorliegende Dissertation selbständig verfasst und mich keiner anderen als der angegebenen Hilfsmittel bedient, bei der Abfassung der Dissertation nur die angegeben Hilfsmittel benutzt und alle wörtlich oder inhaltlich übernommenen Stellen als solche gekennzeichnet habe.

Essen, den 24.07.2024

André Marcel Haase

Erklärung:

Hiermit erkläre ich, gem. § 7 Abs. (2) e) + g) der Promotionsordnung der Fakultät für Biologie zur Erlangung des Dr. rer. nat., dass ich keine anderen Promotionen bzw. Promotionsversuche in der Vergangenheit durchgeführt habe und dass diese Arbeit von keiner anderen Fakultät/Fachbereich abgelehnt worden ist.

Essen, den 24.07.2024

André Marcel Haase

Erklärung:

Hiermit erkläre ich, André Marcel Haase, dass ich mit der Veröffentlichung der Publikationen im Rahmen dieser Dissertation keine Urheberrechte verletze.

Essen, den 24.07.2024   _Andre Haase_

                              André Marcel Haase